A biomimetic approach to adaptive camouflage: The function of iridophore and leucophore cells found in the bright white tissue regions of Sepia officinalis

Parfitt, A. R.

Award date:
2004

Awarding institution:
University of Bath

A Biomimetic Approach to Adaptive Camouflage

The function of iridophore and leucophore cells found in the bright white tissue regions of *Sepia officinalis*

Submitted by
A. R. Parfitt
for the degree of PhD

Department of Mechanical Engineering
University of Bath

2004

ProQuest LLC
789 East Eisenhower Parkway
P.O. Box 1346
Ann Arbor, MI 48106-1346

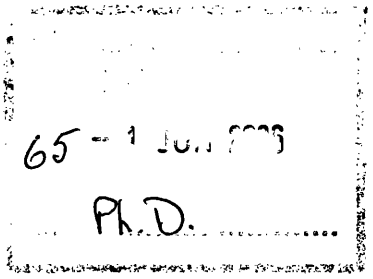
65 - 1
Ph.D.

AUTHOR A R PARFITT YEAR SUBMITTED 2004

TITLE A BIOMIMETIC APPROACH TO ADAPTIVE CAMOUFLAGE

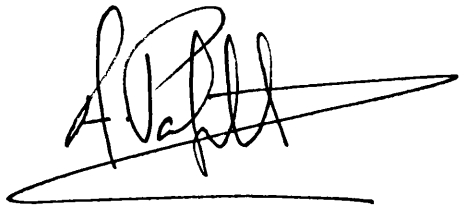

ABSTRACT

This investigation focuses on the ultrastructure and function of (bright) white tissue regions found in the common cuttlefish, *Sepia officinalis*. It illustrates that iridophore cells are orientated in a random manner, within the white regions, and explains how this indiscriminate arrangement may produce structural colours of a low iridescence. Iridescence is also reduced by the presence of leucophore cells. These cells possess Mie light scattering elements, which are responsible for the bright white appearance of the tissue. The direction and area of scatter is presented for a range of wavelengths.

Iridophore and leucophore cell morphology is transformed by physiological quantities of the neurotransmitter acetylcholine. These ultrastructural changes are described, and the advantages to camouflage and communication are considered.

Mechanisms employed by the cuttlefish to utilise natural light for camouflage purposes are mimicked in man-made materials to create a number of colour-changing plastics.

TABLE OF CONTENTS

Part 4 – Colour-changing Materials

LIST OF TABLES AND FIGURES

ACKNOWLEDGEMENTS

I would sincerely like to thank:

Professor Julian Vincent (Centre for Biomimetics and Natural Technologies, University of Bath) for inspiring me to be a diverse scientist and for introducing me to Biomimetics. I thank all members of the CBNT for their continuous support and assistance.

Dr. Elaine Robson (Department of Animal and Microbial Sciences, University of Reading - *retired*) for her patience, perseverance, and in particular for introducing me to electron microscopy.

Dr. Anton Page (Head of the Biomedical Imaging unit, Southampton General Hospital) for a practical introduction to electron microscopy at SGH and for answering many electron microscope questions over the duration of my study.

The Centre for Electron Optical Studies (University of Bath) **Mrs Urshula Potter** and **Professor Glen Love**.

The **Marine Biology Association**, Plymouth. In particular **Professor Roddy Williamson**, and all technicians.

Dr. Tim Birks (Department of Physics, University of Bath) for his continued assistance in all optical related subjects.

Professor Jonathon Knight (Department of Physics, University of Bath) for his guidance through light scattering problems.

Dr. John Hubble (Department of Chemical Engineering, University of Bath) for help in the design of a prototype colour-changing gel.

Professor Robert Eisenthal (Department of Biology and Biochemistry, University of Bath) for his assistance in the experimental design of the prototype colour-changing gel, and the loan of UV equipment.

Lt. Col. Dr. David Moorcroft, **Mr Tony Howard**, and **Dr Lynn Halam** project advisors for the Defence Logistics Organisation.

The **Department of Biology and Biochemistry**, University of Bath.

The **Department of Animal and Microbial Sciences**, University of Reading, for the loan of equipment.

This project has been funded in a joint sponsorship between the Defence Logistics Organisation (Ministry of Defence) and the Engineering and Physical Sciences Research Council.

Part 1 – Background and Introduction

General Introduction

As the cross hairs align over the rear number plate of 007's speeding Aston Martin, James is forced to swerve into a dead-end; he is disarmed and there is no escape. This looks as if it is the end of the Bond saga. However, with the flick of a switch, the car with James completely disappears. 007 escapes thanks to the MOD's latest invention, the chameleon-car. Mirrored surfaces are revealed across the cars bodywork, which reflect the surrounding environment and perfectly camouflages the vehicle (Die another day, MGM films, 2003).

Colour changing objects and materials have often been termed 'chameleon', although their connection with the natural system is trivial. The chameleon is an expert in changing colour and we understand how it, and indeed many animals, uses colours to enhance or reduce communication within their environments (Cott, 1940; Fox, 1953; Fox and Vevers, 1960; Endler, 1978; 1990; 1991). We also know of a more rapid colour-changing group of invertebrate molluscs, the cephalopods. Many cephalopods change their colour display in fractions of a second; this has given them the ability to produce a diverse array of body patterns. This project shall focus on one species of cephalopod, the common cuttlefish *Sepia officinalis*, which frequents European waters. A great deal of research has been conducted on the chromatophore organs of this species, but little consideration has been given to the function and structure of the bright white regions of tissue that are found beneath the chromatophores. These light reflecting regions play an important part in camouflage, and I consider may lend themselves to being mimicked. This investigation therefore focuses on the ultrastructure and optical functions of the iridophore and leucophore

cells found within the bright white regions of the dermis. An attempt will then be made to mimic the properties of these cells to create several prototype colour-changing materials.

MILITARY VEHICLE CAMOUFLAGE

This project shall use ideas from the cuttlefish to create an adaptive colour-changing material that could potentially be developed into a camouflage for military vehicles (operating in the visible spectrum only). By using ideas from the cuttlefish, it is hoped that any colour changing solutions will be reliant upon natural illumination and therefore low energy requiring.

Military vehicles are currently camouflaged in four different coloured paints, appropriate to the operational environment, which are abstractly arranged to create a disruptive pattern (fig.1). When stationary, vehicles are additionally cloaked in camouflage netting that has suitably coloured textiles tied to it (fig. 2). This is used to enhance background matching, and to disguise a vehicle's contour by concealing edges and shadows. Each of these is a very imprecise method of concealment, and may be effective for only a limited duration. Abrupt seasonal changes, or advancing through environments e.g. rural to urban, will often render the camouflage inadequate. To resolve this several different coloured net variants are carried, which creates an additional logistic problem. A more dynamic and accurate method of background matching is therefore desired.

Fig. 1 An operational tank that has been painted in a disruptive pattern suitable for camouflage in a deciduous forest. The inset box shows a sample of the disruptive pattern and colours that would be used in combat uniforms for this environment.

Fig. 2 Brown camouflage netting, suitable for camouflage in the autumn or desert.

INTRODUCTION TO CEPHALOPODS

Cephalopods date from the upper Cambrian period (490 million years ago), making them considerably older than the first chordate fish. Fossil records suggest that early cephalopods developed a hard outer shell for buoyancy. This allowed the originally benthic mollusc group to feed throughout the water column, and additionally provided protection. As competition increased throughout the water column, speed and locomotion became increasingly important, and this led to the gradual internalisation of the cumbersome outer shell (Chamberlain, 1987). It is also thought to have eventually led to the development of fins, and the ability to jet water for rapid propulsion (for detailed evolution see Packard, 1972; Donovan, 1977; Moynihan, 1985).

Nautilus is the oldest remaining cephalopod, and still maintains an external shell. All other cephalopods have either modified and internalised the buoyancy device, or completely discarded it (fig.3). These shell-less cephalopods make up the largest remaining sub-class, the coleoids[1], and they can change colour (with the exception of *Vampyroteuthis*).

[1] The term coleoid is rarely used when referring to squid, octopus and cuttlefish. Cephalopod is more generally written.

NAUTILUS

External shell that possesses no chromatophore organs, iridophores or leucophores.

CUTTLEFISH
Sepia elegans
S. esculenta
S. officinalis

Shell internalised to form the cuttlebone. Their soft muscular bodies contain chromatophores, iridophores and leucophores.

SQUID
Alloteuthis subulata
Loligo forbesi
L. opalescens
L. pealii
L. plei
L. vulgaris
Lolliguncula brevis

Shell internalised to form the pen. Their soft muscular body contains chromatophores, and iridophores, but few species possess leucophores.

OCTOPUS
Octopus dofleini
O. vulgaris
Eledone moschata

Shell completely absent. Their soft muscular bodies contain chromatophores, iridophores and leucophores.

Fig. 3 A summary of the cephalopods mentioned in this text, and a list of the coleoid species that are referenced. (Images from CephBase, 2002).

SEPIA OFFICINALIS

INTRODUCTION

The common cuttlefish *Sepia officinalis* Linnaeus 1758 (fig. 4) migrates between the coastal waters of the North Sea, English Channel, east Atlantic Ocean and Mediterranean (Boletzky, 1983). During migration, this solitary epibenthic mollusc remains mostly in shallow waters where it encounters a wide range of substrates such as rock, sand, mud, kelp forests, and coral. This range of different habitats has undoubtedly increased their camouflage repertoire.

As a consequence of shallow-water dwelling and breeding, together with extraordinary transforming colouration, *Sepia* has long generated scientific interest. Observational records date to Aristotle (translation, 1910), and continue today as we still marvel at the complexity of all cephalopods.

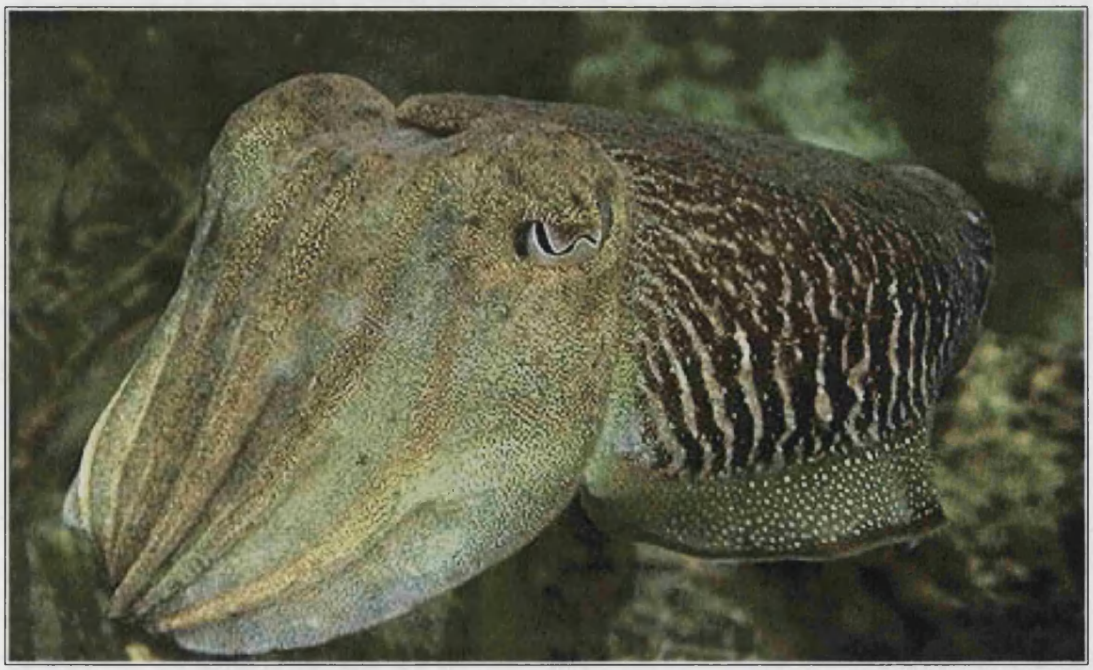

Fig. 4 Common cuttlefish, *Sepia officinalis* (Image, R. Byrne).

The life cycle of *S. officinalis* is under two years, during which 1cm length hatchlings develop to a maximum size of almost half a metre (excluding retractile tentacles). Their soft muscular bodies and continually growing cuttlebone (Boletzky, 1979; 1983) permits this rapid growth. It is therefore not surprising that the cuttlefish is a voracious predator that hunts, like most cephalopods, a variety of prey day and night. Their diet consists mainly of crustaceans such as shrimps and crabs, as well as numerous teleosts fish (full summary of diet see Hanlon and Messenger, 1996). Prey is stalked, or ambushed (Boletzky, 1974, 1996; Messenger, 1968; Moyinhan and Rodaniche, 1982; Boletzky and Roeleveld, 2000), and it is even possible that they mimic other fish whilst in pursuit of prey. However, it is clear that all methods of hunting rely on camouflage and this is used to get to within one mantle's (body) length distance from the prey. It is at this distance that two projectile tentacles are released to catch, recoil the prey (Messenger, 1968; Kier, 1991), and restrain it in eight strong arms.

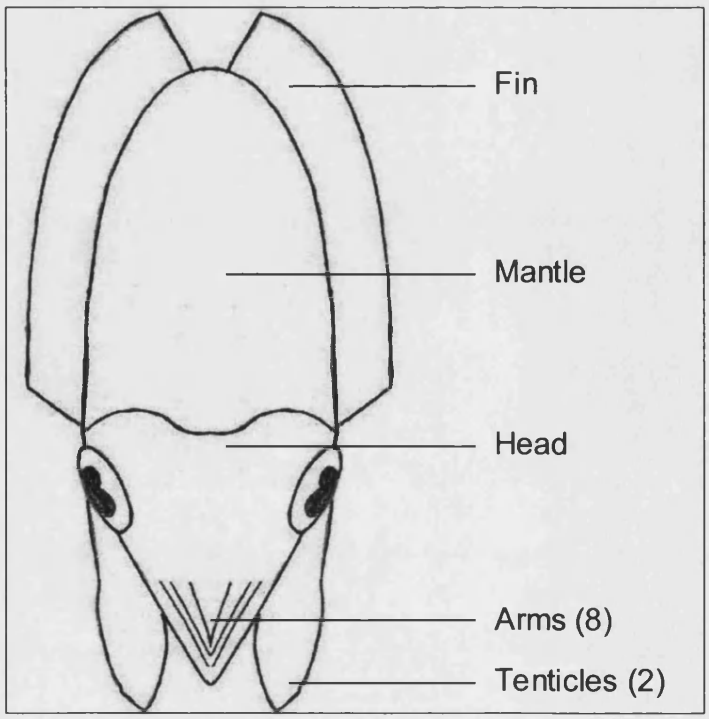

Fig. 5 A sketch illustrating the different part of a cuttlefish, as referred to in the text.

The size range from juvenile to adulthood, subjects *S. officinalis* to a wide variety of predators. In temperate waters they are preyed upon by teleost fish, although Hanlon and Messenger (1996) suggest that a complete predator list would include every carnivore [of that environment]. Numerous defence strategies are used to avert detection, and these are generally termed as crypsis (Cott, 1940; Endler, 1991). Cephalopod crypsis includes general background matching, countershading, disruptive patterning, deceptive resemblance, and even morphological rarity to prevent predator learning (Hanlon and Messenger, 1996). If and when crypsis fails, cuttlefish may also try to startle a predator by flashing patterns or waves (passing cloud display) across the body, before inking and jetting away (defensive strategies see Hanlon and Messenger, 1988; 1996).

Camouflage is therefore uppermost in sustaining a cuttlefish's life, as it is most important for both hunting and escape from predation. Many elements are involved in this camouflage, including morphology and behaviour. However, it is the chromatic components that are primary. These include pigmented chromatophore organs, and light reflecting iridophore and leucophore cells.

CHROMATOPHORE ORGANS: A SUMMARY

The important role of chromatophore organs is emphasised by the extensive amount of research already conducted upon them (summarised in Messenger, 2001). A brief introduction follows:

Chromatophore cells provide skin colouration throughout most of the animal kingdom (Fox, 1953; Fox and Vevers, 1960). It is only the cephalopods that possess a more advanced, and unique chromatophore organ (Parker, 1948, Cloney and Florey,

1968). It consists of an elastic sac, or sacculus, which contains brown, red, or orange[2] pigment granules in *S. officinalis*. The sacculus is surrounded by 6-20 conical muscles (Fuchs, 1914; Reed, 1995) and each of these is innervated by the central nervous system (Florey, 1966; Cloney and Florey, 1968; Florey and Kriebel, 1969; Loi *et al*, 1996; Loi and Tublitz, 2000; Messenger *et al*, 1997). Several neurotransmitting substances have been shown to induce contraction of this muscle; these include glutamate (Bone and Howarth, 1980) and a peptide (FMRFamide) in *S. officinalis* (Loi *et al*, 1996) and *Octopus vulgaris* (Messenger *et al.*, 1997). The latter substance does not affect several squid species, which suggests that differences may occur in chromatophore regulation (previous reference).

This neuromuscular control allows not only a wide range of body patterns (although it is limited) to be displayed, but permits static and dynamic patterns as well. It also means that the chromatophores are driven by information from the eye and brain (Boycott, 1961). However, visual information is limited, given that most cephalopods, including *S. officinalis,* are colour-blind (Marshall and Messenger, 1996).

The optical receptor cells of *S. officinalis* contain only one type of rhodopsin; with a peak absorbance of 492 nm (Brown and Brown, 1958; average for cephalopods is 480 nm). It is similar to vertebrate rhodopsin. However, it does not bleach, due to the presence of retinochrome, an accessory pigment that regenerates rhodopsin (summary in Messenger, 1981). Cuttlefish therefore see in green only. In addition, cephalopods may also perceive polarised light. Fine microvilli found around the edge of each optical receptor cells are arranged at 90° to one another, and are thought to register at least two planes of light polarisation (Moody and Parriss, 1960; Rowell and

[2] The perceived *in vivo* colour of chromatophore pigments will be strongly influenced by light attenuation in the ocean. Optical oceanographic is discussed in the appendix, page 211.

Wells, 1961; Moody, 1962). The limited colour vision and overall simplicity of the cephalopod eye is remarkable, given the degree to which cephalopods can actively camouflage themselves in a range of different environments. The fact that the eye can perceive only a limited spectrum of colour, suggest that chromatophores may not be involved in background colour matching, but instead serve another purpose. This shall be discussed. A common hypothesis is that light reflecting iridophore and leucophore cells, which are found beneath the chromatophore layer, are responsible for background colour matching. It is the role of these cells that is to be investigated. However, in order to characterise and understand their respective optical capacities, the morphology and ultrastructure of each cell must be examined. I consider that our current understanding of iridophore and leucophore cells from *S. officinalis* is insufficient, and does not explain all of the optical phenomena that are evident in the tissue.

MATERIALS AND METHODS

WELFARE OF EXPERIMENTAL ANIMALS

Many marine animals, including cephalopods, are prone to severe physiological stress. Elevated levels of plasma glucose, adrenaline and lactic acid, as well as osmotic effects, have all been observed after handling, exposure to air (for even short periods), low oxygen levels, high temperature, and high ammonia levels (Boyle, 1999). Cuttlefish respond to disturbance by squirting ink. This is composed of melanin, mucus and tryosinases (Prota *et al.*, 1981), which may all cause stress to a cephalopod that is kept in a confined space and limited volume of water. The well-being of captive animals was considered uppermost throughout this entire investigation.

TRANSPORT OF LIVE SPECIMENS

Only adult specimens were used in this investigation as iridophore and leucophore cells are not fully developed in juveniles under the age of 20 weeks (mantle length 45 mm; Hanlon and Messenger, 1988).

Specimens were caught in the Solent and transported from either Portsmouth or Poole harbour during the late spring to early autumn. In the winter, aquarium reared specimens were collected from the Marine Biology Association, Plymouth.

All specimens were transported in heavy-duty polyethylene bags (120 x 60 cm) containing fresh sea water. The bags were additionally covered with a black bin-bag, and each placed in plastic crates to ease lifting. The cuttlefish were transferred into the innermost bags using a bucket, so as not to expose them to air. Two extra containers (25 L) of fresh sea water were also collected per trip, and these were used

to initially fill the aquarium at Bath. Eleven specimens in total were transported by car, at a comfortable temperature, with no fatalities or inking.

On one occasion, due to a low number of aquarium specimens, a cuttlefish was dissected and post-fixed (table 3, page 17) at Plymouth, before transportation on ice (students at Plymouth then used the remains).

Care Of Live Specimens And Aquarium Conditions

Specimens were allowed to recuperate for a minimum of 1 day after transport. The size, and number of specimens determined housing in either a 68 litre or 40 litre plastic aquarium. These were partially filled with fresh sea water from the area of capture and topped-up with synthetic sea water (Tropical Marin, Aquarientechnik). The water was circulated through separate filters (Eheim) containing foam and activated charcoal, at a rate of 840 L/h. Each aquarium was illuminated for 9 hours per day (artificial light), maintained at room temperature ($\approx 17^{o}C$), and fitted with two stones with separate air supplies. All specimens were fed on earthworms and defrosted fish. Earthworms are an unusual, and undocumented diet. Interestingly, the cuttlefish used the luring mode of hunting when feeding on earthworms.

Cuttlefish do not digest prey externally, however they do immobilise it with a toxin (Messenger, 1968). Food and other debris were therefore removed after feeding to contain the toxin and to discourage bacterial growth. Half of the water in the aquarium was replaced with synthetic sea water every ten days.

As there is not an established aquarium at Bath University, specimens were housed for the shortest time possible.

ANAESTHESIA

Two anaesthetics were initially tested in accordance with the Universities Federation of Animal Welfare handbook (Boyle, 1999). These were 7.5% magnesium chloride ($MgCl_2$: $6H_2O$ in distilled water) and 2.5% ethanol (in sea water). Magnesium chloride is a conventional anaesthetic for marine invertebrates, and induces minimal trauma in *Sepia* (Messenger *et al.*, 1985; O'Dor and Shadwick, 1989). It has a lower osmolarity (1210 mOsmol/kg) than ethanol (1431 mOsmol/kg), and should therefore be better suited to the cuttlefish's own osmolarity (1120 mOsmol/kg)[3]. In preliminary tests, ethanol acted far quicker, inducing terminal anaesthesia[4] in 6-10 minutes (Mantle Length 145 – 280 mm). Magnesium chloride required 20 minutes to kill a female cuttlefish of mantle length 160 mm. Examination of the dermal fin tissue subsequent to magnesium chloride anaesthesia, also displayed gross dermal cell damage. No detrimental effects were found with ethanol; its use is also recommended by the Marine Biology Association (MBA), Plymouth (R. Williamson, pers. comm.). Cephalopods will recover from weak ethanol (Packard, 1995; Loi and Tublitz, 1997), and magnesium chloride anaesthetic (Messenger *et al.*, 1985). However, this was not performed during this investigation.

ANAESTHETISING PROCEDURE

Animals were caught in the aquarium and transferred underwater into calibrated buckets. Ethanol was then gently poured into the bucket, and the appearance, behaviour, and respiratory movements of the specimen observed. Respiratory movements cease after 3-6 minutes (depending on specimen size), and a further 3 minutes allowed for terminal anaesthesia. The animal was then decapitated

[3] Average osmotic concentration (mOsmol/kg): Plasma 1160, whole muscle 1103, and muscle cells 1098 (Robertson, 1965).
[4] Terminal anaesthesia is defined here as three minutes after respiratory movements cease.

under the anaesthetic solution using a sharp scalpel placed between the cranium and nuchal cartilage (Tompsett, 1939), before severing the optic lobes and peripheral nerves (Boyle, 1999).

PREPARATION OF THE INTEGUMENT

Pieces of the integument were excised in the anaesthetic solution with a scalpel blade or scissors, before transferring it underwater into plastic Petri dishes containing dental wax. Each dish was twice flooded with artificial sea water (ASW, table 1), to remove the anaesthetic solution, and the integument was pinned out. Accurate pinning of the tissue to its original size was considered important, as disproportional stretching may have induced false optical effects.

Artificial Sea Water (ASW)	**Synthetic Sea Water** (used in aquarium only)
500 mM NaCl 10 mM KCl 12 mM $MgCl_2$ ($6H_20$) 10 mM $CaCl_2$ ($2H_20$) 4mM HEPES buffer pH 7.4 Osmolarity 1000 mOsmol/kg	Tropical Marin (Aquarientechnik) Made with freshly distilled water pH 7.4 Osmolarity 1000 mOsmol/kg

Table 1 Composition of artificial sea water, and the synthetic sea water that was used only in the aquarium.

Light Microscope Slide Preparations		
	Whole Mount	**Strewn Sections**
Fixative*	Overnight 4°C	70 mins at R.T.
Buffered Wash*	20 mins.× 3 changes	6 mins.× 3 changes
Haematoxylin Stain	>10 mins. (examine in microscope)	5 mins.
Tap water Wash (Blueing)	5 mins.	5 mins.
1% Eosin (aqueous)	5 mins.	5 mins.
Dehydration Ethanol 70%, 80%, 95%, absolute x 2	10 mins.	1 mins.
Xylene	10 mins.x 2 changes (examine in microscope)	2 mins.x 2 changes
Mount in DPX	Leave for 2 days and allow to dry	

Table 2 The procedures for preparing light microscope slide.(* Composition, table 3 page 17).

Chemical Fixation Of The Integument For Light Microscopy

Whole and strewn (serial) integument mounts were prepared for light microscope examination (table 2) by pinning the tissue and immersing it in fixative solution. Whole tissue mounts were fixed overnight in a refrigerator. Smaller strewn sections were prepared by first fixing the tissue briefly for 10 minutes at room temperature. This short exposure was to harden the tissue slightly, making it easier to cut thin transverse and longitudinal sections with a high-grade razor blade (Gillette series 5). The fixative was then replenished and left for a further 60 minutes at room temperature.

All preparations were rinsed in buffered wash (tables 2 and 3), and either stained in haematoxylin and eosin, or left unstained, before dehydrating with ethanol and mounting in DPX (distyrene plasticizer and xylene) resin.

Chemical Fixation Of The Integument For Electron Microscopy

Prior to pinning the integument in ASW, the underlying connective tissue and muscle was trimmed with fine scissors as to aid the perfusion of fixatives, in particular the much slower penetrating glutaraldehyde. The skin was not peeled from the muscle as this often damages the tissue. The pinned tissue was then flooded with a primary fixative solution and left for 10 minutes at room temperature. Orientated tissue sections were then cut with freshly broken razor blades (Gillette, series 5) and pipetted into vials containing primary fixative. Once enough sections had been cut, the fixative in the vials was replenished, and all were placed in the refrigerator for 50 minutes. Lowering the temperature of primary fixation is thought to reduce considerably the degree of lipid leaching (Glauert and Lewis, 1998), as lipids are not

ASW (pH 7.4, 4°C), and post-fixed in 2% osmium tetroxide for 1 hour at room temperature. This process fixes and stains lipids. The material was again washed, before tertiary fixation in 1% uranyl acetate for 45 minutes at room temperature. Finally the sections were washed, dehydrated in acetone and immersing in propylene oxide prior to embedding in TAAB hard epoxy resin.

The primary fixative consisted of 1% paraformaldehyde, 2% glutaraldehyde and 0.1M sodium cacodylate buffer, in 50% ASW, pH 7.4 (1228 mOsmol/kg)[5]. A tertiary fixative of 1% uranyl acetate was used as it has been shown to stabilize phospholipid membranes and stain the tissue. This step is almost standard protocol in fixation procedures, and is highly recommend by Glauert and Lewis (1998).

The embedding medium used is not miscible with water, and it is therefore necessary to dehydrate before substituting with propylene oxide. However, dehydration extracts lipids causing the tissue to shrink. Ideally, this should be avoided in order to preserve the optical dimensions of this tissue. It is for this reason that the primary fixative was refrigerated, and 2% rather than 1% osmium tetroxide was used. Acetone was also used instead of ethanol, as it has a lower viscosity, thus penetrates faster and reduces the dehydration time. Using uranyl acetate as a fixative has also been shown to reduce shrinkage to below 4% (Boyde *et al.*, 1997), whilst the presence of calcium in the primary fixative (present in ASW) is also thought to reduce lipid loss (Robards and Sleytr, 1985; D. Knight pers. comm.). To assess shrinkage, measurements of white fin spots were taken during the first 10 minutes of primary fixation, and again after embedding in epoxy resin.

[5] The pH used was determined from Howell and Gilbert's (1976) work on cephalopod haemolymph.

Protocol:	Time:
Anaesthesia Live specimen in known volume of ASW ⇓ 2.5% Ethanol (in ASW) Euthanasia ⇓ Decapitate and pith ⇓ Excise and trim integument	Observe respiratory movements cease (3-6 minutes) + 3 minutes.
Primary fixative solution 1% paraformaldehyde dissolved in ASW (heated to 60°C, 1 drop of 1M NaOH), 2% glutaraldehyde, and 0.1% sodium cacodylate buffer pH 7.4. 1228 msOsmol/kg	10 minutes at RT. (cut orientated sections ≈ 6 minutes) ⇓ 50 minutes at 4°C
Wash ASW and 0.1% sodium cacodylate buffer pH 7.4.	2 × 5 minutes (chilled 4°C)
Post-fixative solution 1 % Osmium tetroxide in sodium cacodylate buffer pH 7.4.	60 minutes
Wash ASW and 0.1% sodium cacodylate buffer pH 7.4.	2 × 5 minutes
Tertiary Fixative 1 % Uranyl acetate in sodium cacodylate buffer pH 7.4.	60 minutes
Dehydration 30%, 50%, 70%, 90% acetone ⇓ 95% acetone ⇓ Absolute (dry) acetone	8 minutes ⇓ 2 × 8 minutes ⇓ 2 × 8 minutes
Embedding Propylene oxide ⇓ 50:50 Propylene oxide:Resin ⇓ TAAB hard resin ⇓ Embed in fresh resin and polymerise at 60°C	30 minutes ⇓ Overnight ⇓ 6 hours ⇓ 20-24 hours

Table 3 Chemical fixation procedure.

EFFECTS OF THE NEUROTRANSMITTER ACETYLCHOLINE (ACh)

Preliminary Observations

Pieces of freshly excised fin were cut into 2 cm square sections (squares with one corner missing) whilst immersed in the anaesthetic solution. These sections contained a number of bright white fin spots. The material was then transferred underwater into one of seven Petri dishes containing wax, and twice flushed with ASW. Each section was accurately pinned out, and a small gap was left beneath them to allow the passage of liquid. The sections were then arranged so that each was in an identical orientation and was positioned along a horizontal line inside a fume cupboard. The dishes were illuminated with a fixed fluorescent light, and viewed at a constant distance and angle of approximately 45°. Any iridescent colours were recorded. The ASW was then pipetted from the dishes and replaced with 5 ml of experimental solution. The colour was again observed (time zero) and at subsequent one minute intervals.

The following experimental solutions were used: ASW, and 1×10^{-8}M (A), 5×10^{-8}M (B), 1×10^{-7}M (C), 5×10^{-7}M (D), 1×10^{-6}M (E), and 5×10^{-8}M (F) ACh concentrations. After 15 minutes all of the experimental solutions were removed, and the tissue was twice flushed with ASW. Observations then continued at one minute intervals with the tissue immersed in 5 ml of ASW (based on an experiment conducted by Hanlon, 1982; Hanlon *et al.*, 1990). ASW was flushed fresh every 5 minutes.

ACh effects on ultrastructure

The above experiment was repeated using thinner tissue sections. Freshly excised squares of tissue were trimmed to remove excess connective tissue and

experimental solutions: ASW, 1×10^{-7}M (G), 2.5×10^{-7}M (H), 5×10^{-7}M (I), 7.5×10^{-7}M (J), and 1×10^{-6}M (K) ACh concentration for 8-15 minutes. Four smaller orientated tissue blocks were then cut per experimental solution. Three of these were immediately frozen (discussed below), and the remaining one fixed chemically (table 3).

CRYOFIXATION

The effects of ACh on the tissue may be masked or eliminated by the time period and processing normally required for chemical fixation.

Cryogenic fixation entails freezing biological tissue within fractions of a second. It has many distinct advantages over chemical fixation as its does not extract anything but heat, and avoids cross-linking and denaturation. Rapid freezing is required to retard ice crystal formation, by quickly increasing the rate of cooling to temperatures below -80°C (193K) at which ice crystal growth is very slow. This extremely fast initial step is ideal for arresting cells when they may be undergoing a physical change (Robards and Wilson, 1993). Cryoprotectants can also be used to retard ice crystal formation, but they have not been used in this investigation due to their extremely high osmolarity.

Contact freezing[6] was used to initially freeze the tissue. This is the preferred method for tissue sections, slices or cell suspensions and entails pressing the tissue against a polished gold-coated copper block that is cooled with liquid nitrogen (-209°C). Once frozen, the tissue is fixed. However, we wish to examine the tissue at room temperature, and in an electron beam. Water within the tissue must therefore be substituted with an organic solvent. This second step is known as freeze substitution

[6] Also termed slam-, metal mirror-, cryoblock-, and impact-freezing.

and prevents secondary recrystallisation as the specimen is elevated to room temperature prior to embedding.

[6]Also termed slam-, metal mirror-, cryoblock-, and impact-freezing.

Cryofixation Method

Bathed tissue was pipetted from the experimental solutions and placed onto a pad (Leica accessories) consisting of a sponge attached to a steel plate. This acts as a shock-absorbent surface. A square piece of Sellotape, and two stacked adhesive plastic rings were fixed in the centre of each pad. These provided a non-porous surface, which would support the specimen in a drop of solution, whilst the plastic 'hole-punch' rings prevent excessive compression (standard laboratory procedure). Each plate was magnetically attached to the stamping arm of a Leica Reichert (MM80 E) impact freezer. Specimens were then slam-froze against the cryoblock with a predetermined control setting of: force 5, speed 6 and thickness 4. The impact force was maintained for 10 seconds, before the stamping arm was lifted, leaving the steel plate and tissue under liquid nitrogen vapour. The specimen was removed from the pad with pre-cooled ceramic forceps, and placed in pre-cooled aluminium vessels containing liquid nitrogen. These vessels were then transferred to a cryogenic freezer that contained cold solvents.

Freeze-substitution Method

In the cryogenic freezer, using cold forceps, each specimen was transferred into labelled vials containing dried acetone and left overnight. A 3% solution of osmium tetroxide was prepared from osmium tetroxide crystals dissolved in cold

dried acetone, before placing it in the freezer to cool overnight[7]. The following morning (~15 h), acetone was replenished twice, before substituting with 3% osmium for 24 hours. The freezer was then switched off. At 273 K osmium was replaced with dry acetone and the specimens washed twice, before placing it in 1 % uranyl acetate in acetone, for 60 minutes. The specimens were finally washed in acetone (two changes 5 minutes each), and embedded in TAAB hard epoxy resin (table 4; procedure based on Maunsbach and Aflzelius, 1999).

Specimen Sectioning

When necessary, embedded tissue sections were re-oriented on blank resin blocks using refrigerated TAAB hard resin, and cured (60°C) prior to sectioning. Thin sections (1μm) were cut using glass knives (LKB cutter) in a Riechert-Jung Ultracut E microtome, and stained with toludine blue. Ultra-thin sections of gold and silver standard (50-60 nm) were cut with a diamond knife (Diatome, Ultra 45°). Ultra-thin sections were collected on a variety of coated (1% Pioloform in chloroform) grids and stained as follows. The grids were immersed in freshly filtered uranyl acetate for 15 minutes in the dark, then washed in freshly distilled water and blot-dried. The grids were then stained in filtered lead citrate for 5 minutes in the presence of sodium hydroxide pellets, before finally washing and blot drying. Sections were examined in a transmission electron microscope (Jeol JEM1220, calibrated regularly).

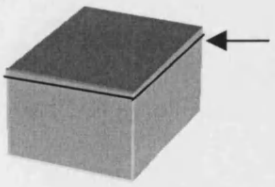

Planar

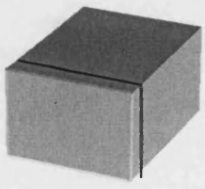

Transverse

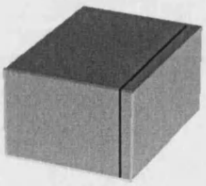

Longitudinal

[7] Osmium tetroxide rapidly reduces in acetone unless mixed cold, and chilled immediately. It also gives off harmful fumes, even at cryogenic temperatures, which penetrate plastic vial lids. All material was therefore placed inside a sealed metal container inside the freezer unit. This is standard procedure within the laboratory.

Protocol:	Time:
Anaesthesia Live specimen in known volume of ASW ⇓ 2.5% Ethanol (in ASW) Euthanasia ⇓ Decapitate and pith ⇓ Excise and trim integument	Observe respiratory movements cease (3-6 minutes) + 3 minutes.
Bathe Tissue ASW or ACh (1×10^{-7}M, 2.5×10^{-7}M, 5×10^{-7}M, 7.5×10^{-7}M, and 1×10^{-6}M)	8 -15 minutes at RT. (cut orientated sections)
Cryofixation Impact Freeze ⇓ Immerse in liquid nitrogen	Immediately after excision ⇓ Transfer under liquid nitrogen vapour
Freeze Substitution Dry Acetone (-90°C)	Overnight (>12 hrs, plus 3 changes), -90°C
Fixative 3% OsO_4 in dry acetone (-90°C)	24 hours, -90°C (then turn off freezer)
Wash at 273 K Dry Acetone (0°C)	2 × 5 minutes
Fixative 1% Uranyl acetate in dry acetone (same temperature as freezer) ⇓ 95% acetone ⇓ Absolute (dry) acetone	60 minutes, 0°C – RT ⇓ 2 × 8 minutes ⇓ 2 × 8 minutes
Wash Dry Acetone ⇓ Propylene oxide	2 × 5 minutes ⇓ 30 minutes
Embedding 50:50 Propylene oxide:Resin ⇓ TAAB hard resin ⇓ Embed in fresh resin and polymerise at 60°C	Overnight ⇓ 6 hours ⇓ 20-24 hours

Table 4 Cryofixation and freeze substitution of ACh treated tissue.

OSMOLARITY

Osmolarity was measured and not calculated, using calibrated freeze-point depression (CamLab equipment).

STEREOLOGY

Sectioned microstructures were measured automatically using image analysis software (Optimas v.6.1, Optimas UK Ltd., West Malling, Kent). Electron micrographs were first digitised using a flat bed scanner and calibrated using the above software. Adjusting the threshold value then sharpened the images. This eliminated many of the small sub-nanometer particles, making the microstructures more prominent. The image was then converted to back and white, before double-checking the calibration. Computed values were also validated against manual measurements. Adjusting the threshold value of each image did not affect the measured values.

The size and distribution of microstructures were also measured manually. Several lines were drawn through the mid-region of each cell, and the size of intersected microstructures measured. The space between each intersected microstructure was also measured (based on Cooper, *et al.*, 1990).

Strewn ultra-thin sections were used to determine the overall size of sectioned microstructures. Micrographs of each ultra-thin section were placed in series, so that an estimate of element size could be made. This is known as a directional counting rule, or dissector principle (Sterio, 1984; see also Howard and Reed, 1998).

The distribution of white fin spots, and organelles within iridophore and leucophore cells was analysed using Clark and Evans (1954) nearest-neighbour method (previously used by Hanlon and Messenger, 1988, to measure chromatophore

distribution). The equation for this method is given in the appendix, page 214.

POLARISATION

Both fixed tissue, and fresh un-fixed un-stained tissue were examined using a Wild polarised light microscope. Each section was examined in both transmission and epi-illumination (separate cold lamp and polarising light filter). The polariser and analyser were set at maximum extinction and the stage rotated 360° to determine if the bright white patches are birefringent (results negative).

Part 3 – Light Reflecting Cells

Introduction To White Skin Components

Two white areas of differing intensity are apparent in the dermis of octopus and cuttlefish. These are located below the chromatophore organs, and are collectively termed the white or light chromatic components (Packard and Sanders, 1971; Hanlon and Messenger, 1988; 1996). The lower intensity of white (a paler creamier white colour) is formed by connective tissues and muscle found deep in the dermis and is widespread throughout the tissue (however, it is notably absent from the translucent fin). Regions of a higher intensity of white, or bright white are also found within the dermis. These bright white areas are located directly beneath the chromatophore organs and above the much deeper underlying pale white muscle. It is the bright white areas that constitute the dermal light-reflecting layer, or iridocyte layer (Packard and Hochberg, 1977), and consists of light reflecting iridophore cells and light scattering leucophore cells. The iridophore cells provide a structural colour, and give the bright white areas a pale iridescent green appearance. They are not however responsible for the bright white appearance. This is instead due to the leucophore cells. The ultrastructural and optical properties of the bright white areas are to be investigated.

The distribution of bright white areas changes considerably during the development of a cuttlefish (Hanlon and Messenger, 1988), and it is for this reason that juvenile specimens were not used. In adult *S. officinalis* a range of intense white areas can be seen, and these differ greatly in size. The largest and most conspicuous are the bright white 'zebra-bands', which are displayed on the dorsal sides of the mantle (fig. 6a), and on the tentacles. Progressively smaller white patches are located at the fin-end of each of these white bands. The fin itself contains even smaller bright

white spots, which are evenly distributed throughout it. A bright white line also borders the fin edge in adult males (fig. 6b).

The retractable nature of the overlying chromatophore organs, combined with their high density (Hanlon and Messenger, 1988) ensures that both the pale and bright white regions of the tissue can be obscured (fig. 7). Retracted chromatophore organs expose both of the white areas to incident light, whilst opened chromatophores shadow the white regions. The chromatophore organs therefore indirectly control the illumination of both of the white areas. This permits the formation of contrasting body patterns, and is also used to vary the overall brightness of the tissue (fig. 8).

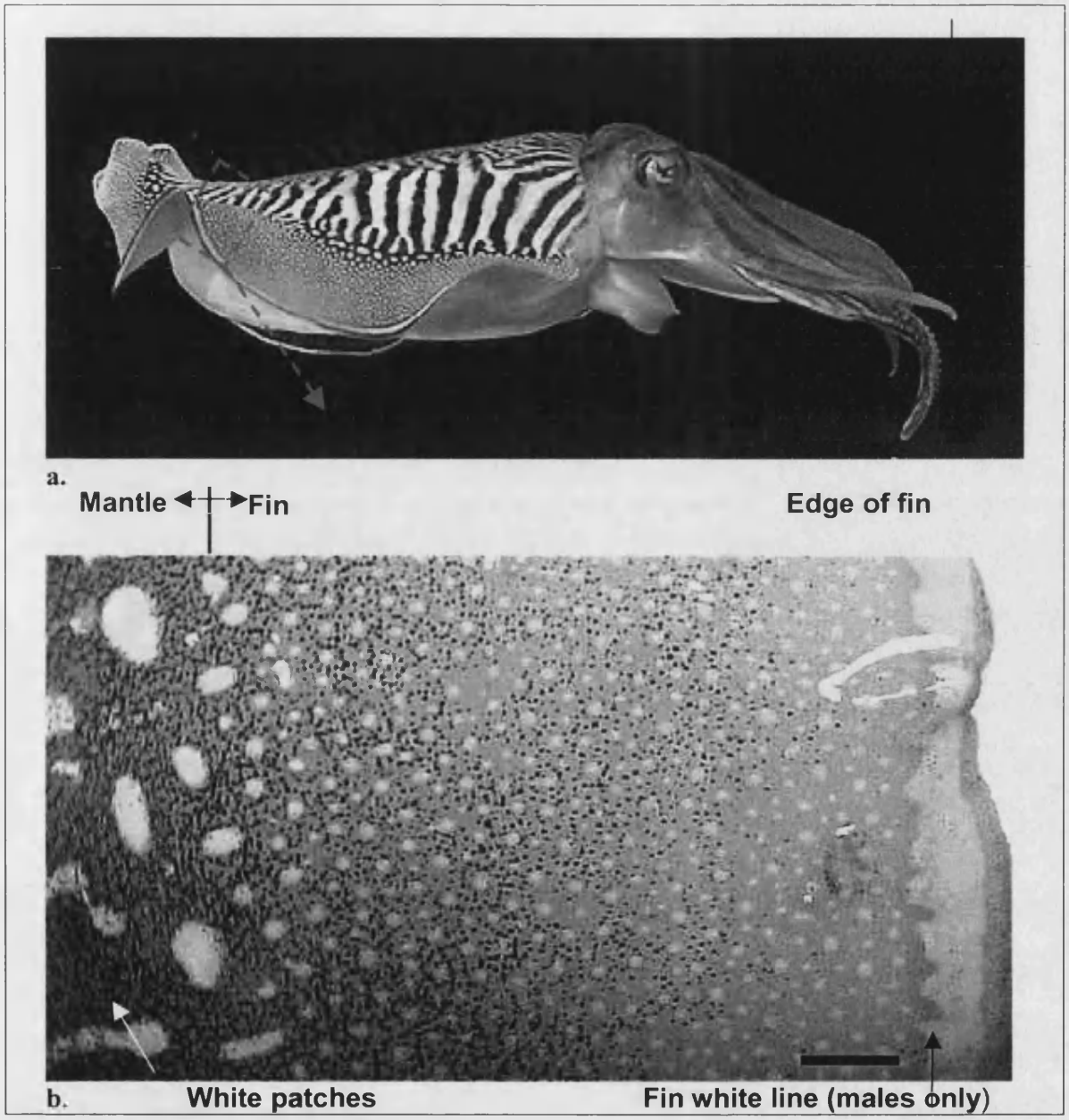

Fig. 6 Intense bright white regions in adult *S. officinalis* ♂.

a. Bright white 'zebra bands' are displayed on the dorsal mantle. Each of these bands is graded to progressively smaller white patches, and eventually to small white fin spots. (Image from CephBase).

b. The transition from bright white patches to much smaller bright white spots, occurs on the boundary between the mantle and the translucent fin. A white fin line is also apparent along the edge of the fin in adult male cuttlefish. Scale bar = 5 mm.

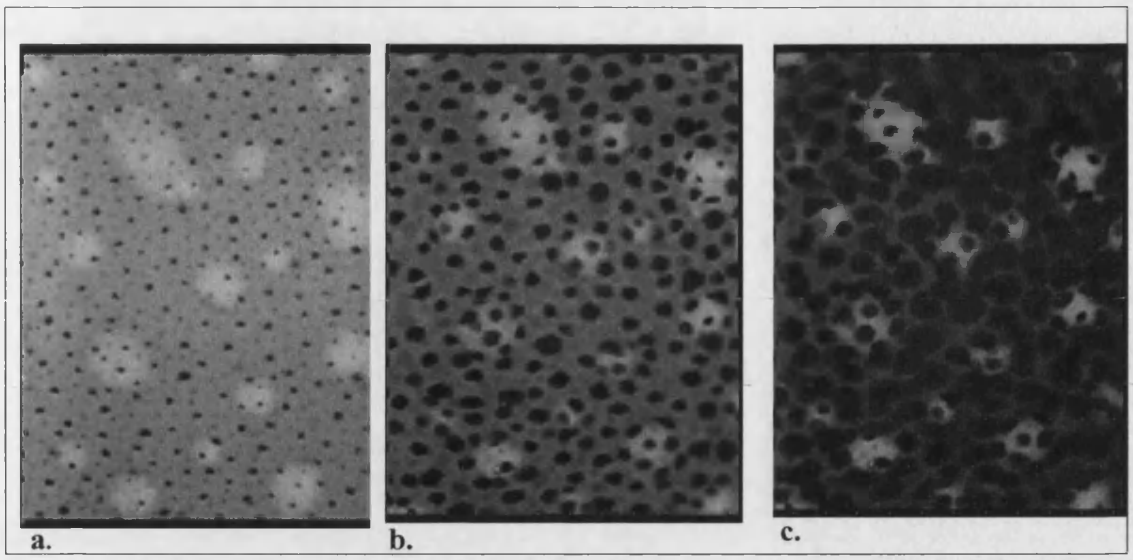

Fig. 7 The contractile chromatophore organs are located above both the pale and bright white areas of the tissue. The chromatophores indirectly control the amount of incident light upon the white regions.
a Retracted chromatophores expose both of the white areas to incident light.
b Partially expanded chromatophores reduce the amount of light incident on the tissue below, which dramatically darkens the white connective tissue areas.
c Fully opened chromatophores virtually conceal all of the white areas.
(Images from BBC, 1983 – permission granted for thesis)

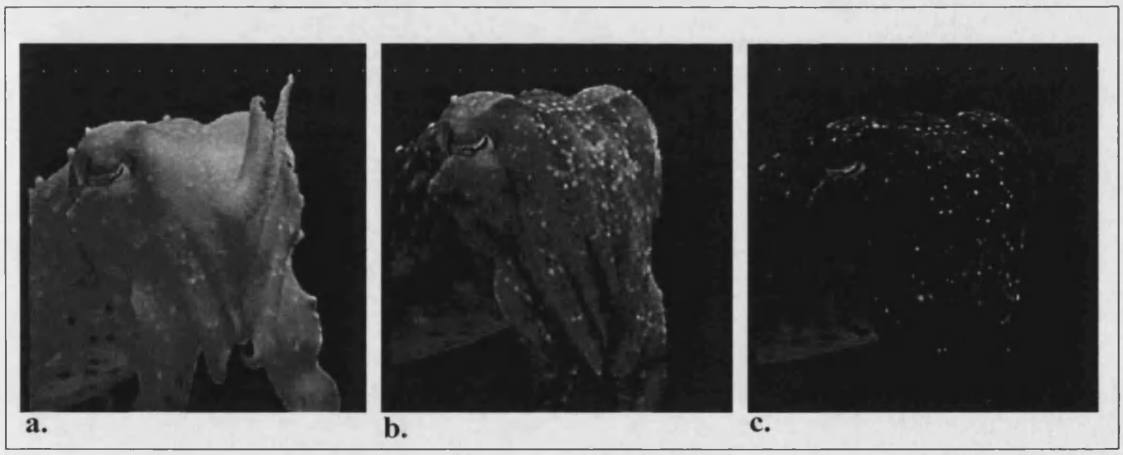

Fig. 8 Cuttlefish control their overall luminance.
a When all of the chromatophores organs are retracted the cuttlefish appears white and conspicuous
b. Partially opening the chromatophore organs reduces the intensity of white and significantly darkens the skin. The cuttlefish is less conspicuous.
c Fully opening the chromatophore organs conceals most of the white areas and dramatically darkens the overall appearance of the tissue. In this instance the cuttlefish matches the surrounding luminance.
(Images from BBC, 1983 – permission granted for thesis)

RESULTS: WHITE SKIN COMPONENTS

Sections of the fin, mantle and head were examined at various viewing angles in both natural and artificial light. Similar observations were also made *in vivo*. All of the bright white regions examined displayed a pale iridescent green sheen, that was not angle dependent. This colour was of a low intensity and appeared relatively faint against the brighter white areas. It also did not appear to alter between the bright white regions, and was of a perceivably constant intensity. This intensity of green iridescence appeared the same in each specimen within the aquarium. Intensity did however appear to fluctuate immediately after transport of the animals. A more intense green iridescence was noted on several occasions after transport from the sea. Unfortunately, this intensity could not be invoked again in the aquarium. Previous authors have also noted a brighter iridescence in squid immediately after wild capture (Cooper *et al.*, 1990).

Light microscope examination of the bright white areas (unstained) reveals little information about the light reflecting cells. This is because they cannot be resolved sufficiently, since the cells are naturally colourless and do not contain pigment granules (figs. 9-10). The regions appear bright chalk-white under epi-illumination, and dark cream in transmitted light. This phenomenon has been noted in octopus (Packard and Sanders, 1971; Brocco, 1976). Stained tissue sections confirm that the bright white regions are composed of an aggregation of light reflecting cells (figs. 11-12), which possess nanometer scale structures that are beyond the resolving power of a light microscope.

Each of the bright white areas is typically 4-10μm below the chromatophore organ layer, and is located within the connective tissue matrix above the pale white underlying muscle (fig. 11). The bright white regions extend through the depth of this

connective tissue and are typically 150-200 μm in depth. Iridophore and leucophore cells are found throughout this depth, and are arranged in no particular order (fig. 13).

Attention was paid to the white fin spots since their location and size is ideal for excision and ultrastructural examination. The white fin spots are lenticular in shape and have a mean diameter of 0.66 (±0.02) mm, and depth of 0.17 (±0.02) mm (mantle length = 13.8-19.5 cm). They are almost uniformly distributed throughout the transparent fin, and having a nearest-neighbour value (R) of 1.71, where 1.00 is random and 2.15 perfectly uniform (see appendix, page 214).

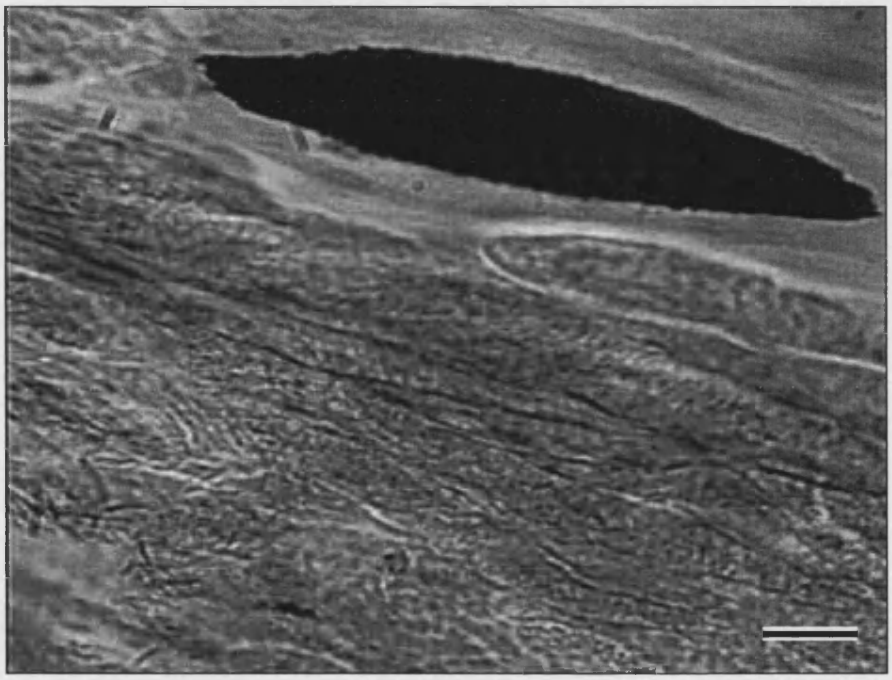

Fig. 9 This is an unstained cross-section through a chromatophore organ (dark black oval) and white patch that has been viewed using phase contrast. It is a strewn hand cut section and is slightly oblique, which clearly shows a partially contracted chromatophore organ above an indistinct layer of cells. It is these underlying cells that constitute the bright white area. Scale bar = 2 μm

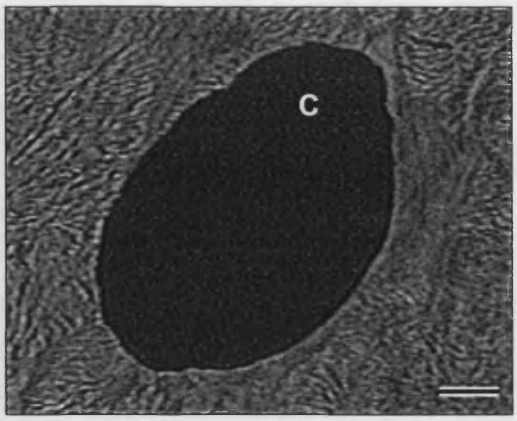

Fig. 10 Plan view of an unstained bright white fin spot and chromatophore organ, that is viewed using phase contrast. A partially retracted chromatophore organ (C) is positioned directly above a bright white fin spot (all of background). Insufficient contrast means that the naturally colourless light reflecting cells cannot be resolved. Scale bar = 2 μm.

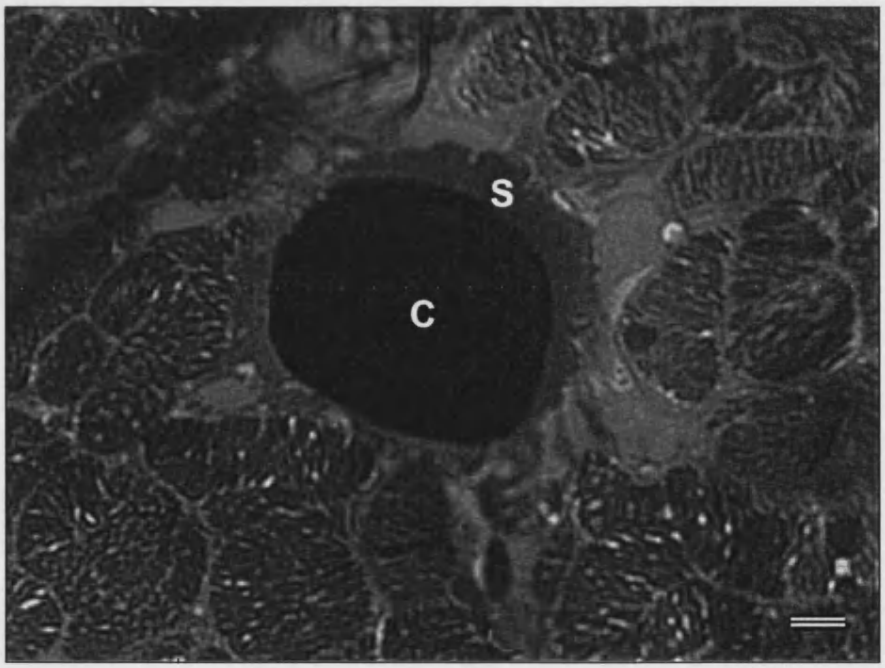

Fig. 11 Plan view of a bright white fin spot and chromatophore organ. This thin section has been stained with toludine blue and is viewed using normal brightfield illumination. The retracted chromatophore organ (C) and its folded elastic sacculus (S) can be seen directly above the light reflecting cells of the bright white fin spot (all of background). Scale bar = 2 μm.

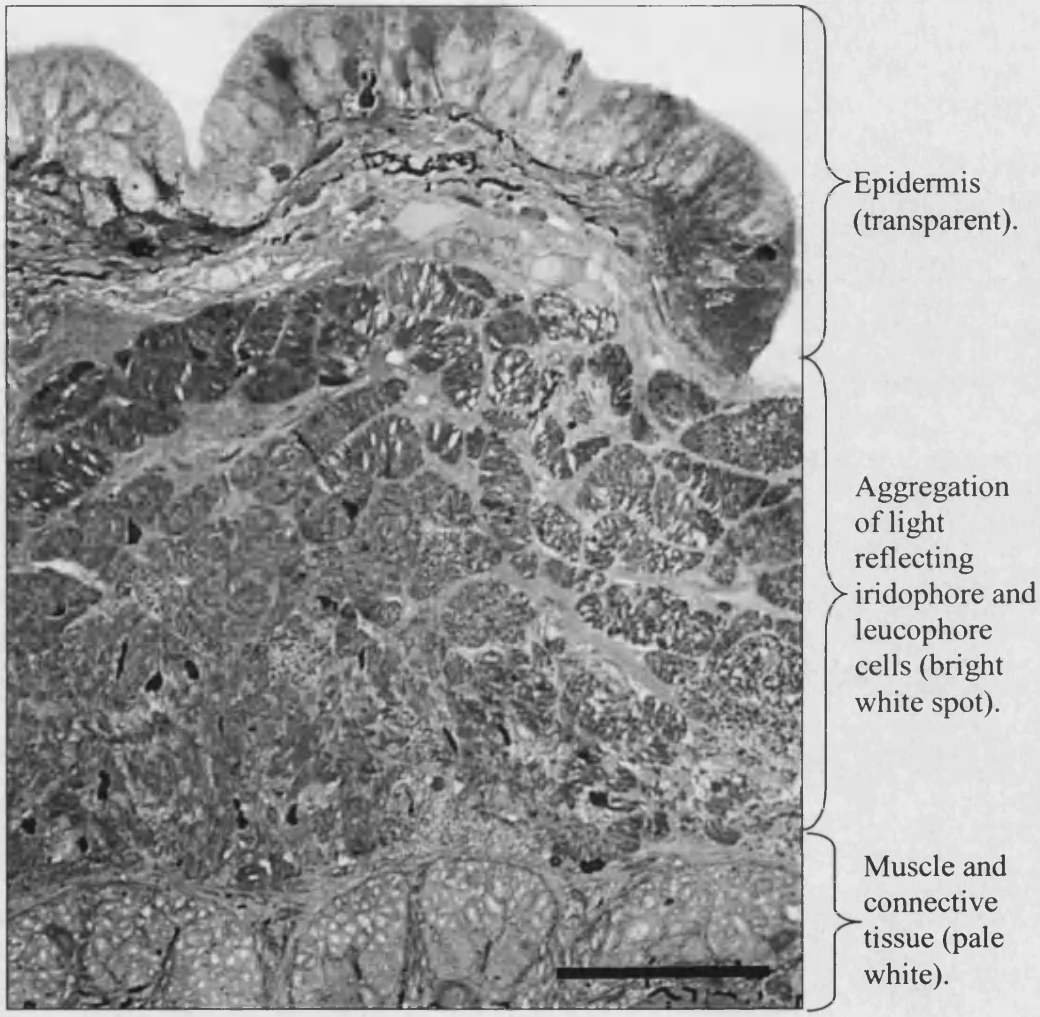

Fig. 12 A cross-section through the centre of a bright white fin spot that has been stained with haematoxylin and eosin. Scale bar = 50 μm.

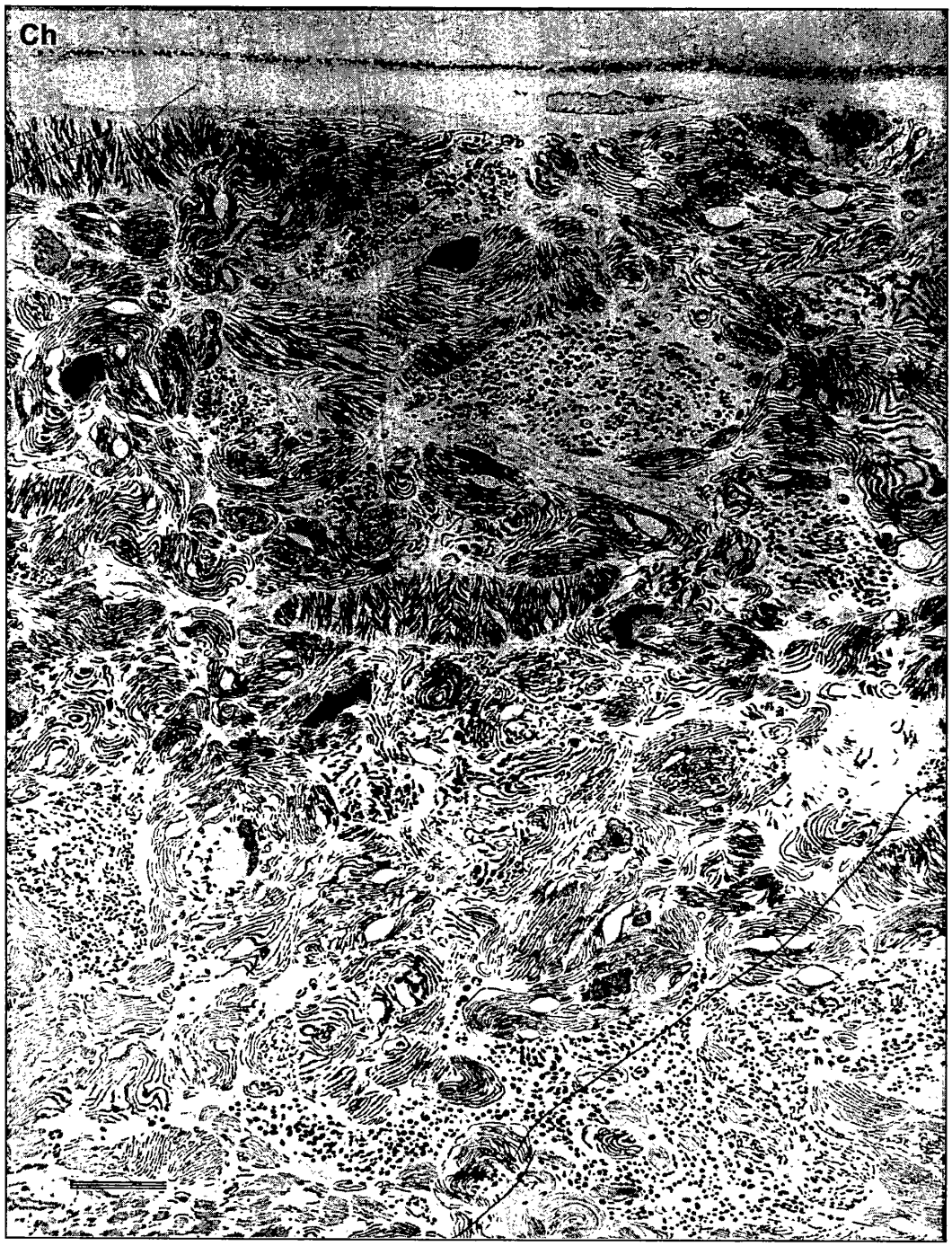

Fig. 13 Ultra-thin (approx. 60 nm) cross-section through a chromatophore organ (Ch) and white fin spot. A high density of iridophore and leucophore cells is found in the bright white spot directly beneath this open chromatophore organ. Note the orientation of these cells with respect to the chromatophore organ, and also the distribution of iridophore and leucophore cells. Scale Bar = 10 μm

DISCUSSION: BRIGHT WHITE SKIN COMPONENTS

The brighter white regions in the mantle, head and fins of *S. officinalis* display only a pale iridescent green colour. This is unlike the iridescence seen in squid. Although squid generally lack leucophores, they do possess iridophores and the iridescent colour produced by these cells varies greatly as viewing angle and incident light angles are changed (Cooper *et al.*, 1990; Mäthger and Denton, 2001). The maintenance of one iridescent colour by *S. officinalis* is therefore intriguing, particularly if we wish to later utilise structural colours within a camouflaging material.

Given that iridescent green is seen at the surface of the tissue, it is not surprising that in transmitted light the bright white regions appear dark cream. Green light is reflected by the bright white patches, and is therefore absent from transmitted light. If we extract short wavelength blue light from white, it will appear yellow, and similarly extracting green will produce brown. It is therefore conceivable that reflecting pale green wavelengths will result in a yellow-brown (dark cream) colour being transmitted.

Particular attention was paid to the bright white fin spots as it is these regions that I consider will be the basis for a biomimetic camouflage netting. This is because the fin has an additional role, which is similar to that fulfilled by current military netting. The fin is used not only in low speed swimming and hovering, but also during ventral adhesion to hard substrates (Boletzky and Roeleveld, 2000), as well as burying into softer substrates. When settled on the bottom the fin is spread out to conceal shadows cast by the mantle; butterflies and moths demonstrate the same behaviour. Since the fin is transparent it also provides a region of integration, where the underlying background can merge with the chromatophore organs and bright white

spots, which are both used to camouflage. It is for these reasons that a camouflage net is skirted around a vehicle, and also why netting (transparent) is used instead of a continuous sheet of camouflaged canvas.

Introduction To Dermal Iridophore Cells

Dermal iridophore cells[8] are responsible for the iridescent structural colours found in cuttlefish, octopus and squid. They are found alongside leucophore cells within the intense white areas of octopus and cuttlefish, and also independently throughout the integument. Iridophore cells are also found in the ink sac (Müller, 1853) and eyes of many cephalopod species, as well as the light organs (photophores) of deep-sea cephalopods (Young, 1977; Herring, 2002).

Iridosomal Platelets and Cytoplasmic Spaces

The most conspicuous feature of an iridophore cell is the regular distribution of intracellular discs. These are termed iridosomal platelets (Arnold, 1967), or reflecting lamellae (Kawaguti and Ohgishi, 1962), and are composed of a material of high refractive index. Each of the platelets is arranged with its broad surface parallel to another and is surrounded by a cytoplasm of much lower refractive index. The iridophores therefore contains alternating layers of high and low refractive indices. The cytoplasmic space between each platelet is termed the intrairidosomal space (Brocco, 1976). These spaces are considered to be extracellular in squid and octopus iridophore cells. This hypothesis was first proposed by Arnold (1967) after examining iridosomal platelets from the eye of *Loligo pealii*, and it has since been confirmed in the dermal iridophores of *L. opalescens* (Brocco and Cloney, 1980) and *Octopus dofleini* (Brocco, 1976). A plasma membrane, in the form of a cytoplasmic channel, retains the platelets within the cell. These channels also contain intracellular cytoplasm. It is therefore hypothesised that in their entirety, the platelets are trilaminar structures, consisting of a central high refractive index platelet, a thin covering of

[8] Iridophore cells have also been referred to as iridiophores, iridocytes, reflecting cells, guanophores and brilliant cells. They are also known as reflector cells in octopus (discussed in main text).

intracellular cytoplasm, and a plasma membrane (Brocco, 1976; Brocco and Cloney, 1980).

The ultrastructure of iridophore cells (and leucophore cells) in *Sepia*, has not been studied to the same degree as in other cephalopod genera. Only one substantial study contains micrographs of dermal iridophore cell (no leucophores) from *S. esculenta* (Kawaguti and Ohgishi, 1962). Three separate micrographs of iridophore cells are published for *S. officinalis*: A bright white area (Hanlon and Messenger, 1988); isolated iridophore cells (Shashar *et al.*, 1996); and iridophore cells found on the ventral side of the mantle (Budelmann *et al.*, 1997).

Refractive Index

The refractive index (n) of the iridosomal platelets found in the eyelids of *L. forbesi* and *S. elegans* is 1.56 (interference microscopy) (Denton and Land, 1971). Similar values of 1.506 (interference microscopy) and 1.554 (refractometer) have also been recorded in the iris and dermis of *O. dofleini* (Brocco, 1976). The refractive index of the intrairidosomal space is generally considered to be 1.33 (interference microscopy) (Land, 1972). A slightly higher value of between 1.339-1.351 was recorded by Brocco (1976), which is comparable with the value generally recorded for the cytoplasm of most living cells (n = 1.353 Sanderson, 1994).

Iridosomal Platelet Composition

The content of the platelets is uncertain. It was first described as guanine (Fox, 1953; Arnold, 1967) before being dismissed by Denton and Land, (1971; Land, 1972) who described it as chitin; most recently in *L. vulgaris* and *Alloteuthis subulata* (Mäthger and Denton, 2001). However, neither chitin nor guanine has been found in the iris or dermal iridophore cells of *O. dofleini* or *L. opalescens* (Brocco, 1976;

Brocco and Cloney, 1980). Instead three sulfur-rich proteins were extracted from each species, and four proteins have been extracted from the dermal platelets of *Lolliguncula brevis* (Cooper *et al.*, 1990). Mirow (1972) also described the composition of dermal platelets from *L. pealii* and *L. opalescens* as 'electron dense', and this term has been adopted by subsequent authors.

Iridosomal Platelet Distribution

The distribution and location of iridosomal platelets within the dermal iridophore cells differs greatly between genera (fig.14). In cuttlefish, the platelets are distributed throughout the cell, approximately parallel to one another (Kawaguti and Ohgishi, 1962) (fig. 14a). A similar arrangement of platelets is found in squid iridophore cells. However, the platelets are not continuous across the cell but are instead grouped into iridosomes consisting of between 2-7 platelets (Arnold, 1967; Mirow, 1972) (fig 14b). *Octopus* iridophore cells are very different, as the platelets are located on the cell surface. Groups of 4 to 32 platelets (called an iridosome, or reflectosome) project out from the cell (Brocco, 1976) (fig. 14c). This greatly alters the morphology of *Octopus* iridophore cells, and they have since been termed reflector cells by Cloney and Brocco (1983).

Three different dermal iridophore cells are therefore apparent in cephalopods.

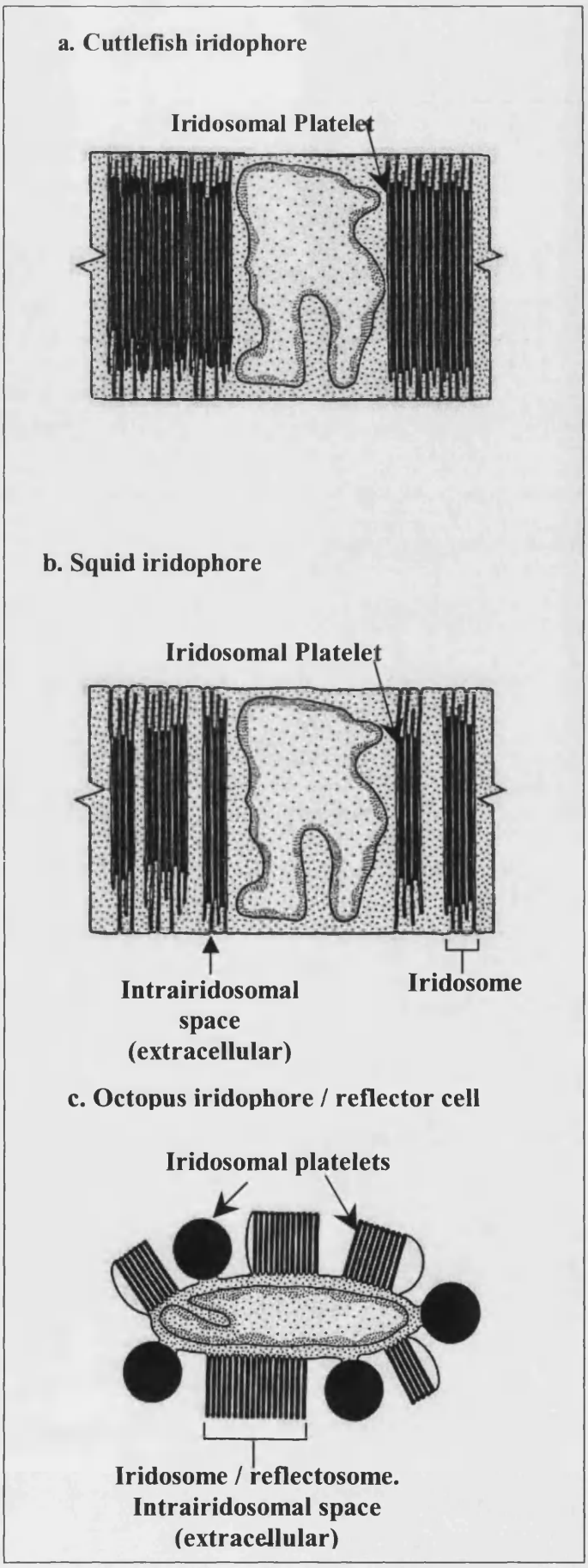

Fig. 14. Cross-sectional diagrams of cephalopod iridophore cells. Images adapted from Brocco and Cloney, 1980.
Not to Scale

IRIDOSOMAL PLATELET ORIENTATION

The orientation of iridophore cells with respect to the integument may also be different between genera. This has led to different interpretation of how the iridophore cells may interact with incident light:

1) MULTI-LAYER INTERFERENCE

This hypothesis was first proposed by Denton and Land (1971) after isolating and examining iridophore cells from the eyelids of *L. forbesi* and *S. elegans*. They propose that the iridosomal platelets of cephalopods are arranged in stacks that are parallel with the integument surface, and are therefore similar to the reflective scales of fish (Denton, 1970). In this orientation the platelets may reflect certain wavelengths via multi-layer interference (see also fig. 29). The wavelengths that will be reflected can be determined with an equation proposed by Huxley (1968, see also Rayleigh, 1917). Huxley suggests that maximum constructive interference (λ_{max}) will occur when alternate layers of high and low refractive index material have an optical thickness (thickness multiplied by refractive index) equal to one quarter of the incident wavelength. A simplified version of Huxley's equations is given by Denton and Land (1971). This equation (1) considers only iridosomal platelet thickness (t) and its corresponding refractive index (n), and was only later modified (equation 2) to include both the thickness of the iridosomal platelets (p) and intrairidosomal space (s) (Land, 1972).

$$\lambda_{max} = 4nt \qquad (1)$$

$$\lambda_{max} = 2(n_p t_p + n_s t_s) \qquad (2)$$

Most of the iridophore cells measured by Denton and Land were found compliant with this ¼ wavelength rule, and the calculation predicts the same wavelengths as are observed in the tissue. Subsequent investigators have also found these equations to fit, and this theory is generally supported. However, Denton and Land measured only isolated *in vitro* iridosomal platelets, and no direct *in vivo* measurements of platelet orientation are published.

2) Diffraction Gratings

One of the earliest investigations into the iridophore cells of *S. officinalis* was conducted by Schäfer (1937). He described and illustrated iridosomal platelets as being perpendicular to the integument surface. In this orientation the edge of each platelet may instead diffract light (see iridophore discussion and fig. 29). However, the diffraction grating equation has not been applied in any published work. I consider that this is because the angles of incident light required for diffraction will be very acute, and this is clearly not the case for the bright white patches of *S. officinalis*. In addition, I consider diffraction theory has been largely ignored simply because Denton and Land's equations are quick and simple to apply.

Several electron micrographs support the diffraction hypothesis. The most substantial is a single micrograph of iridophore cells in the ventral mantle of *S. officinalis* (Budelman *et al.*, 1997). It shows platelets that are orientated perpendicular to the integument. A series of micrographs from *S. esculenta* (Kawaguti and Ohgishi, 1962) also shows perpendicular iridosomal platelets. However, not all of the platelets are orientated in this way. Whilst, a micrograph of *S. officinalis* (Hanlon and Messenger, 1988) suggests that the iridosomal platelets are randomly orientated, although they do not discuss this in their paper.

Other investigators have questioned the orientation of platelets (Brocco and Cloney, 1980; Hanlon *et al.*, 1984). Brocco and Cloney (1980) conclude that octopus iridophores behave as multi-interference layers, and rename them reflector cells. They also propose that the terms 'reflector cell' be used to imply stacked multi-interference platelets, 'iridocyte' for cells that might produce colour by diffraction, and 'iridophore' to be used when orientation cannot be decided upon[9] (Cloney and Brocco, 1983).

DEVELOPMENT OF IRIDOPHORE CELLS

Rabl (1900) hypothesises that the iridophore cells of *Sepiola rondeleti* (a relative of the cuttlefish) arise from mesodermal stem cells that form small granules within their cytoplasm. These granules later coalesce into spheres, before aggregating into rows and ultimately platelets. These observations are supported by Schäfer's (1937) investigation into *Sepia officinalis*, and by Kawaguti and Ohgishi (1962). The latter authors present a micrograph of iridosomal platelets from *S. esculenta*, which they describe as showing the platelets to consist of an assembly of 100 nm particles that were originally created by 5-10 nm granules.

Similar developmental steps are described in other cephalopod iridophore cells. Arnold (1967) suggests that the iridosomes (groups of iridosomal platelets) of *L. pealii* originate from Golgi derived vesicles. Each vesicle and iridosomal platelet is also associated with microtubules, which may later aid in alignment. Microtubules and granular particles are also found in the developing platelets of *O. dofleini* (Brocco, 1976).

[9] The term iridophore shall continue to be used in this work to describe all cephalopod iridescent light reflecting cells.

Active Iridophore Cells

Until recently, iridophore cells have been considered as static structures. However, Hanlon (1982) suggested that the dermal iridophore cell (ventral side of the mantle) of *L. plei* might actively change from non-iridescent (diffuse blue colour) to iridescent, when levels of the neurotransmitter acetylcholine (ACh) are elevated. This claim was rigorously investigated in *Lolliguncula brevis* (Cooper and Hanlon, 1986; Hanlon *et al.*, 1990; Cooper *et al.*, 1990), and suggests that squid possess both passive and active iridophore cells. The neurotransmitter has little or no effect upon the passive cells, while active iridophores become reversibly iridescent upon exposure to elevated levels of acetylcholine. Acetylcholine is naturally found in the dermal iridophore layer of *L. brevis* (Cooper and Hanlon, 1986) and it suggests that the iridophore cells may be subject to neural control. However, neurones have not been directly associated with the iridophore cells, and any optical change takes several minutes to occur. ACh may therefore act more like a hormone (Hanlon *et al.*, 1990). Importantly, this neurotransmitter does not induce chromatophore expansion in squid, or *S. officinalis* (Loi *et al.*, 1996).

Iridosomal platelets located within the photophores of some deep-sea cephalopods have also been shown to emit different wavelengths under changing temperatures (Young and Mencher, 1980). This has not been investigated in dermal iridophore cells.

Polarised Light Reflection and Perception

Octopus are capable of visually discriminating between objects that display different planes of polarised light (Moody and Parriss 1960, 1961; Rowell and Wells,1961; Shashar and Cronin, 1996). More recently this capability has been demonstrated in squid and cuttlefish (Shashar *et al.*, 1996; 2001). The ability to

perceive polarised light may greatly assist in prey capture and could be used to hunt camouflaged fish (Messenger, 1991; Shashar *et al.*, 1998, 2000). Fish with silver scales reflect light downwards in order to conceal themselves, and do so via multi-layer interference (Denton, 1970). This mechanism produces colour (angle) dependant polarisation (Hecht, 1989), and would therefore reveal the position of the shoal to a cephalopod. Similarly, iridophore cells will also polarise light (thin-film interference and diffraction gratings both polarise light, Ditchburn, 1999) and may therefore be used as an intraspecific method of communication. This has been investigated (Shashar *et al.*, 1996) and revealed that prominent polarisation patterns are displayed upon the arms, around the eyes, and 'forehead' of *S. officinalis*. Ultrastructural examination identified isolated iridophore cells within each of these areas, and it is hypothesised that manipulation of them with a neurotransmitter (Cooper *et al.*, 1990) may control polarisation. Similar observations on light polarising areas also correlate with the position of iridophore cells in the arms of *Loligo pealei* (Shashar *et al.*, 2001).

RESULTS: DERMAL IRIDOPHORE CELLS

Isolated and aggregated groups of iridophore cells can be identified within the integument of *S. officinalis*. Each cell is located within the connective tissue matrix, and is situated beneath the layer of chromatophore organs. It is the large aggregated groups of iridophore cells that are of primary interest. These cells are always associated with leucophore cells and are confined to the bright white areas previously described.

Iridophore cells are elongated in shape and typically have tapering ends (fig. 15). Each cell possesses a centrally located nucleus that is surrounded by a distinctive mass of membrane bound cytoplasm. This is then flanked by the iridosomal platelets and intrairidosomal space, and enclosed by an outer cell membrane. The cells have a mean length (± S.E.) of 26.5 (2.7) μm, width of 19.2 (2.3) μm and depth of 7.8 (1.1) μm (N = 30).

Ultrastructural examination of the iridophore cells reveals that the nucleus is elongated perpendicular to the cell's length, and it resembles a central core. It appears roughly circular in planar sections, having a mean diameter of 4.5 (S.E. ±1.0) μm. In transverse and longitudinal sections it is elongated, and has a mean length of 6.5 (S.E. ±0.5) μm. Occasionally, multiple nuclei can incorrectly be seen in an iridophore section. This is because the nucleus is lobed, or kidney-shaped and the edges of each lobe have been sectioned. The nuclear membrane is also undulated and displays numerous infolds.

The nucleus is composed of euchromatin (uncoiled active chromatin), and hetrochromatin (clumped, less active chromatin) that is coiled upon histones (fig. 16). Hetrochromatin stains darker, and is distributed around the periphery of the nucleus. Gaps within the hetrochromatin highlight nuclear pores that are present in the nuclear

Fig. 15 Longitudinal section through an iridophore cell.

A typical iridophore cell that is elongated in shape and has tapering ends. The nucleus is central and extends perpendicular to that of the cell's overall length. Here the two lobes of the kidney-shaped nucleus have been sectioned. It therefore appears as two discrete halves. Highly ordered platelets are found on either side of the nucleus. These are also orientated perpendicular to the cell's length, and are distributed parallel across the cell. Neighbouring iridophores cells display a similar internal distribution of platelets. However, the orientation of these cells is different. As a result neighbouring iridophore cells possess platelets that are horizontal in the top right, 45° in the middle, and vertical on the left.

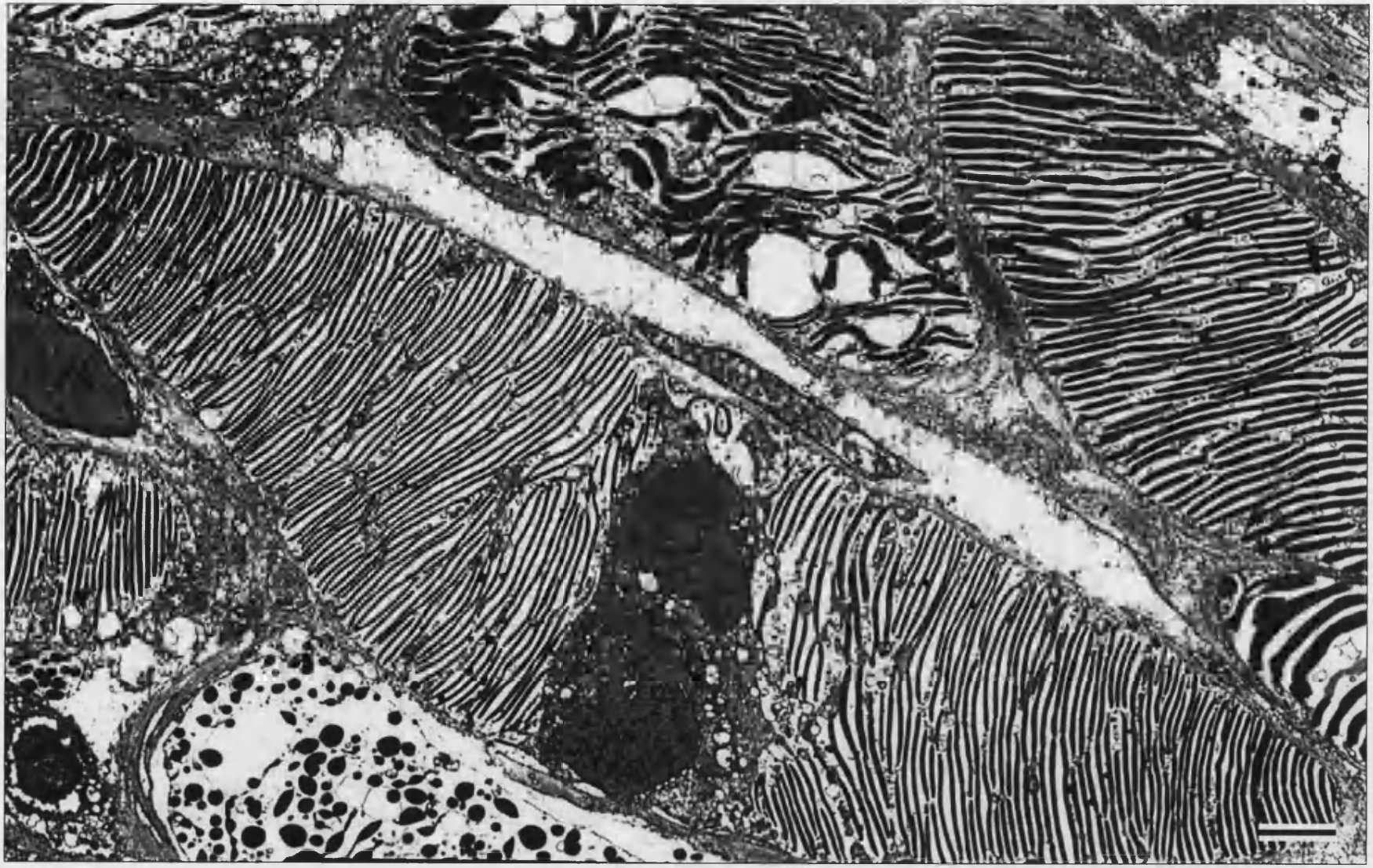

Fig. 15 Scale bar = 2μm

Fig. 16 Planar section through an iridophore cell and nucleus

a) x6,000 **b)** x10,000 (includes labels) **c)** x20,000

The nucleus of an iridophore cell consists of a nucleolus (Nus), euchromatin (Eu), hetrochromatin (Het), and a nuclear membrane (NM). Nuclear pore (NP) openings within the nuclear membrane allow communication with the surrounding cytocentrum (Cyc). The cytocentrum is a thin border of cytoplasm that surrounds the nucleus. It consists of cytoplasm, ribosomal granules, membrane bound vesicles, and the organelles required for cell function and protein synthesis. Developing platelets can also be seen emerging from the cytocentrum (arrows). These platelets project out into the clearer cytoplasm that encircles the cytocentrum. Larger platelets that are not connected to the cytocentrum are also found in the clear cytoplasm, which constitutes the intrairidosomal space.

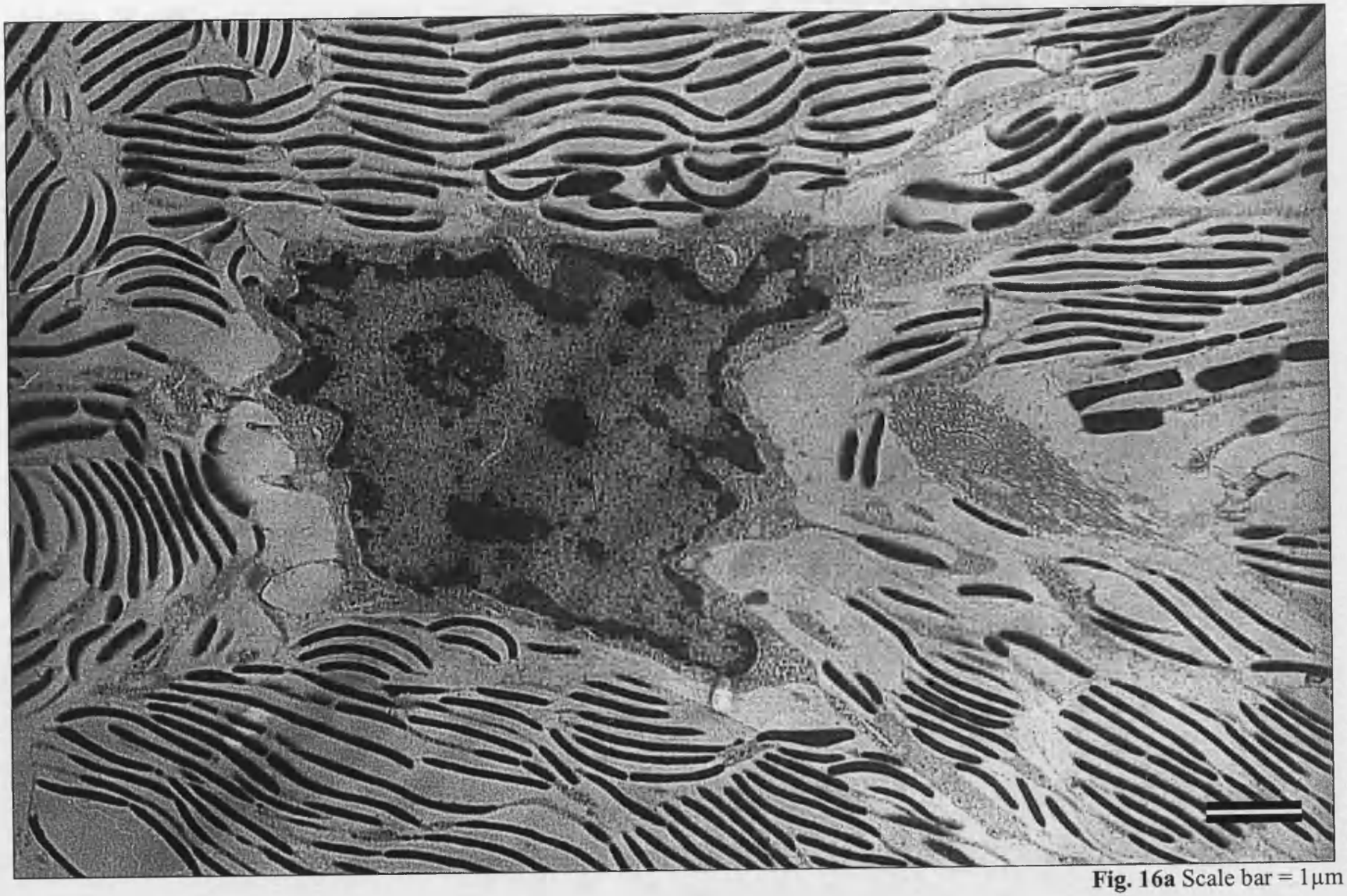

Fig. 16a Scale bar = 1μm

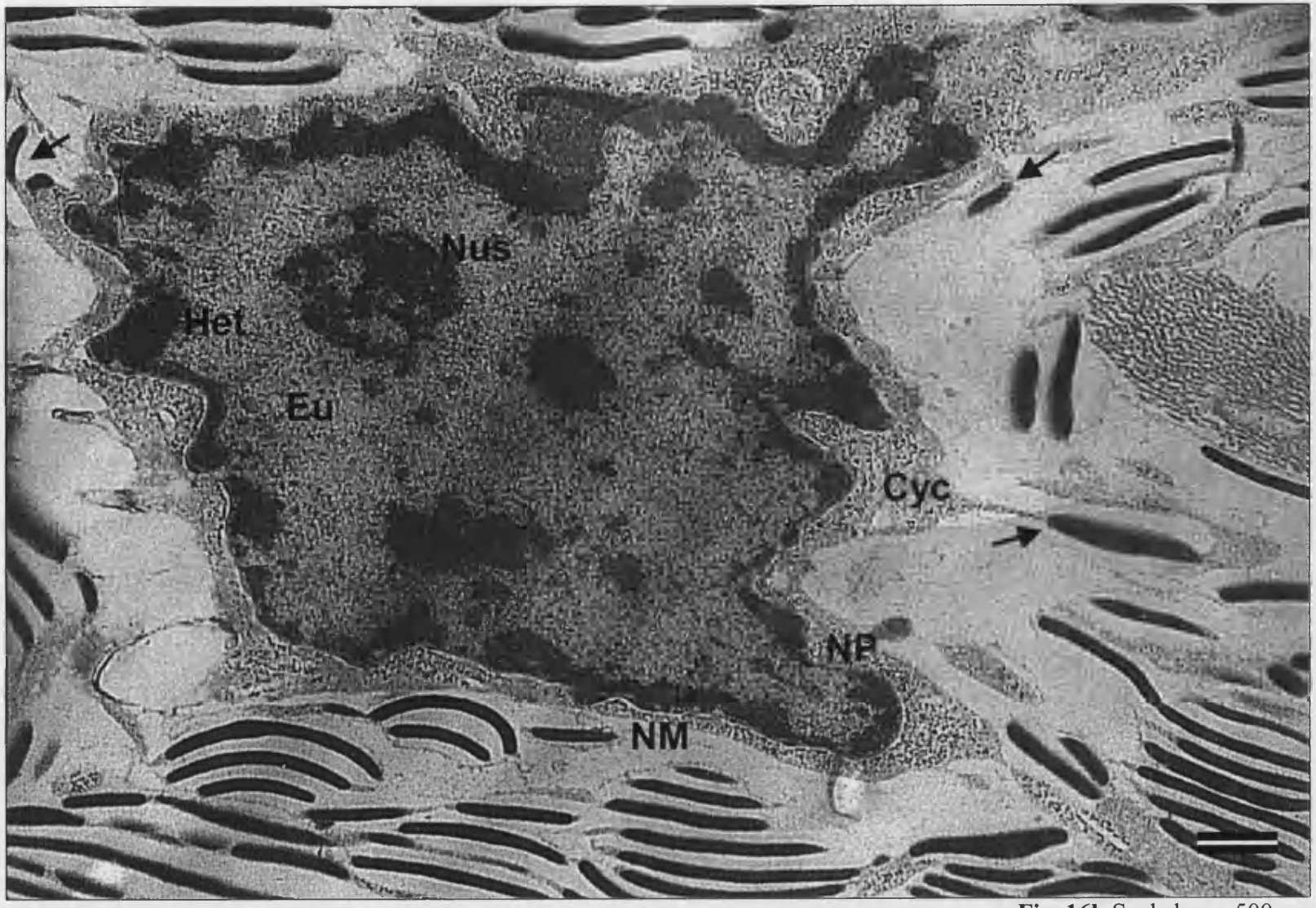

Fig. 16b Scale bar = 500 nm

Fig. 16c Scale bar = 200 nm

membrane, and these lead into the cytocentrum[10]. The cytocentrum is an unusual distribution of cytoplasm that borders the nucleus. It confines all of the organelles required for cell function in a faint membrane. This is unusual since we would normally find these organelles dispersed throughout a typical eucaryotic cell. Most apparent in the cytocentrum are a large number of membrane bound vesicles (≈ 50-70 nm in diameter) and ribosome granules. The vesicles are derived from the Golgi apparatus, and ribosomes from the rough endoplasmic reticulum, all of which are apparent in the cytocentrum. Smooth endoplasmic reticulum is also seen, as well as mitochondria; however the latter are surprisingly sparse. Microtubules could not be resolved within the cytocentrum, and are found only outside it as part of the cells overall cytoskeleton. Similarly, microtubules are not found in the iridosomal platelets, or associated with them.

Densely stained platelets border the cytocentrum. They can be divided into two groups. First, a small number of developing platelets can be seen emerging from the cytocentrum. These are contained within cytoplasmic channels that are confluent with the cytocentrum membrane and its cytoplasm (fig. 16). Typically these platelets are small in diameter, usually only a few 100 nm long, and they do not appear to be orientated in any particular direction. However, their thickness is comparable to that of developed platelets. The second group of iridosomal platelets are much larger in diameter and are considered to be fully developed. It is these iridosomal platelets that are regularly spaced apart and orientated perpendicular to the cells length. These iridosomal platelets are also contained within cytoplasmic channels (figs. 17-21). However, these channels have not been successfully traced back to the cytocentrum.

[10] The term cytocentrum was originally used by Brocco (1976) to refer to the central cytoplasm that surrounds the nucleus of octopus iridophore cells, and this nomenclature is continued here. However, the term is more commonly used in cell biology to refer to the cytoplasm of a dividing cell, which contains two centrioles and no other organelles.

Instead, each channel appears to be a separate inclusion. These meander across the entire width and depth of the cell and encompass several iridosomal platelets as they do so.

The cytoplasmic channels provide a membrane around the platelets, but do not completely surround them. Instead they sheath only the length of the platelets and leave the tips exposed to the cytoplasm contained in the channels (figs. 16-21). Each channel, depending on size, may contain several platelets that are arranged in end-on-stacks. Only one platelet is found within the short cytoplasmic channels that are located at the tapering edges of the cell. Whilst, towards the nucleus the channels get progressively larger, and in longitudinal sections these contain up to 4 iridosomal platelets. A similar stacked arrangement of multiple platelets is seen in the planar sections. In the larger channels with multiple plates, the platelets do not touch each other, but are instead spaced apart by cytoplasmic gaps termed cytoplasmic bridges (figs. 20-21). The channel membrane therefore spans from one iridosomal platelet to the next, and coalesce slightly as it does so.

The cytoplasmic channels of an iridophore cell do not appear to branch.

The iridophore cells are completely enclosed by an outer cell membrane, which extends across the ends of each peripheral cytoplasmic channel and intrairidosomal space (figs. 17-19). The intrairidosomal spaces of *S. officinalis* are therefore intracellular, and not extracellular like those of squid and octopus.

The selective permeability of all membranes (outer cell, cytocentrum and cytoplasmic channel) is evident in the micrographs. A stark contrast can be seen between the clear, relatively unobstructed cytoplasm of the intrairidosomal space and the highly contaminated extracellular cytoplasm (figs. 17-19).

Fig. 17 A longitudinal section through an iridophore cell showing the edge of the nucleus (Nu), cytocentrum (Cyc), iridosomal platelets (IRP), and outer cell membrane (arrow). Each iridosomal platelet is contained within a cytoplasmic channel (CPC) that extends from near to the outer cell membrane across the cell. A gap can be seen between some of the cytoplasmic channels and the outer cell membrane. This suggests that the intrairidosomal spaces (IIS) are continuous around the channels.

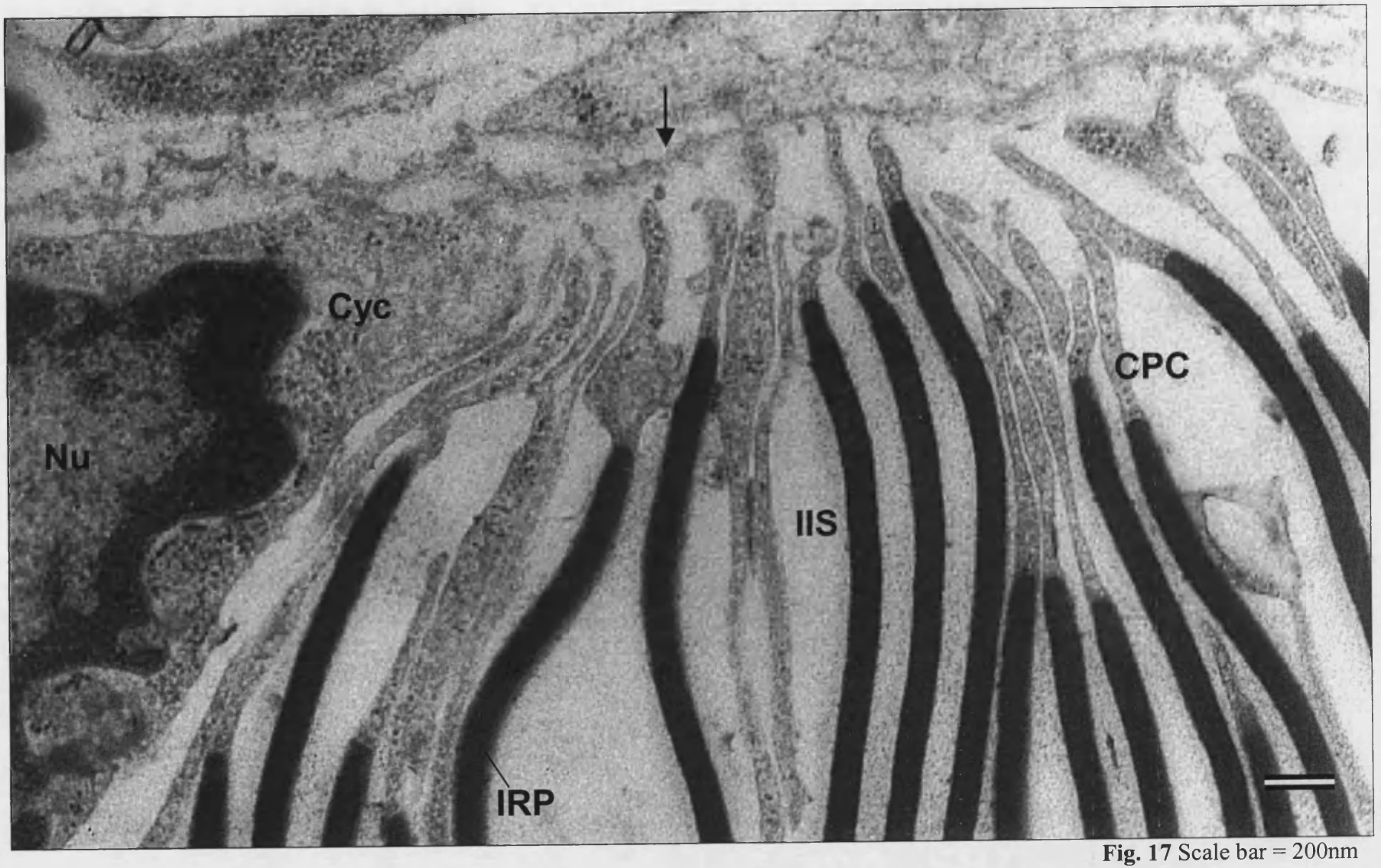

Fig. 17 Scale bar = 200nm

Fig. 18 The outer cell membrane (arrow) of an iridophore cell can be seen extending across the end of numerous cytoplasmic channels and intrairidosomal spaces. This is continuous, and no junctions with the extracellular space are visible. It therefore provides a boundary between the extracellular and intrairidosomal spaces, which maintains the latter contamination free.

The cytoplasmic channels extend to the outer cell membrane, but do not appear to touch or interconnect with it. This is intriguing, since the actual iridosomal platelets may be a considerable distance from the outer cell membrane (*).

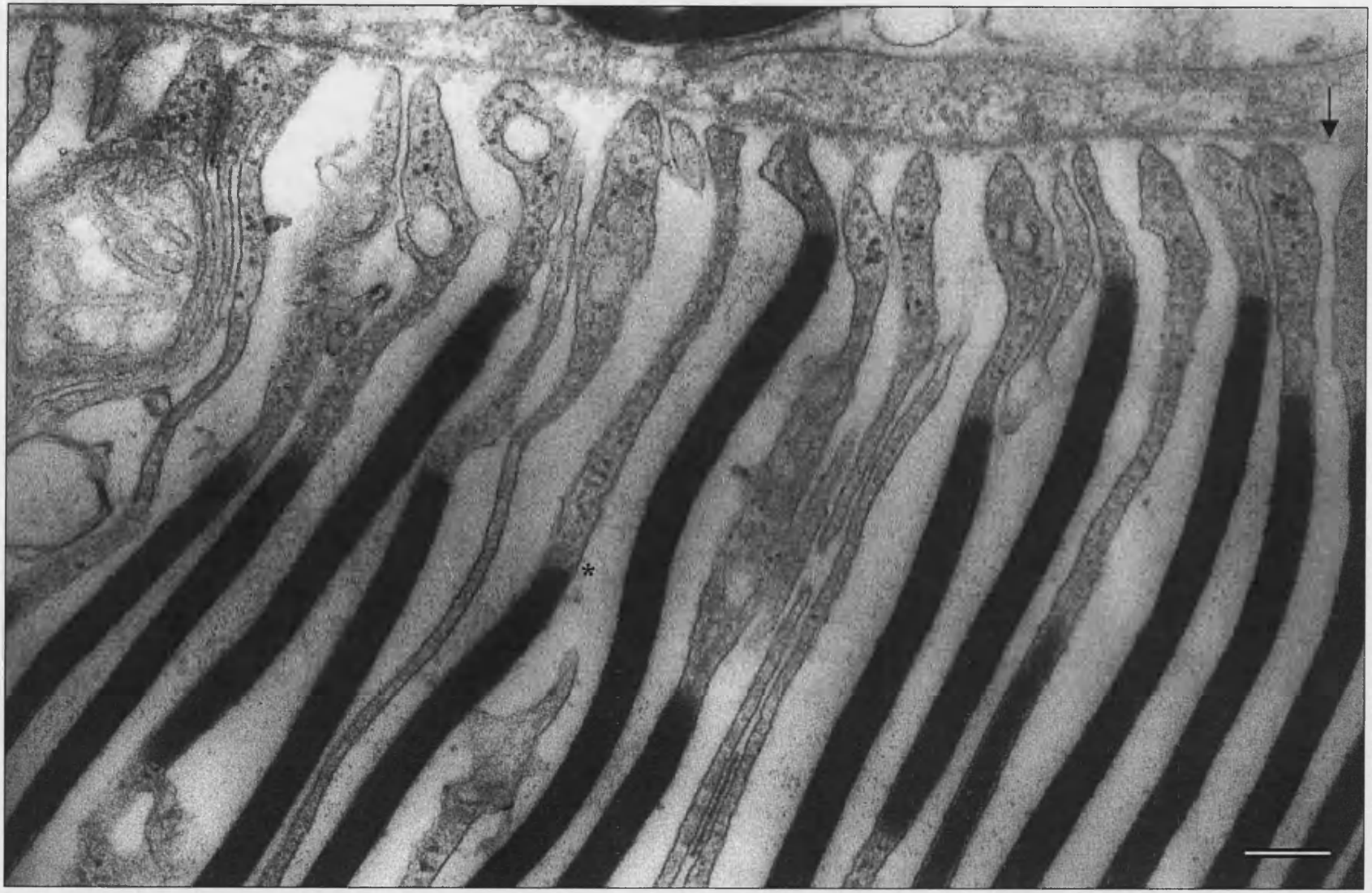

Fig. 18 Scale bar = 200nm

Fig. 19 Planar section through an iridophore cell, focusing upon the outer cell membrane. The outer cell membrane is continuous and follows the profile of the cell. Cytoplasmic channels extend close to it, but do not appear to touch or interconnect with the membrane.

Please note the orientation of the neighbouring iridophore cell's iridosomal platelets

Fig. 19 Scale bar = 200nm

Fig. 20 High magnification micrograph of the iridosomal platelets.

Iridosomal platelets are contained within cytoplasmic channels. These channels have a membrane that is approximately 4 nm thick. It sheaths the length of the iridosomal platelets leaving the tips exposed to the cytoplasm contained within the channel. At the end of each iridosomal platelet the cytoplasmic channel membrane continues and forms a cytoplasmic bridge, which links subsequent iridosomal platelets (arrow). The membrane can be seen to coalesce slightly as it spans these regions. Several iridosomal platelets may therefore be joined together within the same cytoplasmic channel.

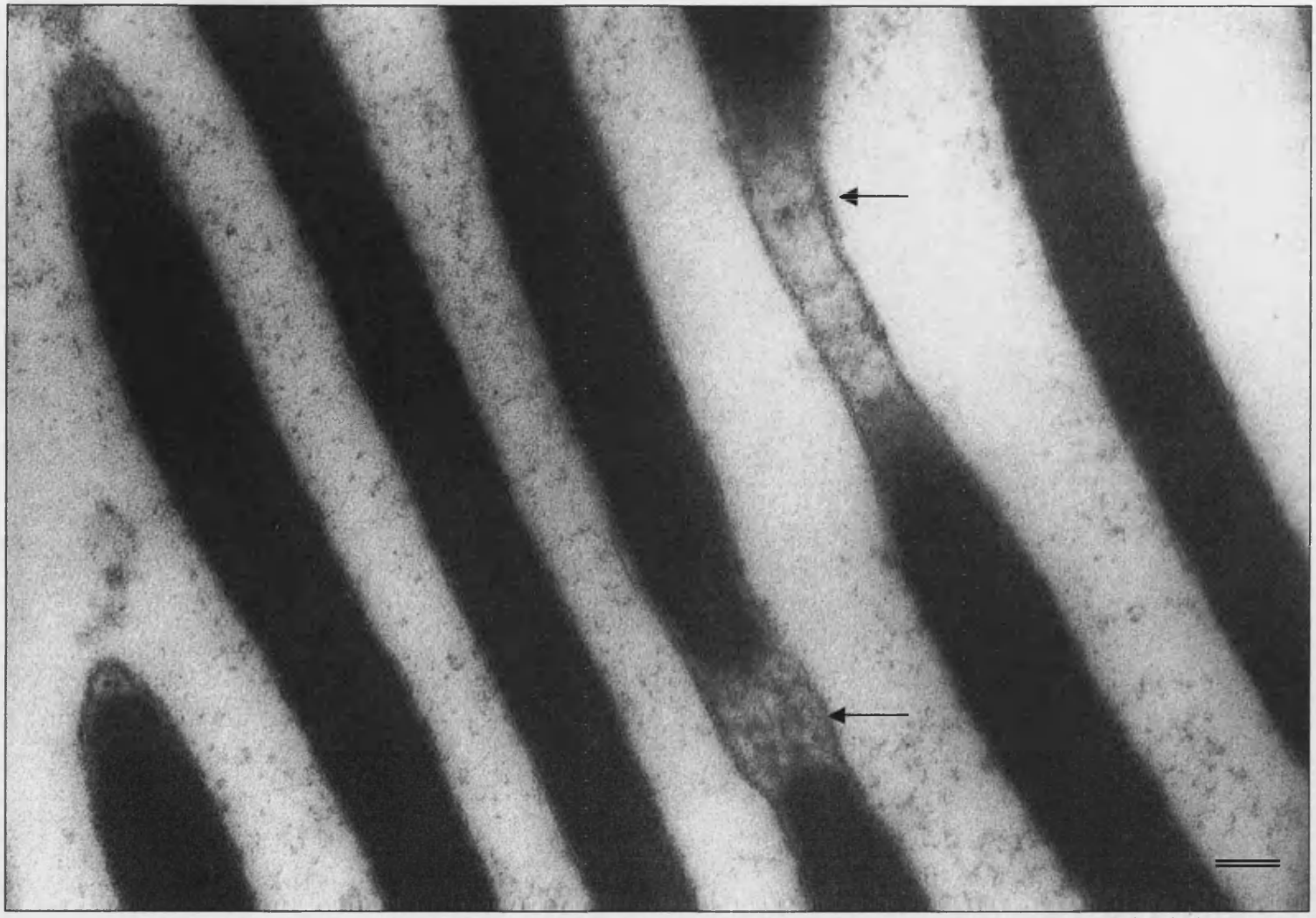

Fig. 20 Scale bar = 50nm

Fig. 21 This micrograph is of an ultra-thin section (50-60 nm) that has been tilted 5° within the transmission electron beam. This was done to examine the continuity of the cytoplasmic channel membrane. Tilting the section induces a shadow around any stained element. A densely stained area, such as a phospholipid membrane, casts a dark shadow and increases the contrast.

The micrograph confirms that the cytoplasmic channel membranes are continuous across the iridosomal platelets and cytoplasmic bridges. The channel membrane does not encircle the iridosomal platelets, and instead leaves the ends of each platelet open to the cytoplasm contained with the channel.

Please note that no dense patches, or granules can be seen in the iridosomal platelets.

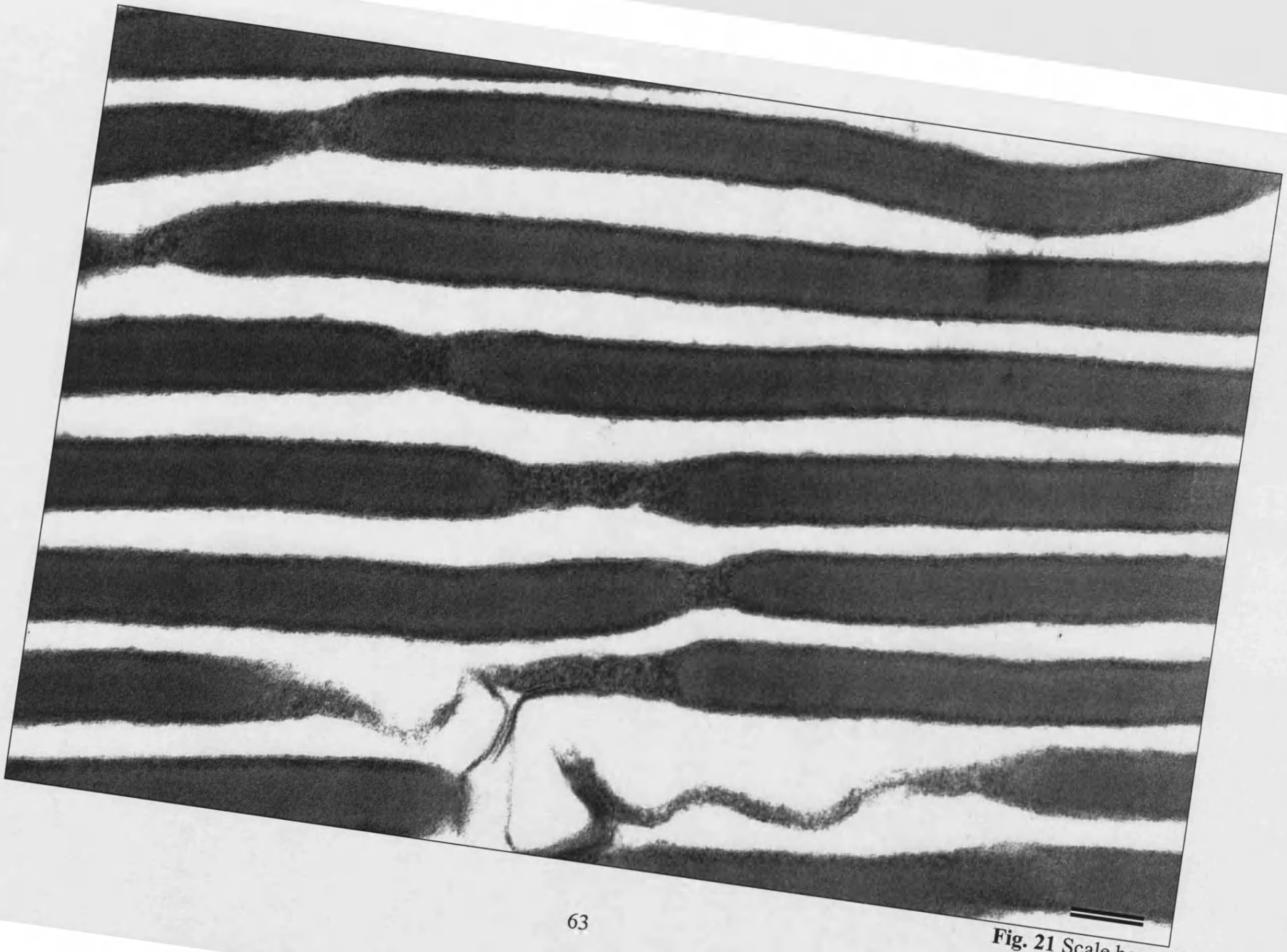

Fig. 21 Scale bar = 100nm

Many of the cytoplasmic channels extend to within a few nanometers of the outer cell membrane (figs. 17-19), but do not touch or interconnect with it. This is surprising given the regimented distribution of the cytoplasmic channels, and the fact that the platelets rarely extend this close to the outer cell membrane. In most instances the platelets are approximately a micron away from the outer cell membrane, yet the channels continue to extend close to it (figs. 18-19). Since the channels do not appear to touch the membrane, it suggests that the clear intrairidosomal cytoplasm is continuous around the ends of the cytoplasmic channels.

Iridosomal Platelets

The platelets are colourless and transparent within the light microscope, and remain so even after primary fixation. It is staining that induces contrast, and the platelets display a high affinity for eosin, toludine blue and osmium tetroxide.

Each platelet is an isolated mass of material that is contained within a cytoplasmic channel (figs. 20-21). Serial sections confirm that the platelets are 'plate-like' discs in shape, and are not rods (fig. 22). However, computer aided 3D reconstruction (IGL Trace v1.26b and sEM Align, Fiala 2001) of serial sections failed. This is due to the scale, density and wavy orientation of the iridosomal platelets as you progress through the cell. Examination of the serial micrographs supports this, as many platelets can be seen to be progressively moving out of the plane of section (shadows around the edge of widening platelets, fig 22). The dissector principle was therefore used to examine continuity between the sections, and also to make progressive measurements of a platelet's sectioned length. These measurements were then used to determine the maximum diameter of individual platelets. Given that the thickness of each section (*L)* is approximately 55 nm (50-60 nm ultra-thin sections), and provided that the sections measured do not pass over the

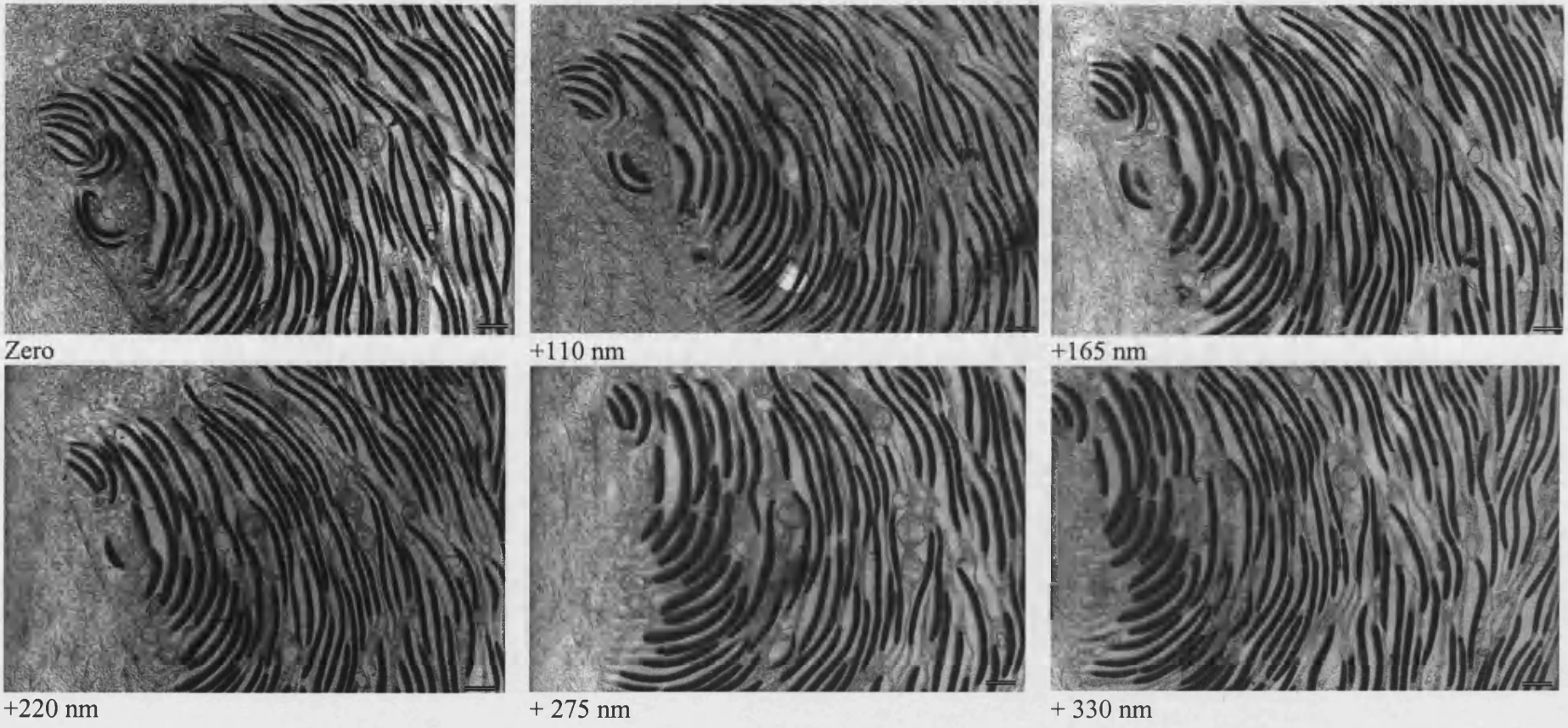

Fig. 22 Longitudinal, serial sections through the tapering end of an iridophore cell. Each scale bar = 500 nm

maximum diameter of the platelet, the maximum radius can be determined (equations given with fig. 23).

The maximum diameter of the iridosomal platelets found in five (serial sectioned) iridophore cells was calculated (fig. 24), and the variance between these cells analysed (table 5). Only four cells gave significant data, which suggests that the platelets vary greatly in diameter (0.7μm – 3.6μm; mean 1.9 ±0.8 μm; fig. 24).

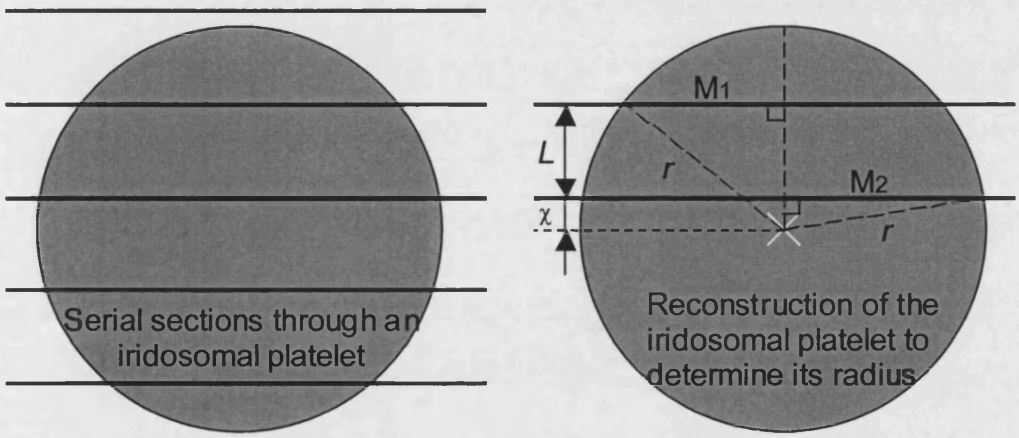

$$M_1^2 + (x+L)^2 = r^2 = M_2^2 + x^2 \qquad (3)$$

$$M_1^2 + 2Lx + L^2 = r^2 = M_2^2 \qquad (4)$$

$$x = \frac{M_2^2 - M_1^2 - L^2}{2L} \qquad (5)$$

$$x^2 + M_2^2 = r^2 \,(= \text{diameter}) \qquad (6)$$

Fig. 23 Serial sections (solid black lines) through an iridosomal platelet (grey circle) are unlikely to have passed directly through the maximum diameter of it. This value can instead be determined, providing that the distance between each section is known (*L*), and the length of each platelet can be measured (½ length = M). The above equation was used to calculate the maximum diameter of the iridosomal platelets, assuming that the platelets are circular and not elliptical.

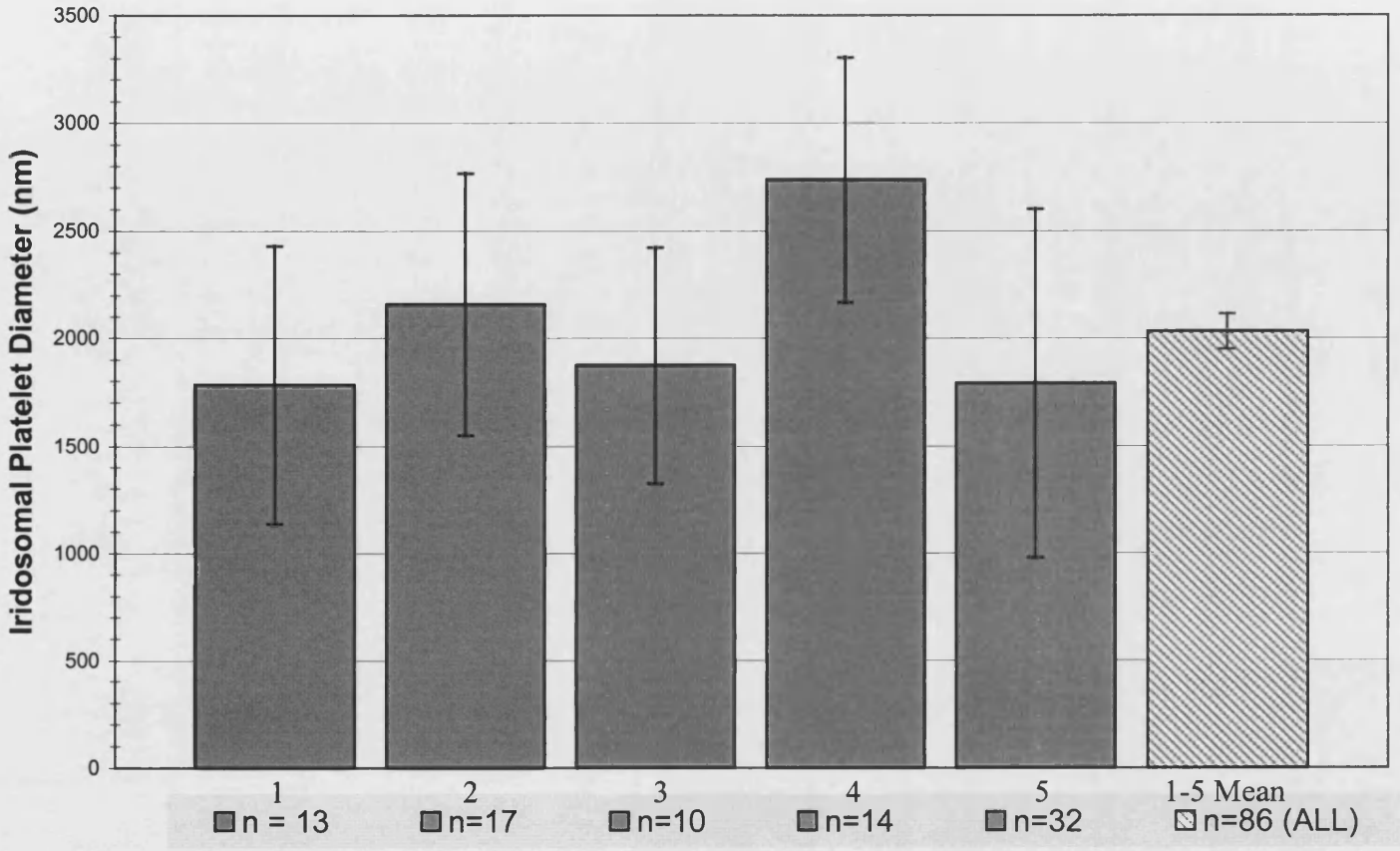

Fig. 24 Iridosomal platelet diameter.
(Columns 1 to 5) Grey columns show the mean iridosomal platelet diameter, and the number of platelets measured (n) for five serial sectioned iridophore cells. These measurements demonstrate a high variability per cell, and to illustrate this the standard deviation for each is given (black error bars).
(Column 1-5 Mean) Striped column represents the mean, and standard error of the mean (red error bar) for all five of the iridophore cells. See also table 5, analysis of variance for this data.

Analysis of Variance – Iridosomal Platelet Diameter

Iridophore Cell 1	Iridophore Cell 2	Iridophore Cell 3	Iridophore Cell 4	Iridophore Cell 5
(n = 13) Mean Iridosomal Platelet Diameter 1.78 µm SD = 0.65 SE = 0.18	(n = 17) Mean Iridosomal Platelet Diameter 2.16 µm SD = 0.61 SE = 0.15	(n = 10) Mean Iridosomal Platelet Diameter 1.87 µm SD = 0.55 SE = 0.17	(n = 14) Mean Iridosomal Platelet Diameter 2.74 µm SD = 0.57 SE = 0.15	(n = 30) Mean Iridosomal Platelet Diameter 1.79 µm SD = 0.81 SE = 0.14
1 vs. 2 **NS** 1 vs. 3 **NS** 1 vs. 4 p <0.001 1 vs. 5 **NS**	2 vs. 3 **NS** 2 vs. 4 p <0.05 2 vs. 5 **NS**	3 vs. 4 p <0.01 3 vs. 5 **NS**	4 vs. 5 p <0.001	

Table 5 Iridosomal platelet diameter.
The mean platelet diameter, standard deviation (SD) from the mean, standard error (SE) of the mean, and analysis of variance for five serial sectioned iridophore cells (graphically represented in figure 24). Probability values (p) equal to, or less than 0.05 are considered significant and suggests a difference between the values for each cell. Not-significant values (NS) support the null hypotheses and suggests that there is no significant difference between the platelet diameters.

Fig. 25 (Graphs **A-E**) Iridosomal platelet thickness( ) and corresponding intrairidosomal space ( ) for five separate iridophore cells (A-E). These two values were then added to give the periodicity ( ). This represents the distance from the leading edge of one iridosomal platelet to the leading edge of the next. A line of best fit has also been applied to the periodicity values. The number of iridosomal platelets measured per cell is denoted by the value 'n' along the x-axis of each graph. (Graph **Mean**) The mean values for each of the five iridophore cells A-E.
See also table 6, analysis of variance for this data.

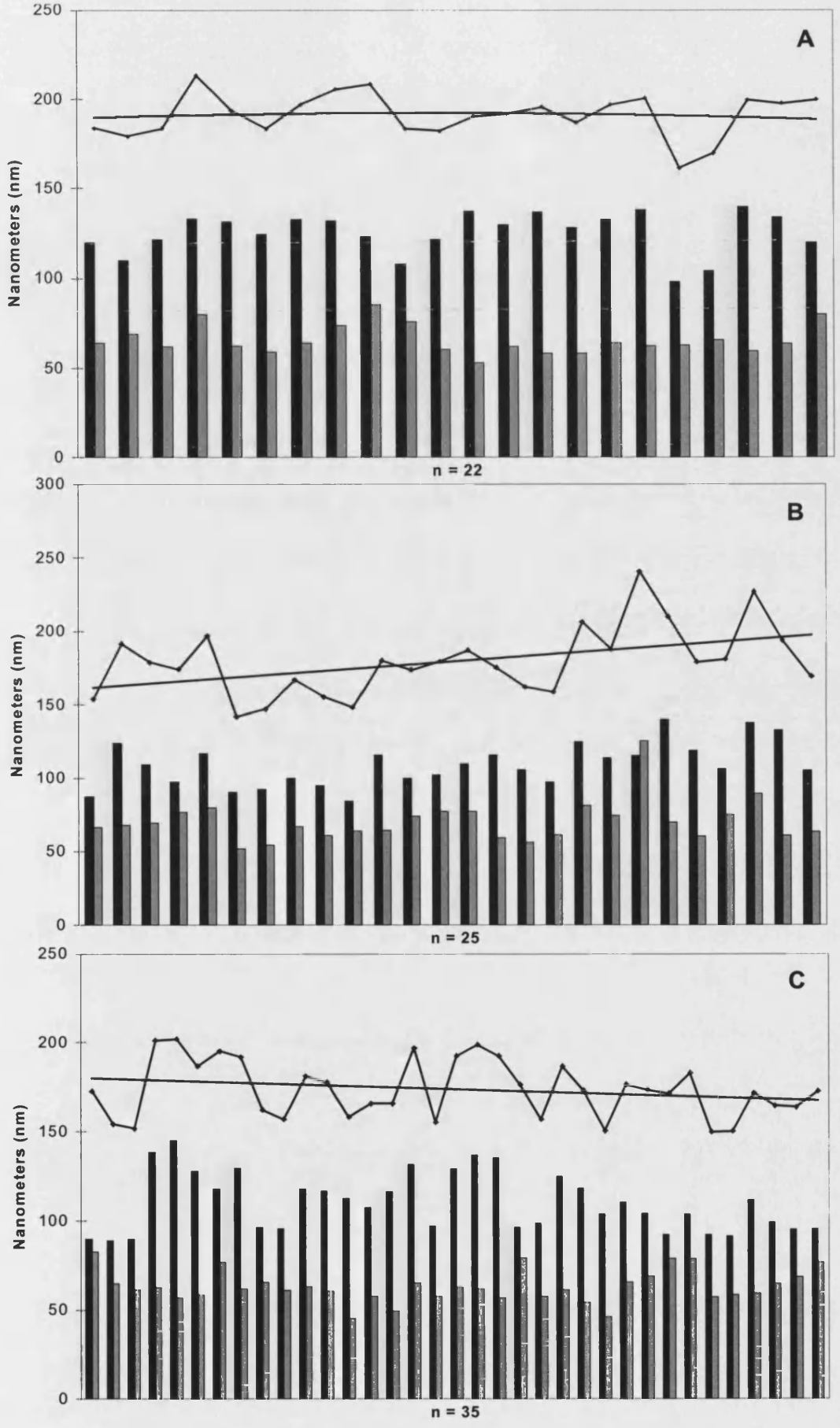
A
Nanometers (nm)
250
200
150
100
50
0
n = 22
B
Nanometers (nm)
300
250
200
150
100
50
0
n = 25
C
Nanometers (nm)
250
200
150
100
50
0
n = 35

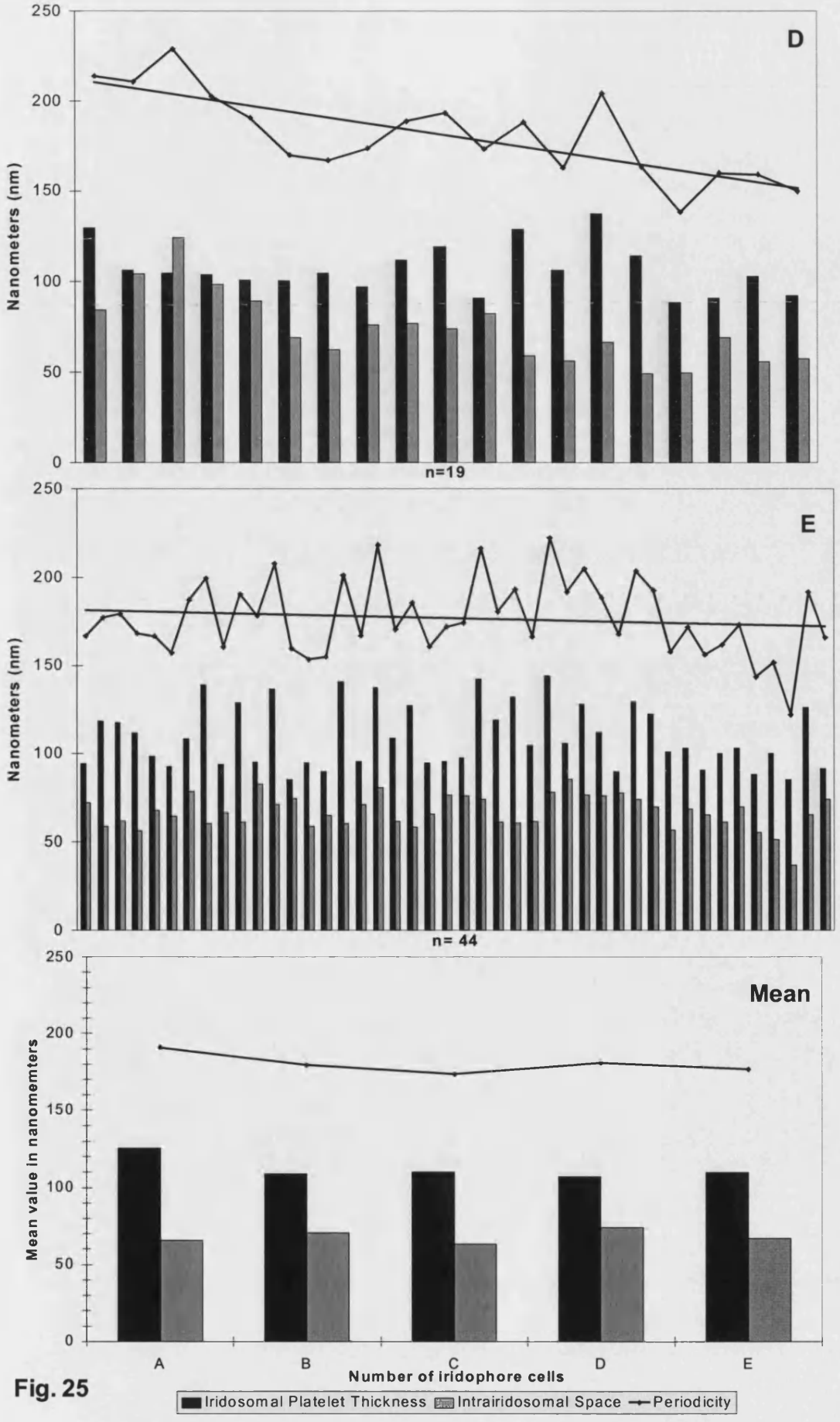
D
Nanometers (nm)
250
200
150
100
50
0
n=19
E
Nanometers (nm)
250
200
150
100
50
0
n= 44
Mean
Mean value in nanomemters
250
200
150
100
50
0
A
B
C
D
E
Number of iridophore cells
Iridosomal Platelet Thickness
Intrairidosomal Space
Periodicity

Fig. 25

Analysis of Variance – Iridosomal Platelet Thickness, Intrairidosomal Space and Periodicity

Iridophore Cell A		Iridophore Cell B		Iridophore Cell C		Iridophore Cell D		Iridophore Cell E	
(n = 22)		(n = 25)		(n = 35)		(n = 19)		(n = 44)	
Platelet	Space	Platelet	Space	Platelet	Space	Platelet	Space	Platelet	Space
125 nm (±2.5)	66 nm (±1.8)	109 nm (±2.9)	70 nm (±2.8)	110 nm (±2.8)	63 nm (±1.5)	107 nm (±3.2)	74 nm (±4.5)	110 nm (±2.7)	67 nm (±1.4)
A vs. B *p*<0.001	A vs. B **NS**	B vs. C **NS**	B vs. C *p*<0.05	C vs. D **NS**	C vs. D *p*<0.05	D vs. E **NS**	D vs. E **NS**		
A vs. C *p*<0.001	A vs. C **NS**	B vs. D **NS**	B vs. D **NS**	C vs. E **NS**	C vs. E **NS**				
A vs. D *p*<0.001	A vs. D **NS**	B vs. E **NS**	B vs. E **NS**						
A vs. E *p*<0.001	A vs. E **NS**								
Periodicity 191 nm (±2.6)		Periodicity 179 nm (±4.7)		Periodicity 173 nm (±2.7)		Periodicity 181 nm (±5.5)		Periodicity 177 nm (±3.2)	
A vs. B *p*<0.05		B vs. C **NS**		C vs. D **NS**		D vs. E **NS**			
A vs. C *p*<0.001		B vs. D **NS**		C vs. E **NS**					
A vs. D **NS**		B vs. E **NS**							
A vs. E *p<0.05*									

Table 6 Iridosomal platelet thickness, intrairidosomal space and periodicity.
The means, standard errors of means, and analysis of variance for the iridosomal platelet thickness, intrairidosomal space and periodicity of the five cells represented in figure 25. Probability values (*p*) equal to, or less than 0.05 are considered significant and suggests a difference between the values. Not-significant values (NS) support the null hypotheses and suggests that there is no difference between the values.

Summary of the iridosomal platelets and their size

The iridosomal platelets are orientated approximately perpendicular to the cells overall length, and are regularly spaced parallel to one another. Their regular distribution gives the iridophore cells a characteristic striped appearance, and more importantly the ability to form structural colours. The reflection of wavelengths is reliant upon the thickness of the platelets and the distance between them (intrairidosomal space). Both these values were measured (see method) in five iridophore cells (fig. 25), and the variance of these measurements assessed (table 6). Analysis of variance suggests that the first cell (iridophore cell A) is significantly different from the rest, and this data shall not be used to calculate the overall mean values. Values B-D (fig. 25) suggests that the iridosomal platelets have a mean thickness of 109 (±1.5) nm and intrairidosomal spaces of 68 (±1.2) nm. The periodicity, i.e. the distance from the leading edge of one platelet to the leading edge of the next, is a mean value of 177 (±1.9) nm.

IRIDOPHORE CELL ORIENTATION

Although the iridosomal platelets are highly orientated and precisely distributed within an iridophore cell, the overall orientation of the iridophore cells appears random. Cross-sections through the bright white skin areas show the organisation of cells to be random. The cells show no regular orientation with respect to the integument, overlying chromatophore organs, or neighbouring iridophore cells (fig. 26). To assess this, each iridophore cell was assigned a line, the direction of which indicated the approximate direction of the platelets. The angle of this line was then measured with reference to an overlying chromatophore organ (0^{o}) using image analysis software (fig. 27).

A random orientation of iridophore cells accounts somewhat for the variety of platelet shapes that can be observed in the micrographs. Any cells that are opposed to the plane of section will have platelets that taper. It is for this reason that I consider the data for iridophore A (fig. 25, table 6) is significantly different.

These observations suggest that iridophore cells found in the bright white patches of *S. officinalis* are not arranged like those of octopus and squid, and raises the question as to how the structural colours found in these regions are formed.

Fig. 26 A cross-section through a white fin spot.

A red line highlights the general orientation of the iridosomal platelets contained within each iridophore cell.

This image can be seen without orientation lines in figure 13.

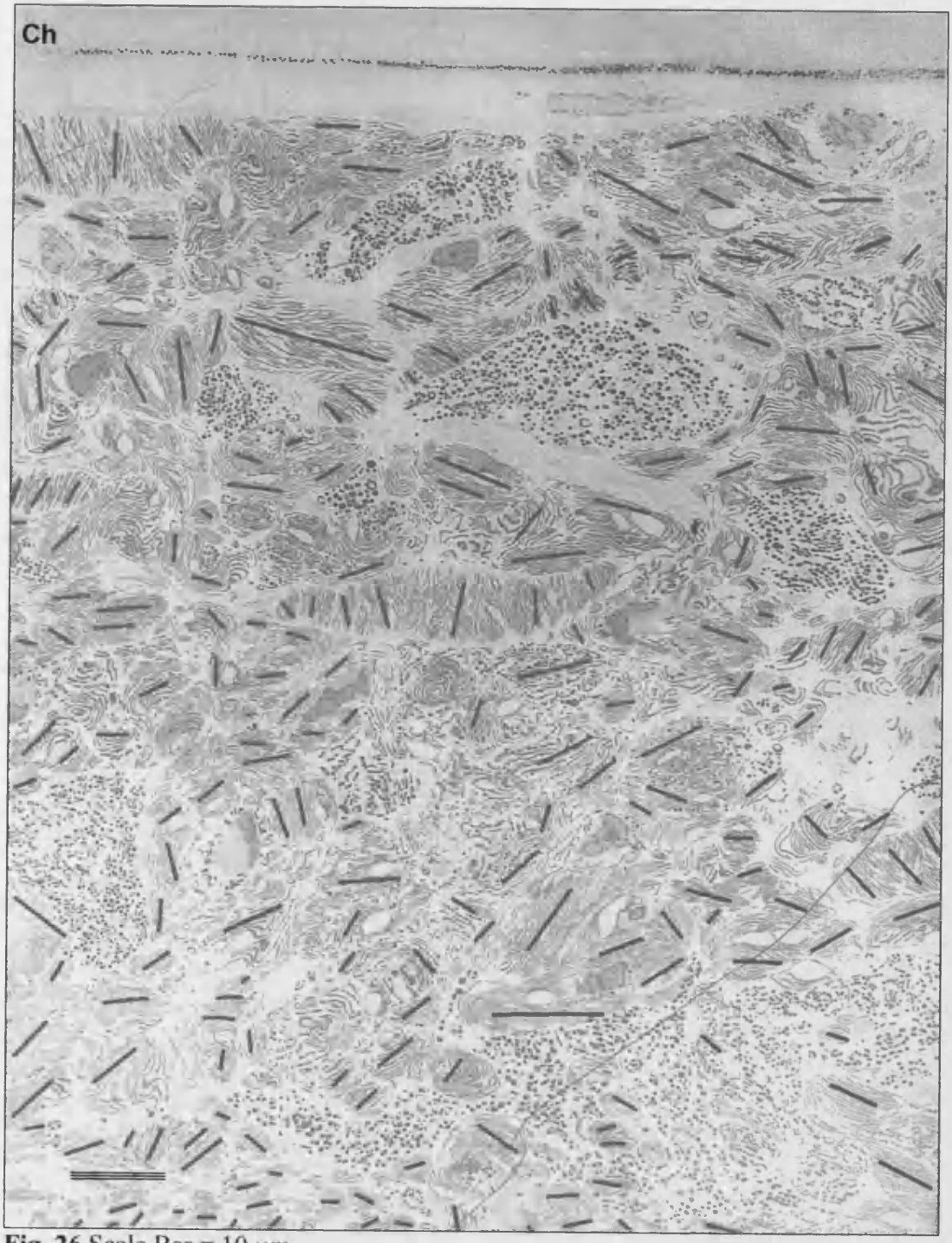

Fig. 26 Scale Bar = 10 μm

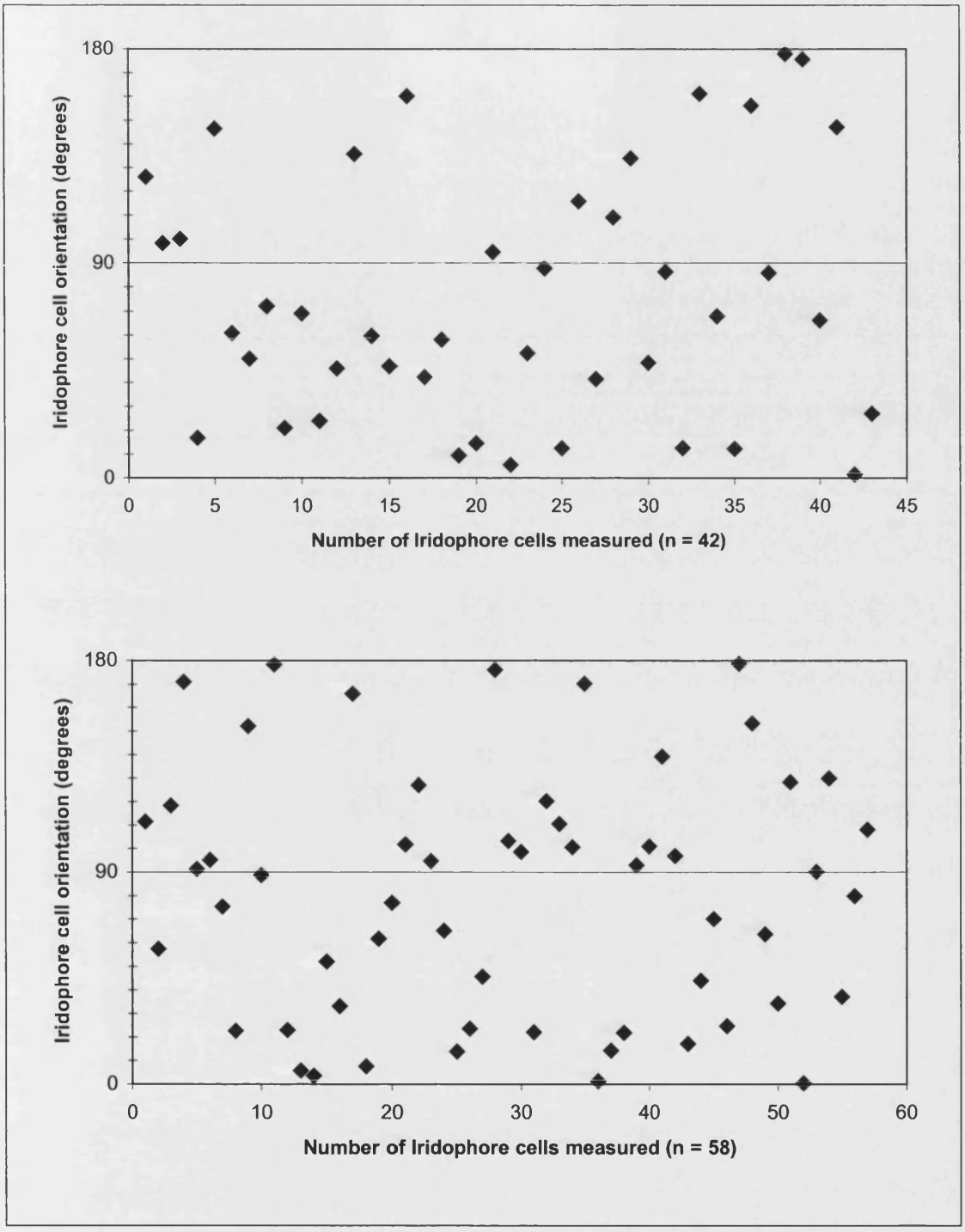

Fig. 27 The orientation of iridophore cells within two bright white fin spots. Each measurement is taken with respect to an overlying horizontal chromatophore organ (0^{o}) and was recorded using Optimas image analysis software.

DISCUSSION: DERMAL IRIDOPHORE CELLS

The precise arrangement of nanometer scale elements within any biological system is remarkable. The platelets contained within the iridophore cells are without exception. As they are of a constant thickness and evenly spaced, it suggests that the platelets are specialised for an optical function. The fact that the cells are then randomly orientated is intriguing, and suggests that this secondary arrangement is highly significant. I hypothesise that a random arrangement of iridophore cell is responsible for a more uniform, less iridescent colour. This colour can therefore be seen at much larger viewing angles, which may prove advantageous during intraspecific communication and camouflage.

MORPHOLOGY

The dermal iridophore cells of *S. officinalis* are similar to those described in squid (Arnold, 1967; Mirow, 1972). Both cells are elongated and have tapering ends. And contain meandering platelets that are orientated perpendicular to the cells length. The nucleus is also similar in that it is lobed, and like those of *Octopus*, possesses a cytocentrum (Brocco, 1976; Brocco and Cloney, 1980). The most contrasting features of *S. officinalis*' iridophores however, is the presence of an outer cell membrane, a lack of iridosomes, and their random orientation in the bright white regions.

The iridosomal platelet are nanometer thick discs and have a mean diameter of 1.9 (± 0.8) μm and thickness of 109 (± 1.5) nm. This description is similar to that of reflecting cells given by Schäfer (1937 – *S. officinalis*), and their thickness is consistent with data presented for *S. officinalis* (Denton and Land, 1971), *S. esculenta* (Kawaguti and Ohgishi, 1962), *O. dofleini* (Brocco, 1976), and the iridophores of *L. brevis* (Cooper *et al.*, 1990). The diameter of the platelet is not documented for each genus, and is published only for *O. dofleini* (1.7 ±0.1 μm; Brocco, 1976).

Surprisingly, this figure is similar to that of *S. officinalis*, which was not expected since the platelets of octopus are located on the cell surface (see fig. 14).

Iridosomal Platelet Composition

The composition of iridosomal platelets was not considered in detail. However, several observations may assist further research. The micrographs suggest that platelets are homogenous, with high affinity for osmium, eosin, and toludine blue stain. This implies that the platelets are composed of a lipid and protein based substance, since osmium tetroxide stains lipids (Glauert and Lewis, 1998) and eosin is a broad protein stain. A similar osmiophilic capacity has also been observed in squid iridophores (Cooper *et al.*, 1990).

The iridosomal platelets do not appear to be electron dense (suggested by Mirow, 1972) as they are transparent and colourless. A high electron density would absorb wavelengths and render the platelets useless as multi-interference layers. It is the tissue stains that are electron dense and it is for this reason they are used.

Substructure could not be resolved within the platelets. Microtubules are not apparent, and the only structural support appears to be the cytoplasmic channel membrane. Previous investigations that have dissolved this membrane also suggest that it provides a structural function (Brocco, 1976 - *O. dofleini*; Cooper *et al.*, 1990 - *L. brevis*).

I hypothesise that the ribosomal granules, which surround the platelets, may contribute to platelet structure. However, it is unclear if the entire platelet is composed of these granules. Granules have been observed at the edges of platelets in *L. pealii* and *L. opalescens* (Arnold, 1967; Cloney and Brocco, 1983) and may form larger (100 nm) globular units in the platelets of *S. esculenta* (Kawaguti and Ohgishi,

1962). These observations support Rabl's (1900) and Schäfer's (1937) hypothesis that platelets arise from granules within the cytoplasm, but cannot confirm this.

Cytoplasmic Channels

The platelets are contained within cytoplasmic channels, and similar channels can be identified in all dermal iridophore cells. The micrographs suggest that each channel may originate at the cytocentrum, since short length cytoplasmic channels can be seen protruding from it. These channels contain ribosomal granules alongside what are hypothesised to be developing platelets. The platelets are of a relatively small diameter, but have a thickness that is similar to developed platelets. This also complements Brocco's (1976 – *O. dofleini*) hypothesis that iridosomal platelets form in the cytocentrum, and that they are of a constant thickness throughout their history.

The much larger peripheral cytoplasmic channels are not connected to the cytocentrum, and instead appear to be isolated inclusions that do not branch. They contain numerous platelets of larger diameter (mean 1.9 μm) and are hypothesised to be fully developed. In all cross-sections the platelets can be seen to be arranged in edge-on stacks. However, the platelets do not touch and are instead separated by a small region of dark staining cytoplasm: a cytoplasmic bridge.

The channels can be seen running across the cell in both planar and longitudinal sections, and suggests that the channels are continuous across the cell, i.e. a large compartment that extends across the circumference of the cell. The channels therefore contain a tessellation of iridosomal platelets (fig. 28). Such an arrangement would explain why sectioned platelets vary in length, and also why they do not all extend to the outer cell membrane. It was hoped that a transverse section

Fig. 28 Cross-sectional diagram of a dermal iridophore cell from *Sepia officinalis*. Large disc shaped iridosomal platelets flank either side of the nucleus and cytocentrum. The platelets are contained within cytoplasmic channels, which resemble large compartments that extend across the circumference of the cell. A number of iridosomal platelets are contained within the channels and they are stacked upon one another. Each platelet is separated from its neighbour by cytoplasmic gaps, which can be seen in cross-section as cytoplasmic bridges.

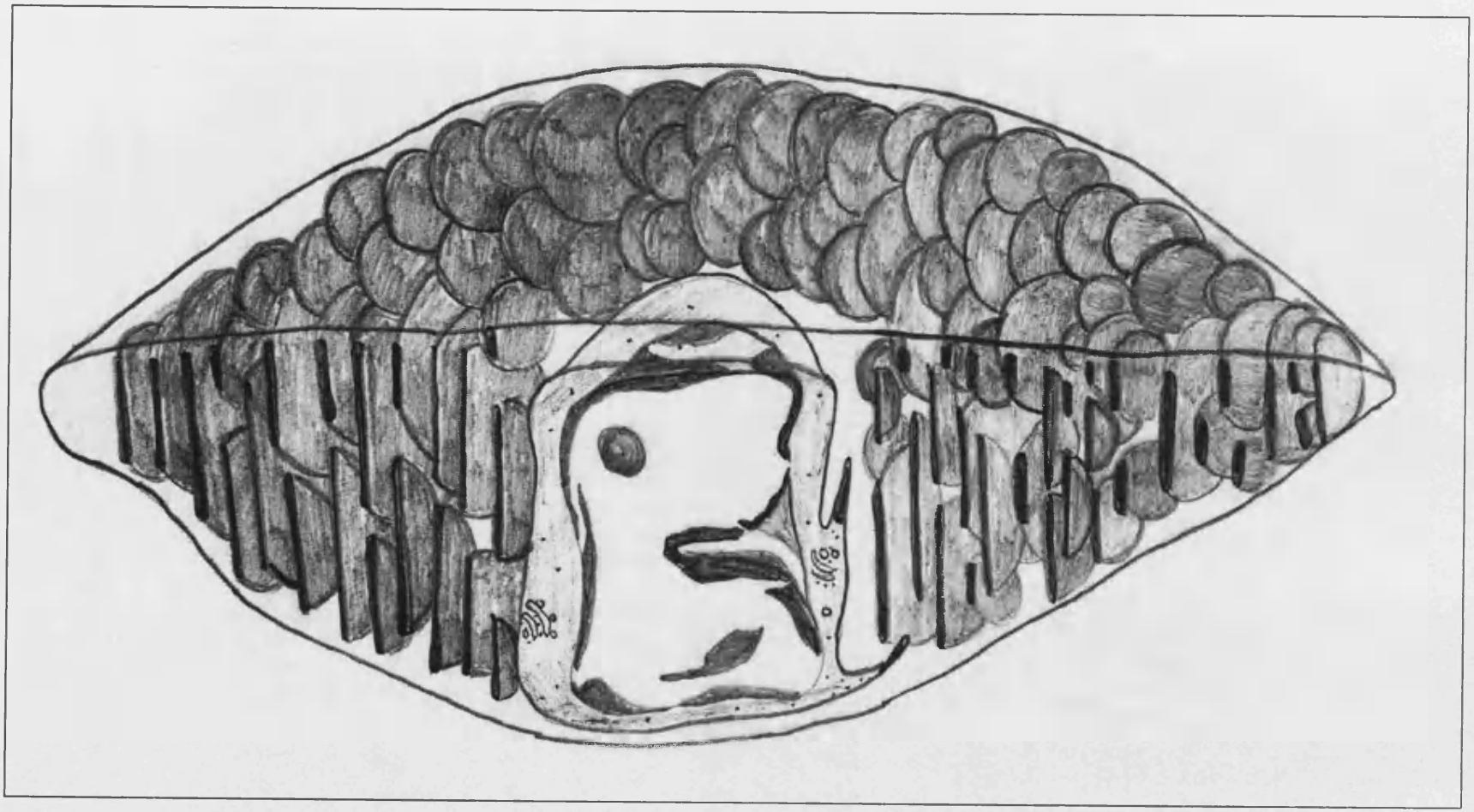

Fig. 28 – Not to Scale

through a cytoplasmic channel would support this hypothesis. However, a suitable section was not obtained. This is not surprising given that the channels are 100 nm thick, and are contained within randomly orientated cells. Serial 3D reconstruction also failed to piece together transverse sections. Shorter length cytoplasmic channels, located at the cells tapering edges, are large enough to contain only one or two (tessellated) iridosomal platelets. Larger cytoplasmic channels, located near the perikaryon, may contain a tessellation of between nine and fifteen iridosomal platelets (see fig. 22).

The cytoplasmic channels sheath the iridosomal platelets, but leave their edges (circumference) exposed to cytoplasm. This observation supports the hypothesis that the platelets are trilaminar (Brocco, 1976), consisting of a platelet that is immersed in cytoplasm, and contained within a membrane. The cytoplasm is not visible along the length of each platelet, as the channel membrane is tight fitting. This tight fit also gives the impression that the channels coalesce slightly along the cytoplasmic bridges, and indicates that the membranes are elastic.

Intrairidosomal Spaces

The most striking feature of the intrairidosomal spaces is that they are unobstructed and appear to contain just cytosol[11]. I hypothesise that this is an optical adaptation, since particles may hinder constructive interference. In order to maintain this clear region, the organelles required for cell function are confined to the cytocentrum. In octopus and squid it appears that the intrairidosomal spaces are kept clear by the iridosome[12] (see micrographs in Mirow, 1972; Brocco and Cloney, 1980), since these iridophores lack an outer cell membrane.

[11] Some fine particles are apparent, however these may be artefacts of the staining procedure.
[12] Groups of iridosomal platelets (see figure 14).

The iridophore cells of *S. officinalis* must communicate with the extracellular space, and I hypothesise that this occurs where the cytocentrum and outer cell membrane make contact (see fig. 15 and 17). This would explain why the nucleus has a central core, elongated perpendicular to cell length.

Optical Mechanisms

The iridophore cells of cephalopods are considered to function as either multi-interference structures or diffraction gratings. I hypothesise that the bright white areas of *S. officinalis* utilise both optical mechanisms. The random orientation of the iridophore cells in these areas may permit both diffraction and multi-layer interference.

Octopus and squid iridophore cells are generally considered to act as multi-interference structures. If this were to be the sole optical mechanism, the majority of platelets would be orientated parallel to the surface of the integument (orthogonal to the direction of incident light). Cuttlefish iridophore cells are generally considered to diffract light (Kawaguti and Ohgishi, 1962; Brocco and Cloney, 1980; Hanlon *et al.*, 1984). In this instance the platelets must predominantly be arranged perpendicular to the surface of the integument (parallel to the direction of incident light). This is clearly not the case in the bright white regions of *S. officinalis.*

The platelets are of a relatively constant thickness within each iridophore cell, and their dimensions do not appear to change in relation to cell orientation. In fact the platelets are similar in thickness throughout the cephalopods (see morphology discussion above).

The two optical theories are distinguished only by the orientation of high refractive index material, with respect to the angle of incident light. From an optical physics point of view the two theories are similar. Both mechanisms require a

collection of transmitting elements, which are separated by a distance that is comparable to the wavelengths of electromagnetic radiation. Upon interaction with this periodic structure, a light beam will have its amplitude, phase, or both, predictably modified (Palmer, 2001). Under these circumstances, orientation is not significant. It is therefore plausible that diffraction may occur within a layered structure, as happens in the gem stone opal (Tilley, 2000). The wavelength formed by a periodic structure is instead dependent upon the geometry of incidence light (fig. 29), and maximum constructive interference will occur only at a certain angle. This is true for both optical mechanisms. Maximum constructive interference generates a peak wavelength of the highest amplitude, and it is this wavelength with which we are most concerned. Either side of the peak wavelength are lower intensity wavelengths, and these form the iridescence. The peak wavelength is therefore visible only at a certain angle and deviation from this angle will result in iridescence.

Given that structural colours have high angle dependence, and they display iridescence, it suggests that they are unsuitable for camouflage. Their conspicuous nature is better suited to communication, and it is for this reason that they are used by shoaling fish and squid (Denton, 1970; Mäthger and Denton, 2001).

Fig. 29 In this figure it can be seen that incident light must complement the angle θ in order to reflect, or diffract the wavelengths. The essential angle can be determined using the equation given in each respective box. Where λ indicates the reflected wavelength and *d* is the optical distance from the leading edge of one platelet to the leading edge of the next. Given the geometry of each system it can be seen that the angle of peak wavelength is directly proportional to the angle of light incidence. Not to scale (based on Nassau, 1983).

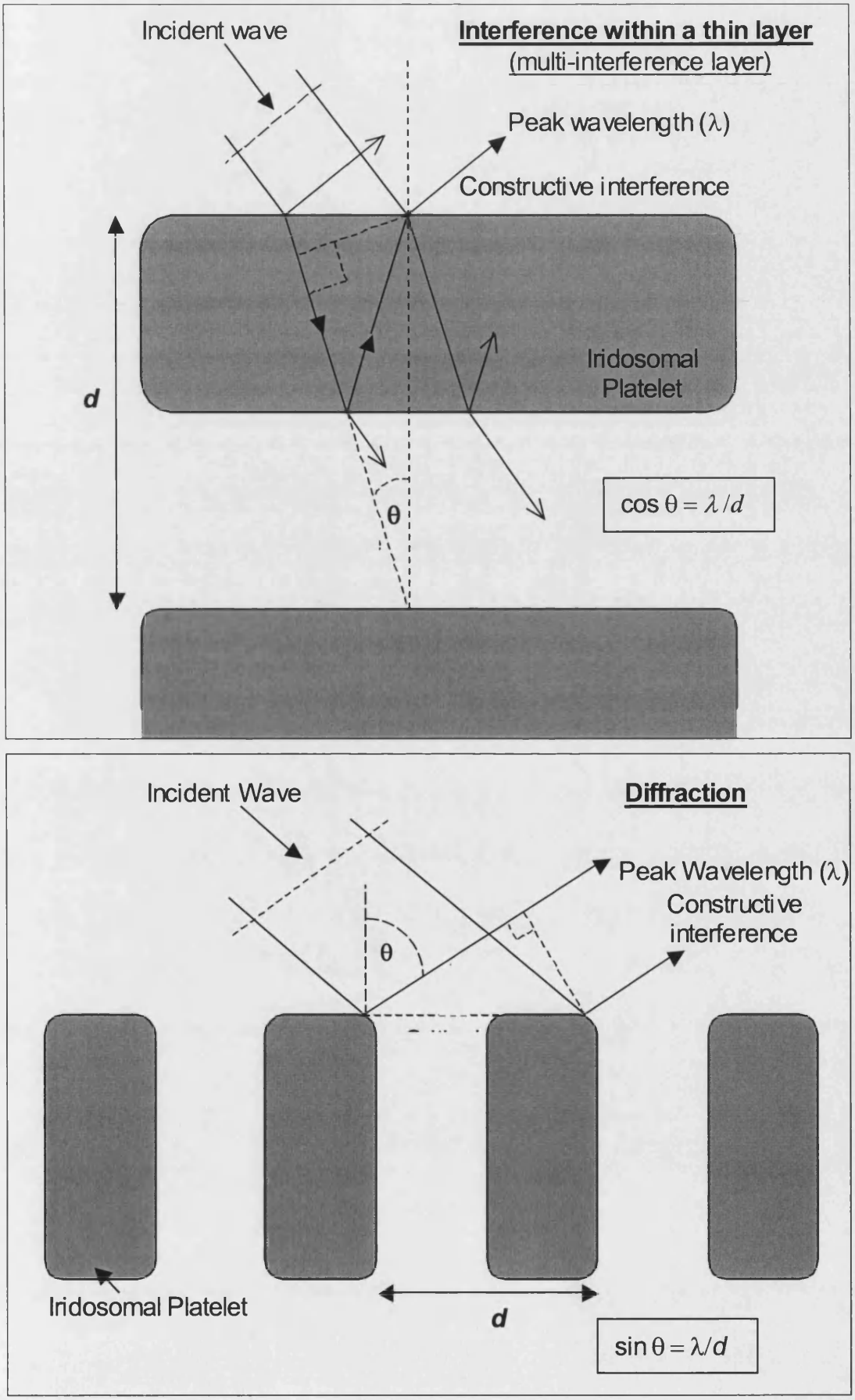
Incident wave
Interference within a thin layer
(multi-interference layer)
Peak wavelength (λ)
Constructive interference
Iridosomal
Platelet
d
θ
cos θ = λ /d
Incident Wave
Diffraction
Peak Wavelength (λ)
Constructive
interference
θ
Iridosomal Platelet
d
sin θ = λ/d

Fig. 29

The limiting factor in structural colours is the narrow critical angle at which the peak wavelength is formed (fig. 29). In order for structural colours to be less conspicuous, the angle of peak wavelength must be increased, and ideally be unlimited for camouflage. This creates a dilemma, since constructive interference is highly angle dependent, and we wish to have a peak wavelength that is not. I hypothesise that this is resolved by the random orientation of iridophore cells.

Hypothesis for random orientation

S. officinalis is shallow dwelling and naturally illuminated by light at a large angle of incidence. This may approach 90° depending on the position of the sun (see appendix page 211). The angle of incidence is therefore compatible with an equally wide range of critical angles[13]. The latter being provided by the random orientation of iridophores.

In order for the iridosomal platelets to function optically, the critical angle of diffraction / multi-layer interference must be met. Given that the iridophores are randomly distributed, countless critical angles will exist throughout the bright white regions. This means that a wide angle of light incidence will compliment many of the critical angles, i.e. numerous iridophores of different orientations will be illuminated at the corresponding angle. An equally wide angle of peak wavelength will then result, since this angle is proportional to the angle of incident light (fig. 29). This means iridophores may function as both diffraction gratings and a multi-layered structures depending upon the angle of light incidence. It is also possible that iridophores (typically those orientated at $\approx 45^{\circ}$) may perform both optical mechanisms at the same time (fig. 30).

[13] The angle of light incidence may also be increased by the light scattering properties of neighbouring leucophore cells.

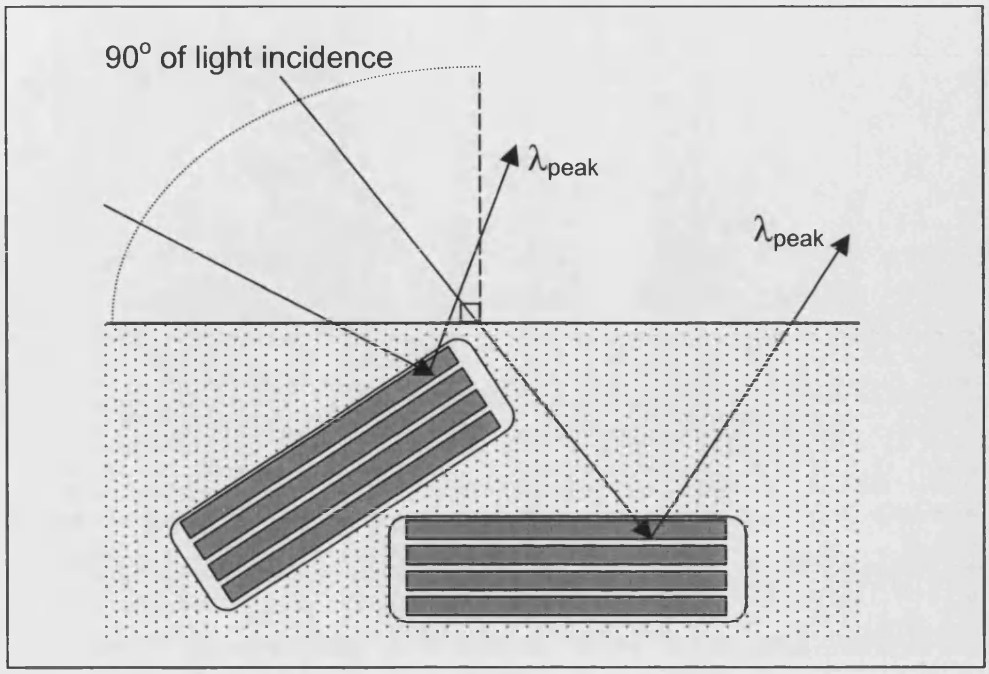

Fig. 30 Randomly orientated iridophore cells illuminated in 90° of incidence may function as independent multi-interference layers, but produce the same peak wavelength. Not to Scale.

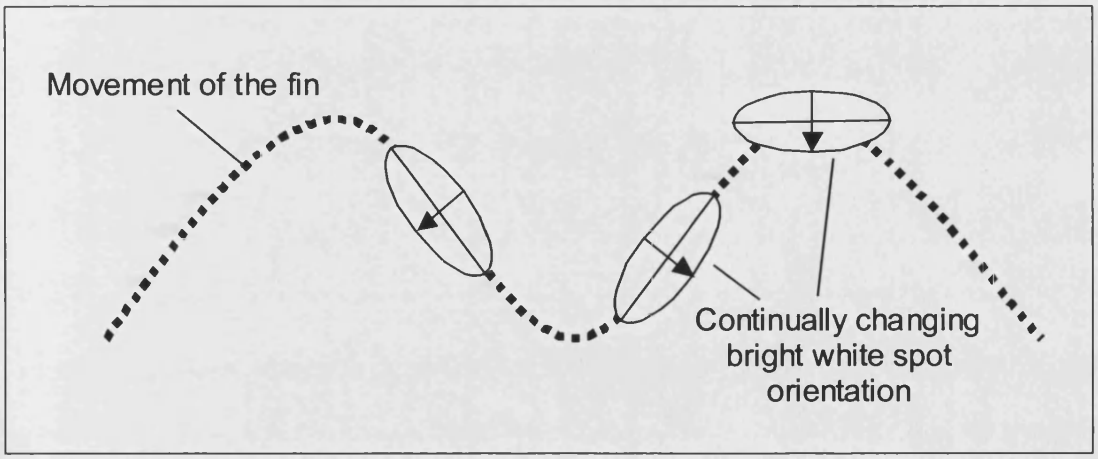

Fig. 31 Movements of the fin will also alter the angle of the iridophore cells. This would produce a rainbow of colour if all iridophores were highly orientated with respect to the integument. However, a random arrangement inhibits this. Not to Scale

A random orientation of iridophores may also enable the peak wavelength to be sustained during movement and textural skin changes. Bright white spots, located on the fin, continually shift as the fin is moved (fig. 31). If these regions contained highly orientated iridophores, we would expect a high degree of iridescence. However, a random orientation may suppress this since λ_{max} will predominate and bleach lower intensity iridescence. Similarly, the orientation of the bright white regions may alter, when elevated on papillae (similar to large goose-pimples, Packard and Sanders, 1971; Froesch and Messenger, 1978 [14]). This activity does not result in a change in peak wavelength.

An equation to determine the peak and band of wavelengths that would result from a random orientation of iridophore cells was kindly derived by Dr. T. Birks (Physics Department, University of Bath):

Peak wavelength:
$$\lambda_{peak} = \frac{4 \times n_p \times n_s \times d}{(n_p + n_s)} \quad (7)$$

Band of Wavelengths:
$$\lambda_{band} = \frac{\pi \lambda_{peak}}{2\chi} \quad (8)$$

$$\chi = \cos^{-1}\left\{\pm\left[\frac{n_p - n_s}{n_p + n_s}\right]\right\} \quad (9)$$

See also appendix p.226

Where n is the refractive index of the iridosomal platelets (p) and intrairidosomal space (s), and d is the distance from the leading edge of one platelet to the leading edge of the next (iridosomal platelet 109 nm + intrairidosomal space 68 nm). The refractive index used is that most commonly published for cephalopod iridophore

[14] Both references refer to elevated bright white regions in octopus only.

cells (n = 1.55 iridosomal platelets, and n = 1.33 intrairidosomal space). The calculated peak wavelength is 506 nm (pale green), and the iridophores are capable of producing an iridescent band of wavelengths between 482.5-531.9 nm (blue-green). This is comparable to the colour that can be seen in the tissue (fig. 4, page 6), and that which is generally regarded to be scattered from the iridophores of *Octopus* and *Sepia*. Observations of the bright white regions also confirm that pale green iridescent colour can be seen at a wide range of viewing angles.

Several factors suggest that the iridophores are efficient reflectors. First, their location 150-200 μm beneath the skin surface means incident wavelengths should easily penetrate. Second, their random orientation is ideal for reflecting a broad angle of light incidence. Third, the large number of equally spaced platelets suggests that iridophores are specialised for constructive interference. It is because iridophores are an efficient reflector that the white regions appear dark cream in transmitted light.

The band of reflected wavelengths complements the chromatophore organs, and suggests they may contribute to camouflage. However, it is more likely that this band of wavelengths contributes to intraspecific communication. Short wavelength blue and green penetrates much further than long wavelength red, which is rapidly attenuated in water. Blue light of 430 nm travels the furthest; it is for this reason the sea is blue, and it is the most abundant wavelength below 10 metres. Wavelengths above and below the 430 nm threshold will penetrate similar distances, but are of a slightly lower intensity. I hypothesise that the band and peak wavelengths, generated by the iridophore cells, operate as an intraspecific pathway for communication. Although the generated intensity is not high, the eyes of *S. officinalis* are tuned specifically towards pale green wavelengths of 492 nm (Brown and Brown, 1958). This fits perfectly within our calculated band of 483 – 532 nm. Importantly, this band is outside the visual range of other cephalopods, which are hypothesised to perceive

480 nm wavelengths. The idea that iridophores convey visual information may also explain why freshly caught specimens (presumably highly stressed) display a very intense iridescent green. This is interpreted as a warning / threat colouration to other cuttlefish.

INTRODUCTION TO CEPHALOPOD LEUCOPHORE CELLS

Leucophore cells are responsible for the bright white appearance of tissue in octopus, cuttlefish and the squid *Sepioteuthis*. Their white appearance is thought to be due to fine ultrastructural elements called leucosomes, and these are hypothesised to have light scattering properties. The formation of white via light scattering mechanisms is common, and the extent of this phenomenon in nature is summarised by Fox (1953).

Packard and Sanders (1971) first used the term leucophore (meaning white-bearer) to describe cells found above iridophore cells in the white patches of *Octopus vulgaris*[15]. The optical properties of these cells were assessed by Messenger (1974), who used coloured light filters to illuminate the tissue of *O.vulgaris, Eledone moschata*, and *S. officinalis*. Each specimen had their chromatophores surgically disabled so that they remained retracted, revealing the underlying tissue. All illuminating wavelengths were reflected by the tissue. This is not surprising since any white surface will do the same. However, Messenger's experiment is significant as it demonstrates that cells other than the chromatophore organs may be involved in background colour matching. It also suggests how colour-blind animals such as cephalopods may effectively camouflage themselves.

Our current understanding of leucophore cells is limited, and is based mainly on observations from *O. dofleini* (Brocco, 1976) and *O. vulgaris* (Froesch and Messenger, 1978). In *Octopus*, leucophore cells are orientated with their broadest surface towards the integument, and each cell possesses approximately 20,000 'club-like' protrusions on its surface. These protrusions have been termed leucosomes, and are thought to be responsible for light scattering. Each leucosomes is composed of a

[15] Froesch and Messenger (1978) describe leucophores below the iridophore cells of *O. vulgaris*.

high refractive index material (Brocco, 1976), similar to that found in the iridosomal platelets (Cloney and Brocco, 1983). Packard and Sander (1971) confirm that the material is not guanine[16], and it is considered to be heterogeneous. As Froesch and Messenger (1978) describe dense centres within the leucosomes of *O. vulgaris.*

The leucophore cells of cuttlefish have not been investigated in detail. A brief description is given by Hanlon and Messenger (1988) in their paper outlining the development of *S. officinalis*. They describe leucophore cells as possessing 1000-2000 electron dense clubs, which are located on the surface of each cell. A micrograph accompanying this statement depicts a cross-section through the tissue, but does not justify their hypothesis. The image illustrates that leucophores are found above and below iridophore cells in *S. officinalis*. It does not suggest that the leucosomes are found on the surface of any cell, and instead shows leucosomes within the intracellular space of leucophore cells. I therefore hypothesise that the leucophore cells of *S. officinalis* are considerably different from those previously described in *Octopus*.

The optical mechanism, or mechanisms, by which leucophore cells scatter light have also not been considered in the literature.

[16] Iridosomal platelets were originally considered to be composed of guanine (Fox, 1953; Arnold, 1967).

RESULTS: LEUCOPHORE CELLS

The leucophore cells of *S. officinalis* are substantially different to those previously described in *Octopus* species. The cells are however, morphologically similar to their neighbouring iridophore cells. The exception being only that the leucophore cells contain spherical leucosomes rather than iridosomal platelets.

Cell morphology

Microscope examination of haematoxylin stained integument, reveals that the leucophore cells are located within the bright white tissue regions of the fin, mantle, arms, and head of *S. officinalis*. The leucophore cells are assorted amongst iridophore cells, which are also found in these regions. No hierarchy is apparent between the two cell types. Each is present in roughly equal numbers, and their distribution is random.

The leucophore cells are elongated, or ovular in shape and have a mean (± S.E.) length of 28.6 (3.1) μm, width of 26.2 (2.6) μm and depth of 10.8 (1.0) μm. In the centre of each cell is a lobed nucleus and cytocentrum. An arrangement which resembles that seen in the iridophore cells. Outside the cytocentrum, dense staining spheres of assorted sizes are found. These are the leucosomes, and they are situated within the clear cytosol, which fills the space between the cytocentrum and outer cell membrane (figs. 32-38).

Nucleus

The nucleus is lobed and elongated in shape, extending perpendicular to the cells overall length. It has a mean (± S.E.) length of 9.7 (1.0) μm and width of 5.3 (0.9) μm. Large infolds in the nuclear membrane, give the nucleus a multi-lobed appearance (fig. 33). It is composed of euchromatin and peripherally distributed hetrochromatin (figs. 32-35). Sporadic gaps within the hetrochromatin highlight the

position of nuclear pores, and these pass directly into the cytocentrum. The cytocentrum immediately borders the nucleus, and contains all of the organelles required for cell function. Most apparent in the cytocentrum are free ribosomal granules along with rough and smooth endoplasmic reticulum. Vacuoles of various sizes can also be seen, together with Golgi apparatus, and mitochondria (figs. 33-34).

In a number of micrographs developing leucosomes can be seen emerging from the cytocentrum (fig. 32-35), and two different developmental states has been observed. First, leucosomes can be seen emerging / budding out from within the cytocentrum (figs. 32, 33, and 34). Second, short cytoplasmic channels with one or a number of leucosomes can be seen extending from the cytocentrum (fig. 32, 35).

Cytoplasmic channels

Developed leucosomes (found outside the cytocentrum) are contained within cytoplasmic channels, along with ribosomal sized granules and a dark staining cytoplasm. These channels extend to the periphery of the cell, but are not ordered like those of an iridophore cell. Instead each channel is branched and highly convoluted. It is therefore difficult to map the entire length of a cytoplasmic channel within a leucophore cell.

Several cytoplasmic channels originate at the cytocentrum, extending directly from it. These channels are a continuation of the cytocentrum membrane, and contain ribosomes and cytoplasm from within the cytocentrum. Several of these attached channels extend to the periphery of the cell (fig. 32).

The meandering path of peripheral cytoplasmic channels means that they regularly taper out of the plane of section. It is in only one micrograph that a number of cytoplasmic channels have remained in section. These peripheral cytoplasmic

Fig. 32 Longitudinal section through a leucophore cell.

A typical leucophore cell that is elongated in shape. The multi-lobed nucleus is central to the cell and is surrounded by a cytocentrum (light grey). Organelles with the cytocentrum regulate protein synthesis and general cell processing, whilst dense staining spherical leucosomes outside the cytocentrum are responsible for light scattering. A cytoplasmic channel connects each leucosome, and in this section a channel can be seen extending from the cytocentrum to the periphery of the cell (arrow).

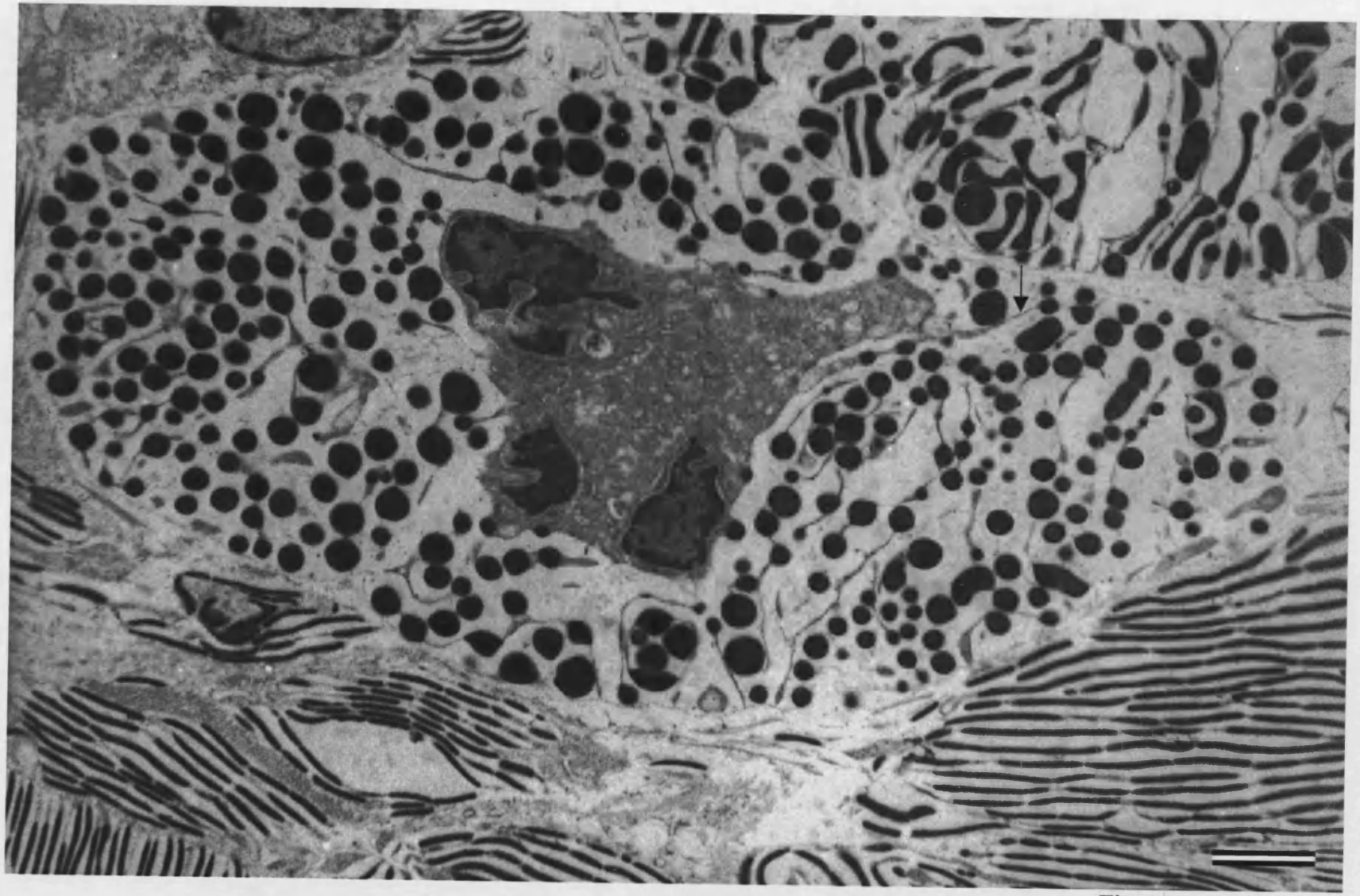

Fig. 32 Scale bar = 2 μm

Fig. 33 Leucophore cell nucleus.

The nucleus is composed of a central nucleolus (Nus) that is surrounded by euchromatin (Eu) and a darker staining hetrochromatin (Het). Nuclear pores within the nuclear membrane pass into the cytocentrum (Cyc), which surrounds the nucleus. Many of the organelles contained within the cytocentrum can be clearly seen in this section. These include rough endoplasmic reticulum (RER), mitochondria, Golgi apparatus and developing leucosomes (arrow) that can be seen emerging from the cytocentrum membrane. Fully developed leucosomes (Ls) are found outside the cytocentrum and throughout the periphery of the cell.

Fig. 33 Scale Bar = 1μm

Fig. 34a and **34b** Three developing leucosomes can be seen within the confines of the cytocentrum membrane. Each appears to be emerging, or budding out from the cytocentrum membrane.

Please note the developing leucosomes are large.

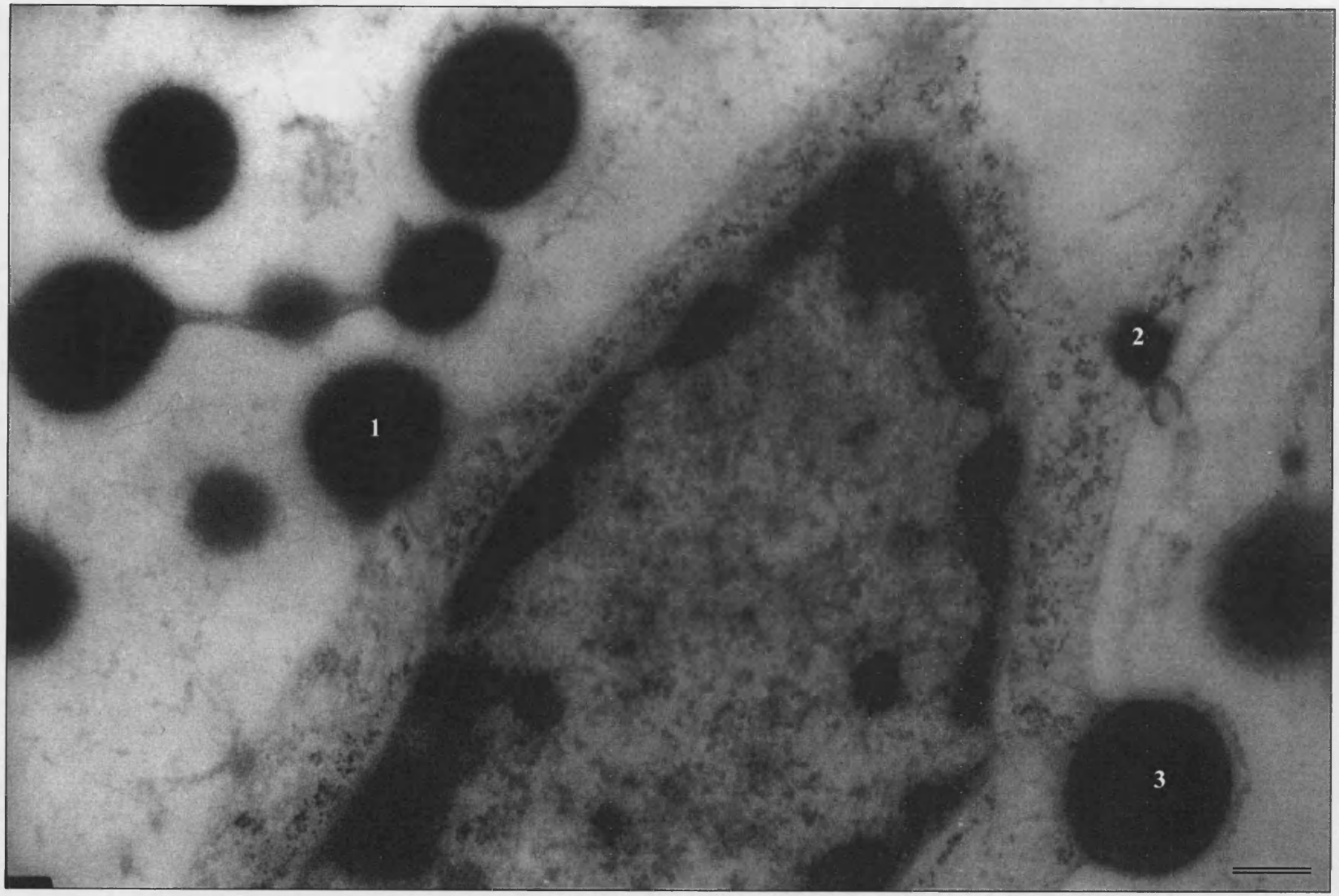

Fig. 34a Scale Bar = 200nm

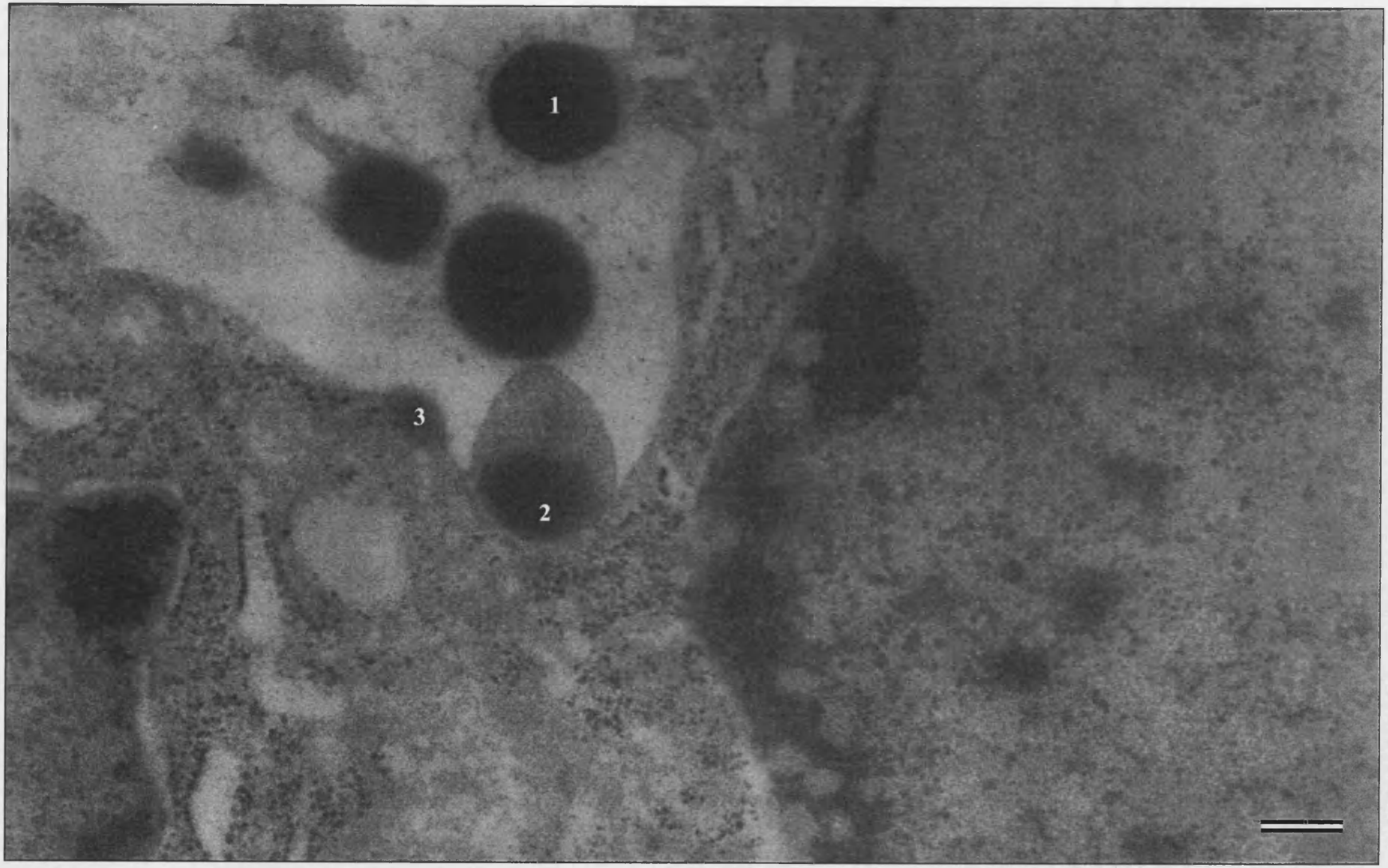

Fig. 34b Scale bar = 200 nm

Fig. 35 Developing leucosomes can be seen extending from the cytocentrum in short cytoplasmic channels. Each of these channels is an extension of the cytocentrum membrane, and some components of the cytocentrum can be seen within the connected channels.

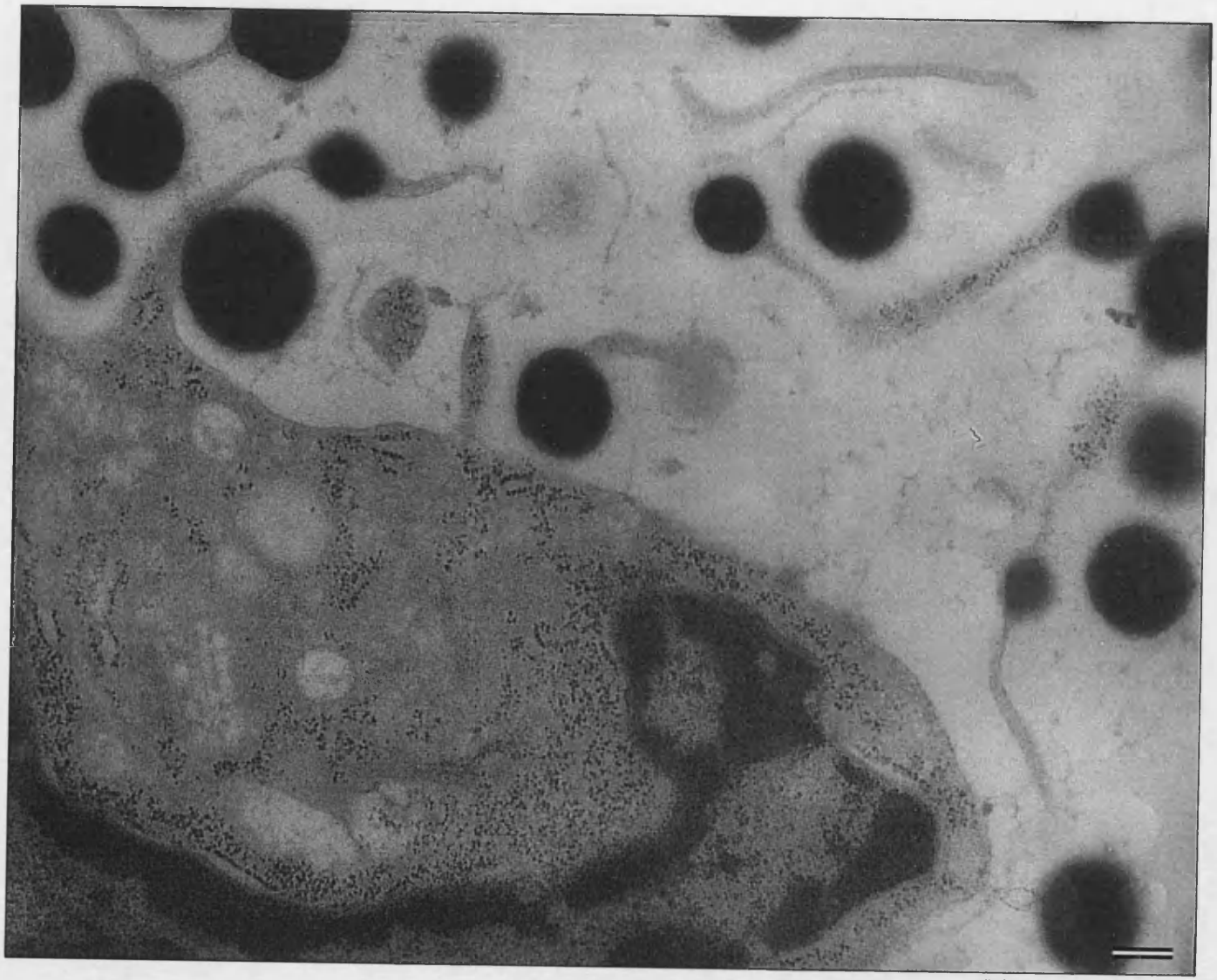

Fig. 35 Scale Bar = 200nm

Fig. 36 This figure illustrates some of the similarities between a leucophore and a neighbouring iridophore. It also highlights the different sizes of the optical organelles found in each cell.

Each optical element is contained within a cytoplasmic channel, and they are all linked via cytoplasmic bridges. The bridges have a similar content, which includes a dark staining cytoplasm, and ribosomal granules. The width of each bridge is also similar in both cells, and this is surprising given the size of each respective optical element.

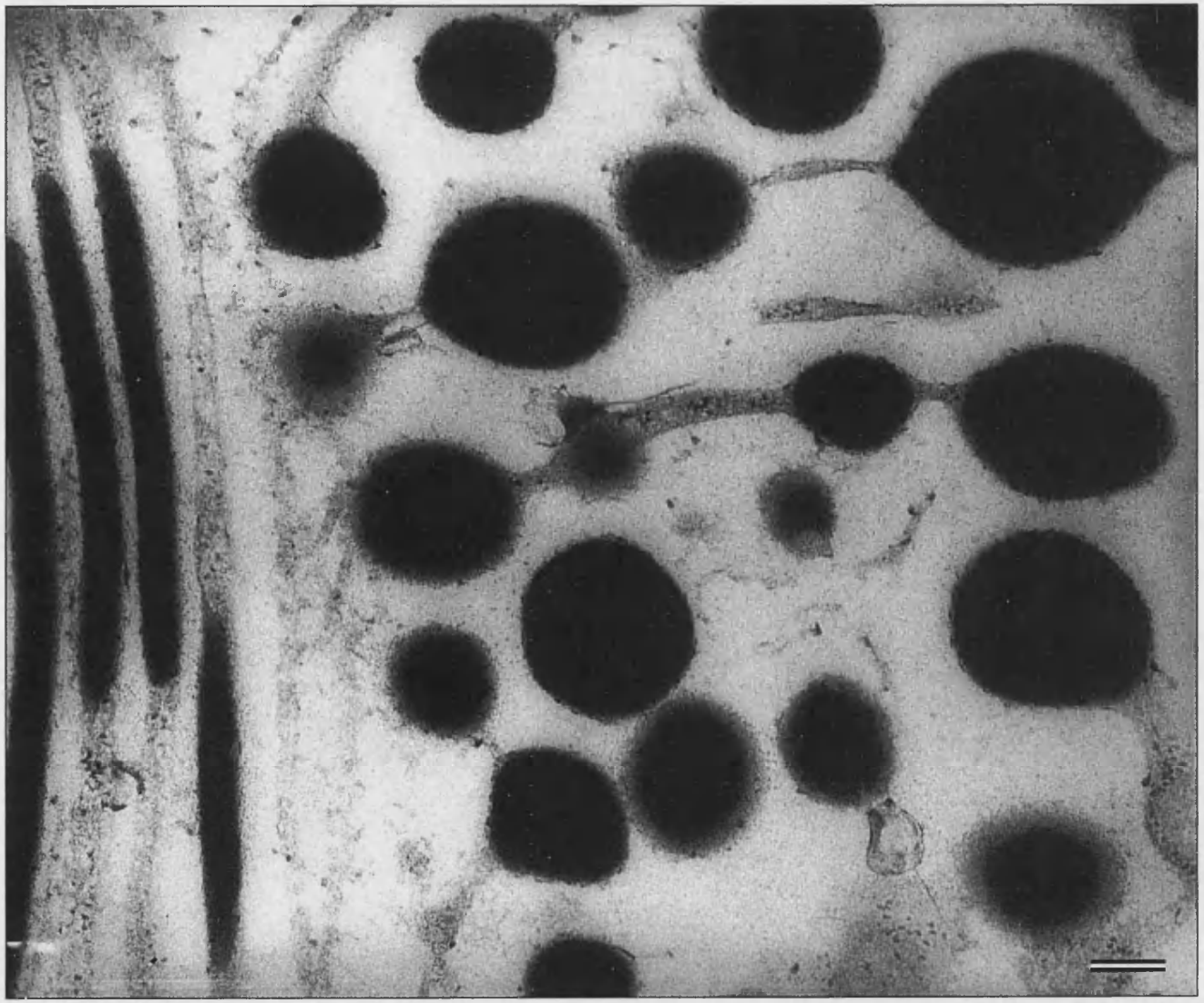

Fig. 36 Scale Bar = 200nm

Fig. 37 A planar section through a leucophore cell.

The peripheral leucosomes located near the outer cell membrane (line that extends diagonally from the scale bar) are joined by a circular arrangement of cytoplasmic channels.

Fig. 37 Scale Bar = 200nm

Fig. 38 Higher magnification of figure 37.

Each cytoplasmic channel sheaths the leucosomes that it contains. The cytoplasmic channel membrane extends over each leucosome, following its profile and covering the majority of its circumference. However, the membrane does not fully encircle the leucosome; a small region is left uncovered on either side. The cytoplasmic channel then continues to the next leucosome, forming a cytoplasmic bridge.

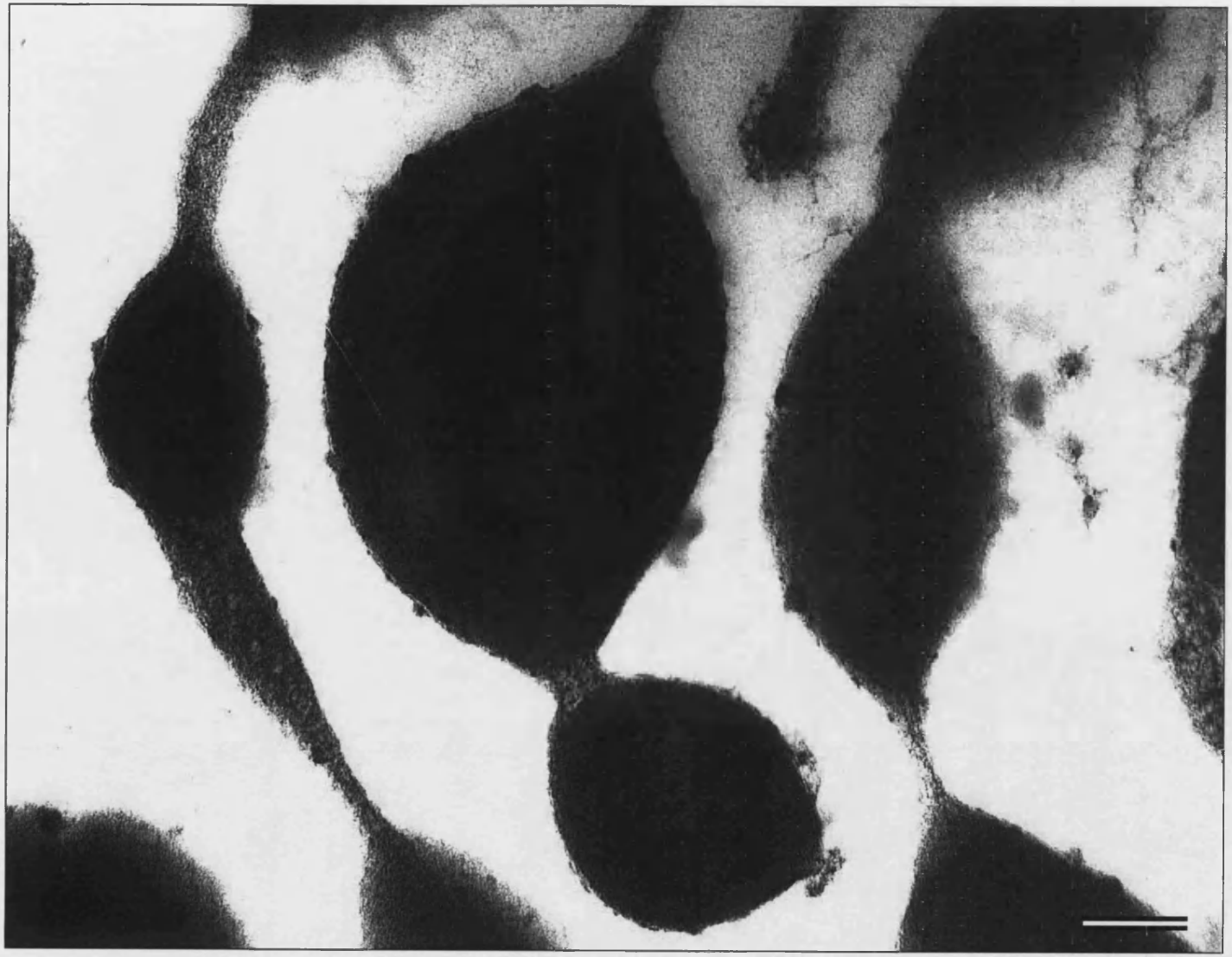

Fig. 38 Scale Bar = 100nm

channels appear to be joined in ring-like structures (figs. 37 and 38), and suggest that the leucosomes are connected in a series of concentric rings.

Cytoplasmic channels extend around the leucosomes, sheathing them in the same way as an iridosomal platelet. Again, the channel membrane does not completely enclose the leucosomes, but leaves a small region on either side exposed to the cytoplasm contained within the channel (figs. 32-39). Each cytoplasmic channel then extends from one leucosome to the next, forming a series of cytoplasmic bridges (fig. 38).

The channel membrane appears to retract around each of the leucosomes before forming a cytoplasmic bridge. The bridge is therefore considerably thinner (≈ 40 nm width) than the leucosome it encloses. Interestingly, the width of each bridge is similar to that observed in the iridophore cells, which contain significantly thinner platelets (figs. 21 and 37).

Leucosomes

Each leucosome is an isolated mass of material that is approximately spherical, and varies greatly in size (fig. 39). Serial sections suggest that diameters may range from 166 - 992 nm within a single cell (leucophore 5, fig. 39; determined using equations 3-6, page 66).

Leucosomes are naturally colourless and transparent, and do not appear to be electron dense. A stain is required to resolve the leucosomes clearly, and they displayed a high affinity for eosin, osmium tetroxide and toludine blue. This affinity, and intensity of staining is identical to that observed for the iridosomal platelets. However, unlike the iridosomal platelets, leucosomes appear to be heterogeneous. Under high magnifications densely stained granules can be observed within the

leucosomes (fig. 40). Each granule is between 12 and 25 nm in diameter, and no other substructure is apparent.

The leucosomes are distributed randomly with in a leucophore cell. Nearest neighbour calculations (see appendix page 214) from four leucophore cells provide an R-value of between 0.47 and 0.63 (R = 0 is aggregated, and R=1 indicates a random distribution; Clark and Evans, 1954), suggesting that distribution is half way between random and aggregated.

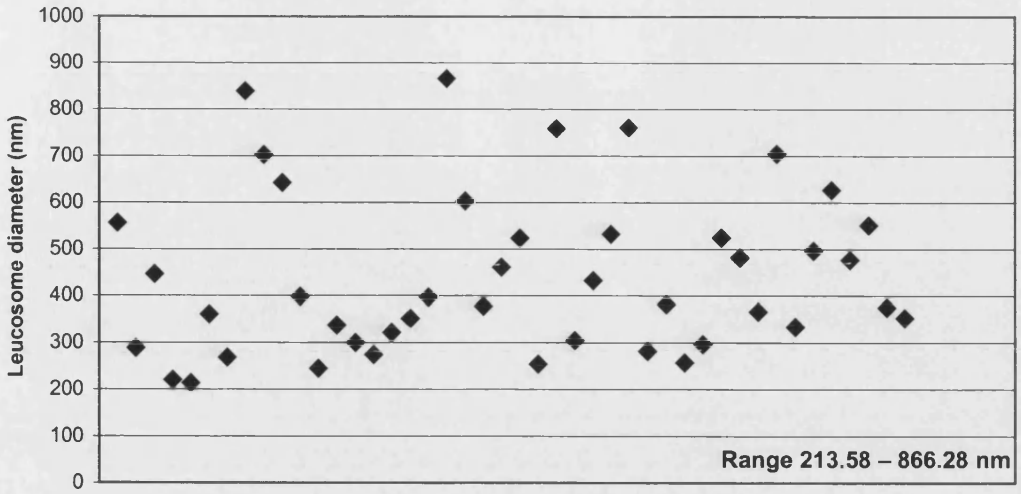

Leucophore cell 1 (leucosomes n = 44)

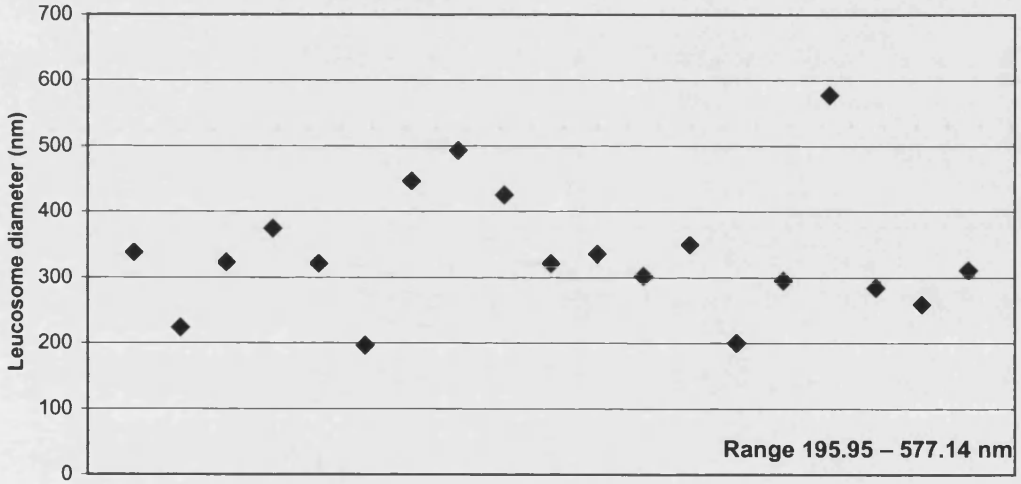

Leucophore cell 2 (leucosmes n=19)

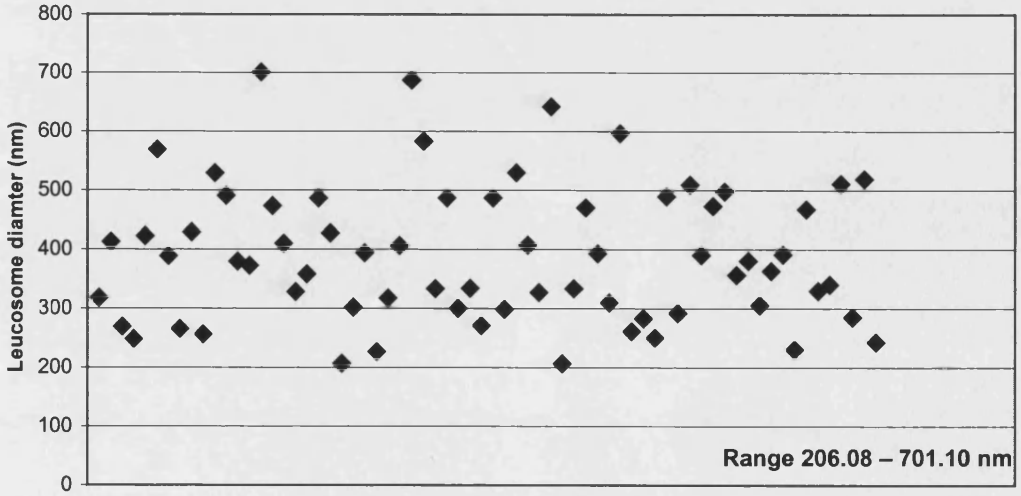

Leucophore cell 3 (leucosomes n = 68)

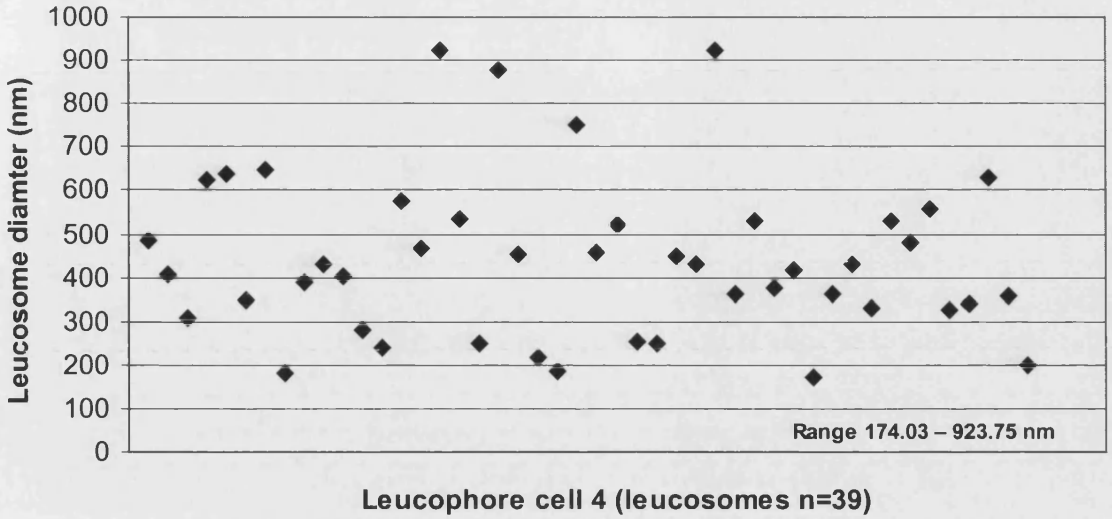

Leucophore cell 4 (leucosomes n=39)

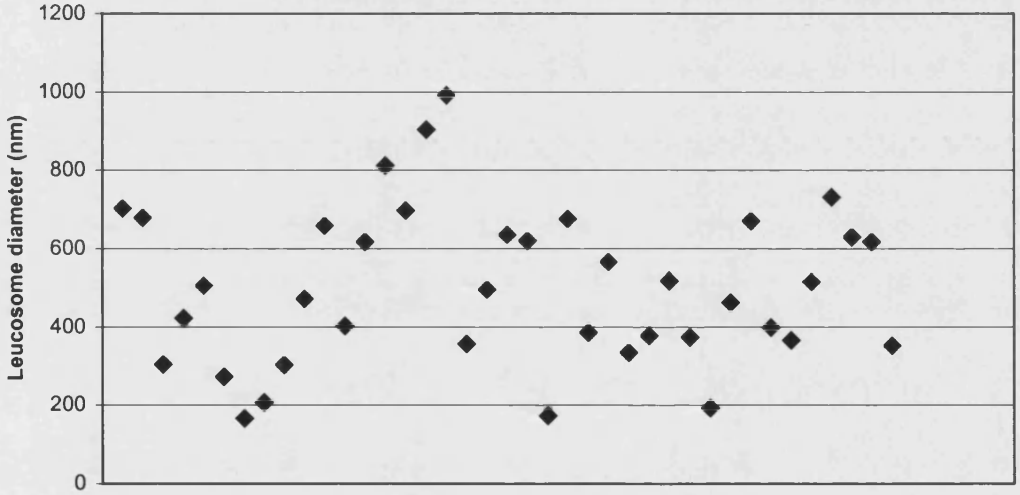

Leucophore cell 5 (leucosmes n = 40)

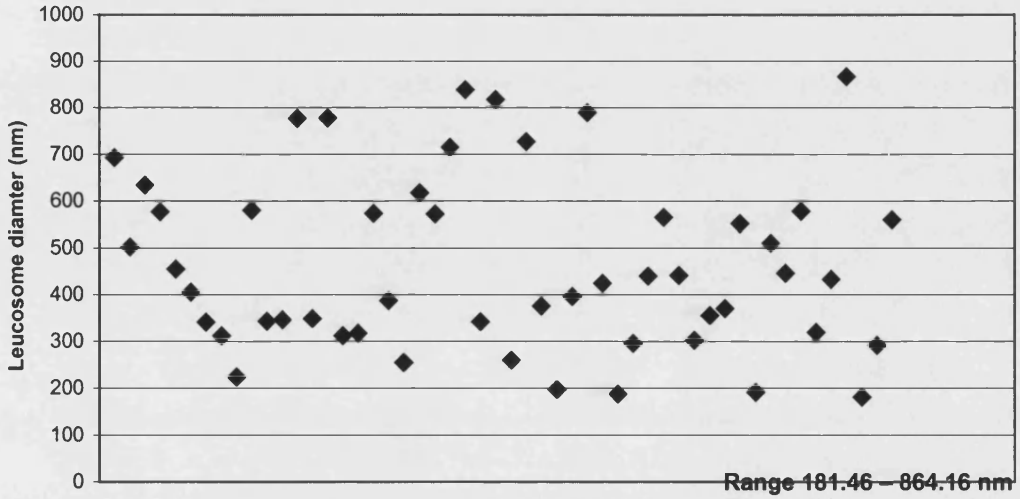

Leucophore cell 6 (leucosomes n=52)

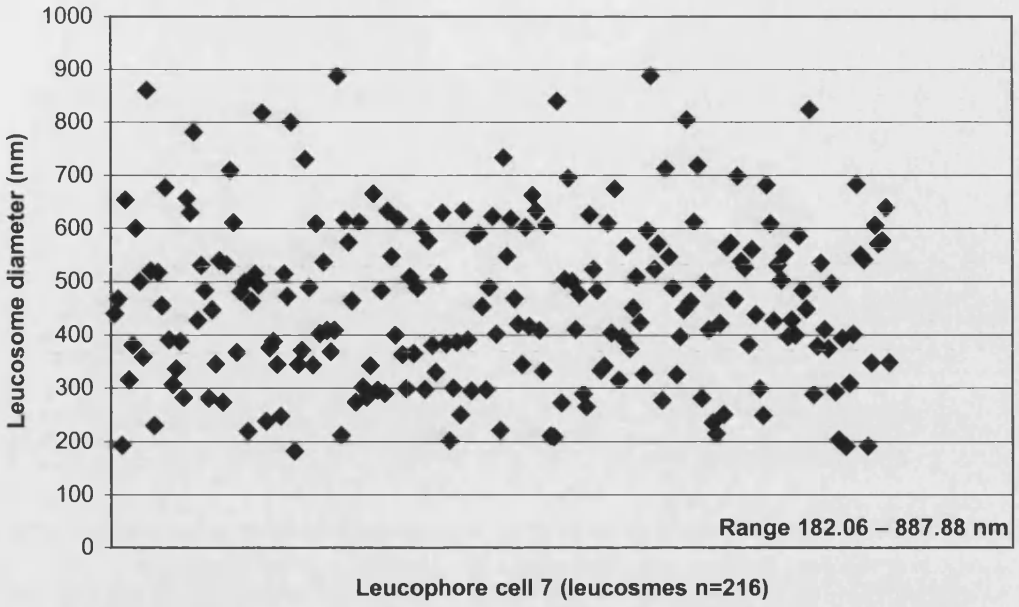

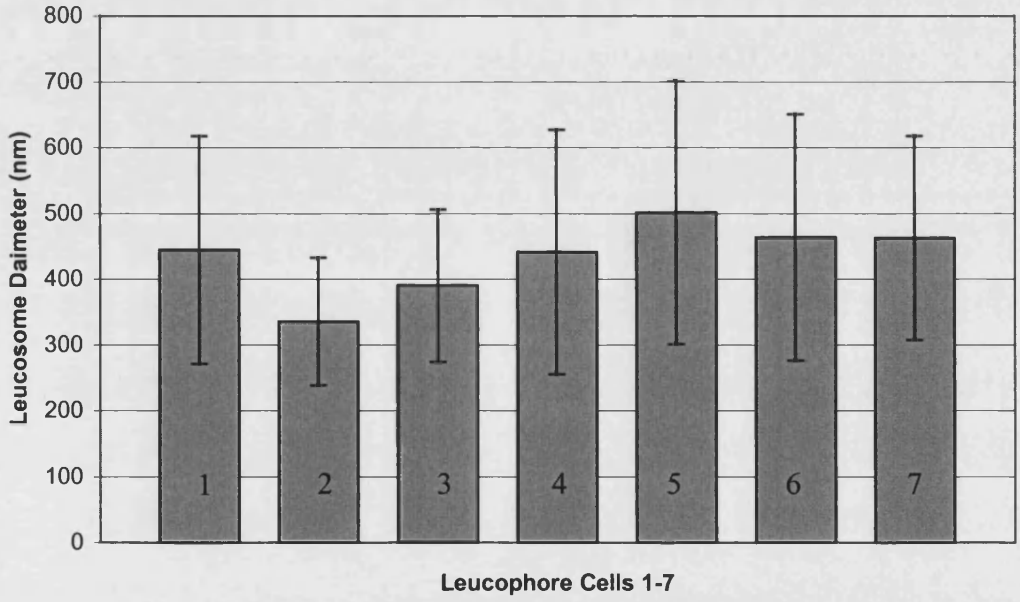

Fig. 39 The diameter range of leucosomes found in seven different leucophore cells. Graphs 1-6 show the maximum calculated diameter of each leucosome found in six serial sectioned leucophore cells. Graph 7 shows the diameter of leucosomes from one longitudinal section through a leucophore cell (i.e. not serial sections). Graph 8 shows the mean leucosome diameter, and standard deviation from the mean for all seven leucophore cells.

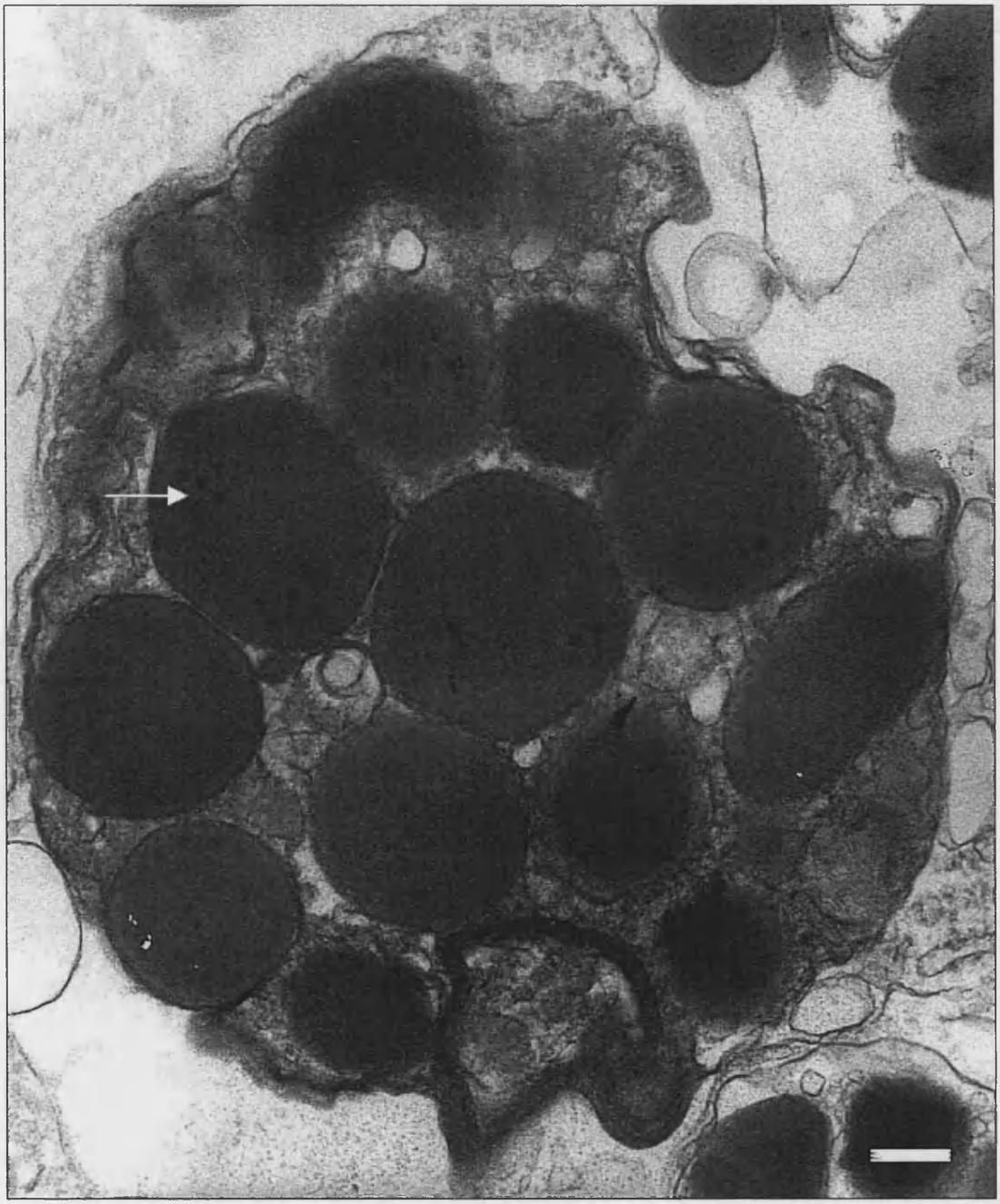

Fig. 40 Transverse section through a leucophore cell (tilted 10°). Dark granules (arrow) can be seen inside the leucosomes, suggesting that their composition is heterogeneous.

Scale bar = 200nm.

DISCUSSION: LEUCOPHORE CELLS

The leucophore cells of *S. officinalis* contain spherical leucosomes of various diameters. Each leucosome is contained within a cytoplasmic channel, and is located within the cell rather than on the cell surface (as in *Octopus*). The spherical shape and intracellular distribution of leucosomes confirms that the leucophore cells of *S. officinalis* are significantly different from those previously described in *Octopus*. However, their function as a light scattering cell is hypothesised to be the same.

MORPHOLOGY

The overall morphology of *S. officinalis* leucophores is surprisingly similar to that of their neighbouring iridophore cells. Both cells are comparable in shape and size, and both possess a cytocentrum. Their only distinguishing feature is the size and shape of their respective optical elements. Disc-shaped iridosomal platelets are considerably larger (diameter ≈1.9 μm) than the spherical leucosomes (≈166-992 nm) found within a leucophore cell.

Function of the Cytocentrum

The cytocentrum is a specific region of the cell, which contains all of the organelles required for cell regulation. This means that cellular processes, and leucosome development occur within a confined region, and does not hinder the cells optical function. As a result, the surrounding cytosol is clear. It does not contain any organelles, other than leucosomes.

Leucosome Development

Leucosomes develop within the periphery of the cytocentrum (fig. 32-35). Each is approximately 450 nm in diameter, and can be distinguished from the developing platelets observed in iridophore cells. As they develop, the leucosome

bulge out from the cytocentrum, and form small cytoplasmic channels. These attached channels then extend into the periphery of the cell and in doing so recruit more developing leucosomes from the cytocentrum. Whether or not the channel then detaches from the cytocentrum is not clear. However, given the large number of channels within a leucophore cell, and the relatively low number that are attached to the cytocentrum, it suggests that most channels are unattached.

The hypothesis that channels extend from the cytocentrum implies that all cytoplasm channels are created from cytocentrum membrane. This would explain why peripheral unattached channels contain ribosomal sized granules and a dark staining cytoplasm that is identical to that of the cytocentrum. Also the fact that developing iridosomes and leucosomes have been observed in their respective cell types is highly significant. It suggests that the cells are predetermined to be either an iridophore or a leucophore cell, and does not support Brocco's (1976) hypothesis that iridophore cells differentiate into leucophores [in *S. officinalis*].

Cytoplasmic channels

Each cytoplasmic channel follows the profile of the leucosomes that it contains, and also links the leucosomes together in a series of cytoplasmic bridges. The micrographs suggest that the channels are tight fitting, as little can be seen between the channel membrane and a leucosome. Each cytoplasmic bridge is also considerably smaller in width ($\approx$ 95 nm) than the leucosomes it contains, giving the impression that the channel membrane is elastic. Interestingly, the width of each cytoplasmic bridge is similar in both iridophore and leucophore cells (fig. 36).

Hanlon and Messenger (1988) noted the leucophore cells contain branching cytoplasmic channels, a phenomenon that has not been recorded in iridophore cells. The reason for channel branching is unclear. However, the mechanism is probably

similar to that involved in cytoplasmic channel formation, i.e. leucosomes that bud out from the cytocentrum may also branch out from cytoplasmic channels.

The tangled distribution of cytoplasmic channels usually found in the periphery of the cells does not support the hypothesis that the channels form concentric circles. Figure 37 depicts a circular array of cytoplasmic channels, which suggests that they are arranged in rings, like the skin of an onion or annual rings of a tree. This pattern was observed in only one micrograph, and could not be found again. It is therefore regarded as a sectioning artefact. However, this micrograph and other higher magnification images confirm that the leucosomes are trilaminar, consisting of a central core composed of high refractive index material, a thin layer of cytoplasm, and cytoplasmic channel membrane.

The cytoplasmic channels may have a number of functions. First, their tight fit suggests that they maintain optical element shape, since an internal substructure cannot be seen. And removal of the channel membrane has been shown to disrupt iridosomal platelet shape (Kawaguti and Ohgishi, 1962). Second, the membrane separates the leucosomes from the clear intracellular cytosol which surrounds them. It is therefore a boundary between low refractive index regions. Third, the channels help to disperse the leucosomes throughout the cell.

Intraleucosomal Space

Extracellular components are excluded from the intraleucosomal space by the outer cell membrane. This cytoplasmic region is therefore relatively clear and unobstructed, so as not to interrupt with the optical function of this cell.

Leucosomes and their composition

The leucosomes are naturally transparent and colourless; they are not electron dense. They show a high affinity for toludine blue, eosin and osmium tetroxide, and

stain to the same contrast as the iridosomal platelets. However, the internal composition of a leucosomes is different to that of a platelet. Each leucosome is instead heterogeneous. Dense granules can be observed throughout the leucosomes, and these are similar in size to the ribosomal granules contained within the cytoplasmic channels. This supports Rabl's (1900) and Shäffer's (1937) hypothesis that optical elements arise from granules within the cell, and also Froesch and Messenger (1978) description of heterogeneous leucosomes in *O. vulgaris.*

The leucosomes of *S. officinalis* are approximately spherical, and range greatly in diameter (fig. 39). Their shape is different from the club-like profile described in *Octopus.* This is probably because cuttlefish leucosomes (like the iridosomes) are positioned inside the cell, rather than protruding out from the surface of it. The advantage of this is that spherical objects are considered to scatter light more efficiently.

A wide range of leucosome diameters was expected, since it is hypothesised that the leucophore cells scatter a broad range of visible wavelengths. This is discussed below.

OPTICAL MECHANISMS

I hypothesise that the bright white appearance of the leucophore cells is due to a combination of both Rayleigh and Mie light scattering. Some very large leucosomes may even reflect, rather than scatter the incident wavelengths.

In lay terms Rayleigh and Mie scattering can be thought of as the redirection of an incident wavelength. As a photon interacts with the particle it causes the particle to resonate at the same frequency as the incident wavelength. The particle will therefore radiate this same frequency in many directions. Consequently, the incident wavelength is not altered, it is simply redirected, i.e. scattered (fig. 41). This is known as elastic scattering (see any A-level physics book). The efficiency at which a particle may scatter a wavelength is known as the scattering coefficient[17] and this is dependant upon a particles size. As a general rule, the ideal scattering particle is half the size of the incident wavelength (Tilley, 2000). As a rough guide therefore (not taking into account *n*) leucosomes between 195 nm to 370 nm in diameter are approaching the ideal light scattering point for day light (390–740nm). However, leucosome size range (≈166-992 nm in diameter) far exceeds the requirements of a light scatterer. Given the precise size and distribution of the iridosomal platelets, the size range of leucosomes must be considered as significant. Perhaps there are several different light scattering mechanisms in addition to the general light scattering rule.

Light scattered by particles smaller than the incident wavelength is generally considered to be Rayleigh light scattering. This theory is normally applied to very small particles, typically less than one-tenth the wavelength of the light. But it is also applicable to larger particles (J. Knight - Physics Dept., Univ. Bath, pers. comm.).

[17] The scattering coefficient (μ_s [cm^{-1}]) is analogous to absorption, and indicates the efficiency to which a particle scatters light. It denotes essentially the area around a particle, which that does not receive scattered wavelengths.

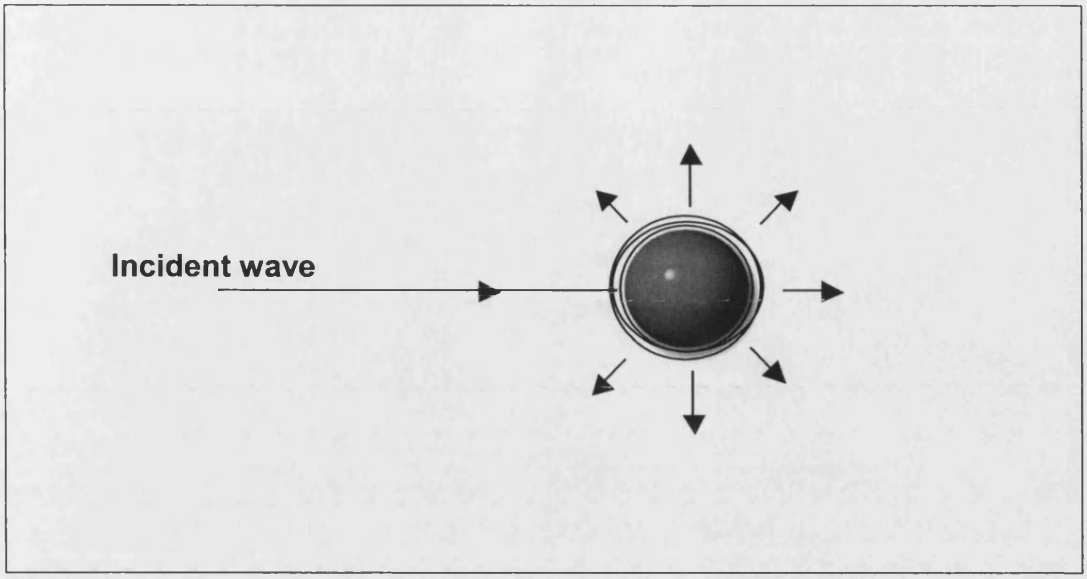

Fig.41 An incident wave may interact with a particle causing it to resonate at the same frequency. The particle will therefore radiate, or scatter, this frequency in a number of different directions.

Small Rayleigh particles scatter light in all directions; this is one of the distinctions of Raleigh light scattering. As particles increase in size the direction of scattering alters, so that more light is radiated forward (fig. 42). This is distinguished as Mie light scattering. There is no clear cut-off between the two methods of scattering and both mechanisms are similar. As a lay rule, particles larger than the incident wavelength are considered as Mie.

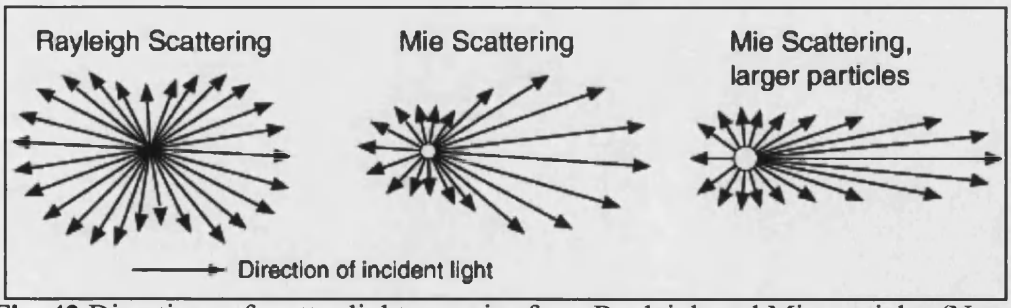

Fig. 42 Directions of scatter light energies from Rayleigh and Mie particles (Nave, 2003)

Mie light scattering occurs predominately in air and water, where large particles in comparison to the incident wavelength scatter light. The theory was

developed in 1908, and has the advantage of being all-embracing; giving the same predictions as the Rayleigh theory for small spherical particles. The complexity of Mie theory is beyond the scope of this project; an online calculator (OMLC, 2001) was used to determine the scattering area and scattering coefficient for a range of leucosomes (fig. 34).

Mie Scattering Calculation

The scattering pattern and coefficient for a range of leucosome diameters was mathematically determined and plotted in figure 43 (1-15). The graphs suggest that the leucosomes demonstrate Mie, rather than Rayleigh scattering, and display predominant forward light scattering. Some backscatter may result from the smaller leucosomes (graphs 1-3). The efficiency of forward scattering can be seen to increase with particle size, and this follows the general rule for Mie scattering. Similarly, as size increases it is the blue, short wavelengths that are scattered most efficiently; small wavelengths incident upon considerably larger particles result in predominately forward scattering. It is important to note that the OMLC programme was not used to calculate multiple light scattering events. The high density of leucosomes within a leucophore cell strongly suggests that multiple light scattering dominates. However, the programme will only calculate the scattering events for objects of the same diameter and uniform spacing. A leucophore cell presents a complex light scattering model, since it consists of a range of leucosome diameters and random spacing. An indication of multiple light scattering paths can instead be interpreted from the individual graphs below. I suggest that the forward propagation of light will become more diffuse with successive scattering.

Fig. 43 (1-15) Displays light scatter from a range of leucosome sizes. The size of each leucosome and incident wavelength is given before each graph. Each wavelength is incident along the x-axis (180-0), and this is indicated in graph 1 by a black arrow.

The leucophore sizes are: the smallest recorded, standard deviation from the mean, mean, and largest leucosome recorded.

The incident wavelengths are: blue (465 nm), peak diffracted wavelength green (506 nm), and red (650 nm). Wavelengths in between these were calculated (in 10 nm increments), these simply compliment the gradual decrease in scattering coefficient.

Each graph includes the direction of scatter for unpolarised (black line), parallel (red line), and perpendicular (blue line) wavelengths. These were calculated to examine any effects of local polarisation, which may occur following scattering.

(For full equation and explanation please refer to OLMC, 2001).

Refractive index of Medium: 1.33 Refractive Index of Sphere: 1.55

1. Blue light (465 nm) by the smallest leucosome recorded (165 nm)

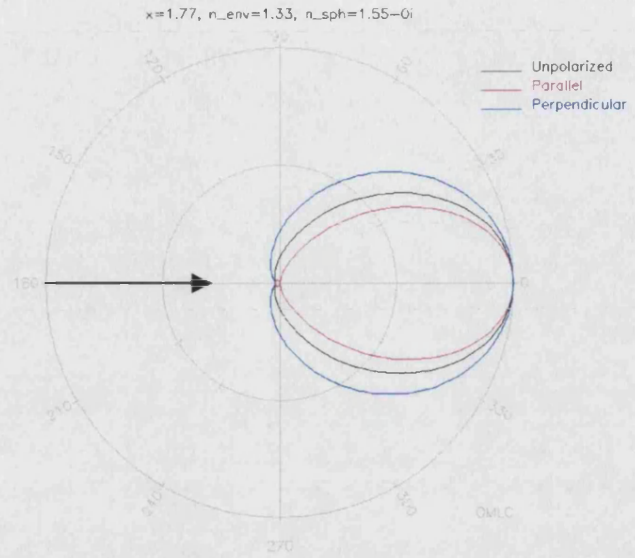

$\mu_s = 2.55$

2. Green light (506 nm) by the smallest leucosome recorded (165 nm)

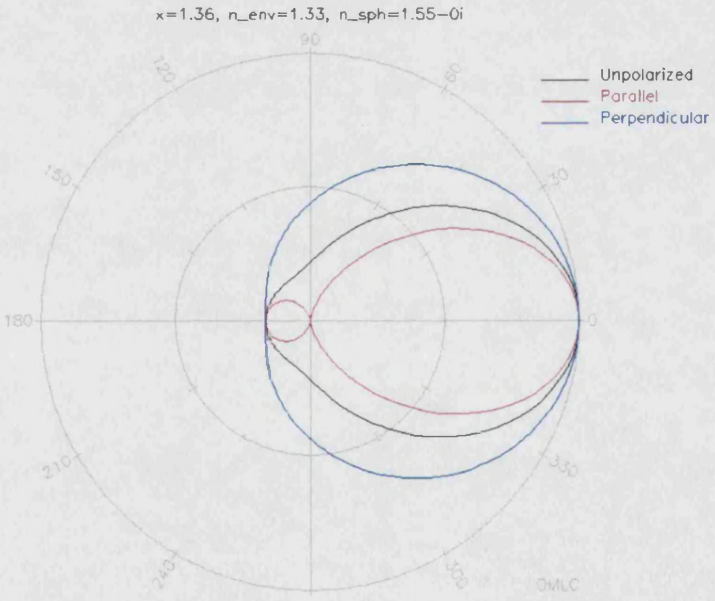

$\mu_s = 1.3$

3. Red light (650 nm) by the smallest leucosome recorded (165 nm)

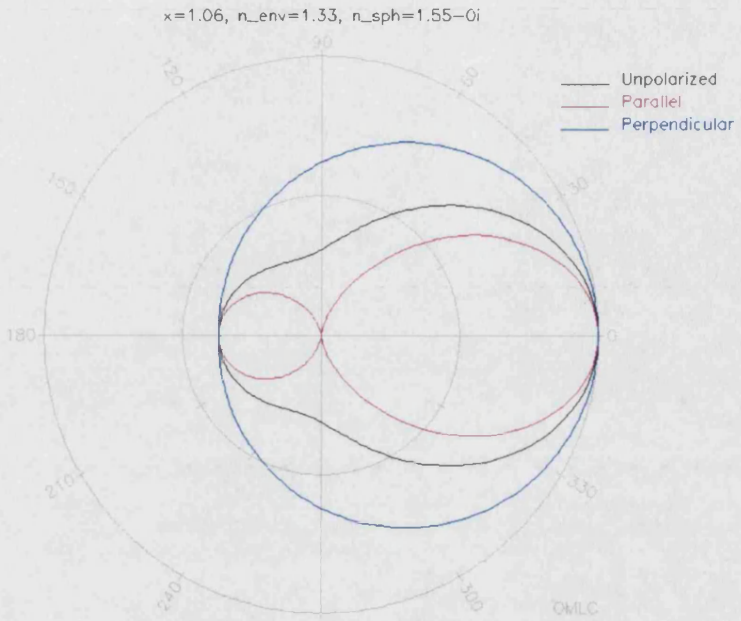

$\mu_s = 0.603$

4. Blue light (465 nm) by leucosome 301nm in diameter (St. Dev. from mean)

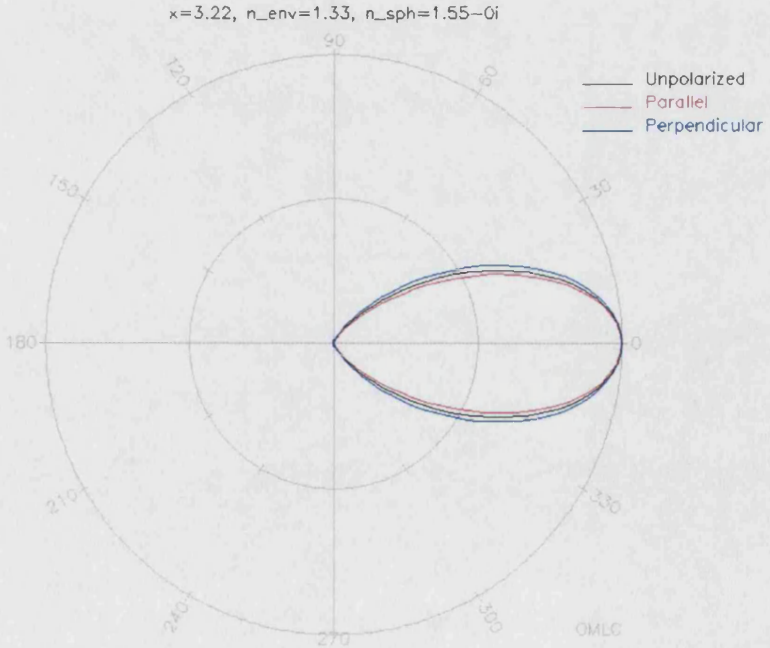

$\mu_s = 36.9$

5. Green light (506 nm) by leucosome 301nm in diameter (St. Dev. from mean)

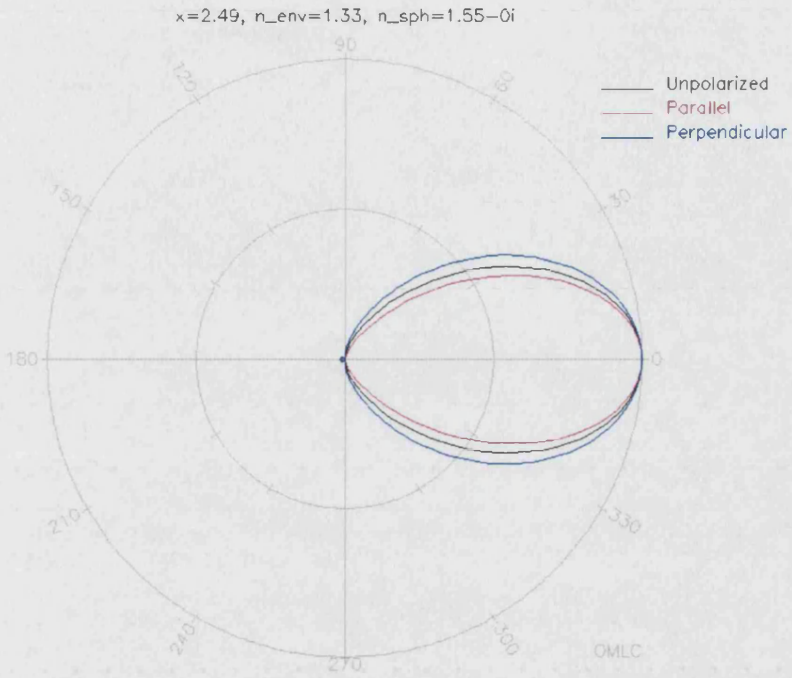

$\mu_s = 20.5$

6. Red light (650 nm) by leucosome 301nm in diameter (St. Dev. from mean)

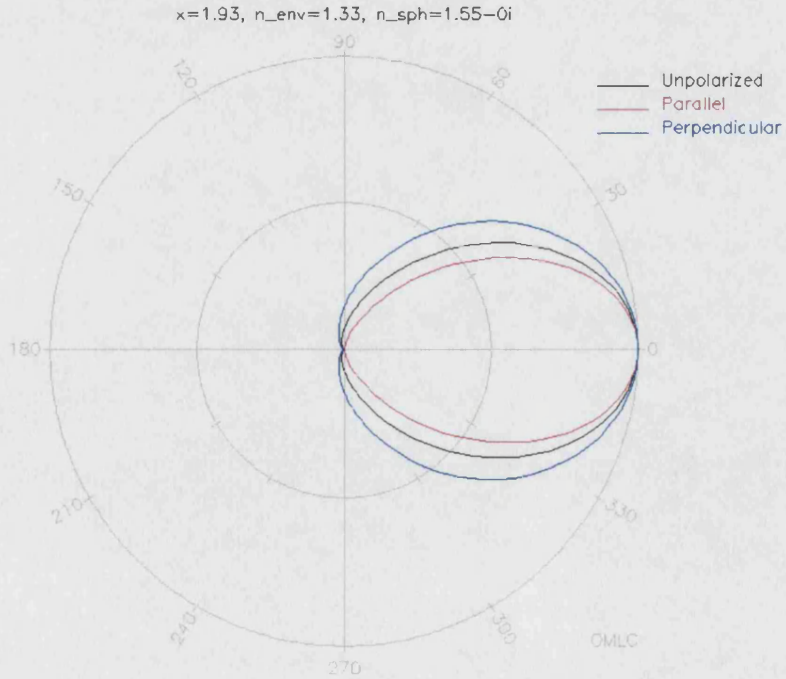

$\mu_s = 10.6$

7. Blue light (465 nm) by mean leucosome diameter (501 nm)

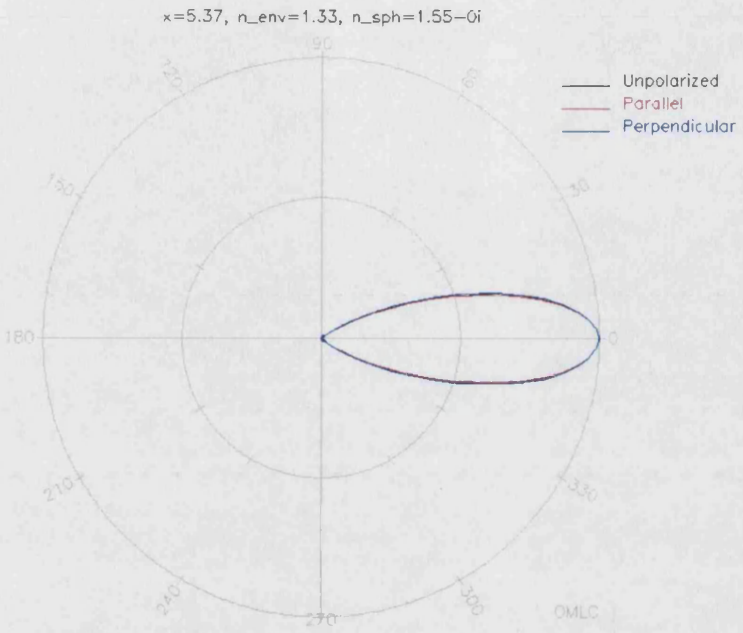

$\mu_s = 283$

8. Green light (506 nm) by mean leucosome diameter (501 nm)

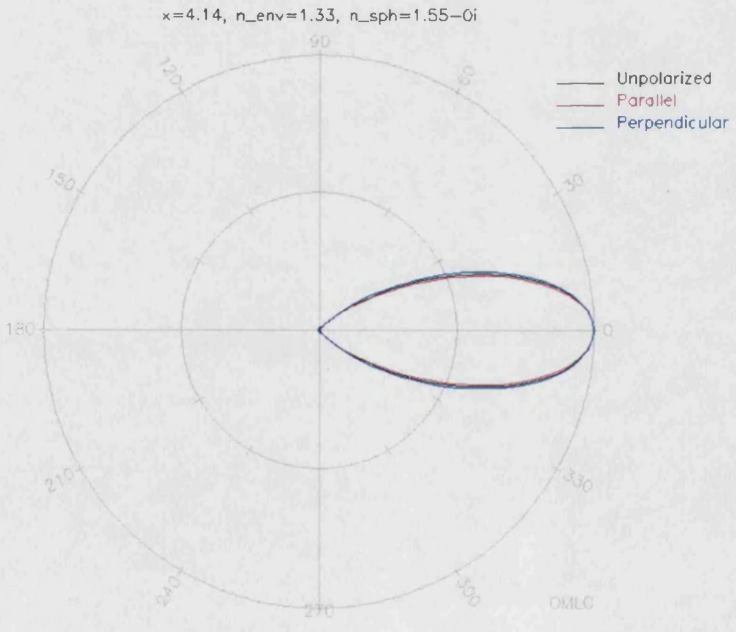

$\mu_s = 173$

9. Red light (650 nm) by mean leucosome diameter (501 nm)

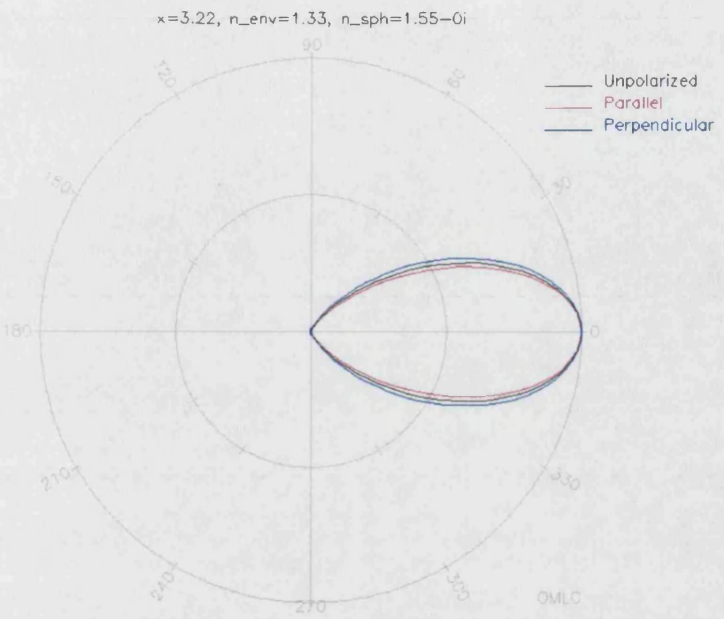

$\mu_s = 102$

10. Blue light (465 nm) by leucosome 702 nm in diameter (St. Dev. from mean)

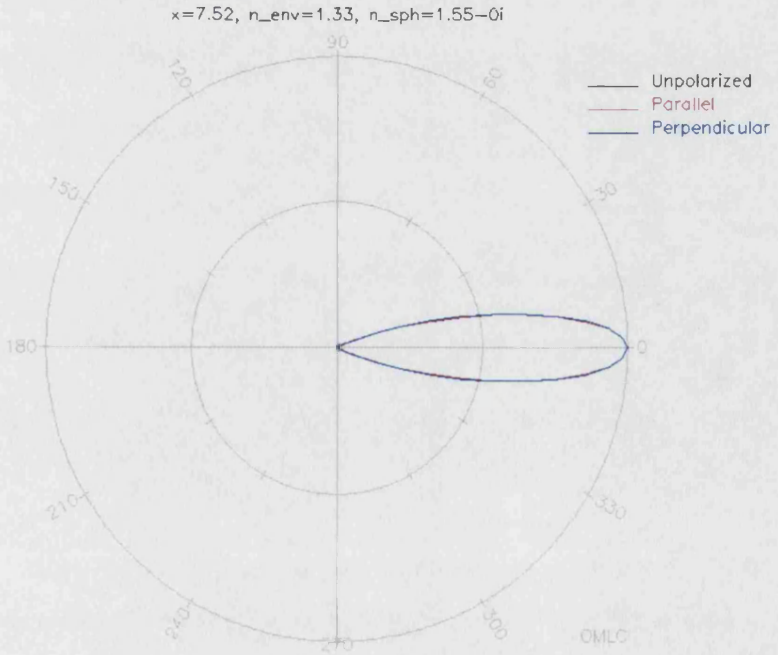

$\mu_s = 945$

11. Green light (506 nm) by leucosome 702 nm in diameter (St. Dev. from mean)

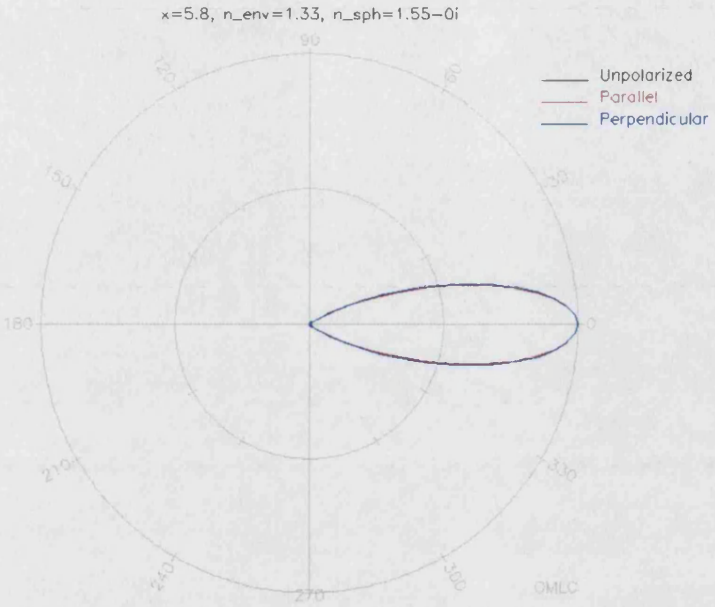

$\mu_s = 633$

12. Red light (650 nm) by leucosome 702 nm in diameter (St. Dev. from mean)

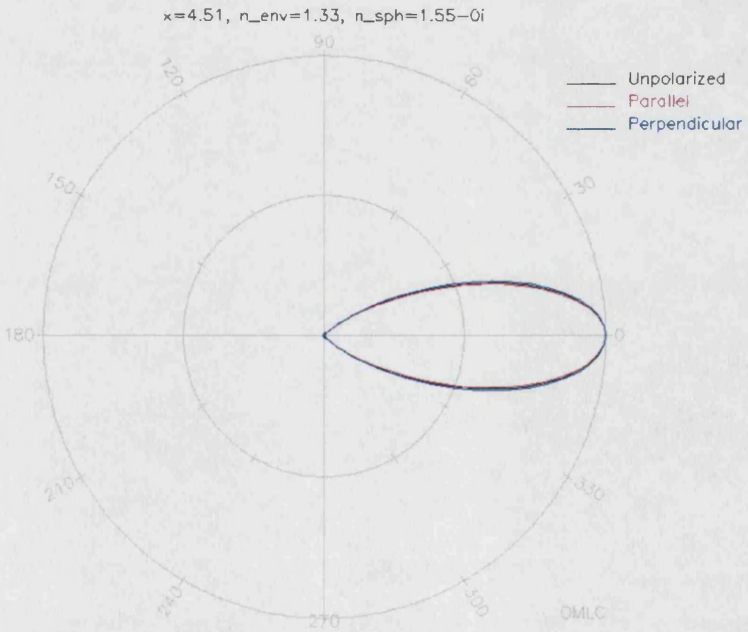

$\mu_s = 403$

13. Blue light (465 nm) by largest leucosome recorded (992 nm)

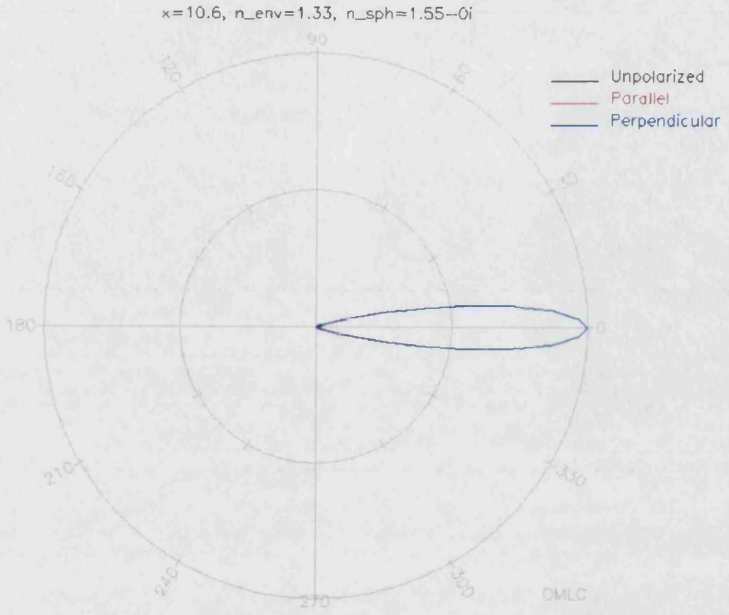

$\mu_s = 2660$

14. Green light (506 nm) by largest leucosome recorded (992 nm)

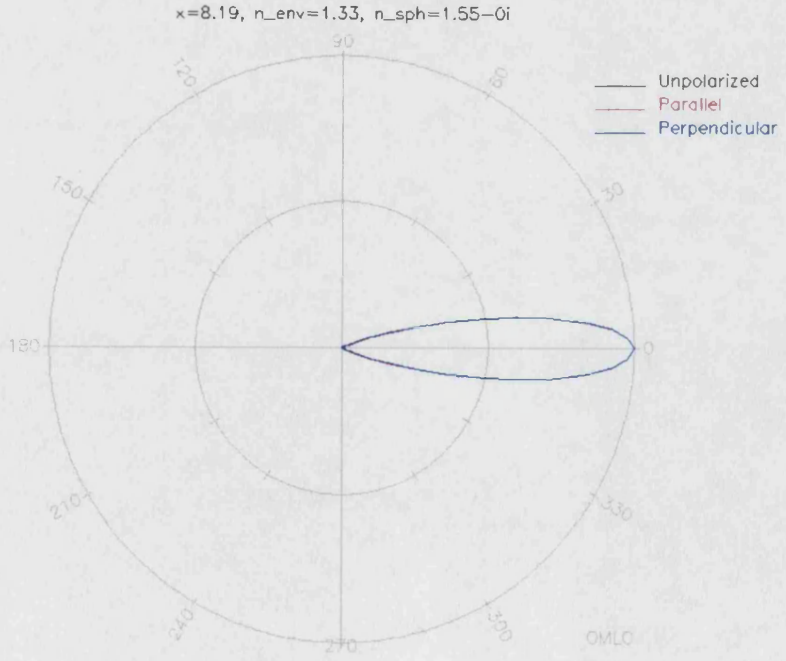

$\mu_s = 2100$

15. Red light (650 nm) by largest leucosome recorded (992 nm)

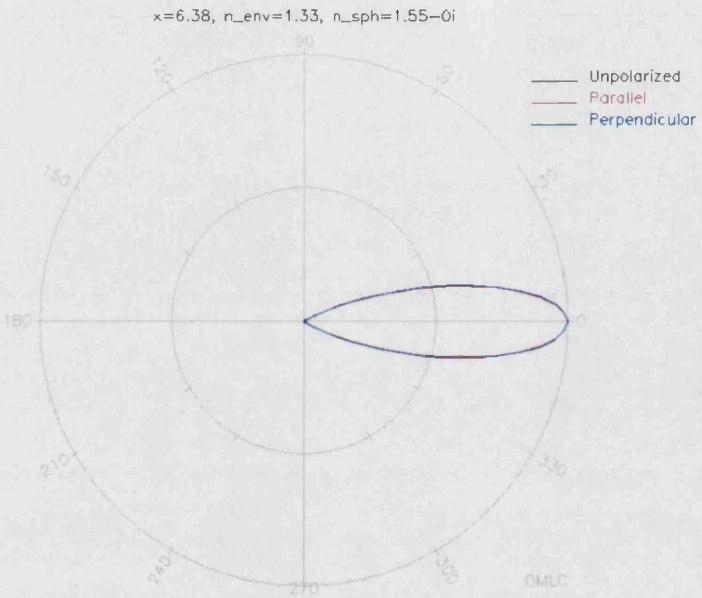

$\mu_s = 1480$

Fig. 43

I hypothesise that leucophore light scattering may better complement a random, rather than uniform, arrangement of iridophores. The scattering of incident wavelengths will increase the efficiency at which the correct angle for multi-layer interference is met (refer back to fig. 29). Plus, the resulting band of reflected wavelengths will undergo further (or secondary) scattering as they return back to the integument surface. This will reduce iridescences. This hypothesis would explain why iridophore and leucophore cells are not found layered one above the other, but are random throughout the bright white regions. A similar arrangement may be found in *Octopus*. Confusion exists over the ordering of cells (Packard and Sanders, 1971; Froesch and Messenger, 1978). Figures *38*, *39*, and *69* of Brocco (1976) suggest *O.*

dofleini iridophores and leucophores are randomly positioned above one another and that neither is orientated in anyway towards the overlying chromatophore organs.

RESULTS: ACETYLCHOLINE INDUCED CHANGES

Preliminary observations

Bathing excised fin tissue in various concentrations of ACh did not induce a spectral shift as expected. Instead, green iridescence gradually diminished as concentration increased.

Tissue Samples bathed in solutions A, B, C and Artificial Sea Water (ASW) Bathing tissue in low ACh concentrations (A = 1 x 10^{-8}, B = 5 x 10^{-8}, C = 1 x 10^{-7} M) and ASW control, resulted in no visible difference to the tissue after 15 minutes of being immersed.
Tissue Samples bathed in solution D Green iridescence diminished slowly after 7-8 minutes in solution D (5 x 10^{-7} M ACh). This tissue appeared pale green in comparison to the ASW control.
Tissue Samples bathed in solution E and F No iridescence could be seen in the tissue after 8 minutes of being immersed in solutions E (1 x 10^{-6} M ACh) and F (5 x 10^{-6} M ACh).
After 15 minutes all solutions were removed by twice flushing with ASW
Rinsed tissue samples A, B, C and ASW ASW wash had no effect on tissue samples A – C, or ASW control. Iridescent green was visible throughout the entire experiment.
Rinsed tissue sample D After a total of 27 minutes (12 minutes in ASW wash) a green iridescence returned to tissue samples D, and each was a similar intensity to that seen in the control.
Rinsed tissue samples E and F After 38 - 45 minutes (23 - 30 minutes in ASW) faint green iridescence returned to tissues E and F. However, this did not match the control, and appeared nothing more than faint after a total of 90 minutes. **Table 7**

ACh affects on ultrastructure

Dramatic morphological differences can be seen in both the iridophore and leucophore cell of *S. officinalis* after bathing the tissue in increasing ACh concentrations (figs. 44-53).

Iridosomal platelets and Leucosomes

The platelets and leucosomes of each cell appear to be sensitive to ACh concentration changes. High concentration of ACh results in structural modification. The light reflecting elements of both cell types undergo morphological change. ACh does not appear to affect the nucleus, cytocentrum, cytoplasmic channels, or outer cell membrane.

Small increases in ACh concentration (1×10^{-7} - 2.5×10^{-7} M) primarily influence the morphology of the iridosomal platelets (figs. 44 – 46). These normally long, thin plates appear short and fat (figs. 45), having a mean diameter of 992 nm (S.E. ±42 nm) and width of 218 nm (S.E. ±18 nm; cells N = 10). This is almost half as long as previously recorded (1.9 μm), and twice as wide (109 nm). Despite these changes, the regular distribution of the iridosomal platelets does not appear to have altered.

Increasing the concentration of ACh (5×10^{-7} M) further disrupts the optical organelles, making it difficult to distinguish between the cell types. Many of the cells contain both platelets and leucosomes, and resemble a transition between iridophore and leucophore cells. A few iridophore cells containing just platelets (fig. 47 [cell 1])

Fig. 44 A planar view of a white fin spot that has been bathed in 2.5×10^{-7} M ACh.

Iridophore (Ird) and leucophore cells (Le) can be identified within the tissue, however they are less well defined than in untreated tissue. The iridosomal platelets remain evenly distributed and maintain a periodic distribution. However, many of them are considerably shorter in length.

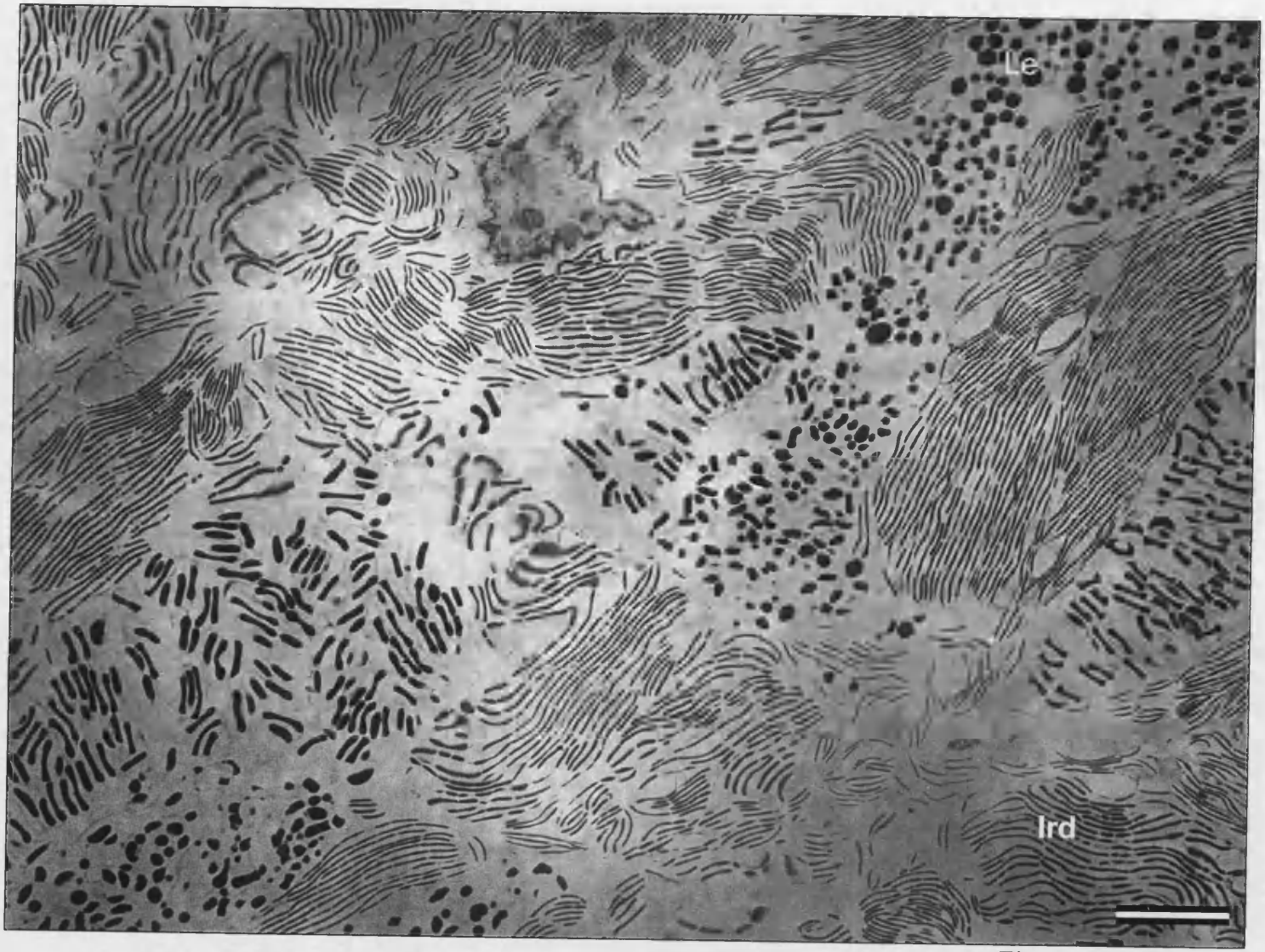

Fig. 44 Scale bar = 5μm

Fig. 45 Closer examination of the iridosomal platelets confirms that some are considerably shorter and thicker after ACh treatment (2.5×10^{-7} M ACh). Despite this change in morphology, the platelets are still bound by cytoplasmic channels, which do not appear to have been ruptured or damaged in any way. Small ribosomal granules can also be seen within the cytoplasmic channels.

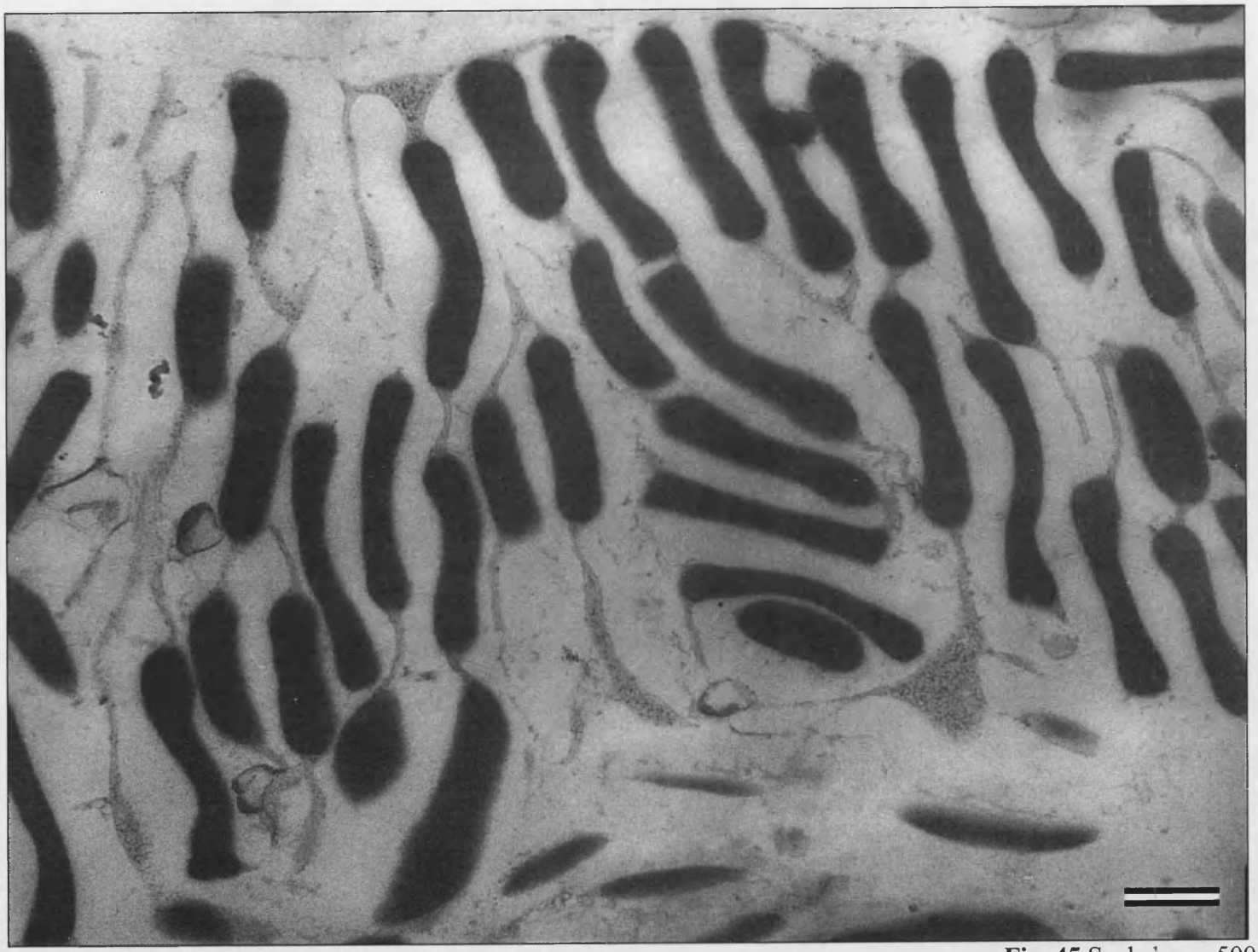

Fig. 45 Scale bar = 500 nm

Fig. 46. Morphological changes can also be seen in the leucophore cells. Spherical leucosomes appear to have become elongated slightly (arrow), making it difficult to differentiate iridosomal platelets and leucosomes. This suggests that both iridosomes and leucosomes undergo morphological changes in the presence of ACh (2.5×10^{-7} M).

Fig. 46 Scale bar = 200nm

Fig. 47 As ACh concentration increases (5×10^{-7} M ACh) it becomes increasingly more difficult to differentiate between iridophore and leucophore cells. Iridophore cells that contain just platelets (**1**) are still evident, but many of the cells appear to contain structures that resemble both platelets and leucosomes (**2**). These cells look as if they are in transition from one type to another. In this figure cell 2 contains predominantly platelets, suggesting that it is an iridophore. The nucleus of each cell remains intact.

Fig. 47 Scale bar = 5 μm

Fig. 48 Leucophore cells, that contain spherical leucosomes, are not found after bathing the tissue in 5×10^{-7} M ACh. Instead, they contain distorted leucosomes and iridosomal platelets; again resembling a transition from one cell type to another. Here the cell containing predominantly more leucosomes (**3**) may be a former leucophore cell.

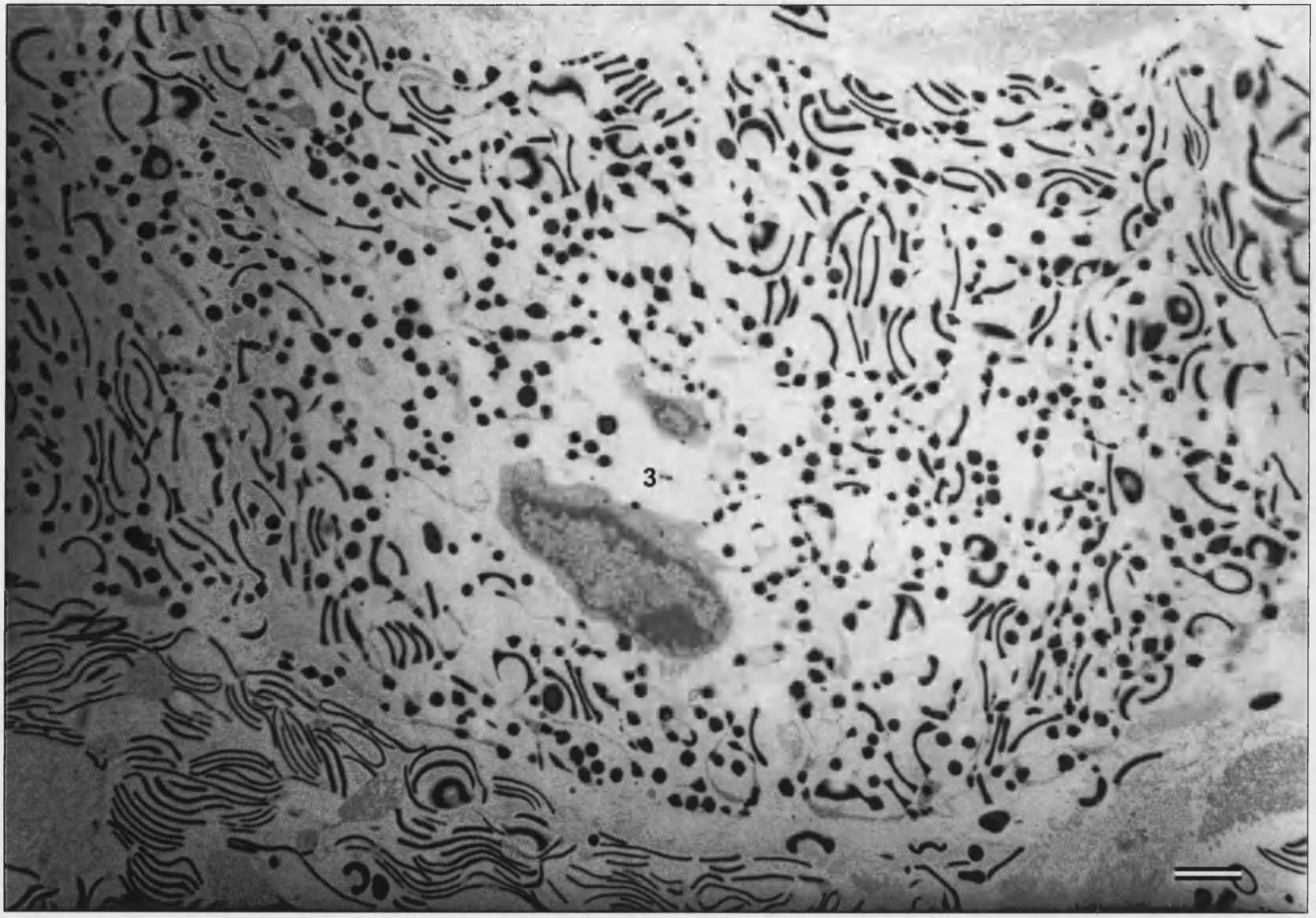

Fig. 48 Scale bar = 2μm

Fig. 49 Peripheral iridosomal platelets appear to have broken up within their cytoplasmic channels. However, the position of the channels does not appear to have altered, as they still extend to the outer cell membrane (arrow) and are still regularly spaced (ACh 5×10^{-7} M).

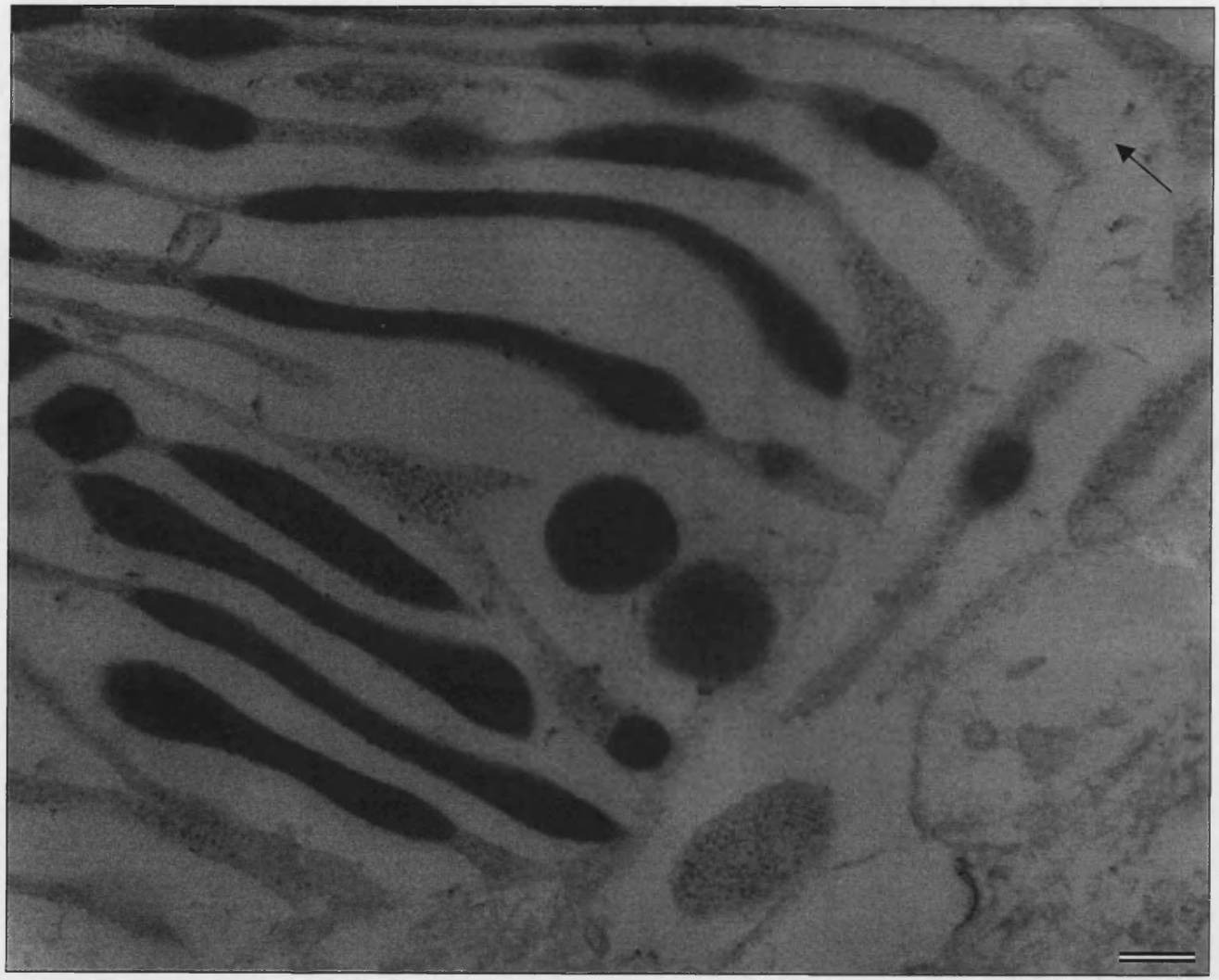

Fig. 49 Scale bar = 200 nm

Fig. 50 The cytoplasmic channels of this cell can be seen to contain both iridosomal platelets and leucosome elements. The dense staining, high refractive index material contained in the channels has become segregated into smaller regions. However, there is no sign of cell damage; the cytoplasmic channels, cytocentrum, and nucleus are all intact. (ACh 7.5×10^{-7} M).

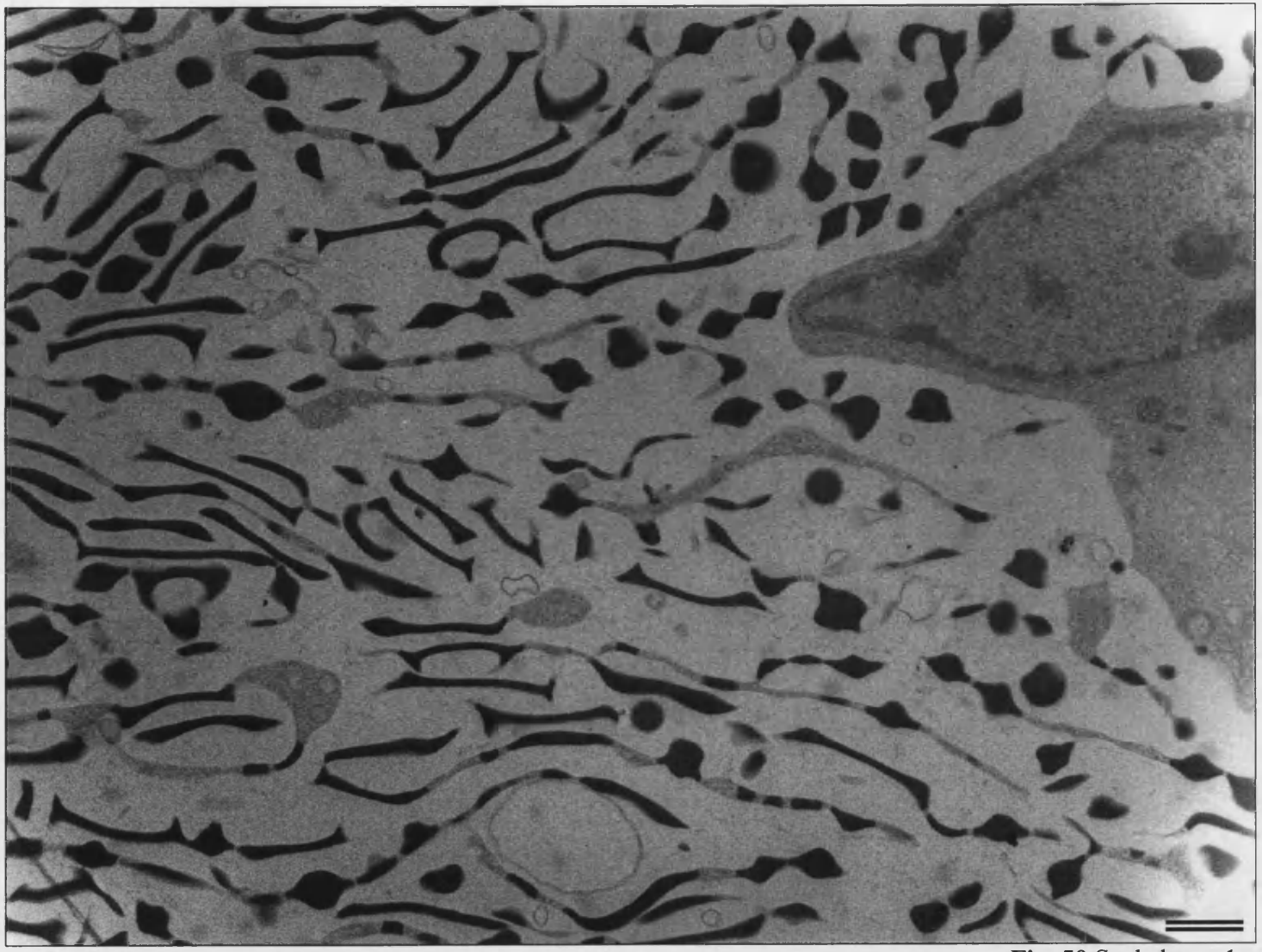

Fig. 50 Scale bar = 1 μm

Fig. 51 Despite the morphological changes that have occurred outside the cytocentrum of this cell, the numerous organelles and developing leucosomes contained within the cytocentrum are unaffected. (ACh 1 x 10^{-6} M).

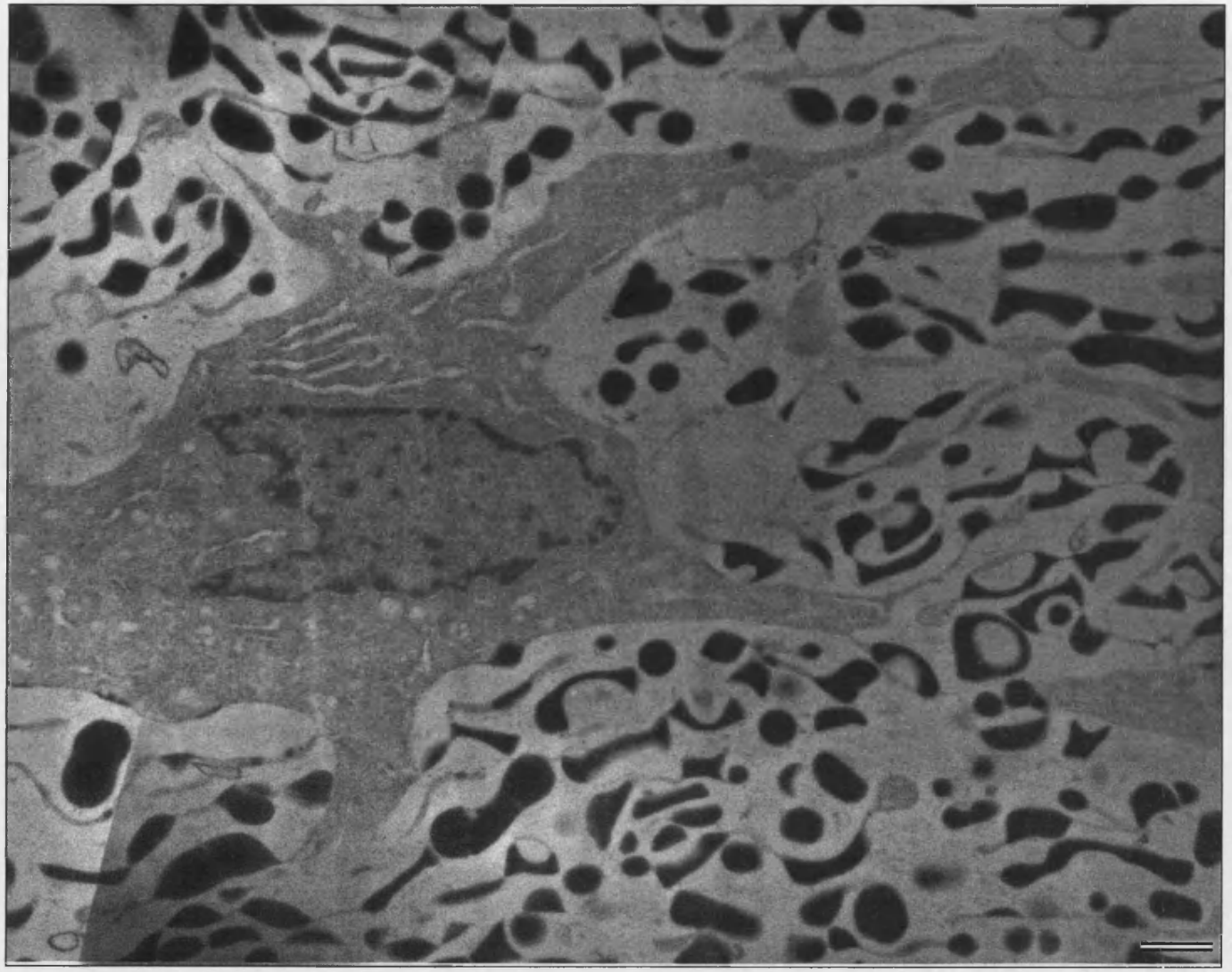

Fig. 51 Scale bar = 500 nm

Fig. 52 High magnification of the nucleus, cytocentrum and developing optical elements.

A high ACh concentration (1×10^{-6} M) does not appear to have damaged the nucleus, nuclear membrane, cytocentrum, or any of the attached cytoplasmic channels. It has however caused a significant change in the shape of developing iridosomes / leucosomes, so much so that it is difficult to distinguish which they are.

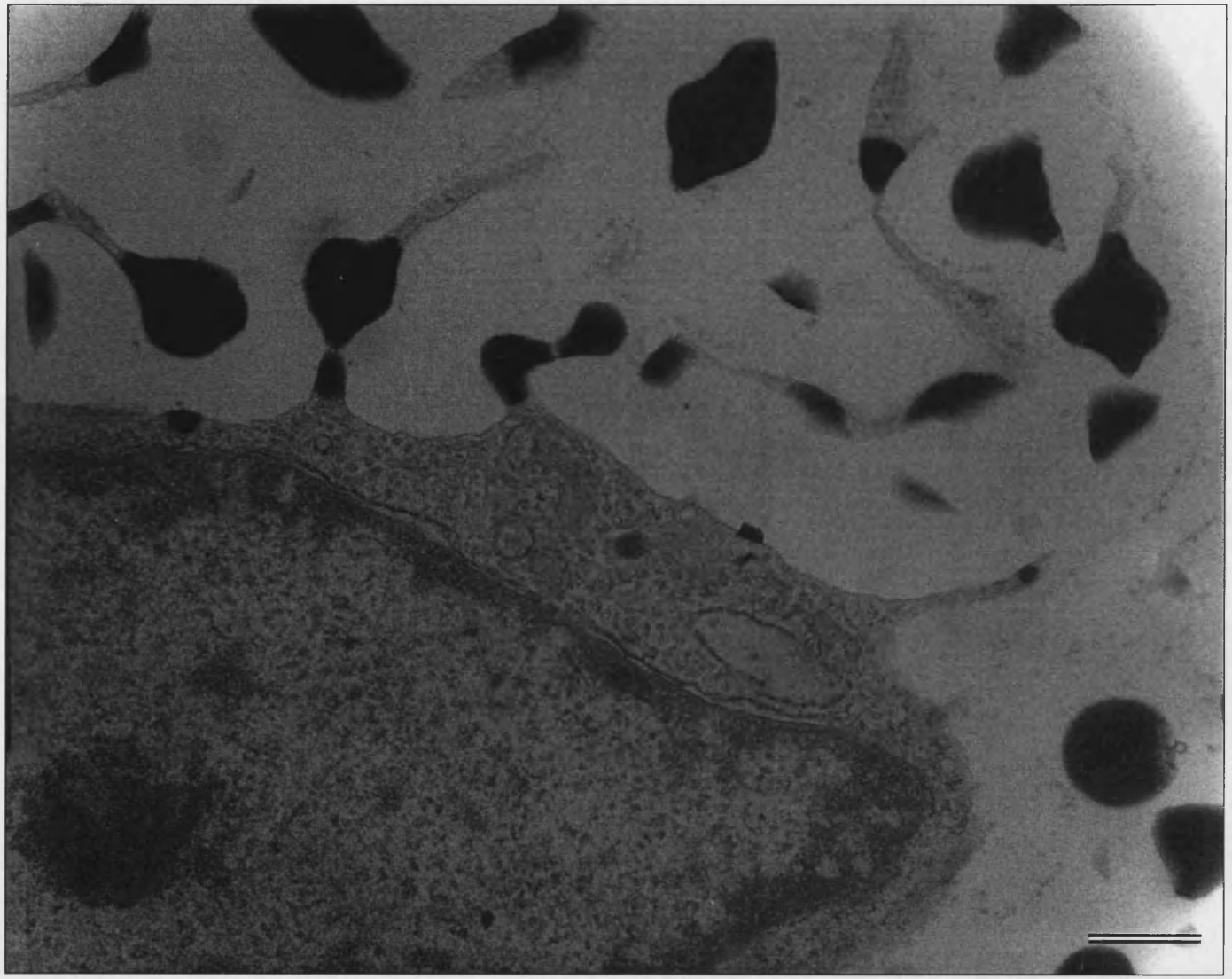

Fig. 52 Scale bar = 500 nm

Fig. 53 Short iridosomal platelets are joined together by a cytoplasmic channel. At the end of this channel is a high concentration ribosomal sized granules. (ACh 5×10^{-7} M).

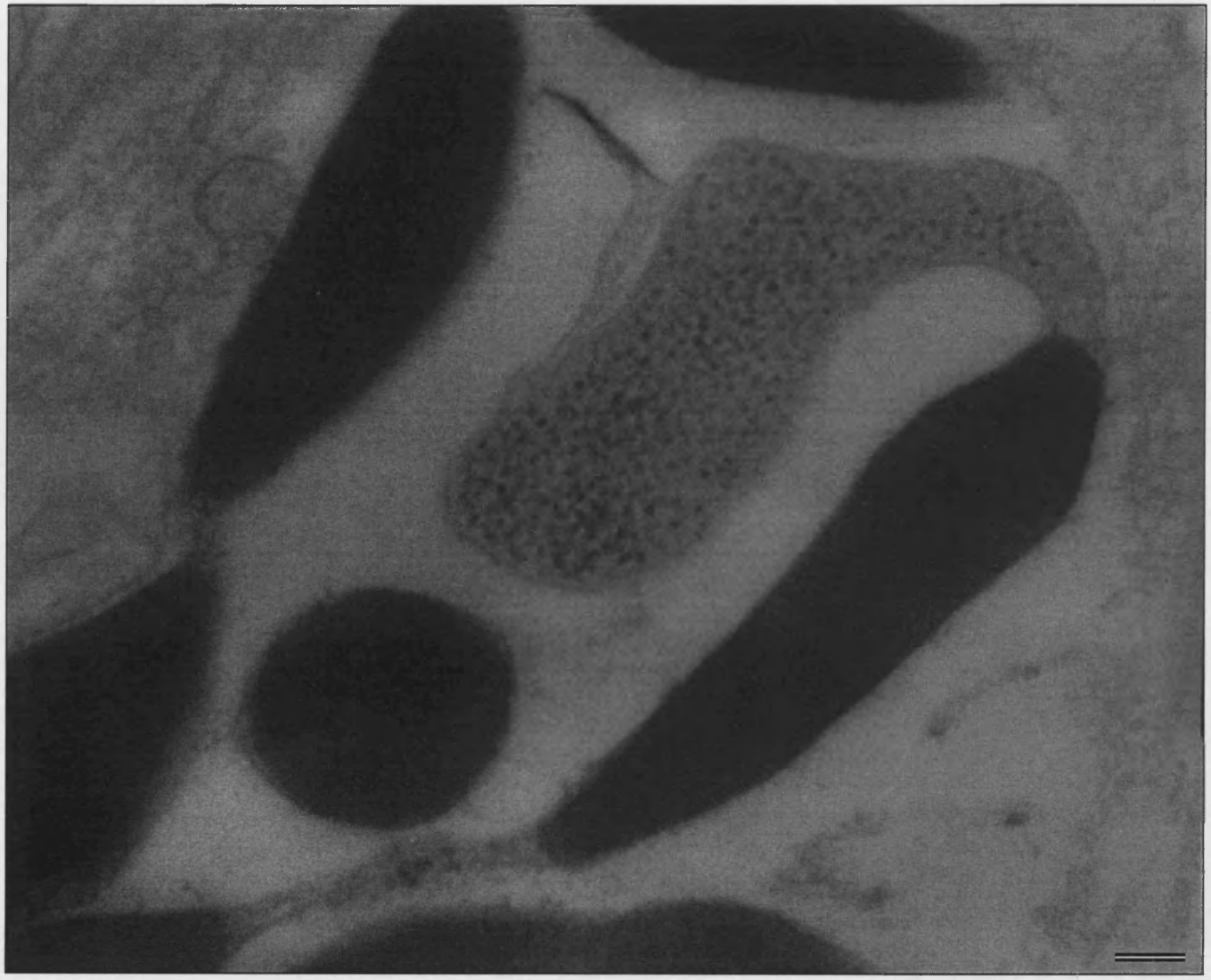

Fig. 53 Scale bar = 100 nm

Fig. 54 High magnification of the cytoplasmic channels reveals that this membrane is intact and that it contains elements that resemble both iridosomal platelets and leucosomes. (ACh 7.5×10^{-7} M).

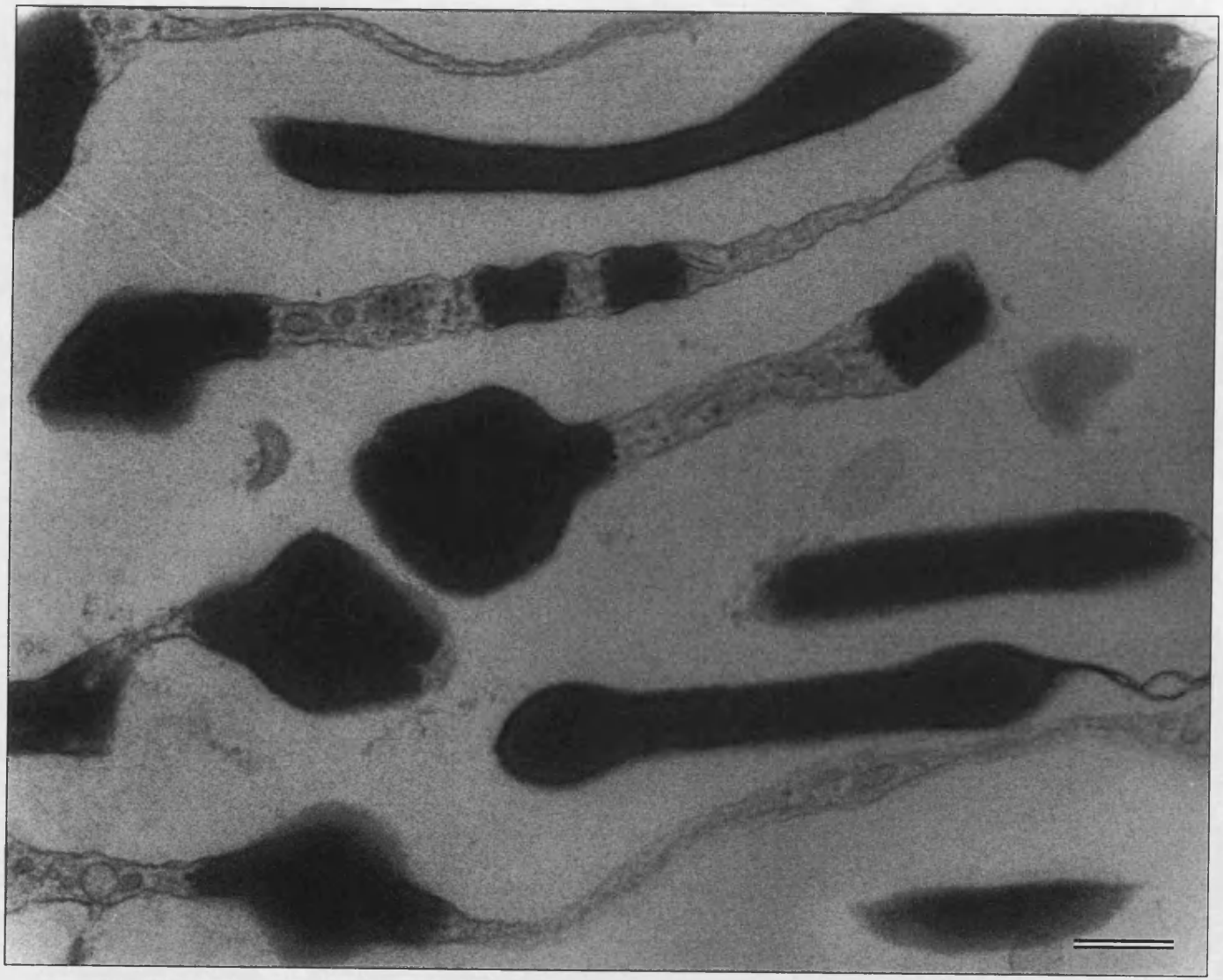

Fig. 54 Scale bar = 200 nm

can still be observed. These platelets remain regularly spaced, and still resemble a constructive interference structure (coherent scattering). However, all the leucophore cells contain distorted leucosomes and also iridosomal platelets. The majority of cells therefore appear to be transitional, and these may be sub-categorised into two groups: those containing predominantly platelets (fig. 47 [cell 2], and those containing predominantly leucosomes (fig. 48 [cell 3]).

After bathing the tissue in 7.5×10^{-7} M ACh and above, the optical organelles of both iridophore and leucophore cells are indistinguishable (figs. 50 – 52). Each organelle represents an asymmetric globule, and these range greatly in size (~100 nm – 2μm). They are more akin to a leucosome than a platelet. A definitive size range of these elements was not made, as it was not possible to reconstruct serial sections of these obscure shapes.

Some elongated platelet-like structures do remain (fig. 48). These have bulbous ends, and resemble 'dumbells'. They are no longer regularly spaced throughout the cell, and do not appear to form any periodic structure.

No cells can be found that have a regimented distribution of cytoplasmic channels, i.e. channels cannot be seen extending across the cell as previously described in iridophores. Instead, all cytoplasmic channels meander across the cells in a similar manner to that described in untreated leucophores. Each channel still encases a highly refractive material, but in this instance they contain globular elements that appear to be remnants of both platelets and leucosomes (figs. 48 and 49). High magnification of the channels reveals that each element is still linked via a cytoplasmic bridge, which contains a darkly stained cytoplasm and ribosomal granules. These components are identical to those found in the cytocentrum of treated

and untreated cells (fig. 50 - 53). Several figures (47 – 50) also show developing platelets or leucosomes within the cytocentrum. It is difficult to see if these have become distorted in anyway. However, developing elements contained within short cytoplasmic channels that are attached to the cytocentrum have become distorted by ACh treatment.

DISCUSSION: ACH INDUCED CHANGES

Treatment of *S. officinalis* tissue with increasing physiological concentrations of ACh *in vitro,* caused green iridescence to disappear gradually. No other coherently scattered wavelengths were observed. This suggests that ACh 'turns off' the optical function of the iridophore cells. The reason why diffraction is inhibited can be seen in the TEM. However, the ultrastructure of both iridophore and leucophore cells appears to change in the presence of elevated ACh, and the degree of transformation suggests that a more complex underlying function may also ensue.

ACh induced changes in iridosomal platelet morphology

The morphological changes observed at low ACh concentrations (1×10^{-7} to 5×10^{-7}) are astounding. Not only do the platelets shrivel very abruptly to almost half their normal size, but they retain their light diffracting ability. There is a clear advantage in being able to maintain the original green iridescence, since any abrupt colour change would prove conspicuous within this highly camouflaged animal.

It was originally considered that ACh might affect only a few iridophore cells, since this has been observed in *Lollinguncula brevis* (Cooper *et. al.*, 1990) and would explain the diminishing colour. However, in even the low ACh concentrations tested, few iridophores resembled their former state, suggesting that ACh has a blanket effect in *S. officinalis*. It appears to cause all the platelets to contract in length, and increase in width. As each platelet swells, it occupies more of the cytoplasmic space. However, as all iridophores are affected, each occupies the cytoplasmic space at an equivalent rate. Optimas measurements of 25 iridophore cells (five from each ACh concentration) confirms this (fig. 55). Consequently, the mean periodicity from the leading edge of one platelet to the leading edge of the next remains the same. Since periodicity remains almost constant, the scattered wavelength (in accordance with

equations 7, 8,and 9, page 90) should remain the same (fig. 56). This may explain why low ACh concentrations maintain a green iridescent appearance, whilst it is clear that the iridophore cells have undergone dramatic morphological changes.

Platelet width may continue to expand and maintain coherent scattering for only a short period. A point will be reached when the cytoplasmic space becomes too small to permit coherent scattering. This point is not reached within the iridophore cell. Instead, some of the platelets begin to segment in ACh concentration above 5 x 10^{-7} M. This disrupts the normally regular alignment of the platelets, and fewer can therefore constructively interfere. Consequently, the intensity of reflected green wavelengths becomes less. It is at this stage that we begin to see iridosomes and leucosomes within the same cell. And it is conceivable that less coherent scattering will occur. However, some regions do maintain a periodic structure (fig. 45). Measurement of these areas using the Optimas software confirms that periodicity is equivalent to that required to diffract green wavelengths (figs. 55 and 56). At 5 x 10^{-7} M ACh, few spherical leucosomes can be identified. Instead, the leucophore cells contain non-spherical globules of high refractive index material, and some of the cells contain platelets. It is not clear if the cells that contain platelets are iridophores that have undergone a more advanced transformation into a leucophore. Or, whether they are leucophore cells that have transformed some of their leucosomes into iridosomal platelets. However, it is clear that ACh affects both iridophore and leucophore cells. The effects are just more noticeable within iridophores.

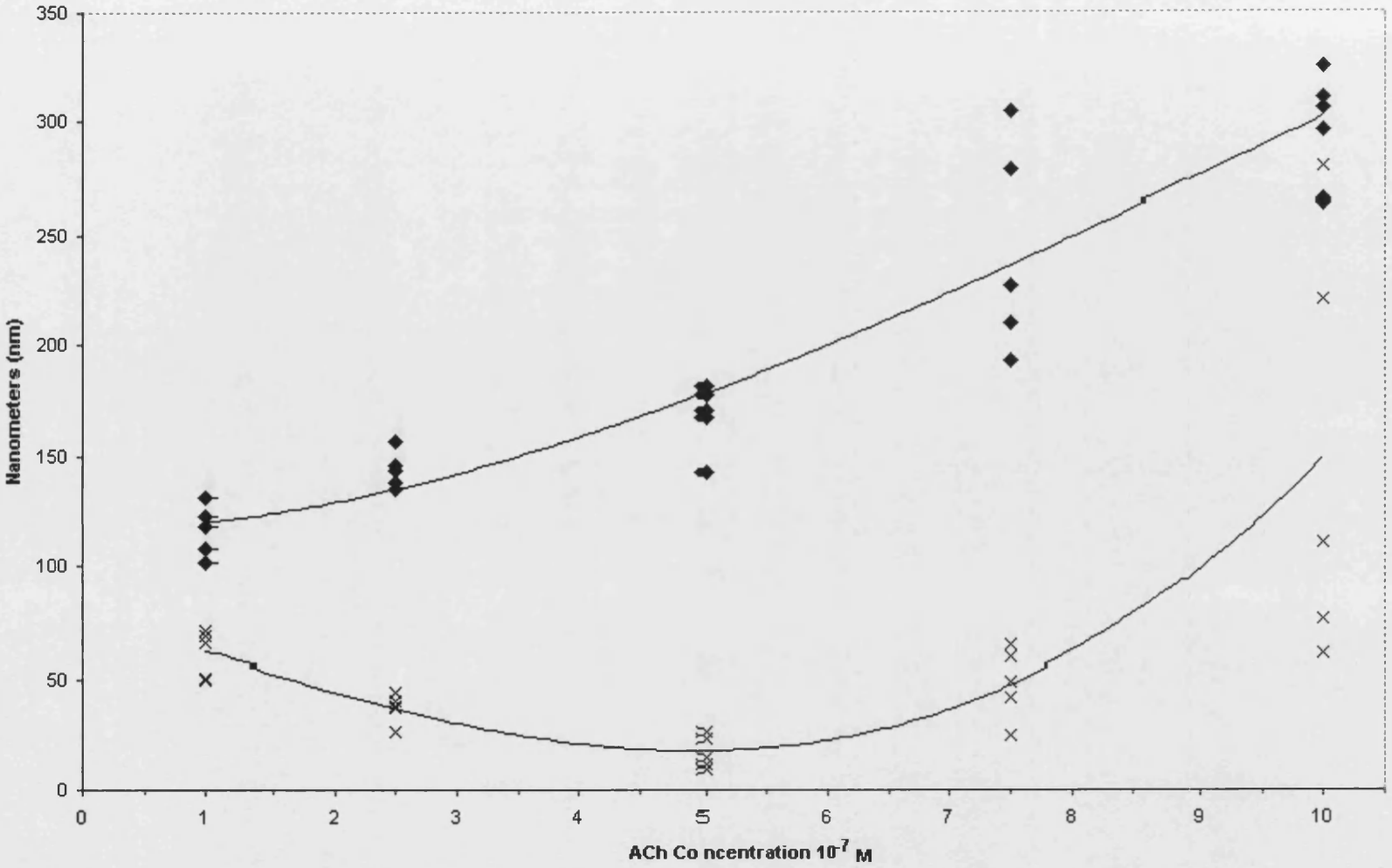

Fig. 55 Graph illustrating the mean iridosomal platelet thickness (**x**) and mean platelet spacing (♦) for 25 iridophore cells (5 in each ACh conc.).

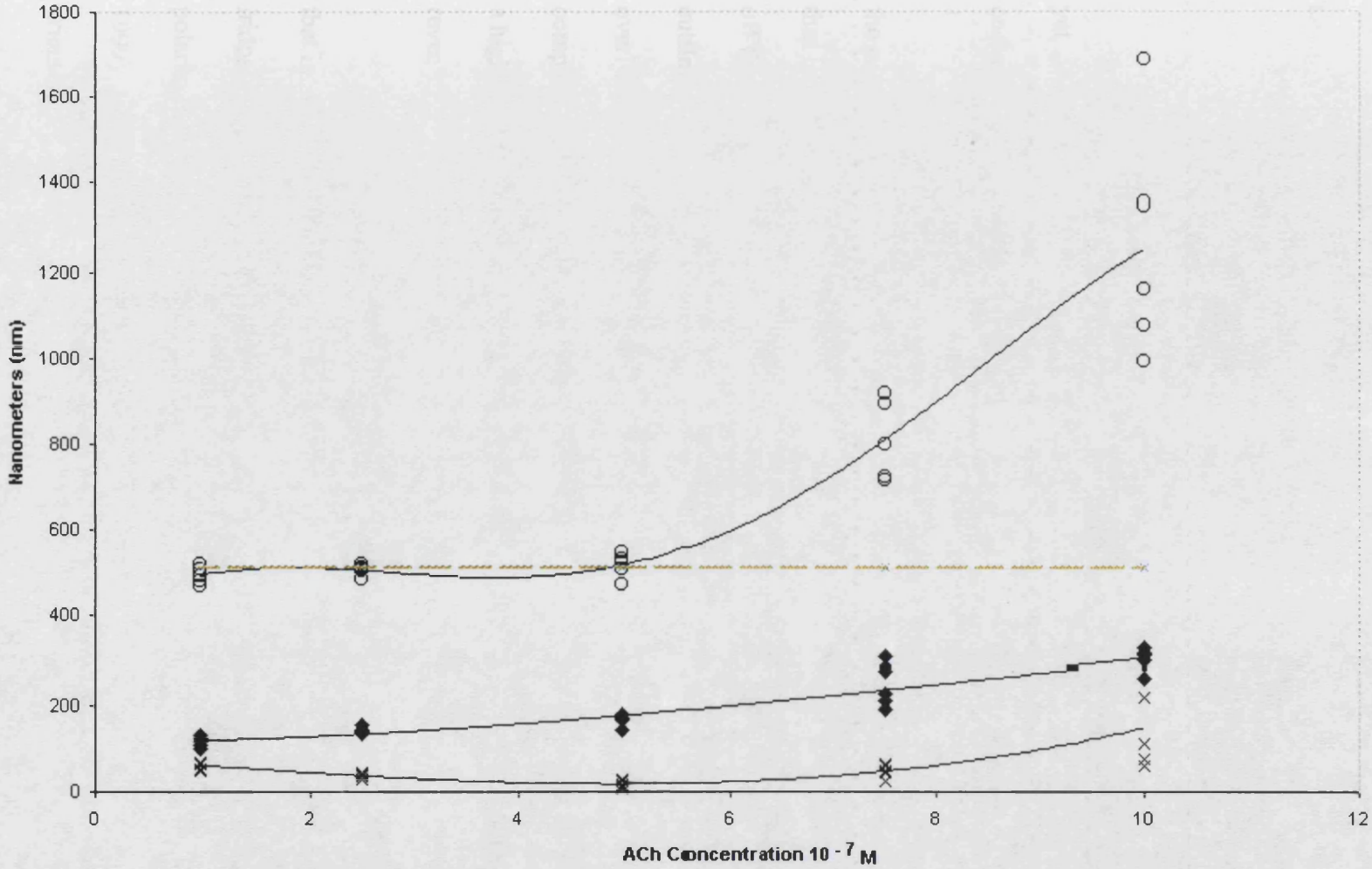

Fig. 56 Graph showing the calculated wavelength for the above 25 iridophore cells (see fig. 55). Green dotted line indicates the peak wavelength reflected from untreated iridophore cells

Non-spherical leucosomes still probably scatter visible wavelengths, since the bright white regions remain visible in even the highest ACh concentrations. Determining the light scattering properties of non-uniform leucosomes is however beyond the scope of this project.

What is the purpose and advantage?

It is difficult to comprehend why iridophore cells should change morphology, yet maintain the same reflected wavelength. Initially this appears to be a waste of energy; however I do not believe this to be the case.

We have already demonstrated that reflected green wavelengths correlate with the peak absorption of retinochrome present in the eye of *S. officinalis*. This suggests that iridophores may be involved in intraspecific communication. Switching on and off the reflected wavelength may therefore be involved in signalling to other cuttlefish. And different intensities of green may convey different information. The overlying chromatophore organs could control intensity, however this may compromise body pattern and overall body luminance. ACh does not, so consequently a highly camouflaged cuttlefish could communicate intraspecifically without revealing its position to predators.

Altering the morphology of the iridophores may also serve another purpose that is also involved in intraspecific communication. Changing the dimensions of each iridosome may not change the reflected wavelength, but may alter the degree of light polarisation. It is well-understood that diffraction gratings polarise light (Ditchburn, 1999). This effect is not perceived within the bright white spots, since the random orientation of iridophores, and the presence of light scattering leucosomes produce a random polarisation (non-polarised). However, isolated iridophore cells present on the

head and arms of *S. officinalis* do polarise light (Shashar *et. al.*, 1996). The observation that ACh induces change within the aggregated iridophores of *S. officinalis* supports Shashar's (*et. al.*, 2000) hypothesis that neurotransmitters may change the polarisation characteristics of iridophore cells.

SUMMARY 1

The bright white regions of tissue found directly below the chromatophore organs in *S. officinalis*, predominantly contains iridophore and leucophore cells.

Although these cells are specialised for different optical purposes, their shape, size, and structure are similar. Both are slightly elongated in shape and are typically 25 - 30 μm in length. They possess a central nucleus, which is immediately surrounded by a cytocentrum, which contains all the non-optical organelles. All cellular processes therefore occur within the confines of the cytocentrum, away from the optical regions. In the area outside the cytocentrum are the optical organelles, termed iridosomal platelets and leucosomes. Each is composed of a high refractive index material (N = 1.55), and the cells differ only in the morphology of this material. The iridosomal platelets are thin discs, whilst the leucosomes are spherical. All of the optical organelles are then encased within long cytoplasmic channels, which connect them and create cytoplasmic bridges between them.

Iridosomal platelets are 1.9 (± 0.8) μm in diameter and 109 (± 1.5) nm thick. They are arranged perpendicular to the cell's long axis, and are evenly spaced apart (68 ±1.9 nm) to form a grating. It is this regimented distribution of high refractive platelets which functions optically. However, iridophores and leucophores are randomly arranged throughout the bright white regions of tissue, and are orientated at all angles with respect to the integument surface. This forms a three-dimensional complex of randomly arranged gratings. This apparently indiscriminate arrangement of gratings is probably unique to cephalopods.

It is hypothesized that a random distribution of gratings reduces iridescence, and maintains a much larger angle of coherent scattering at the peak wavelength (equ. 7). Both of these factors are determined by the angle of incident light (and viewing

viewing angle). If the cells were all orientated in the same direction, the cells would produce structural colour only when the incident light was at the correct angle for coherent scattering (θ, see fig. 29). It is at this point the peak reflected wavelength (λ_{max}) is formed. Deviation from this angle gives iridescence. The bright white tissue regions of *S. officinalis* do not display much iridescence, and a green colour can be seen at all angles. In a random arrangement of iridophores, θ becomes less significant, since light incident at any angle can form λ_{max}. The intensity of λ_{max} is considerably higher than any iridescence, which will simply become unsaturated. However, a slight iridescent green is still apparent, as a full complement of iridophores, arranged at all angles, does not occur within the white regions.

In the shallow waters inhabited by *S. officinalis*, light incidence may approach 90°. In these circumstances the iridophores may function at many different angles, all permitting coherent scattering. This random arrangement of optically significant cells in unusual and I consider undocumented. Although, I hypothesise that the bright white regions described in many *Octopus* species may also contain a random arrangement of iridophores.

The random arrangement of leucophores is less significant, since the high refractive index leucosomes are approximately spherical. Leucosomes range greatly in size (~166-992 nm), and are not regularly spaced. They probably scatter all visible wavelengths in a predominantly forward direction, via Mie light scattering. However, the high density of leucosomes in each cell means the forward propagation of light becomes greatly diffused as multiple light scattering events occur in each cell. The scattering of incident light by these cells has two important roles. First, the white regions reflect predominant wavelengths within an environment, so in the saturated green light of a kelp forest the white regions will appear green (Messenger, 1974).

This is important for camouflage, as it permits immediate background matching. Second, scatter will increase the angles of light incident upon an iridophore, and similarly the light reflected from it.

The ultrastructure of both iridosomal platelets and leucosomes is affected by the neurotransmitter substance, acetylcholine, which alters the high refractive index material within each optical organelle. The long slender platelets halve in length, becoming short and fat in the presence of elevated ACh. Surprisingly, this dramatic structural alteration does not influence the structural colour produced. A pale iridescent green remains. As each platelet contracts in length it increases in width. The space between each platelet is therefore reduced, which means periodicity is unaffected. Coherent scattering may still therefore occur. Changes in platelet morphology may instead influence polarization of reflected light. This may play a vital role in intraspecific communication.

In higher ACh concentrations, the iridophores do not form any structural colour. The platelets appear to break into smaller fragments, which roughly resemble leucosomes. However, it is difficult to distinguish between either optical organelle. The leucosomes are stressed, no longer spherical, and many cells contain both platelets and leucosomes. All of the cells may now scatter light and give a white appearance, however none appear capable of coherent scattering. This is supported by the fact that the bright white regions are still visible in the tissue, but no structural colours are observed. ACh is therefore hypothesised to switch off structural colour formation and any consequent polarization, both of which may be involved in intraspecific communication.

Structural colour can be restored to ACh treated tissue by rinsing in seawater; a phenomenon also recorded in the squid *Lollinguncula brevis* (Cooper *et. al.*, 1990).

It is intriguing that the organelles undergo such distortion and then return to shape. It suggests that the high refractive index material displays shape memory properties. Further work should focus on the full classification of this material and its regulation. Control, composition and configuration of this material have not been investigated. A material that undergoes such rapid and reversible morphological changes is of interest to developmental biology.

Part 4 – Colour-changing materials

Adaptive Camouflage: Iridophore Cell Mimics

Numerous elements within the dermis of a cuttlefish contribute to its diverse camouflage repertoire. In order to attain the same degree and diversity of camouflage within a man-made material, a mimic of each of these cells and organs is required. Theoretically, a number of 'off the shelf' components could be substituted for these biological elements. For example: The function of chromatophores to match environmental brightness could be easily replaced with photochromatic dyes. As light levels increase the intensity of a coloured dye could diminish. The light scattering properties of the bright white patches could be easily mimicked by light scattering particles, e.g. white paint, or calcium carbonate. And iridophore cells could be replaced by a random arrangement of diffraction gratings. The limitation of this haphazard assembly would be that the material could not be tuned to specific wavelengths; a requirement of military adaptive camouflage. The only method, by which it could be tuned, would be to address individual iridophores and control peak wavelength diffraction.

Methods of producing a colour changing iridophore cell mimic shall be discussed in this chapter.

Deformable Diffraction Gratings

Since iridophore cells can diffract light, their primary function can be mimicked using diffraction gratings. Currently, man-made diffraction gratings are either broadband reflectors of very high iridescence, or specific-band reflectors with very low iridescence. This does not fulfil the demands of camouflage. Ideally, camouflage that uses diffraction must be capable of producing a broad band of tuneable colours that have no iridescence.

Novel methods of producing a manipulable diffraction grating are discussed.

Background to Diffraction Gratings

Diffraction gratings reflect (or transmit) wavelengths that range from ultraviolet to near infrared. They separate (disperse) polychromatic light into its constituent monochromatic components, and are therefore an important analytical tool as well as commercial commodity. Their spectroscopic quality has improved through advances in the formation and reproduction of their surface profile. More conventional, diamond tooled or ruled gratings are now being replaced by computer generated (CG), mass-producible diffraction gratings.

Ruled gratings typically diffract a wide range of wavelengths, and are commonly used in spectrophotometers. In these applications the grating has a saw-tooth profile composed of right-angled triangles. This is known as a blazed grating, and the peak diffracted wavelength alters greatly with angle. Ruled gratings are also known as continuous level gratings. This is because each period is identical, having the same depth, orientation, and size (5-20 μm). A computer is used to generate more complex multi-level, or three-dimensional gratings. Here each period can be addressed separately and a variety of profile shapes (e.g. square, rectangular, triangular, stepped) can be produced with different sizes (smallest 0.1 μm), lengths, widths, depths, and orientations. A photolithographic mask of this pattern is produced and used to expose secondary plates, which are then electroplated (fig. 57; summary of process Swanson and Weldkamp, 1990). The increased degrees of freedom means that complex CG diffraction gratings and holograms can be formed very easily. Mass production is possible by either re-using the masks, or by embossing the electroplated grating (negative image) onto other materials. In the latter process the grating is wrapped around a roller (fig. 58) and typically embossed into thin foil.

Fig. 57 Holographic metal shims used in the embossing process.

Fig. 58 A holographic metal shim is mounted on the top roller prior to embossing. Thin foil is then fed between the two rollers. This imprint is then coated in a thin protective plastic.

PROCEDURE 1 – DEFORMABLE DIFFRACTION GRATINGS

The hue of structural colours can be altered by mechanical pressure, distortion, swelling and shrinkage (Fox, 1953). It is therefore possible to change the periodicity of a grating, simply by extending the substrate. This would change the angle at which the diffracted orders were coherently scattered. Ideally, the resting state of an elastic

grating would diffract a wavelength of 400nm (violet). A 90 % deformation would cover the entire visible spectrum, resulting in a wavelength of 740 nm (red). In practice 90% deformation may not be required, as many applications including camouflage may need only a limited spectrum. 40% deformation extending from dark blue (445 nm) to red (623 nm) would be more efficient.

Embossing

The possibility of embossing directly onto a deformable material was tested at the holographic printing company, Light Impression Ltd., Leatherhead. A number of different methods, based upon standard embossing techniques, were tested. These included elevated temperature and pressure tests, all of which proved ineffective.

Moulding

A diffraction grating was directly cast by painting a thin layer of Latex rubber on to its surface. A negative impression of this grating was then left in the cured rubber (fig. 59). Strong iridescent colours could be seen upon the surface of this highly flexible and deformable material (I have found no reference to this method). Unfortunately, only a 5 –10 % deformation was possible with this material, as it contained numerous air bubbles, which caused the material to fracture easily. To reduce the number of air bubbles, the Latex was cast under vacuum, using a desiccating chamber and water-driven pump. This however had the opposite effect as it rapidly withdrew the ammonia, and formed a sponge-like Latex material. Silicone rubber was suggested as an alternative material, as this deformable material is regularly cast under vacuum when moulding intricate three-dimensional shapes.

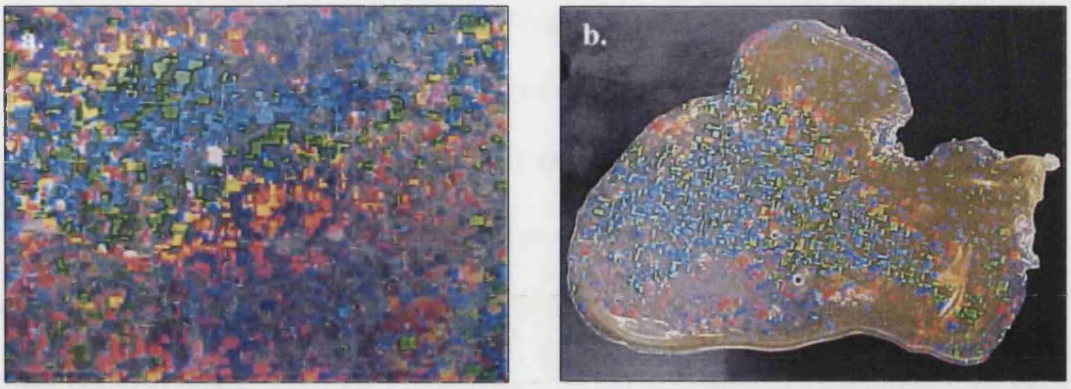

Fig. 59 Casting a hologram in Latex rubber.

Latex rubber was painted onto the surface of a holographic metal shim (a) and allowed to cure at room temperature and pressure. The transparent Latex rubber was then pealed from the shim, and revealed iridescent structural colours on its surface (b). Although replication was successful, the cured Latex contained many air bubbles and pockets (c, indicated in red).

METHOD: OPTIMUM CASTING PROCEDURE

MATERIALS

Silicone Rubber (Alchemie RTV 240, or Axson Essil R291)

Catalyst (Alchemie C240, or Axson Essil C291)

Ruled grating or CG holographic shim

Optional:

Coloured Dye: Ethanol based art dye (Pantone TRIΛ by Letraset).

White scattering particles: Sodium Chloride (table salt).

High-grade clear silicone resin was added to the appropriate catalyst (ratio 10:1) and mixed thoroughly for several minutes. At this stage ethanol based dyes or

other contaminates, e.g. white light scattering particles, may be added. The quantity of contaminates must not exceed the volume of catalyst, as the resin will not cure.

The entire mixture is then degassed at an optimum pressure of -1 Bar, for 25 minutes (MK technology, vacuum casting machine). The removal of gases from a resin such as silicone rubber will cause it to foam, creating a temporary four-fold increase in volume.

The degassed material is then poured, ideally under vacuum, onto the diffraction grating, before degassing for a further 25 minutes. The pressure is then equalised slowly, and the silicone rubber is left to cure at room temperature for 12 hours. This curing time can be reduced to as little as 2 hours (depending upon volume) by elevating the temperature to 60°C. However, I have found that accelerated curing times result in a slightly higher modulus rubber; plus heating will cause expansion and therefore distortion of the metal grating. If a minimal curing time is desired, for example in mass production, quartz gratings could instead be used as these do not soften under high temperature or pressure, and have a low coefficient of thermal expansion.

Small segments of original and silicone rubber grating were sputter coated in carbon, and examined in a scanning electron microscope (Jeol JSMT330).

PROCEDURE 1: RESULTS AND DISCUSSION

The intensity of colours observed in the first Latex cast is no different to that seen in the vacuum cast silicone rubber (fig. 60 and 61a-b). Strong iridescent colours are formed using both methods. All that is different is the quality of the end-cured material. No air bubbles, or other degradation result in the vacuum cast silicone rubber, creating a more uniform and resilient material.

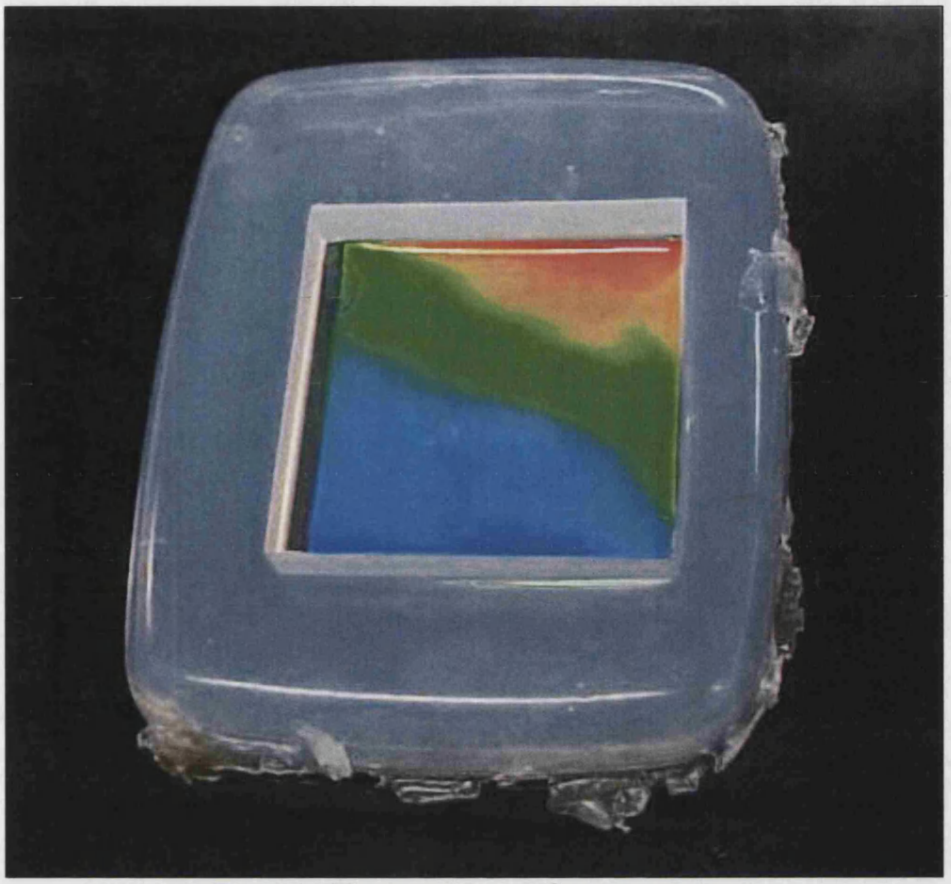

Fig. 60 Silicone rubber diffraction grating

Adding impurities to the silicone resin can alter the intensity of diffracted colours. A black ethanol based dye greatly improves colour intensity by absorbing non-diffracted wavelengths (fig. 61e-f), whilst intensity will diminish when light scattering particles are added (fig. 61c).

SEM examination of the silicone rubber gratings shows each period is the exact mirror image of the original metal grating. A high degree of surface uniformity is clearly seen, and the scale of replication is astonishing (fig. 62). The only defects found on the silicone rubber replica are small nanoscale fragments located on the tips of each grating period. These are small enough not to affect light diffraction and resemble fettling fragments, which are common to all moulded structures. These SEM images confirm that vacuum casting can be used not only to replicate diffracting gratings, but it can also be used to mould nanoscale structures.

The disadvantage of using silicone rubber is that it becomes dirty very quickly. Dust and grease adhere to the grating surface, and all free sides of the rubber. This does not significantly affect diffraction, although it may limit outdoor applications. Washing the plastic in warm soapy water soon removes the dirt and grease, without damaging the iridescent surface. The same cannot be said for standard diffraction gratings (uncoated), which easily become scratched when touched, and are often destroyed when washed.

Fig. 61 Silicone rubber gratings, moulded from a holographic metal shim that is normally used to emboss holograms.

a) Clear silicone rubber grating, viewed upon a black background. b) Clear silicone rubber grating, viewed upon a white background. c) Silicone rubber grating with white scattering particles mixed in the resin, viewed on a black background.

d) Holographic metal shim used to mould the silicone rubber gratings. e) Silicone rubber grating with black dye mixed in the resin, viewed upon a white background. f) Silicone rubber grating with black dye mixed in the resin, viewed on the holographic metal shim.

All photographs were taken with the same Sony digital camera, no flash. A tripod was used to maintain photographic angle, and the artificial ceiling lights within the laboratory illuminated all samples.

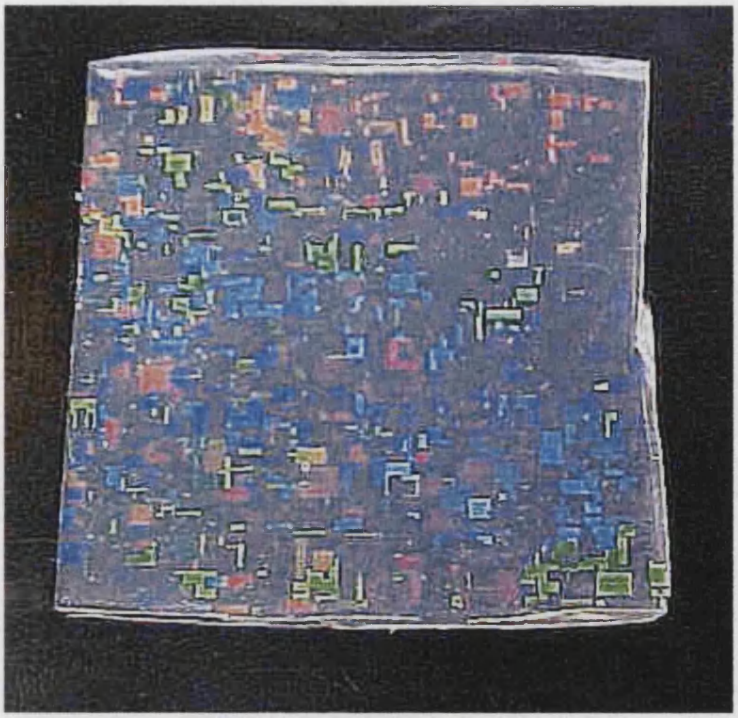

a) Clear silicone rubber grating

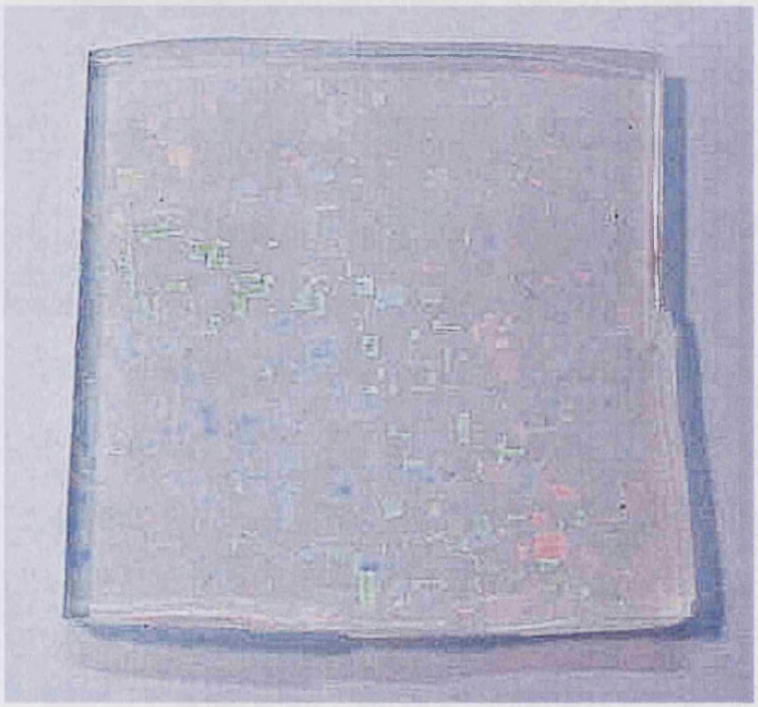

b) Clear silicone rubber grating

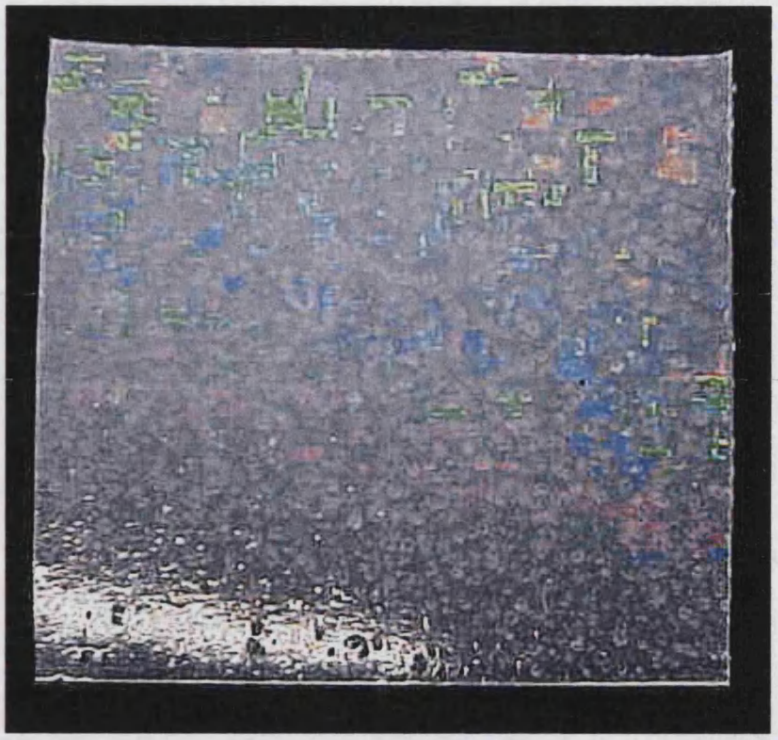

c) Silicone rubber grating containing white light scattering particles

d) Original holographic metal shim

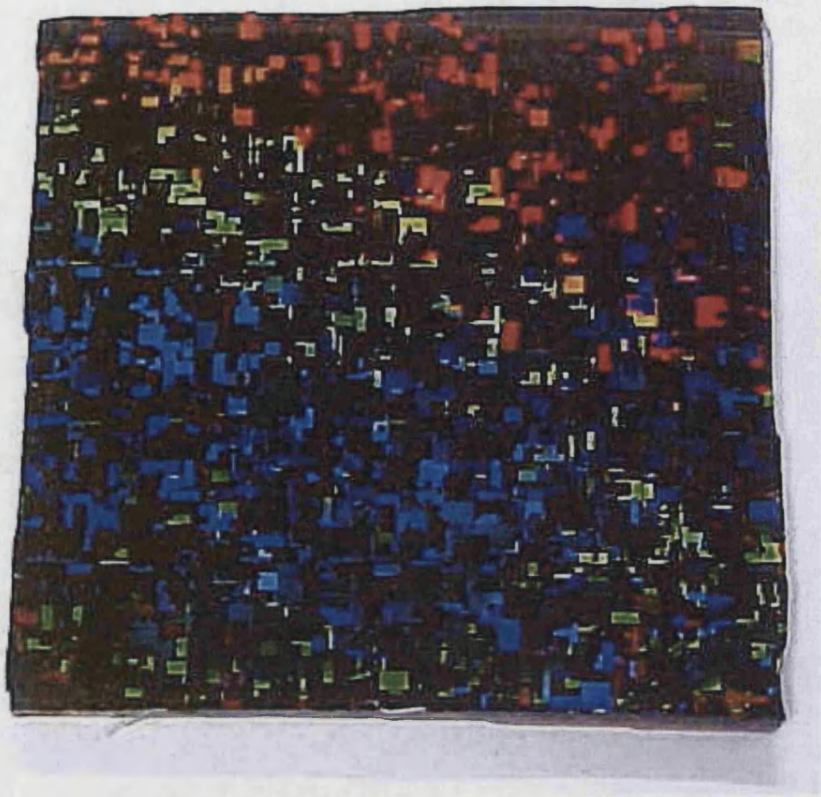

e) Silicone rubber grating containing black dye

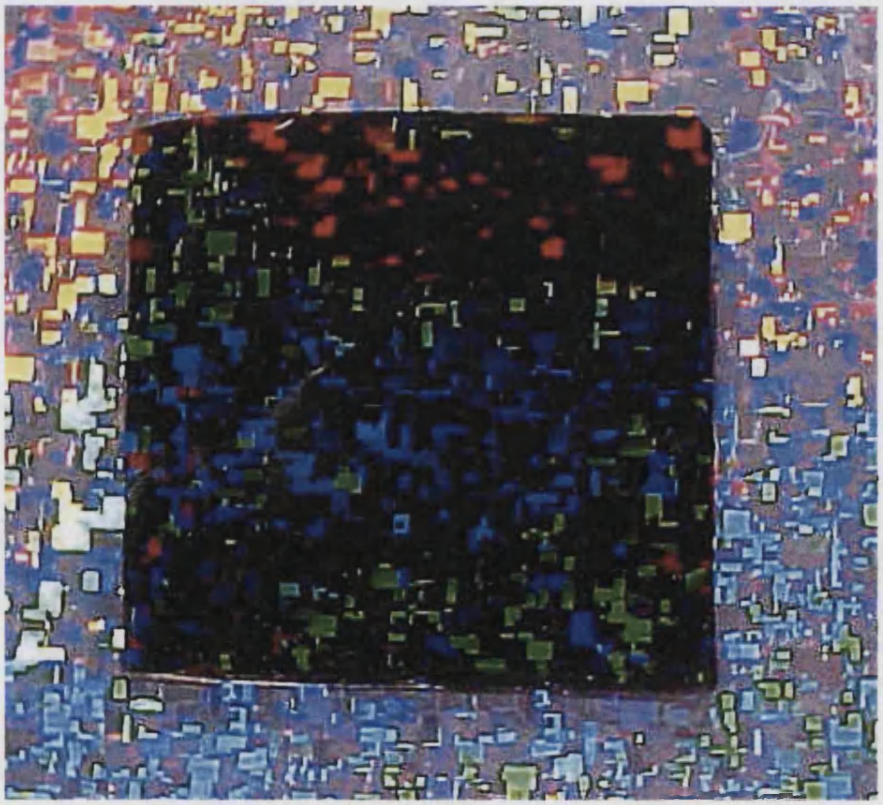

f) Silicone rubber grating containing black dye

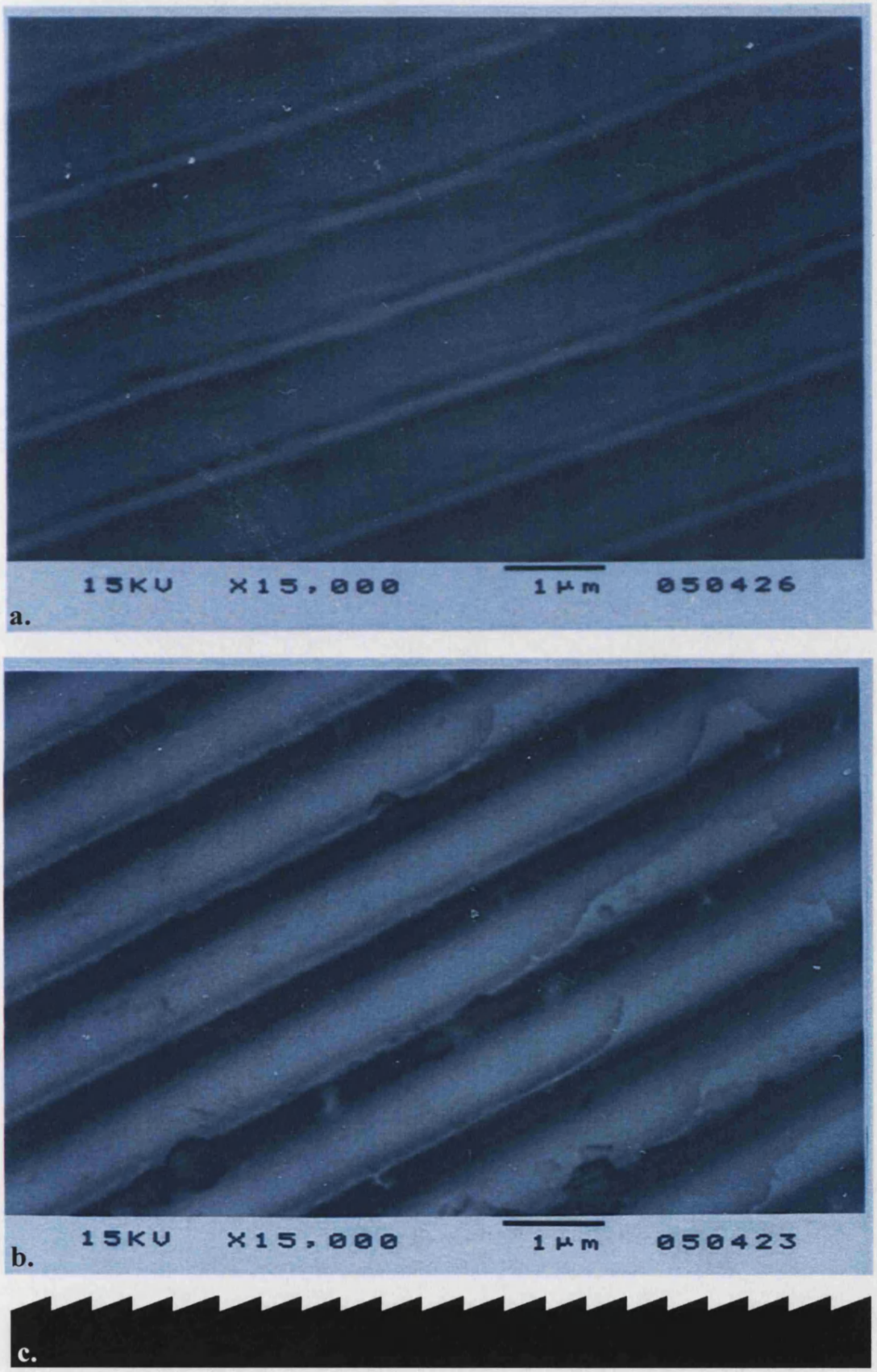

Fig. 62 Scanning electron micrographs of a holographic metal shim (a) and clear silicone rubber grating replica (b) after casting. The grating profile is blazed in cross-section (c).

CONTROLLED DEFORMATION OF SILICONE RUBBER GRATINGS

The Poisson ration of silicone rubber prevents unidirectional deformation. As the material is stretched its length increases, whilst width reduces. The surface of the silicone rubber may also buckle slightly as it is stretched. These natural effects of rubbery materials become a major problem when trying to induce uniform diffraction within this material, and results in a wide spectrum of diffracted colours.

Ideally, a single colour will be displayed, and incremental stretching of the grating will result in larger wavelengths. It may be possible to compensate for Poisson effects within a computer generated hologram, however the high cost associated with producing a bespoke grating are not warranted for this preliminary research. Instead, a far cheaper experimental rig (fig. 63) was designed to support the silicone rubber, and minimise buckling.

PROCEDURE 2 – CONTROLLED DEFORMATION OF A SILICONE RUBBER GRATING

Silicone rubber was vacuum cast into the experimental (fig. 64) rig and allowed to cure at room temperature. Once set, the rig and attached silicone rubber was lifted out from the mould and mounted within an Instron testing machine. The large metal plates of the rig were clamped into the machine (fig. 65) and the rubber stretched. The entire rig was illuminated at 90° with a swan-neck lamp fitted with a 60 Watt bulb, and photographed using a Sony digital camera. The camera was mounted on a tripod to maintain a constant viewing angle and distance.

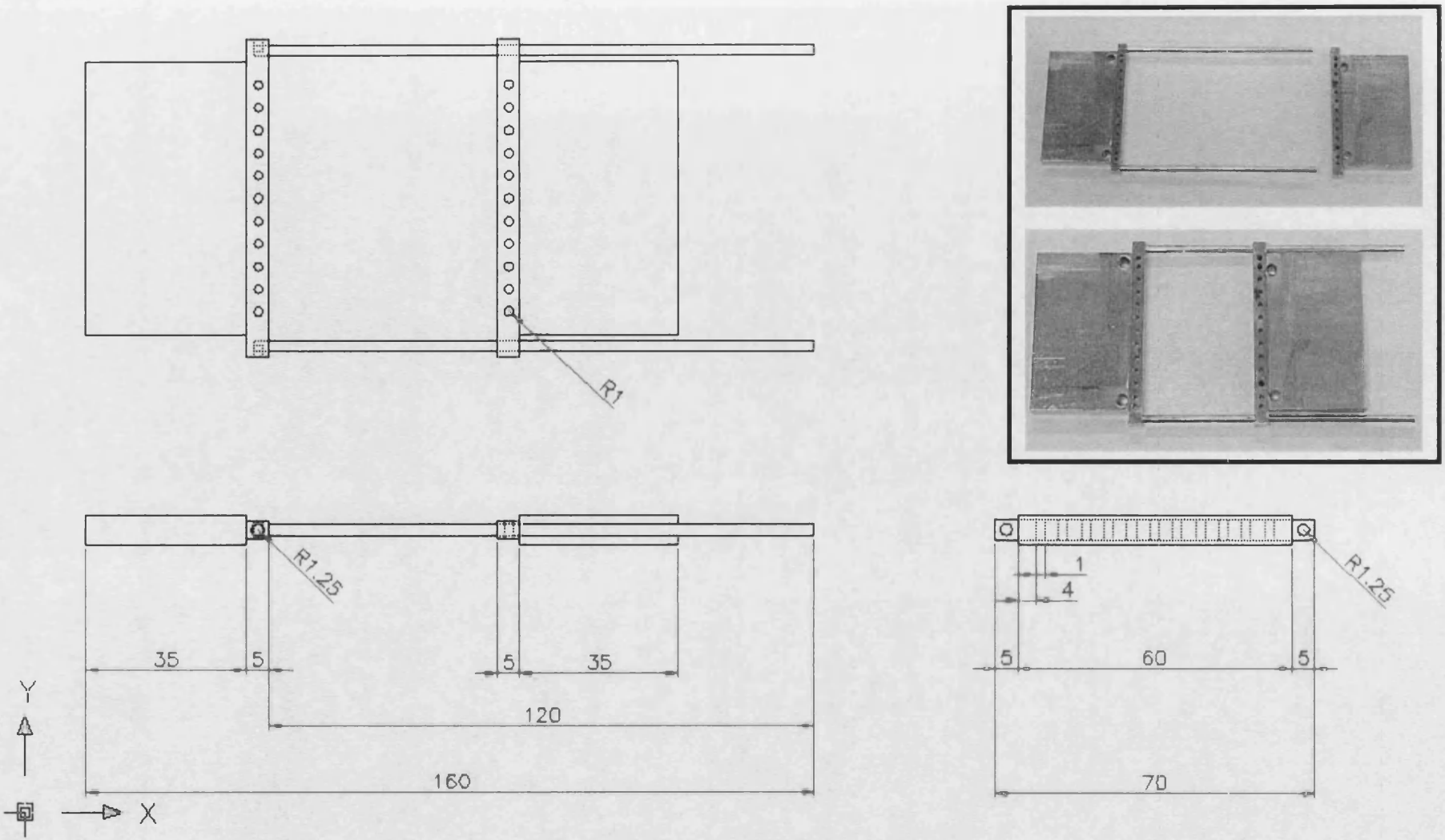

Fig. 63 Experimental rig design and measurements (drawn using AutoCAD software). Inset box, shows two pictures of the machined stainless steel rig. All measurements are in millimetres.

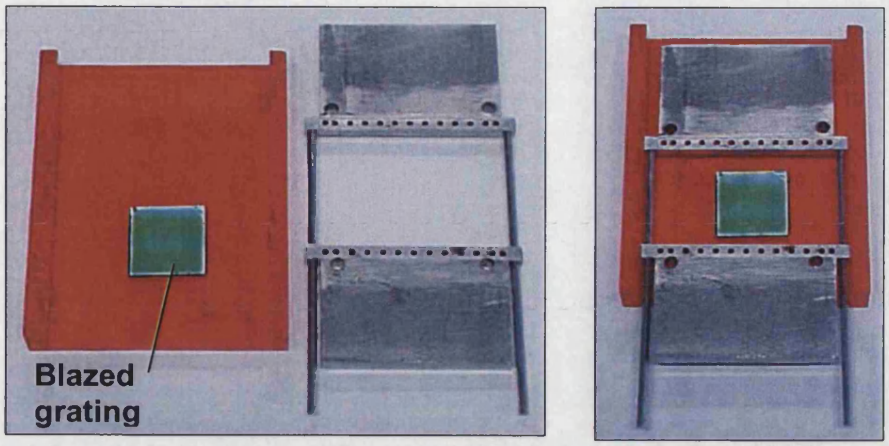

Fig. 64 Stainless steel rig and mould containing a blazed diffraction grating.

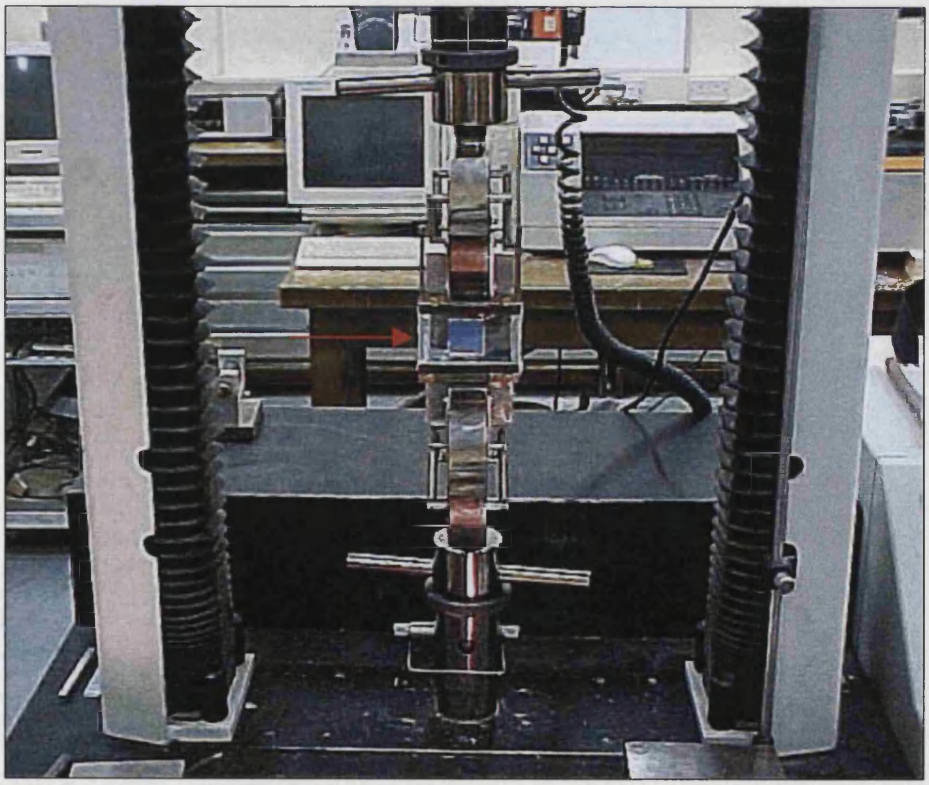

Fig. 65 Stainless steel rig and clear silicone rubber grating (red arrow) are clamped in an Instron testing machine.

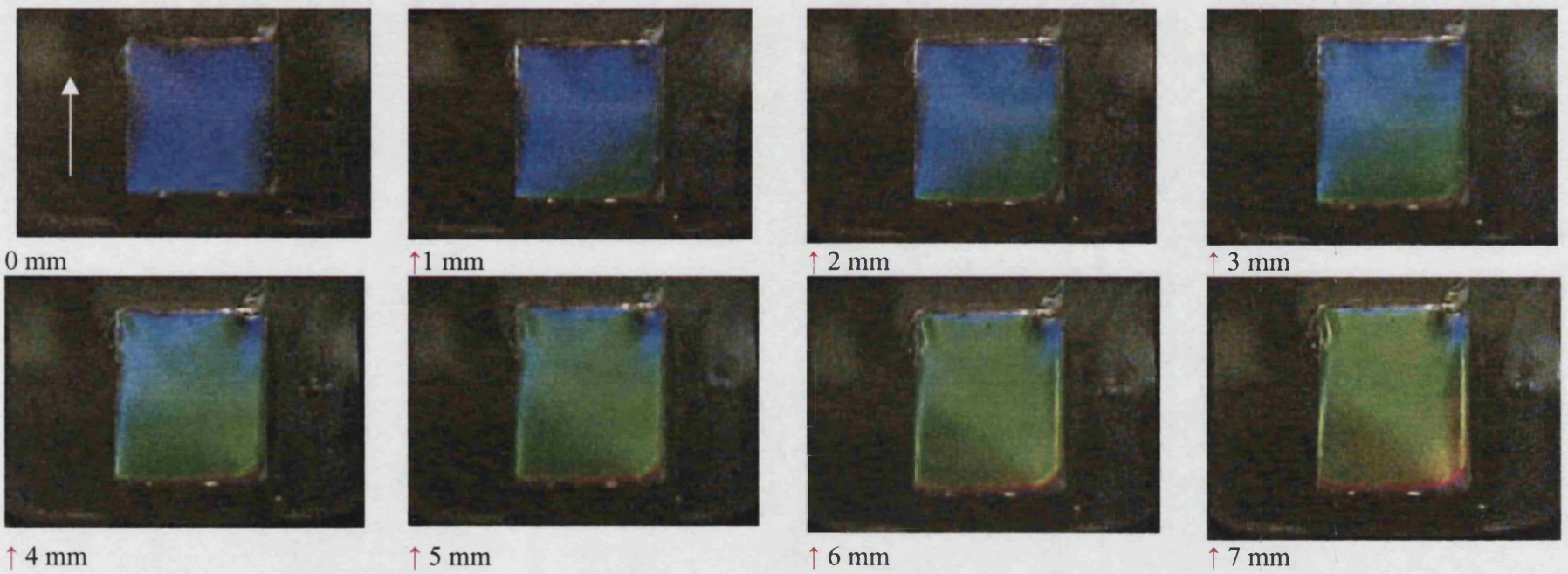
0 mm
↑1 mm
↑ 2 mm
↑ 3 mm
↑ 4 mm
↑ 5 mm
↑ 6 mm
↑ 7 mm

↑ 8 mm

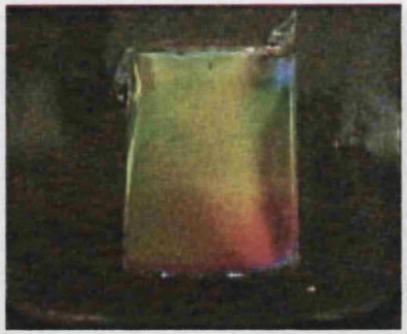

↑ 9 mm

↑ 10 mm

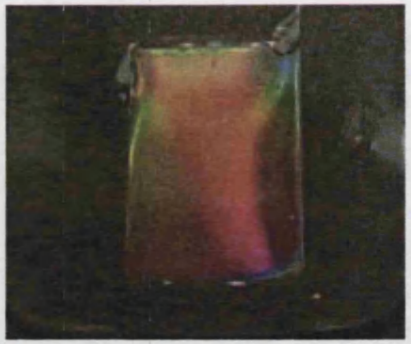

↑ 11 mm

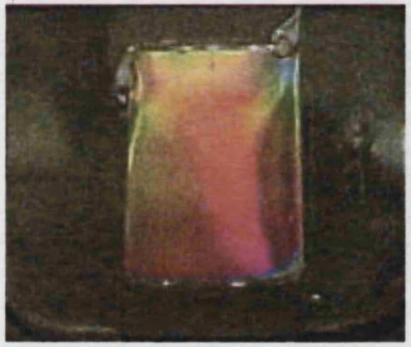

↑ 12 mm

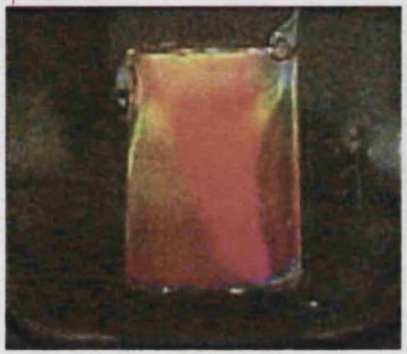

↑13 mm

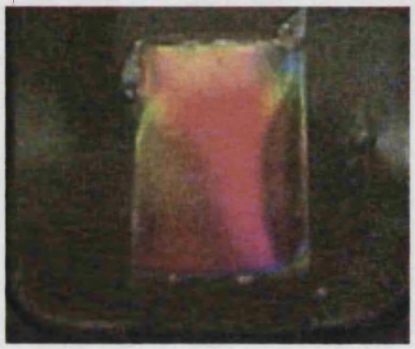

↓ 12 mm

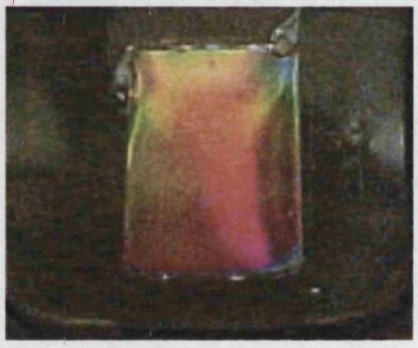

↓11 mm

↓10 mm

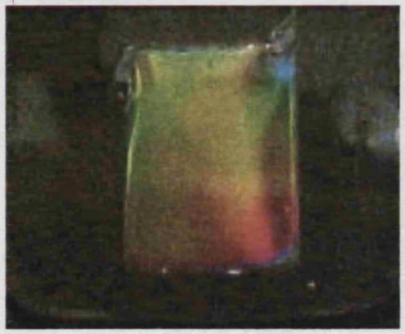

↓9 mm

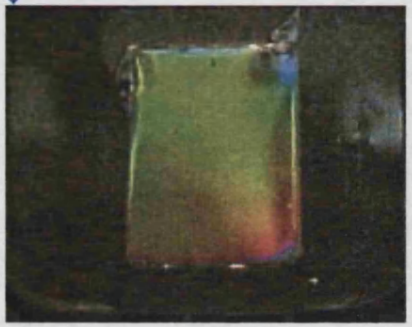

↓ 8 mm

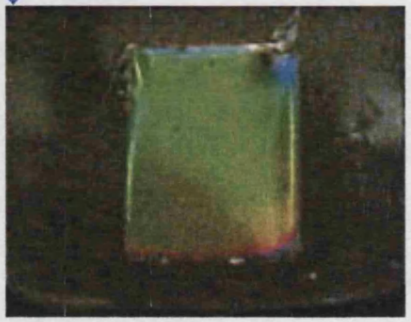

↓ 7 mm

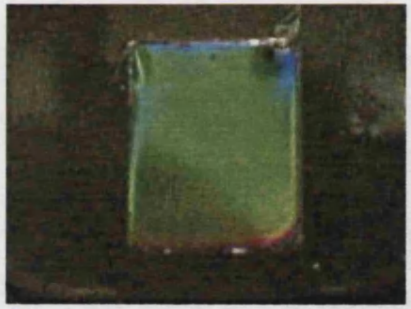

↓ 8 mm

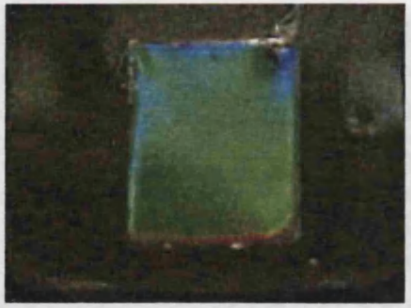

↓ 7 mm

↓ 6 mm

↓ 5 mm

↓ 4 mm

↓ 3 mm

↓ 2 mm

↓ 1 mm

↑2 mm

↑ 3 mm

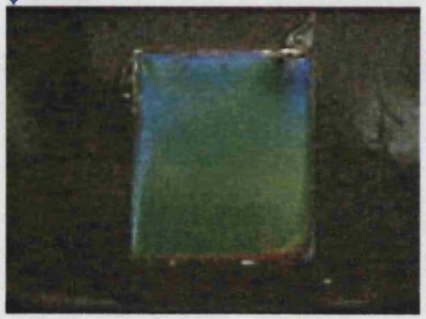

↑ 4 mm

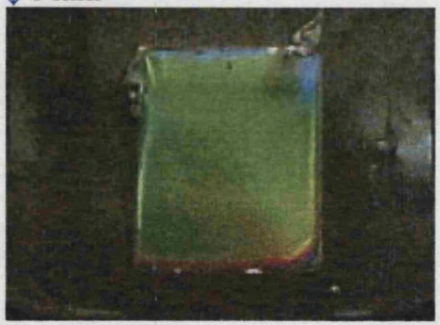

↑ 5 mm

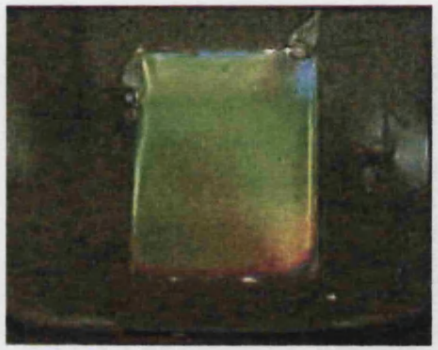

↑ 6 mm

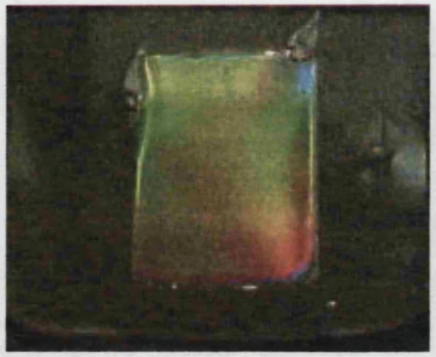

↑ 7 mm

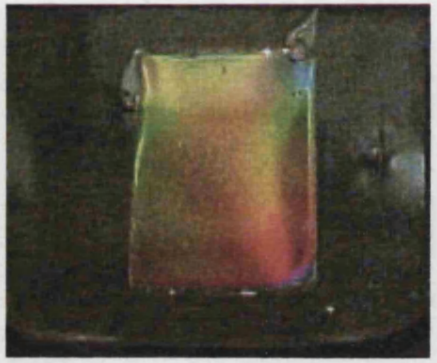

↑ 8 mm

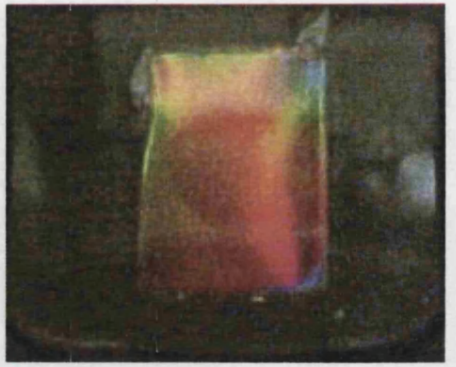

↑ 9 mm

↑ 10 mm

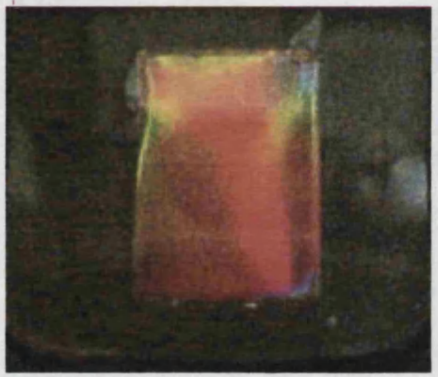

↑ 11 mm

Fig. 66 Cycled extension and contraction of a deformable black silicone rubber grating.

The blazed grating was aligned upwards in the test rig (direction indicated by white arrow in first picture) before it was extended (↑)in one millimetre steps and resulted in larger wavelengths being diffracted (dark blue to red). Reversing the direction of stretching in the Instron (↓), therefore retracting the rubber in one millimetre steps, resulted in shorter wavelengths being diffracted (red to blue).

This silicone rubber grating is a replica of a blazed diffraction grating taken from a spectrophotometer. The blazed angle is pointing toward the top of each page, i.e. same direction as the red arrows. All images were photographed with a Sony digital camera mounted upon a tripod, which remained at a fixed distance and angle. The grating was illuminated at 90° with a swan-neck lamp fitted with a 60W bulb only.

PROCEDURE 2: RESULTS

The unwanted surface buckling effects of silicone rubber were reduced by the design of a supporting rig. The rig allowed the rubber to be freely stretched in one direction, but prevented deformation in the orthogonal direction. This gave a more uniform distribution of colour when the rubber grating was stretched and relaxed. Stretching the silicone rubber increased the grating's periodicity, giving a controlled spectral shift towards red. Releasing the strain allowed the rubber grating to retract and return to its original shape and colour (spectral shift towards blue, fig. 66). A total deformation of 52 % (13 mm) was required to span the visible spectrum, progressing from a dark blue to pale red. This is slightly higher than the theoretical deformation of 40%, and is due to the fact that the grating profile (as well as the spaces in between) increases in size as the grating is stretched. The more conservative hypothesis of 40% deformation did not consider that the actual grating profile would deform.

A maximum deformation of 72 % (18 mm) was achieved with a very thin film of silicone rubber (≈ 1mm thickness) before it broke from the supporting rig. However, cycling up to 60% deformation had no detrimental effects upon the silicone rubber, colours formed, or resting colour of the grating.

PROCEDURE 2: CONCLUSIONS

The formation of deformable diffraction gratings is a novel and patentable idea. It has provided one solution as to how an iridophore cell could be mimicked. It does not however lend itself to a camouflage application at this stage. The non-uniform strain effects of silicone rubber are too severe, and even with the addition of a support rig does not diffract a uniform peak wavelength. Embedding fibres within the silicone rubber may reduce unwanted deformation along the sides of the material. Horizontal fibres may resist any narrowing of the material as it is stretched vertically.

This uniform strain could be established by embedding chitin fibres (per. comm. J. Vincent). It is also possible to activate a colour change with vertically embedded fibres. Fine 0.25 mm Nitinol wires (shape memory alloy) were cast into a silicone rubber grating. Once cured, the wires were caused to contract with a 9 V battery causing a shift in diffracted colour. However, repeated activation caused the wires to work free from the silicone rubber.

The need for mechanical stretching does not lend itself as a practical solution to a cephalopod skin mimic. It would also be difficult to randomly orientate rubber diffraction gratings and induce a spectral shift. The idea may however have a number of different commercial applications.

Please see appendix (page 217) for additional work on non-deformable, injection-moulded diffraction gratings, and colour changing fibres for the textile industry.

PROCEDURE 3: A NON-MECHANICAL APPROACH

MOTILE DIFFRACTION GRATING

This procedure is concerned with the formation of a diffraction grating that can be switched on and off, and has been inspired by the ACh induced morphological changes seen in cuttlefish iridophore cells. The following methods are based upon the combination of a number of well-established procedures. These include the formation of diffraction gratings using light interference, electrophoresis, and the affinity binding of chemical dyes to proteins.

Hypothesis

Electrophoresis is a commonly used technique which moves oppositely charge molecules within or upon a material. I intend to use electrophoresis to align particle so

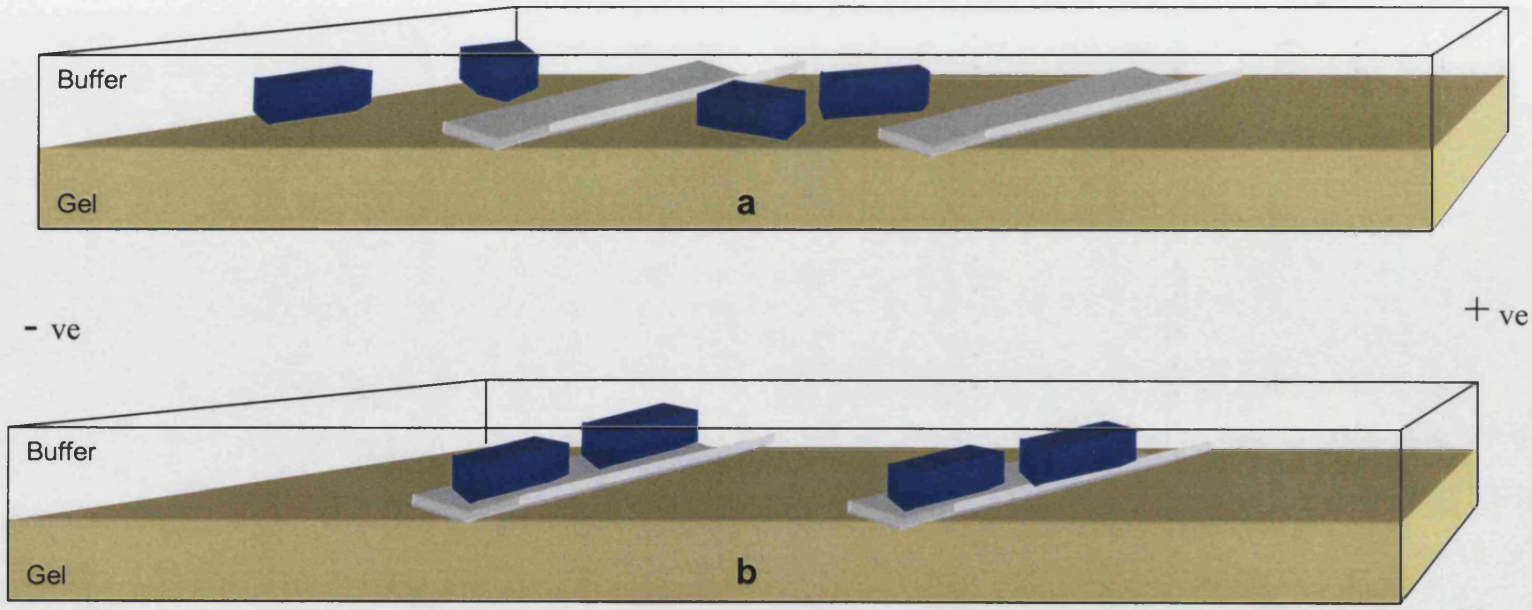

Figure 67. Motile diffraction grating.

A photo-reactive cross-linking agent (grey chevrons) will be used as the invisible diffraction grating. This will bind specific particles of a higher refractive index (blue blocks), thus creating a visible diffraction grating. **a.** Non-diffractive as particles are dispersed. **b**. Diffractive, as particles are bound to the cross-linking agent. Not to scale.

that they may form a diffraction grating, and then by reversing electrophoresis distort the grating, i.e. switch it off. The difficulty is aligning particles in nanoscale lines that are equally spaced apart so that they may diffract light. It would be easier if particles could bind to an invisible grating (i.e. low refractive index), and then use electrophoresis to detach them. Simply by reversing the polarity of electrophoresis, the particles could be made to bind and un-bind (dissociate) from the invisible grating (fig. 67).

I have briefly discussed how holograms and diffraction gratings can be generated within a computer, but they can also be formed using coherent beam interference. This more conventional approach works by exposing a photographic plate to interference patterns that are generated by an object placed between two coherent light beams (Outwater and Hammersveld, 1995). It does not create a physical grating profile, but instead a photographic profile that can diffract incident wavelengths. The photographic plate could be substituted by any material coated in a photo-reactive chemical. I used a Dextran gel as the supporting material, and covered this in a photo-reactive cross-linking agent. The cross-linking agent would ideally have a refractive index that is equal to the gel base, and would therefore appear invisible, as it does not diffract light. It would however have a high affinity for a dye molecule and bind it when the two come in contact.

The disadvantage of this method is that the grating can be formed only on the surface of a material.

Electrophoresis

Electrophoresis is the migration of a charged particle under the influence of an electric potential. It is widely used in biochemistry and chemical engineering as a method of separating molecules of differing charges or molecular weight, such as

proteins, enzymes and nucleic acids. Separation occurs within a matrix (normally a gel) immersed in a conducting solution, and molecules migrate at different rates through the matrix according to their charge and / or molecular weight. However, we wish to perform electrophoresis on the surface of a material, i.e. in free solution. This is rarely done, as heat generated by electrophoresis induces convention currents within the conducting solution and disrupts separation.

The bio-specific binding interaction between two molecules, can occur both in free solution or within the pores of a hydrogel matrix. These are termed affinity interactions. Again, these interactions are commonly used in biochemistry to provide the basis for a number of separation techniques (Hermanson *et al.*, 1992). However, in this situation we should like to be able to reverse the affinity interaction under isocratic conditions (i.e. without changing the chemical environment). This is not a common procedure. Consequently, a student project, under the supervision of Dr. J. Hubble (Department of Chemical Engineering, University of Bath), was carried out. This work is summarised below:

Summary of Student Project (Sinclair, 2002)

The aim of this work was to move a charged dye molecule through a support matrix using a weak electric field. An area within the matrix contained a bound protein, to which the dye has a high affinity. Upon meeting this protein the dye will bind, become immobilised, and form a coloured boundary. Increasing and reversing the electrical current, so as to break the dye-protein bond, will then disperse the coloured dye.

Dissociation of a triazine dye and lysozyme

The triazine dye, Cibacron blue F3GA (Sigma chemicals), was selected as the most suitable for this experiment. It is widely used as an affinity ligand in the

purification of proteins, due to its strong colour, net negative charge, and its ability to bind to a variety of proteins in particular the protein lysozyme. Lysozyme is an enzyme found in chicken egg white, and can easily be coupled to dextran molecules, which were used to make the gel matrix. In this instance lysozyme shall be bound to dextran (a carbohydrate) in the support matrix, and then used to reversibly bind the moving triazine dye (fig. 68).

Dextran was used to form the supporting gel matrix. It is a glucose polymer with an abundance of hydroxyl groups which makes it suitable for covalently bonding further proteins. This matrix material has been extensively studied and is routinely used by Dr. Hubble's group.

PROCEDURE 3A: METHOD

The student produced a dextran gel matrix consisting of three layers. This consisted of two 'sandwich' layers of dextran, and in between a layer of dextran and bound lysozyme (fig. 68).

Each gel plate was placed in a vertical electrophoresis bath filled with a buffer solution (number of buffer solutions and concentrations tested). Cibacron blue was placed in wells at the top of each gel using a long needled pipette. A voltage between 80-250V and current between 25-30 mA was then applied across the plate. Successful forward propagation of the dye and immobilisation at the lysozyme interface would then prompt a reversal of current, by simply switching the electrode connectors.

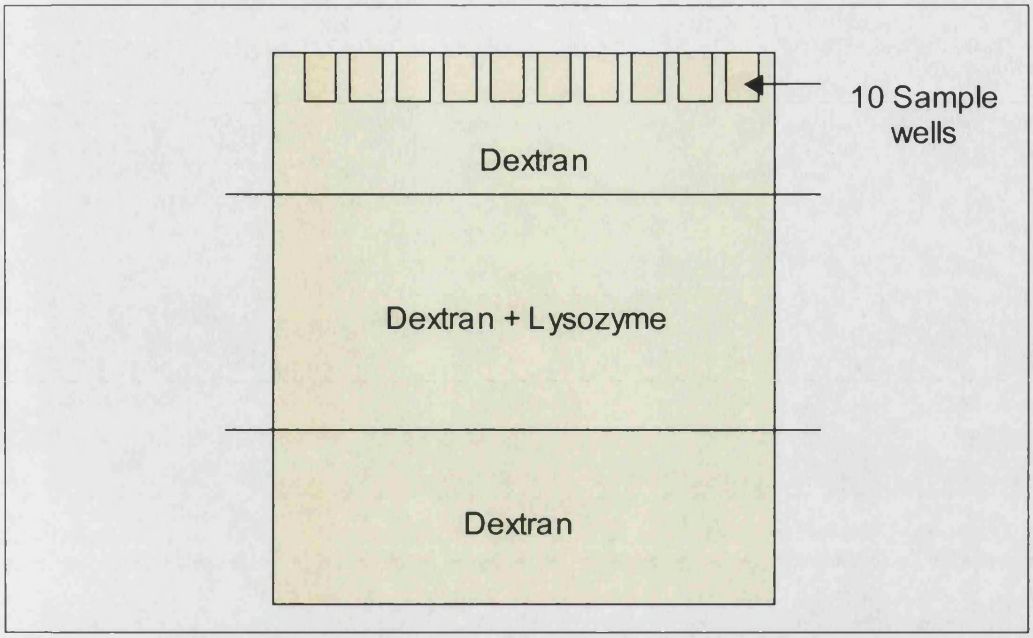

Fig. 68 Composition of the experimental gel plates.

PROCEDURE 3A:RESULTS

Only Dextran gels with a large pore size permitted the forward migration of Cibacron blue to the lysozyme interface. The ideal composition of this gel was determined to be 28 % 43K and 42 %513K Dextran (dextran-DUS-NH_2-Triazine) and

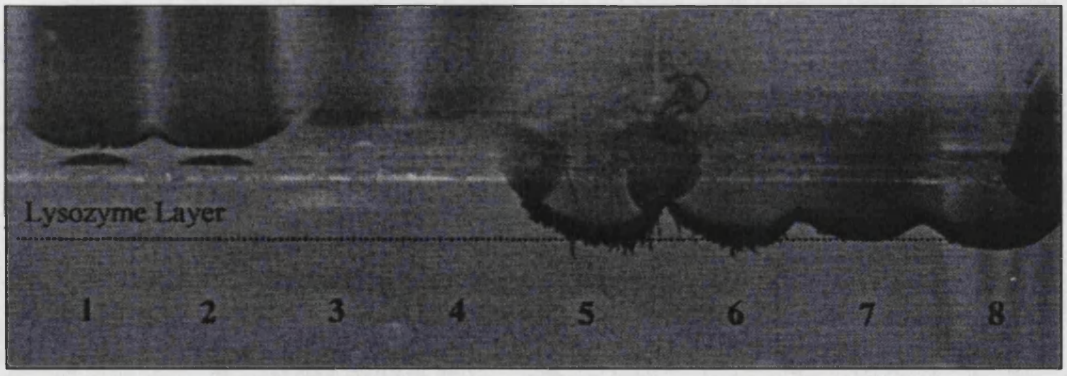

Fig 69 Lysozyme binds Cibacron blue in wells 5 to 8.

Samples: 11K dyed Dextran-CB (1,2), Haemoglobin (3,4), Cibacron Blue 7 days old (5,6), Cibacron Blue 24 hours old (7,8).

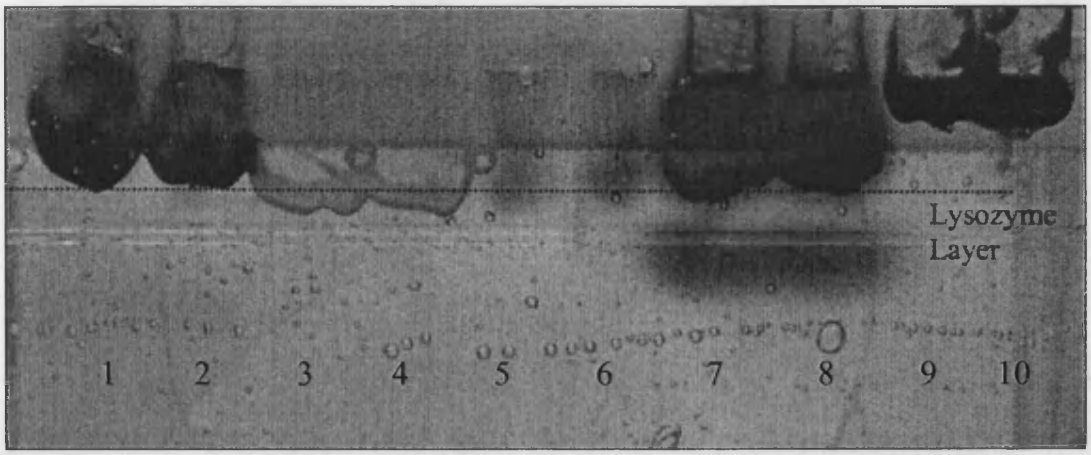

Fig. 70 After material had bound at the lysozyme layer the electrical potential was reversed. As a result material can be seen in the wells and also bound at the interface. This figure suggests that both Cibacron blue and Procion red dissociate from lysozyme after the electrical potential has been reversed for 3 hours.

Samples: Procion Blue (1,2), Procion Yellow (3,4), Haemoglobin (5,6), Cibacron Blue (7,8), Procion Red (9,10).

30% water. The middle, binding-layer contained an additional 75-120 mg/ml of lysozyme. This was sufficient to immobilise Cibacron blue in the range of buffers tested (0.01 - 0.1 M Tris-HCL plus 0 - 0.7 M glycine, pH 8-9). Lowering the ionic strength of the buffer increased velocity, and this had a far greater effect than increasing the voltage.

Cibacron blue binds at the immediate interface with lysozyme, and does not migrate though it (fig. 69). This affinity of binding is so great that subsequent unbound molecules cannot penetrate into the lysozyme, and a back-log of unbound dye results. The channel therefore becomes blocked, and the dye spread horizontally within the gel (figs. 69 and 70).

Reversing the potential across the gel did not induce full dissociation of bound Cibacron dye, as the affinity is too great. Instead, unbound dye, that did not reach the

lysozyme layer due to backlogging, simply migrated upwards. However, in additional test with much lower affinity Procion red dye, preliminary results suggest that dissociation can be induced by reversing electrophoresis (fig. 70).

PROCEDURE 3A: CONCLUSION

Although controlled dissociation using Cibacron Blue was not achieved in the short project above, the results are encouraging. Lysozyme can effectively immobilise dyes within a dextran gel matrix. And importantly, lysozyme is transparent. It could therefore be used to form an invisible binding layer. It is now my intention to form this invisible binding layer photochemically, so that ultimately a lysozyme diffraction grating can be formed on the surface of a matrix.

PROCEDURE 3B: PHOTO-REACTIVE BINDING OF LYSOZYME

This procedure addresses the possibility of photo-chemically binding lysozyme to a dextran matrix. It is hoped that a photo-induced cross-linking reaction may ultimately enable a nanometer scale diffraction grating to be formed on the surface of dextran. Lysozyme must therefore be chemically modified so that it includes a photo-reactive portion. Bound lysozyme will then be used to reversibly bind triazine dyes such as Cibacron blue F3GA, or Procion red (see above procedure). To test the feasibility of this idea millimetre scale lines, rather than nano, will be formed at this very preliminary stage.

In order to use light as a method of controlling the distribution of lysozyme, a photo-reactive group will be added to the enzyme. Suitable photo-reactive cross-linking agents are the aryl-azide group (Fleet *et al.*, 1969). These are unreactive in the dark, but rapidly convert into a highly reactive nitrene upon photolysis. This

derivative is electron deficient aryl nitrene, which has a half-life of milliseconds. The high reactivity of this derivative means that it will non-specifically insert into target molecules (e.g. dextran), or it will quickly be destroyed (Hermanson, et al., 1992). The disadvantage of non-specific insertion is that the yield is low, often less than 10%. This may be a problem for nanometre scale applications. Prof. R. Einsthaal (Biology and Biochemistry Dept., Uni. of Bath) suggested I use phenyl azide as it is slightly electrophilic, thus will preferentially bind to hydroxyl groups abundant in dextran (Jakoby and Wilchek, 1977; Dean, 1985).

The high reactivity of the nitrene derivative also demands that photolysis be the last step, lysozyme must therefore be conjugated to the phenyl azide prior to any photo-reactive cross-linking with dextran. Consequently, lysozyme must covalently bind to the phenyl azide in the dark prior to photolysis.

The aryl azide, *4,4'-dithio-bis(phenyl azide)* (DTPA, $C_{12}H_8N_6S_2$) was selected as the most suitable cross-linking agent (Sigma, UK). It contains two photo-reactive phenyl azides, linked via a disulfide bond (fig. 71). Reduction of the disulfide cross link with either *dithiothreitol* (DTT), or *tris-(2-carboxyethyl)phosphine* (TCEP) will induce a thiol group on DTPA (fig. 72). TCEP was selected, as excess TCEP would not have to be removed before carrying out the subsequent cross-linking reactions (Molecular Probes, 2002). The amine group ($-NH_2$) of lysozyme was then modified and bound to this new thiol group (-SH). Amine-thiol cross-linking is the predominant method of forming such hetroconjugates, and results in a stable thioether bond. The amine itself is not reactive with thiol, and must be modified into a thiol-reactive group called maleimide prior to conjugation. *Sucinimidyl trans-4-(maleimidylmethyl) cyclohexane* (SMCC) is the preferred reagent for inducing thiol-reactive groups at an amine site. Cross-linking thiol and maleimide will then result in lysozyme being

bound to the photo-reactive DTPA (fig. 73). Irradiation will then bind this complex to the dextran matrix.

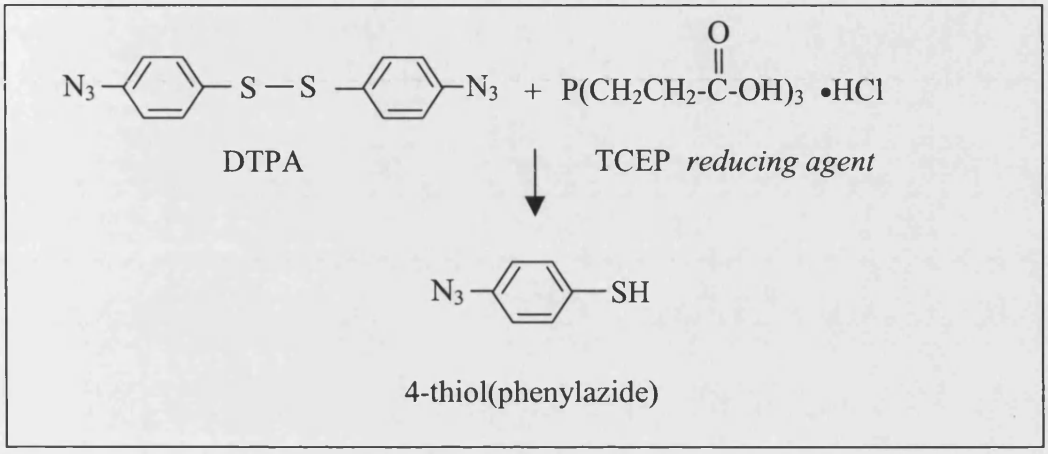

Fig. 71 Thiolation of DTPA

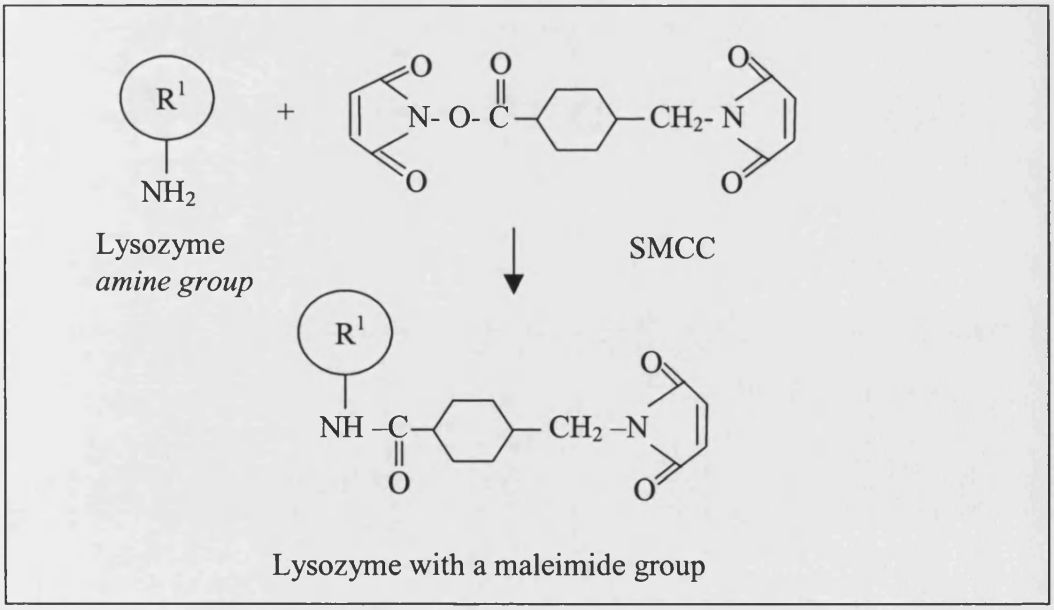

Fig. 72 Inducing a maleimide group on lysozyme.

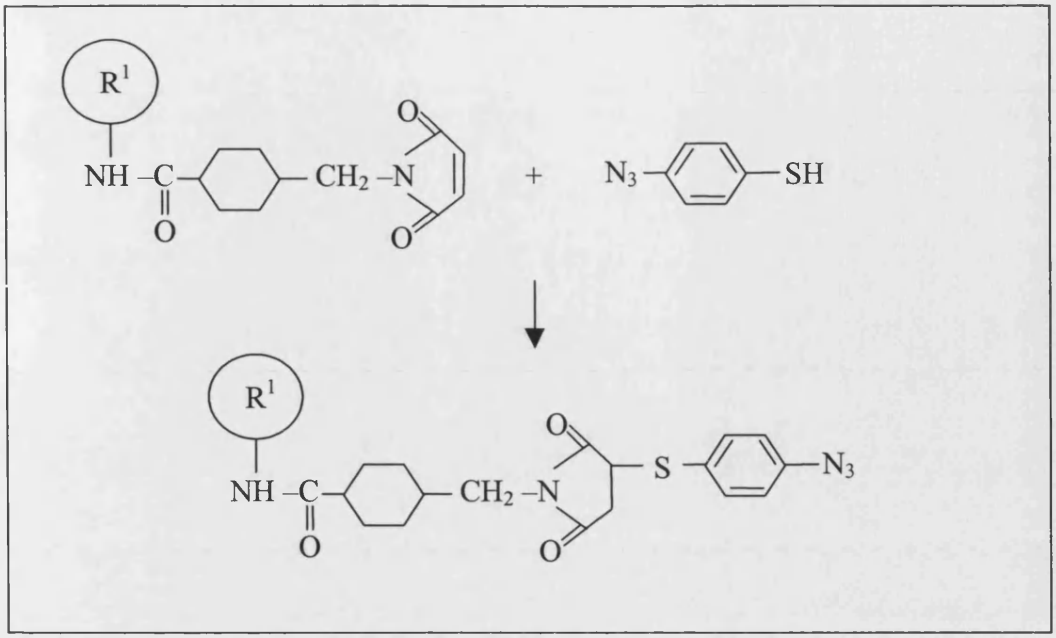

Fig. 73 Thiol and maleimide conjugation. The lysozyme is now bound to the photo-reactive cross-linking agent phenyl-azide.

PROCEDURE 3B: METHOD

(Advice on experimental procedure from Prof. R. Eisenthal, and approved by Prof. P. Holman, Dept. of Biology and Biochemistry, Univ. of Bath).

All procedures using DTPA were conducted in a photographic dark room, equipped with three Kodak safe lights, and an electronic balance.

Maleimide derivatisation of lysozyme (based on Molecular Probes, 1999):

A 5 mg/ml solution of SMCC was prepared by adding 100 µl of DMSO (*Dimethylsulfoxide*) to 500 µg SMCC. The solution was then pipetted up and down until it was completely dissolved. The amount of SMCC solution required to modify 200 µl of lysozyme was then calculated:

$$\mu\text{l of 5 mg/ml SMCC} = \frac{15\text{ mg/ml Lysozyme}}{5\text{ mg/ml SMCC}} \times \frac{\text{MW } 334}{\text{MW } 14{,}400} \times MR \times 1000$$

A molecular ratio (*MR*) of 1.25:1, SMCC to lysozyme[18], was advised and thus 87 µl of SMCC solution was added to 200 µl of lysozyme, and stirred for 1½ hours to allow maleimide conjugation.

Purifying lysozyme conjugate (based on Molecular Probes, 1999):

Two resin spin columns, which exclude 30,000 MW proteins, were used to separate the conjugated lysozyme. Each resin column retains molecules smaller than 30,000 MW, and allows larger to pass through. However, a maximum of 250 µl of solution can be loaded per column. The maleimide derived solution was therefore split evenly between the two columns and centrifuged for 5 minutes at 1100 rpm. (The resulting lysozyme-maleimide conjugate must be used within 3 hours).

Thiolation of DTPA (based on Molecular Probes, 1999):

CARRIED OUT IN THE DARK

TCEP solution was prepared by dissolving 3 mg of TCEP in 3 ml of 0.1 M NaCl (pH 7.5). In a separate vial 500 µl of TCEP solution was then added to 200 µl of DTPA (15 mg/ml, dissolved in DMSO) and mixed before incubation at room temperature for 15 minutes.

Conjugation to dextran (based on Sigma Aldrich DTPA product information):

The conjugated lysozyme-azide solution was poured onto freshly prepared dextran plates[16] (under safe light). It was then irradiated using a broad band UV bulb (range 250-400 nm; Applied Photophysics Ltd.). This was carried out inside a protective light box, to minimise operator exposure. UV protective goggles were also worn throughout the experiment. The bulb was set at a distance of approximately 10

[18] *Lysozyme*, MW 14,400. 15mg/ml in 0.1M sodium phosphate (di-sodium hydrogen orthophosphate anhydrous). *Dextran*, 28 % 43K and 42 %513K Dextran (dextran-DUS-NH_2-Triazine). Both prepared by Ronshang Zhang, Dept. of Chemical Engineering, Univ. of Bath.

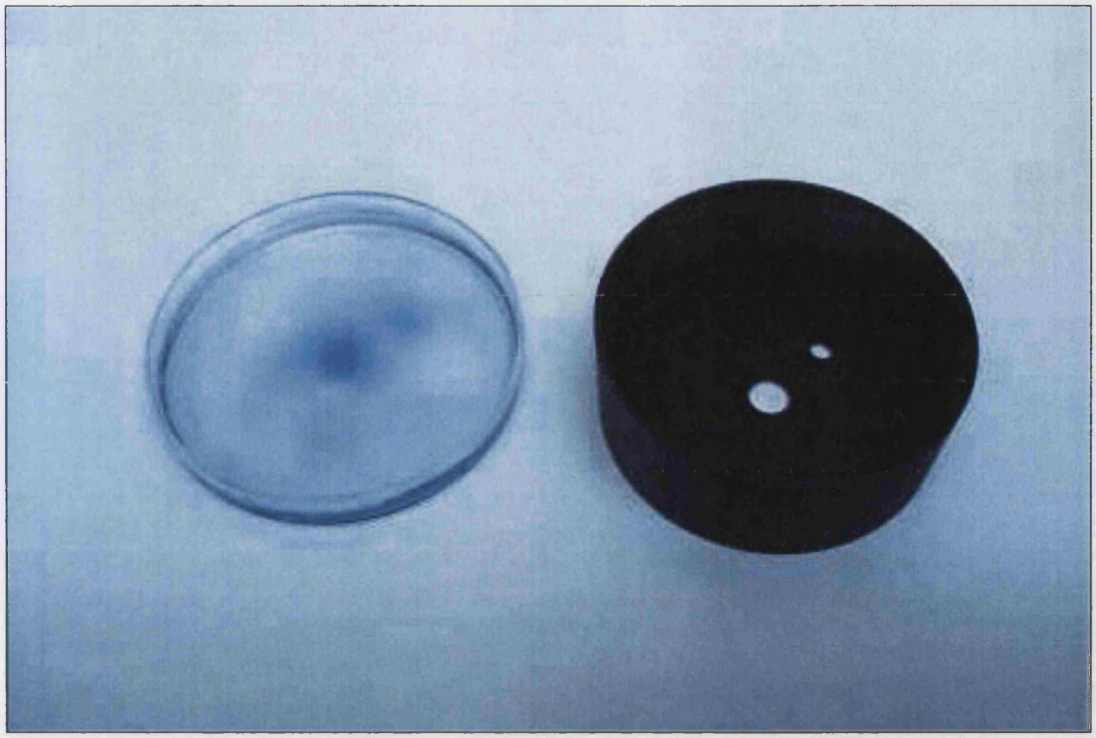

Fig. 74 Dextran gel plate and photo-chemically bound lysozyme stained with Cibacron blue. The corresponding black exposure mask is also shown. Exposure time 3 minutes.

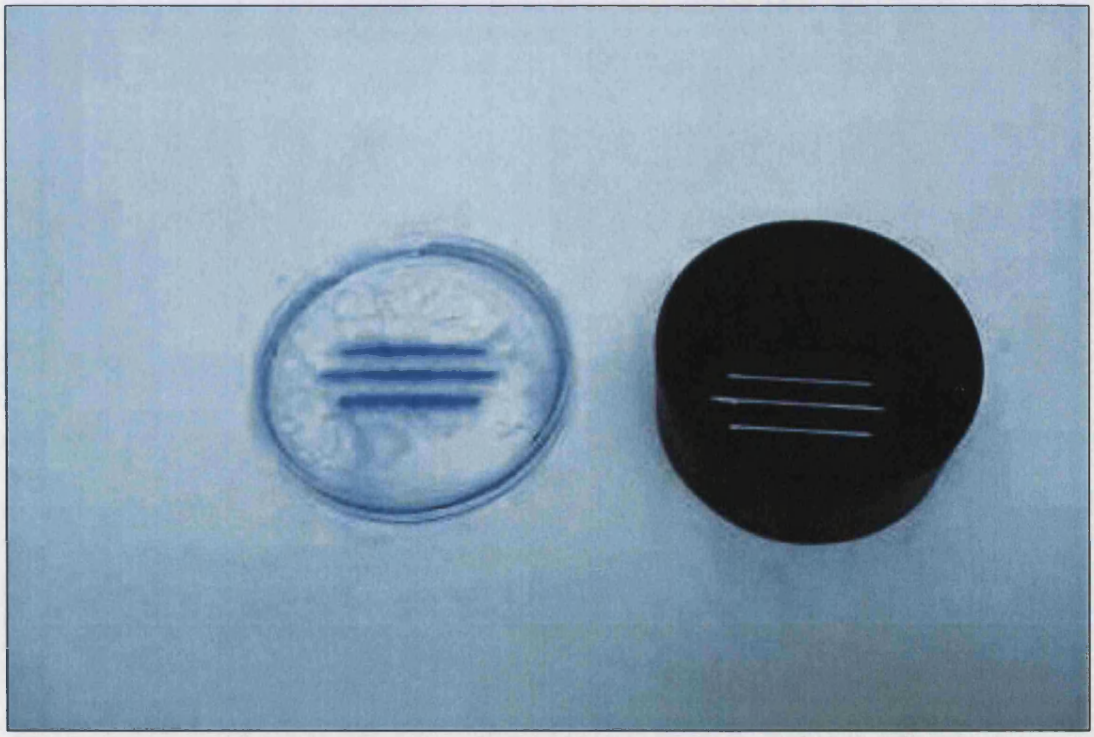

Fig. 75 Dextran gel plate and photo-chemically bound lysozyme stained with Cibacron blue. The corresponding black exposure mask is also shown. Exposure time 5 minutes. This higher exposure time gives a more definite pattern, suggesting more of the lysozyme bound to the surface. However, it damaged the dextran surface and as a consequence it appears mottled.

cm away from the gel surface, and a mask (grid of circular holes) was placed directly on the gel. UV exposure time was 3-5 minutes.

Each dextran plate was then rinsed in tris-buffer and flooded with a very weak solution of Cibicron blue, before rinsing again (figs. 74 and 75).

PROCEDURE 3B: DISCUSSION

The photoactive binding of lysozyme is encouraging, and lends itself to further development. The results suggest that the same chemical method could be used to produce much smaller lysozyme gratings. However, in order to produce a motile diffraction grating that is electrophoretically switched on and off, a more suitable dye is required. It is suggested that weak affinity Procion red dye be tested more rigorously.

SUMMARY 2

A true iridophore cell mimic has not been produced. Although, a number of prototype materials have been successfully developed. I do not consider that any of these at present, are suitable for military camouflage. This is due to inherent iridescence problems. However, a random arrangement of plastic diffraction gratings, supported within a low refractive index material, may produce less iridescent colours. Further work is required to accomplish this, and I suggest collaboration between biologists, physicists, and material scientists.

The prototype gratings that have been developed are patentable (as discussed with Abel and Imray, University of Bath patent attorney) and may have commercial value. A recent article in New Scientist (Hogan, 2004) discusses the industrial demand for non-pigment based colours, and highlights diffraction grating and multi-layer interference as a replacement for paints and dyes (see also appendix, page 217).

Deformable gratings may offer other military applications, which diffract wavelengths outside the visible spectrum. These may include anti-reflective coatings, infra-red dispersal mechanisms, or stealth materials.

Appendix:

Optical Oceanography

We wish to investigate an aquatic camouflage system for possible land based applications. It is therefore important to consider how *S. officinalis* is illuminated in the ocean.

When light strikes the interface between two dissimilar refractive media, such as air and water, it can be both reflected and transmitted (see also fig. 29). Some polarisation may also occur. The amount of reflection (and degree of polarisation) depends mainly upon the angle of incident light, and this can be determined using Fresnel's law of reflection. However, it is generally approximated that 5% of incident sunlight is reflected back into the atmosphere at the ocean surface. The remaining light is transmitted into the sea where it is slowed down ($\approx$ 1/3 slower than in air) by this denser, higher refractive medium and as a consequence changes direction. This is known as refraction, and any directional change is in accordance with Snell's Law.

Light that is transmitted through the ocean (and atmosphere) must also contend with interactions between suspended particles, gasses, dissolved substances, and plankton. Each of these components, including water itself, may absorb or scatter portions of the light. This may again alter the course of photons, or completely absorb them. These factors determine the rate of decrease of light intensity, and the process is known as light attenuation. Within the terrestrial environment we can appreciate that intensity alters greatly over the course of a day, and that this directly influences marine light intensity. However, the intensity of individual wavelengths, as a function of the overall intensity, remains almost constant within the terrestrial environment (Le Grand, 1952). This is not the case in water; its strong absorptive properties have a profound effect upon transmitted light. Long wavelengths such as red disperse first,

often within the first few metres of the water column and are almost extinct at 10 metres. A gradient thus exists towards the least absorbed wavelength, short wavelength blue light (≈ 430 nm), which may penetrate several hundred metres. Different wavelengths are therefore attenuated at different rates and this will affect the appearance of colours at depth. Consider, cuttlefish chromatophores (discussed on pages 8 - 9) being viewed at 20-30 metres, red chromatophores will appear black (Packard and Hochberg, 1977). Similarly, white spots will not appear white, but a combination of the incident light present. Light attenuation will also greatly reduce viewing distances, and therefore communication. Green light (483 - 531 nm, page 90) scattered by the iridophore cells will therefore travel considerably further than long wave red. The limited area of light transmission is called the euphotic zone

The direction of light and its intensity are proportional to the sun's position. However, even on a cloudy day light is considered to be ambiguous within an open space. Clouds greatly reduce the overall intensity of light, and the intensity will be reduced further in the ocean by differing degrees of scattering and absorption. Scattering increases radiant distribution, and within the ocean this is predominately downward (fig. 76; another example of Mie light scattering). The scattering of light in air (via both Rayleigh and Mie light scattering) and sea means shallow dwelling *S. officinalis* is illuminated at a wide range of incident angles.

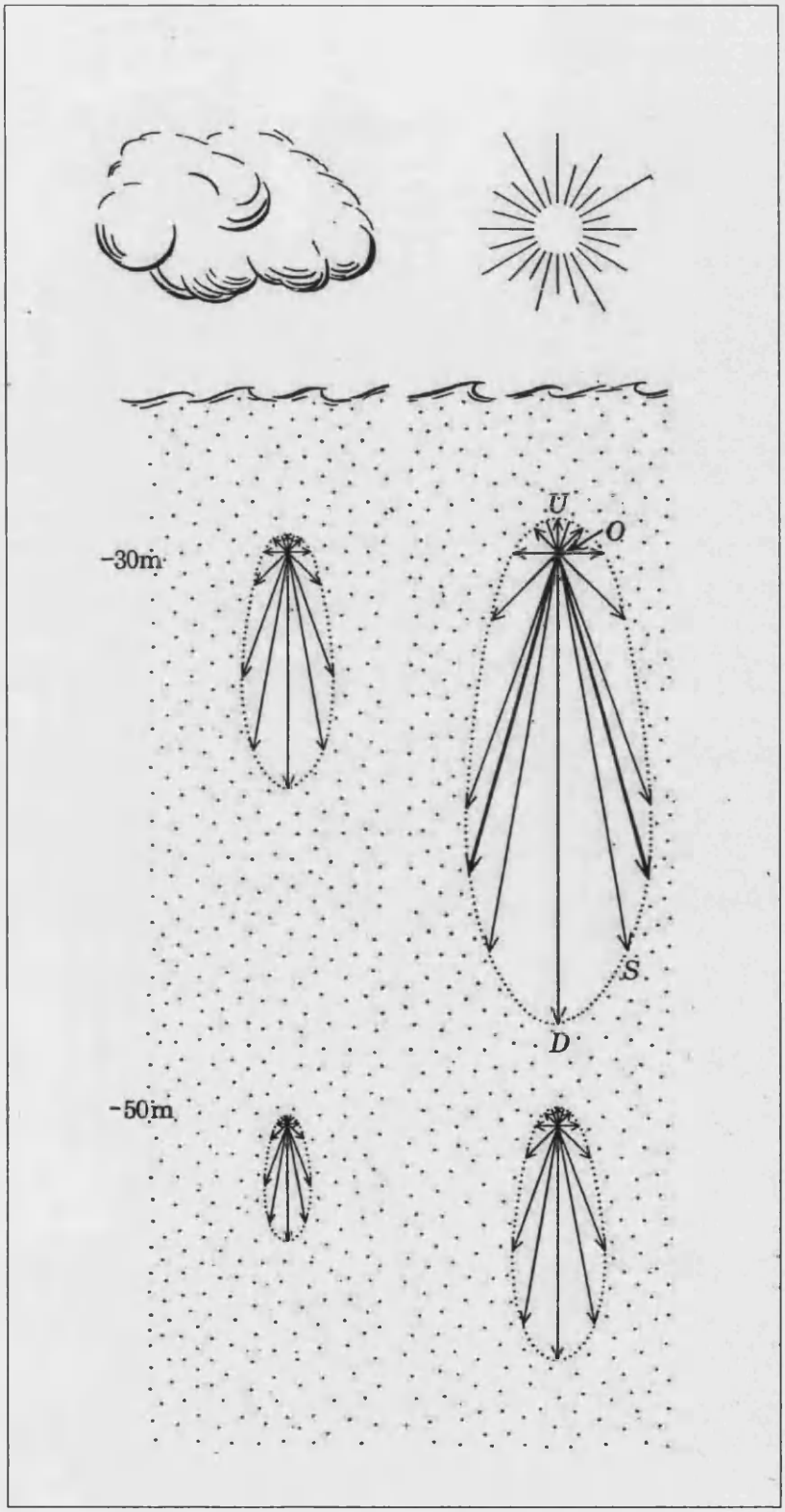

Fig. 76 Radiance distribution in the sea. At the given point *O*, the distribution of light intensities in three-dimensions is given by the dotted line *S* around the axis *UD*. The length of the line gives the relative intensity of light. (From Denton, 1970).

Nearest Neighbour Calculation
Clark and Evans (1954)

This method is used to estimate the distribution of objects and it considers the distance from an individual to its nearest neighbour (r), irrespective of direction. The mean actual nearest neighbour distance (r_A) is calculated as:

$$\bar{r}_A = \frac{\sum r}{N}$$

where 'r' is the distance and 'N' the number measured.

This actual value is then compared to the expected (r_E) distance if the samples were randomly distributed:

$$\bar{r}_E = \frac{1}{2\sqrt{p}}$$

where p is the observed density of samples.

The difference between the actual and expected results is then used to measure the degree of random distribution (R), where R = 1.00 for a random distribution, R = 0 shows maximum aggregation, and R = 2.1491 when distribution is perfectly uniform.

$$R = \frac{\bar{r}_A}{\bar{r}_E}$$

Nearest Neighbour Examples: Distribution of White Fin spots

Specimen 1 (ML = 195 mm)	
White Spot Diameter (mm)	R Nearest neighbour
0.65	1.25
0.93	1.64
0.56	1.54
0.75	2.11
0.63	1.87
0.56	2.28
0.68	1.85
0.66	2.08
0.57	1.75
0.71	1.32
1.02	1.03
0.64	0.88
0.81	1.22
0.73	0.95
0.62	1.25
0.54	1.73
0.56	1.44
0.4	1.42
0.8	1.12
0.48	1.4
0.61	1.76
0.83	1.28
0.32	1.6
0.81	1.56
0.75	1.26
0.66	1.77
0.63	1.28
0.55	1.44
0.75	1.6
0.6	1.1
0.83	1.92
0.9	1.18
0.73	1.8
0.58	0.96
1.04	0.8
0.68	1.6
0.82	1.45
0.45	1.22
OBSERVED MEAN:	
0.68	1.466052632
rA0.147 cm	
ESTIMATED MEAN:	
P = 47.25 cm sq	
rE	0.072739296
R = rA/rE	**2.015**

Specimen 2 (ML = 153 mm)	
White Spot diameter (mm)	R Nearest neighbour
0.72	1.6
0.4	0.83
0.32	1.12
0.48	1.15
0.51	1.44
0.4	1.28
0.64	0.96
0.4	1.04
0.56	0.88
0.66	0.72
0.45	0.8
0.73	0.99
0.8	1.2
0.76	1.33
0.72	1.1
0.4	1.56
0.56	1.35
0.48	1.53
0.8	1.04
0.68	1.02
0.56	1.58
0.48	1.28
0.32	1.2
0.6	0.96
0.74	1.12
0.82	0.9
0.99	0.88
0.56	0.75
1.3	1.37
0.62	0.8
0.56	1.28
0.75	0.9
0.6	1.42
0.66	1.51
0.72	1.23
1.01	1.54
0.89	0.96
0.54	1.04
OBSERVED MEAN:	
0.636578947	1.148947368
rA0.115 cm	
ESTIMATED MEAN:	
P = 43.6 cm sq	
rE	0.075722816
R = rA/rE	**1.517**

Specimen 3 (ML = 138 mm)	
White Spot diameter (mm)	R Nearest neighbour
0.48	1.65
0.67	1.15
0.8	0.96
0.32	0.8
0.72	1.18
0.56	1.44
0.7	1.28
0.35	1.25
0.55	0.88
0.85	0.96
0.5	1.45
0.45	1.62
0.38	1.42
0.9	1.22
1.05	1.56
0.56	1.3
0.8	0.98
1.03	1.34
0.65	0.99
0.8	1.28
0.61	1.52
0.55	0.97
0.58	1.18
0.85	1.36
0.53	0.92
0.42	1.34
0.77	1.44
0.84	0.96
0.48	1.64
0.6	1.62
0.81	1.34
0.75	1.36
0.45	0.89
0.83	1.64
0.94	0.95
0.67	1.42
0.58	1.3
1.02	1.53
OBSERVED MEAN:	
0.668421053	1.265526316
rA0.127	
ESTIMATED MEAN:	
P = 40.4 cm sq	
rE	0.078664596
R = rA/rE	**1.609**

Leucosome Distribution within four leucophore cells:

Leucosomes of Leucophore A	
Dia. (nm)	**R** Nearest neighbour
515.48	373.46
415.54	396.51
305.08	368.20
203.14	310.34
389.24	405.02
241.96	184.12
215.62	441.84
273.52	420.80
473.40	473.23
578.86	526.61
263.22	399.76
368.28	426.06
331.53	273.52
504.96	610.16
373.46	436.52
462.84	483.92
316.05	762.27
252.48	536.52
OBSERVED MEAN:	
360.26	434.94
rA	0.435
ESTIMATED MEAN:	
P = 0.38748 µm sq	
rE	0.80324
R = rA/rE	**0.540**

Leucosomes of Leucophore B	
Cell Dia. (nm)	**R** Nearest neighbour
351.85	551.89
388.31	404.71
666.59	592.83
740.02	545.21
324.47	453.7
518.04	481.45
425.93	537.15
314.51	583.41
509.25	500.48
546.36	500.48
462.32	471.44
248.65	407.03
425.92	416.49
342.59	472.27
296.54	416.78
305.48	703.34
OBSERVED MEAN:	
429.18	502.42
rA	0.502
ESTIMATED MEAN:	
P = 0.396721 µm sq	
rE	0.79383
R = rA/rE	**0.632**

Leucosomes of Leucophore C	
Cell Dia. (nm)	**R** Nearest neighbour
322.01	330.36
408.75	366.5
460.85	464.25
378.46	403.44
450.56	235.62
307.24	563.04
296.08	412.29
305.07	263.35
235.52	433.86
363.52	397.81
204.84	291.07
266.41	428.64
358.44	598.57
209.54	526.24
199.68	190.06
245.76	474.9
491.45	418.12
404.84	305.14
501.76	748.55
563.32	392.31
256.37	268.15
OBSERVED MEAN:	
344.31	405.35
rA	0.405
ESTIMATED MEAN:	
P = 0.329498 µm sq	
rE	0.871051
R = rA/rE	**0.465**

Leucosomes of Leucophore D	
Cell Dia. (nm)	**R** Nearest neighbour
501.76	466.5
404.48	330.68
296.96	361.13
199.68	304.58
378.88	397.47
235.52	180.67
209.92	433.6
266.24	412.91
460.07	564.58
563.12	516.02
256.77	418.12
358.45	392.31
322.56	268.45
491.8	598.79
363.52	428.44
450.56	574.9
307.24	748.24
245.76	312.79
204.13	303.47
407.29	270.88
OBSERVED MEAN:	
346.24	414.23
rA	0.414
ESTIMATED MEAN:	
P = 0.410568 µm sq	
rE	0.780328
R = rA/rE	**0.530**

Additional Work:

1) Cast diffraction gratings (pages 172 - 191)

Deformable silicone rubber diffraction gratings are a novel and relatively inexpensive way of replicating a diffraction gratings or holograms, and may have commercial applications. I considered that this might be broadened further by the ability to form gratings and nanometer scale structures in a range of plastics with higher moduli.

Injection moulding

Given the ease with which diffraction gratings can be cast into Latex and silicone rubber, I considered whether other plastic casting techniques could be used to replicate diffraction gratings. I therefore decided to investigate if a grating could be moulded onto the surface of a thermosetting plastic by standard injection moulding. Two plastics were available for this test: a high-grade, high-flow rate, virgin polypropylene with a black colouring additive (Lexan black, GE plastics Ltd; suggested by Prof. A. Medland, Mechanical Engineering, Bath); and a recycled mixture of grey coloured polypropylene, which was reground into pellets.

METHOD

In accordance with GE plastic's technical data sheets the Lexan black was pre-heated with an air-drying oven (120°C for 3 hours) prior to moulding. This is to remove excess moisture (>0.02%), which can disrupt surface detail. The recycled plastic was not pre-heated, as a suitable drying temperature and time could not be determined. The plastics were then placed in separate hoppers ready for moulding (fig. 77) and the machine flushed of residual material.

A holographic shim was inserted into a standard injection-moulding tool (master mould; fig. 78) and held in position with double-sided sticky tape. This was

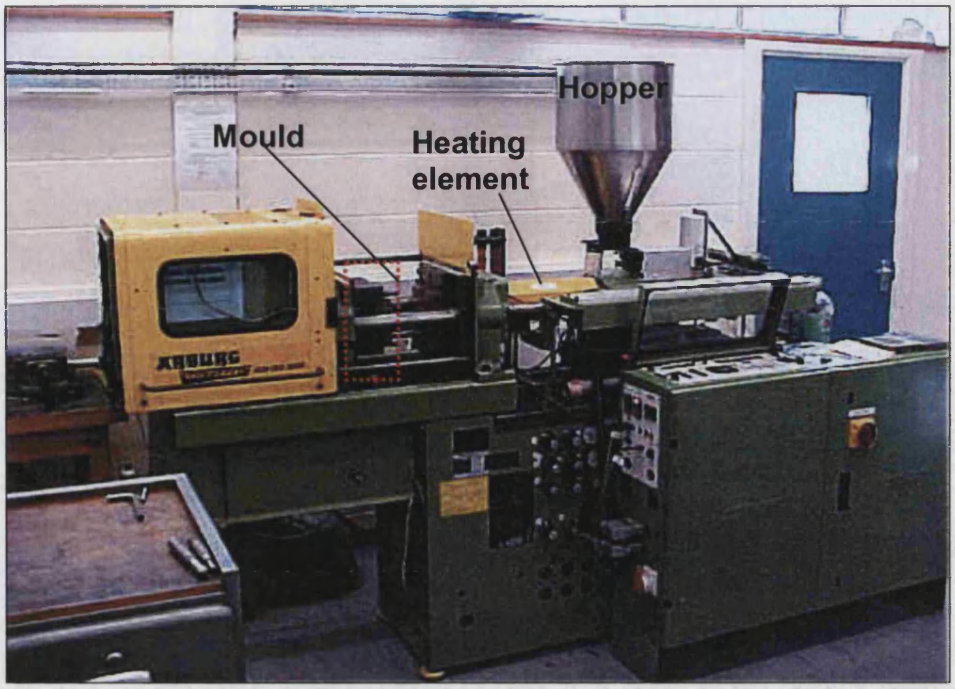

Fig. 77 Arburg injection moulding machine complete with master mould attached (red box) and hopper.

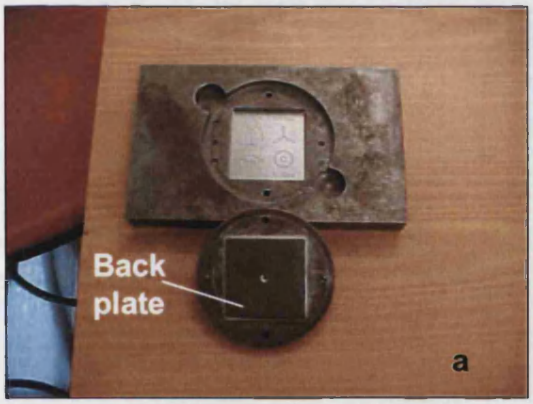

Fig. 78 An injection mould (master) complete with back plate. The polished mould surface is inscribed with four pictures and the Department of Mechanical Engineering logo. **a** Shows the mould 'naked' as normally used. **b** A holographic metal shim has been inserted (red arrow), and then cast. The resulting holographic plastic replica is still attached the back plate (blue arrow). **c** The grating can be easily removed after repeated moulding without damage to the original master.

then cast in an Arburg injection-moulding machine, under a range of temperatures and pressures.

RESULTS AND DISCUSSION

The holographic shim was successfully replicated onto the surfaces of both grades of polypropylene (fig. 78 and 79).

The optimum machine setting for injecting both plastics was found to be the same as that normally used to cast the master mould:

S27:16	t_1 = 1.6 seconds
S29:18	t_2 = 1.1 seconds
S28:25	t_3 = 1.1 seconds
S26:16	Plasticising speed = 160 rpm

Table 8 Optimum settings for the Arburg injection-moulding machine. As determined by Mr. R. Peplar (Dept. of Mech. Eng., Univ. of Bath).

Fig. 79 Injection moulded hologram made from Lexan black polypropylene.

No visible difference in the quality of reproduction was found between the plastics. This suggests that even low-grade recycled polypropylene can be used to replicate diffraction grating and nanoscale structures. Only 30 replicas were produced in each plastic, and the quality of reproduction did not diminish. During this production the hologram did not appear to deteriorate, or become dislodged. This is

encouraging, as mass production would require a continuous manufacturing of thousands of items. Full-scale production cannot be simulated with the Arburg machine, as it is designed for small batch production only. Instead, I suggest that a local plastics company is licensed to carry out R&D on this new procedure. I envisage that a company will be interested as holograms could be incorporated onto the surface of any injection-moulded plastics without having to design and produce a new and expensive master mould. Examples include:

Holographic Packaging – To increase shelf appearance of a product. It is a well-established fact that holograms dramatically increase shelf presence and sales of a product within supermarkets. Embossed holograms are therefore used in cardboard packaging, and can be commonly seen on toothpaste, razor blade, and cereal boxes. I have not found any holograms of plastic packaging. However, the above process could used to form holograms on the surface of any injection moulded plastic e.g. shampoo and fizzy drink bottles.

Security and Anti-Tamper packaging - Damage / opening the package would change the colour of the plastic seal.

2) Light Diffracting Fibres For The Textile Industry

Acrylic fibres are formed in much the same way as injection moulded plastics. The same machine is used, but is instead used to force a molten plastic through a spinneret, from which fine fibres are then extruded. Acrylic fibres therefore vary greatly in diameter, from a few millimetres to several hundred microns. I hypothesise that a diffraction grating, similar to that cast in silicon (periodicity ~1 μm, fig. 62) could be formed on the surface of a fibre by extruding it through a spinneret that incorporates a grating profile (figs.80 - 83).

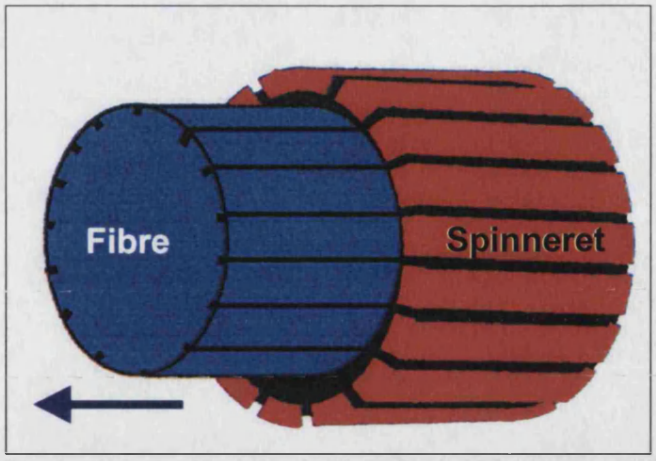

Fig. 80 Diagram illustrating the hypothetical method of forming a diffraction grating on the surface of an acrylic fibre (per. comm. V. Kapsalis, Student at Chelsea College of Art and Design).

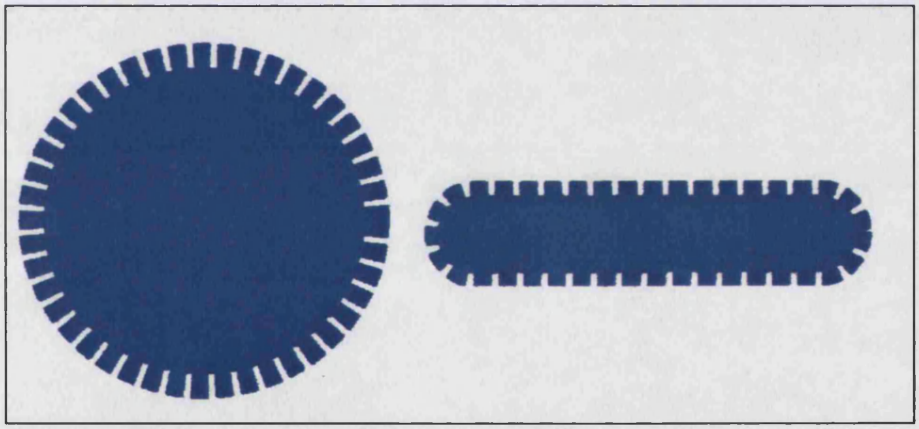

Fig. 81 Spinnerets can be used to produce a range of fibre cross-sections. This diagram illustrates how circular and elongated fibres would be suitable for light diffraction.

Prototype spinneret

A standard spinneret is a circular metal disc (15 cm in diameter and 3 mm thick) that contains approximately 100 small holes (>0.5 mm), through which the plastic is extruded. In order to form a grating on the surface of a fibre, the holes could be etched. However, this would be expensive and may not work for the simple reason

that plastic expands slightly as it cools, which may distort the surface grating. Expansion also occurs during injection moulding, and it was whilst carrying out the previous experiment that I hypothesised how plastic expansion could be used to assist in the formation of diffraction grating fibres.

Hypothesis

Molten plastic is forced through a small lead hole (in the same way as it would when injection moulding). The plastic will then enter a slightly larger channel, which contains the diffraction grating profile. It is in this channel that the plastic will begin to cool, expand and the grating pattern imprinted.

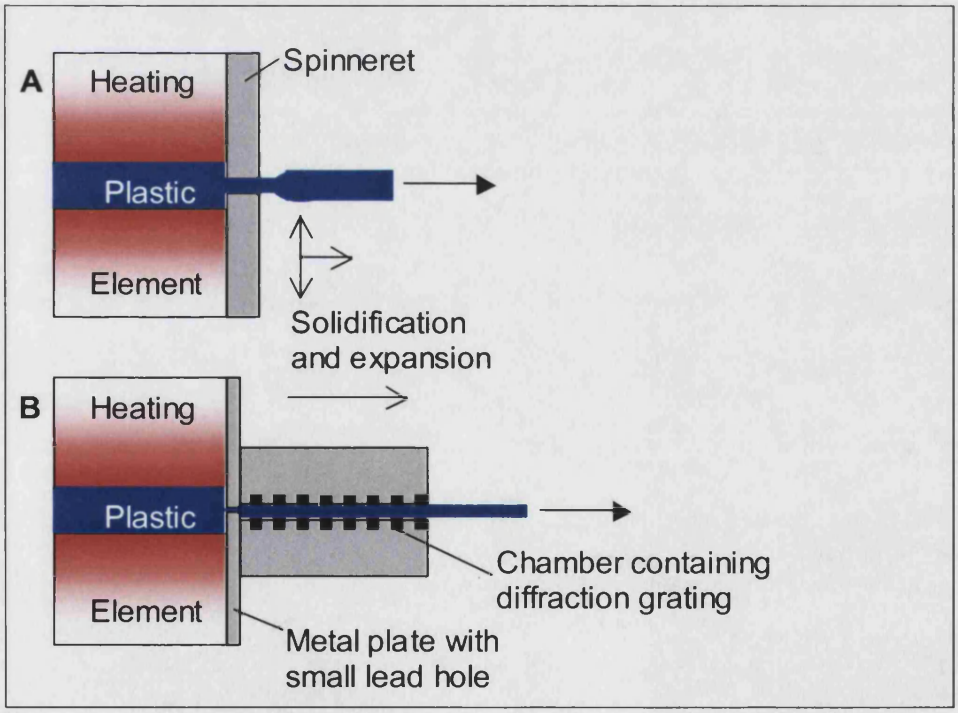

Fig. 82 Diagram illustrating how expansion of a plastic can be used to form diffraction grating fibres. **A.** How a spinneret is typically used to form a fibre. **B.** A small lead hole is used to inject molten plastic into a chamber containing a diffraction grating (profile must run in same direction as plastic).

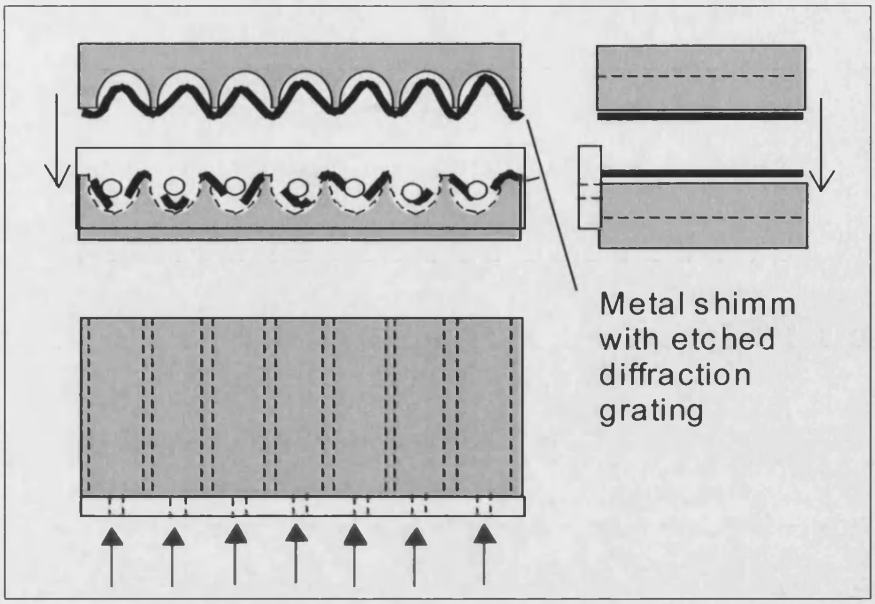

Fig. 83 Isometric drawing of the proposed spinneret for producing 7 light diffracting fibres. This is an exploded diagram of the spinneret, and the two black arrows indicate that the grey plates are clamped together. Two holographic metal shims are therefore sandwiched between the two plates. Blue arrows indicate the direction of molten plastic injection (drawing not to scale).

It is hypothesised that as the plastic solidifies in the expansion chamber, a grating will be formed on the surface of the resulting fibre. Experiments must be carried out to determine the force of injection required, and any effects induced by the speed of solidification. It may also be necessary to heat a section of the expansion chamber in order to maintain some degree of fluidity.

This hypothesis was presented to Prof. Chris Lawrence (Dept. of Textile Manufacture, Univ. Leeds), who fully supports the idea, and wishes to work with the Univ. of Bath in the development of this highly novel fibre.

3) COLOUR CHANGING HYDRO GELS

(Dr. J. Hubble)

Diffraction gratings were cast into the surface of hydrogels. Hydrogels are being developed by Dr. Hubble which incorporate biological molecules. These are capable of selectively recognising specific signals, and responds by changing gel porosity. Larger molecules may then permeate through the gel (Tang *et al.*, 2003). As porosity increases, the gel swells, and this is proportional to specific signal concentration. By incorporating a diffraction grating onto the surface of a hydrogel, the degree of swelling may be quantified. Professor Chris Lowe's group at the University of Cambridge has also conducted similar work to this.

Derivation of Equations 7-9

Personal communication with Dr. T. Birks

The model assumes (a) normal incidence on a multilayer stack with (b) equal path lengths. That is:

$n_p h_p = n_s h_s$

where h_p is the thickness of the iridosomal platelets, and h_s the thickness of the intrairidosomal space. Hence $h_p+h_s = d$ [#].

The motivation for these assumptions is (a) simplicity and (b) this gives the biggest stop bands.

The equation is derived from Russell *et al.* (1995), which provides general results for the behaviour of multilayer stacks. The key results from that paper are eq. 28 on p. 597, and eq. A8 on p. 631:

$ky = \cos^{-1}(A)/d$

where ky is Bloch wavevector, d is the pitch.

A = a fairly complicated expression involving the layer thicknesses, indices and propagation angles, via a parameter p defined in eq. 2 on p. 587.

Assuming normal incidence (beta = 0 hence, $\pi = k\,ni$, where i is P (platelets) and S (space) in turn) and equal pathlengths (see [#] above), you then get a simpler expression for A:

$A = \cos^2(k\,n_p\,h_p) - 1/2\,(n_p/n_s+n_s/n_p)\,\sin^2(k\,n_p\,h_p)$.

The equations [#] can also be manipulated to give

$h_s = d\,n_p / (n_P + n_s)$ and something analogous for h_p.

The centre of the stop band (the first Bragg condition) is given by setting the optical phase change across a complete period to π (so that a partial wave reflected at the second period interferes constructively with one reflected at the first period: round-trip phase change = 2 π), i.e.:

$k\,(n_p\,h_p + n_s\,h_2) = \pi$

which using $k = 2\,\pi / \lambda$ and the expressions for h_p and h_s in terms of d gives the equation for λ_{peak}.

The edges of the stop band are given by setting A = -1 (go closer to the centre of the stop band and A < -1 and ky becomes complex). If chi is defined by

$\chi = k\,n_p\,h_p$

then solving A = -1 for chi gives:

$\cos(\chi) = +/-\,(n_p - n_s) / (n_p + n_s)$

and hence k and then λ_{band}.

λ_{band} therefore has two values (+/-) which indicate the edges of the stop band. It seems right therefore that the two values tend to each other and to λ_{peak} as n_p approaches n_s, meaning the stop band shrinks to nothing.

MEDIA COVERAGE AND PRESENTATIONS OF WORK

News Items:

EPSRC Newsline Winter 2001, Nature's Secret Agents - p12-13

Telegraph newspaper, Cuttlefish gives clue for tank camouflage - 03/02/2002

The Guardian newspaper, Eluding the Enemy -16/01/2003.

The Sun newspaper , Tanks 'to disapear' - 11/04/ 2002

The Bath Chronicle - Thursday June 20 2002, p20

Western Daily Press - 2002

National Geographic News - March 2003
http://news.nationalgeographic.com/news/2003/03/0311_030312_secretweapons1.html

Topics - Univ. of Bath Newspaper 29 July 2002

Innovazione, Arrivano i robot biomimetici – 2002

University of Bath, "Best People" - Annual Report 2001-2002.

Book:

Roger Highfield (2002). The Science of Harry Potter. Headline Press

Significant Presentations:

Meet the Scientist - TechniQuest Cardiff

Institute of Mechanical Engineering (IMechE), South West Regional presentation.

Chelsea College of Art, London Institute (every academic year)
(Project Assistant - Royal College of Art, London)

Prize:

University of Bath, Ede and Ravenscroft Prize July, 2002

REFERENCES

Aristotle (1910). *Historia Animalium.* Translation by D. Wentworth-Thomson. Oxford: Clarendon Press.

Arnold, J.M. (1967). Organellogensis of the cephalopod iridophore: cytomembranes in development. *Journal of Ultrastructure Research*, **20**, pp. 410-421.

BBC, 1983. [VHS Video] *Wildlife on One: Aliens form inner space.* Producer Andrew Cooper (reference no. NBSC24ST).

Bayley, H. and Knowles, J.R. (1977). Photoaffinity Labeling. **In:** *Methods in Enzymology* (eds. W. B. Jakoby and M. Wilchek) **XLVI,** pp. 69-114.

Boletzky, S.v. (1974). The »larvae« of cephaolopoda: A review. *Thalassia Jugoslavica* **10**(1/2), pp. 45-76.

Boletzky, S.v. (1979). Growth and Life-span of *Sepia officinalis* under artificial conditions (Mollusca, Cephalopoda). *Rapp. Comm. Int. Mer. Médit* **25/26**(10) pp. 159-168.

Boletzky, S.v. (1983). *Sepia officinalis.* **In:** *Cephalopod life cycles, Volume 1: Species accounts*, (P.R. Boyle, ed.) pp. 31-52. London: Academic Press.

Boletzky, S.v. (1987). Cephalopoda. **In:** *McGraw-Hill Yearbook of Science and Technology 1988.* pp. 50-53. New York: McGraw-Hill.

Boletzky, S.v. (1996). Cephalopods burying in soft substrata: agents of bioturbation? *No reference, paper direct from author.*

Boletzky, S.v. and Roeleveld, M.A.C. (2000). "Ventral adhesion" to hard substrates: A thigmotactic response in sepiid cuttlefish (Mollusca, Cephalopoda). *Vie et Milieu* **50**(1), pp. 59-64.

Bone, Q. and Howarth, J.V. (1980). The role of $_{L}$-glutamate in neuromuscular transmission in some molluscs. *Journal of the Marine Biology Association, U.K.* **60**:619-626.

Boycott, B.B. (1961). Functional organisation of the brain of the cuttlefish *Sepia officinalis. Proceedings of the Royal Society of London B,* **153**, pp. 503-534.

Boyde, A. Jones, S.J. and Tamarin, A. (1977). Dimensional changes during specimen preparation for scanning electron microscopy. *Scanning electron microscopy*, **I**, pp. 507-518.

Boyle, P.R. (1999). Cephalopods. **In:** *The UFAW handbook on the care and management of laboratory animals*, 7th Edn., **2**: *Amphibious and aquatic vertebrates and advanced invertebrates* (ed. T. B. Poole), pp. 115-139.

Brocco, S.L. (1976). The ultrastructure of epidermis, dermis, iridophores, leucophores

and chromatophores of *Octopus dofleini* Martin (Cephalopoda: Octopoda). Ph.D. thesis, University of Washington.

Brocco, S.L. and Cloney, R.A. (1980). Reflector cells in the skin of *Octopus dofleini*. *Cell and Tissue Research*, **205**, pp. 167-186.

Brown, P.K. and Brown, P.S. (1958). Visual pigments of the octopus and cuttlefish. *Nature*, **182**, pp. 1288-1290.

Budelmann, B.U, Schipp, R. and Boletzky S.v. (1997). Cephalopoda. **In:** *Microscopical Anatomy of Invertebrates: Volume 6A, Mollusca* (eds. W.A. Fredrick and A.J. Kohn). Wiley-Liss, Inc.

CephBase (2002). [WWW] http://www.cephbase.utmb.edu (20/03/02)

Chamberlain, J.A. (1987). Locomotion of *Nautilus*. **In:** *Nautilus. The biology and paleobiology of a living fossil* (eds. W.B. Saunders and N.H. Landman) pp. 489-525. New York: Plenum Press.

Clark, P.J. and Evans F.C. (1954). Distance to nearest neighbour as a measure of spatial relationships in populations. *Ecology*, **35**(4), pp. 445-453.

Cloney, R.A. and Florey, E. (1968). Ultrastructure of cephalopod chromatophore organs. *Zeitschrift für Zellforschung*, **89**, pp. 250-280.

Cloney, R.A. and Brocco, S.L. (1983). Chromatophore organs, reflector cells, iridocytes and leucophores in cephalopods. *American Zoologist*, **23**, pp. 581-592.

Cooper, K.M. and Hanlon, R.T. (1986). Correlation of iridescence with changes in iridophore platelet ultrastructure in the squid *Lollinguncula brevis*. *Journal of Experimental Biology*, **121**, pp. 451-455.

Cooper, K.M., Hanlon, R.T., and Budelmann B.U. (1990). Physiological color change in squid iridophores: II. Ultrastructural mechanisms in *Lollinguncula brevis*. *Cell and Tissue Research*, **259**, pp. 15-24.

Cott H.B. (1940) *Adaptive colouration in animals*. London: Methuen and Co.

Dawkins, R. (1998). *Unweaving the rainbow*. London: Penguin.

Dean, P.G.G., Johnson W.S. and Middle, F.A. (1985). *Affinity Chromatography: a practical approach*. Oxford: IRL Press.

Denton, E.J. (1970). Review lecture on the organisation of reflecting surfaces in some marine animals. *Philosophical Transactions of the Royal Society of London, B.*, **258**, pp. 285-313.

Denton, E.J. and Land, M.F. (1971). Mechanism of reflexion in silvery layers of fish and cephalopods. *Proceedings of the Royal Society of London. A.*, **178**, pp. 43-61.

Ditchburn, R.W. (1999) Light. New York: Dover.

Donovan, D.T. (1977). Evolution of the dibranchiate cephalopoda. *Symposia of the Zoological Society of London*, **38. In:** *The Biology of Cephalopods* (eds. M. Nixon and J.B. Messenger), London: Academic Press.

Endler J.A. (1978). A predator's view of animal colour patterns. *Evolutionary Biology* **11**, pp. 319-364.

Endler J.A. (1990). On the measurement and classification of colour in studies of animal colour pattern. *Biological Journal of the Linnean Society*, **41**, pp. 315-352.

Endler, J.A. (1991). Interactions between predators and prey. **In:** *Behavioural Ecology. An Evolutionary Approach* (eds. J.R. Krebs and N.B Davies), pp. 169-196. Oxford: Blackwell Scientific.

Ferguson, G.P., Messenger, J.B., and Budelmann, B.U. (1994). Gravity and light influence the countershading reflexes of the cuttlefish *Sepia officinalis*. *Journal of Experimental Biology*, **243**, pp. 63-67.

Fiala, J.C. (2001). IGL Trace / IGL Align / sEM align [WWW] http://synapses.bu.edu/

Fleet, G.W.J., Porter, R.R. and Knowles, J.R. (1969). Affinity labelling of antibodies with aryl nitrene as a reactive group. *Nature,* **224**, pp. 511-512

Florey, E. (1966). Nervous control and spontaneous activity of the chromatophores of a cephalopod, *Loligo opalescens*. *Comparative Biochemistry and Physiology* **18**, pp. 305-324.

Florey, E. (1969). Ultrastructure and function of cephalopod chromatophores. *American Zoologist* **9**, pp. 429-442.

Florey, E. and Kriebel, M.E. (1969). Electrical and mechanical responses of chromatophore muscle fibres of the squid, *Loligo opalescens*, to nerve stimulation and drugs. *Zeitschrift für vergleichende Physiologie,* **65**, pp. 98-130.

Fox, D.L. (1953). Animal biochromes and structural colours. Cambridge, UK: Cambridge University Press.

Fox H.M., Vevers G. (1960). The nature of animal colours. London: Sidgwick and Jackson.

Froesch, D. and Messenger, J.B. (1978). On the leucophores and the chromatic units of *Octopus vulgaris*. *Journal of Zoology, London*, **186**, pp. 163-173.

Fuchs, R.F. (1914). Der Farbenwechsel und die chromatische Hautfunktion der Tiere. In *Handbuch der vergleichenden Physiologie* (ed. H. Winterstein), **3**, pp. 1189-1656.

Glauert, A.M. and Lewis P.R. (1998). Practical methods in Electron microscopy, Vol. **17**: *Biological specimen preparation for transmission electron microscopy*. Portland Press.

Godfrey, D., Lythgoe, J.N. and Rumball, D.A. (1987). Zebra stripes and tiger stripes: the spatial frequency distribution of pattern compared to that of the background is significant in display and crypsis. *Biological Journal of the Linnean Society*, **32**, pp 427-433.

Hanlon, R.T. (1982). The functional organisation of chromatophores and iridescent cells in the body patterning of *Loligo plei* (Cephalopoda: Myopsida). *Malacologia*, **23**, pp. 89-119.

Hanlon, R.T., Cooper, K.M. and Cloney, R.A. (1984). Do the iridophores of the squid mantle reflect light or diffract light in the production of structural colors? *American Malacological Bulletin*, **2**, p. 91.

Hanlon, R.T. and Messenger, J.B. (1988). Adaptive coloration in young cuttlefish (*Sepia officinalis* L.): the morphology and development of body patterns and their relation to behaviour. *Philosophical Transactions of the Royal Society of London,* B, **320**, pp. 437-487.

Hanlon R.T., Cooper, K.M., Budelmann, B.U. and Pappas, T.C. (1990). Physiological color change in squid iridophores. I. Behaviour, morphology, and pharmacology in *Lollingucula brevis. Cell and Tissue Research*, **259**, pp. 3-14.

Hanlon, R.T. and Messenger, J.B. (1996). *Cephalopod Behaviour*. Cambridge: Cambridge University Press

Hecht, E. (1989). Optics, 2nd ed. Massachusetts: Addison-Wesley.

Hermanson, G.T., Mallia A.K. and Smith, P.K. (1992). *Immobilized affinity ligand techniques*. London: Academic Press Inc.

Herring, P.J., Dilly, P.N., and Cope C. (2002). The photophores of the squid family Cranchidae (Cephalopoda: Oegopsida). *Journal of Zoology*, **258**(1), pp. 73-90.

Hogan, J. (2004). Smart surfaces show their colour. *New Scientist* (**28/02**) p. 24.

Howard A.D. (1999). *Project R274T: Project objectives*. Colchester: Defence Clothing and Textiles Agency (now Defence Logistics Organisation).

Howard, C.V. and Reed, M.G. (1998). *Unbiased Stereology: Three-dimensional measurement in microscopy*. Oxford: BIOS Scientific Publishers.

Howell, B.J. and Gilbert, D.L. (1976). pH-temperature dependence of the hemolymph of the squid, *Loligo pealei. Journal of Comparative Biochemistry and Physiology,* **55**A, pp. 287-289.

Huxley, A.F. (1968). A theoretical treatment of the reflexion of light by multilayer

structures. *Journal of Experimental Biology*, **48**, pp 227-245.

Kawaguti S. and Ohgishi, S. (1962). Electron microscope study of iridophores of a cuttlefish, *Sepia esculenta. Biological Journal of Okayama University,* **8**(3-4), pp. 115-129.

Kier, W.M. (1991).Squid cross-striated muscle: the evolution of a specialized muscle fibre type. *Bulletin of Marine Science*, **49**, pp. 389-403.

Land M.F. (1972). The physics and biology of animal reflectors. *Progress in Biophysics and Molecular Biology,* **24**, pp. 75-106.

Le Grand, Y. (1952). *Optique Physiologique*. Paris: Editions de la Revue d' Optique.

Loi, P.K., Saunders, R.G., Young, D.C. and Tublitz, N.J. (1996). Peptidergic regulation of chromatophore function in the European cuttlefish *Sepia officinalis. Journal of Experimental Biology,* **199**, pp. 1177-1187.

Loi, P.K. and Tublitz, N.J. (1997). Molecular analysis of FMRFamide and FMRFamide related peptides (FaRPs) in the cuttlefish *Sepia officinalis. Journal of Experimental Biology*, **200**(10), pp. 1483-1489.

Loi, P.K. and Tublitz, N.J. (2000). The roles of glutamate and FMRFamide-related peptides at the chromatophore neuromuscular junction in the cuttlefish, *Sepia officinalis. Journal of Comparative Neurology*, **420** (4), pp. 499-511.

Mäthger L.M. and Denton E.J. (2001). Reflective properties of iridophores and fluorescent 'eyespots' in the Loliginid squid *Alloteuthis subulata* and *Loligo vulgaris. The journal of Experimental Biology*, **204**, pp. 2103-2118.

Marshall, N.J. and Messenger, J.B. (1996). Colour-blind camouflage. *Nature*, **382**, pp. 408-409.

Maunsbach A. B., Aflzelius B.A. (1999). Freezing and low-temperature embedding. In *Biomedical electron microscopy – illustrated methods and interpretations*, Ch 16, pp. 125-140. Academic Press: California.

Messenger, J.B. (1968). The visual attack of the cuttlefish, *Sepia officinalis. Animal Behaviour*, **16**, pp. 342-357.

Messenger, J.B. (1970). Optomotor responses and nystagmus in intact, blinded and statocystless cuttlefish (*Sepia officinalis* L.). *Journal of Experimental Biology,* **53**, pp. 789-796.

Messenger, J.B. (1974). Reflecting elements in cephalopod skin and their importance for camouflage. *Journal of Zoology, London*, **174**, pp. 387-395.

Messenger, J.B. (1981). Comparative physiology of vision in Molluscs. **In:** *Handbook of Sensory Physiology and Evolution of Vision in Invertebrates* (ed. H. Autrum), pp. 93-200. New York: Springer-Verlag.

Messenger, J.B. (1991).Photoreception and vision in Molluscs. **In:** *Evolution of the eye and visual system* (ed. J.R. Cronly-Dillon and R.L. Gregory), pp. 364-397. London: MacMillan.

Messenger, J.B., Nixon, M, and Ryan, K.P. (1985). Magnesium chloride as an anaesthetic for cephalopods. *Comparative Biochemistry and Physiology*, **82C** (1), pp. 203-205.

Messenger, J.B., Cornwell, C.J, and Reed, C.M. (1997). L-Glutamate and serotonin are endogenous in squid chromatophore nerves. *Journal of Experimental Biology*, **200**, pp. 3043-3054.

Messenger, J.B. (2001). Cephalopod chromatophores: neurobiology and natural history. *Biological Reviews*, **76**, pp. 473-528.

Mirow, S. (1972). Skin color in the squid *Loligo pealii* and *Loligo opalescens*: II. Iridophores. *Zeitschrift für Zellforschung,* **125**, pp. 175-190.

Molecular Probes (1999). *Protein-protein crosslinking kit* (product information). **MP 06305.** Molecular Probes, Inc.

Molecular Probes (2002). *Handbook of fluorescent probes and research chemicals.* Chapter 5.2, *Chemical crosslinking reagents; Thiolation of biomolecules.* [WWW] http://www.interchim.fr/bio/molprobes/cd/docs/sections/0502.htm (12/06/02).

Moody, M.F. (1962). Evidence for the intraocular discrimination of vertically and horizontally polarized light by *Octopus*. *Journal of Experimental Biology*, **39**, pp. 21-30.

Moody, M.F. and Parriss J.R. (1960). Discrimination of polarized light by *Octopus*. *Nature*, **4728**, pp. 839-840.

Moody, M.F. and Parriss J.R. (1961). The discrimination of polarised light by *Octopus*; a behavioural and morphological study. *Zeitschrift für vergleichende Physiologie*, **44**, pp. 268-291.

Moynihan, M. (1985). *Communication and noncommunication by cephalopods.* Bloomington: Indiana University Press.

Moynihan, M., and Rodaniche, A. F. (1982). The Behaviour and Natural History of the Caribbean Reef Squid *Sepioteuthis sepioidea*. With a Consideration of Social, Signal and Defensive Patterns for Difficult and Dangerous Environments. *Advances in Ethology* **25**. Berlin and Hamburg: Verlag Paul Parey.

Müller, H. (1853). Bericht über einige im Herbste 1852 in Messina angestellte, verleichend-anatomische Üntersuchungen. *Zeitschrift f. wissensch. Zool.*, **4**, pp. 299-370.

Nassau, K. (1983). *The physics and chemistry of color*. New York, John Wiley & Sons.

Nave R., (2003). [WWW] http://hyperphysics.phy-astr.gsu.edu/hbase/atmos/blusky.html

O'Dor, R.K. and Shadwick, R.E. (1989). Squid, the Olympian cephalopods. *Journal of Cephalopod Biology* **1**, pp. 33–55.

OLMC (2001). [WWW]. (ed. S. Prahl) http://omlc.ogi.edu/software/mie/

Outwater, C. and Hamersveld, V. (1995). Practical Holography. Dimensional Arts Inc. *Free download from:* http://www.holo.com/holo/book

Packard, A. (1972). Cephalopods and Fish: The limits of convergence. *Biological Review* **47**, pp. 241-307.

Packard, A. (1995) Through the looking-glass of cephalopod colour patterns. **In:** *Behavioural brain research in naturalistic and semi-naturalistic settings* (eds. E. Alleva, A. Fasolo, H-P. Lipp, L. Nadel and L. Ricce), pp. 105-130. Netherlands: Kluver Academic Press.

Packard, A. and Sanders, G.D. (1971). Body patterns of *Octopus vulgaris* and maturation of the response to disturbance. *Animal Behaviour*, **19**, pp. 780-790.

Packard, A. and Hochberg, F.G. (1977). Skin patterning in *Octopus* and other genera. **In:** *The Biology of cephalopods: Symposia of the Zoological Society of London* (eds. Nixon, M. and Messenger, J.B.), **38**, pp. 191-231. New York: Academic Press.

Palmer, C. (2001). *The diffraction grating handbook* (4th edition). New York: Richardson grating laboratory. [WWW] http://www.gratinglab.com/library/handbook4 (30/03/01).

Parker, G.H. (1948). Animal colour changes and their neurohumours. Cambridge: Cambridge University Press.

Prota, G. Ortonne, J.P., Voulot, C. Khatchadourian, C. Nardi, G. and Palumbo, A. (1981). Occurrence and properties of tryosinase in the ejected ink of cephalopods. *Comparative Biochemistry and Physiology*, **68B**, pp. 415-419.

Rabl, H. (1900). Uber Bau und Entwicklung der Chromatophoren der Cephalopoden nebst allgemeinen Bemerkungen uber die Haut dieser Tiere. S.B. Akad. Wiss., Wein III, **109**, pp. 341-404.

Rayleigh, 3rd Baron (1917). On the reflection of light from a regularly stratified medium. *Proceedings of the Royal Society of London A*, **93**, pp. 565-577.

Rao, K.R. and Fingerman, M. (1983). Introduction to the symposium:

Chromatophores and color changes. *American Zoologist*, **23**, pp. 463-476.

Reed. C.M. (1995). Dye coupling in the muscles controlling squid chromatophore expansion. *Journal of Experimental Biology*, **198**, pp. 2631-2634.

Robards A.W., Sleytr U.B. (1985). Low temperature methods in biological electron microscopy. **In:** *Practical Methods in Electron Microscopy* (ed. A.M. Glauert), Vol. **10**. Amsterdam: Elsevier.

Robertson, J.D. (1965). Studies on the chemical composition of muscle tissue. III. The mantle muscle of cephalopod molluscs. *Journal of Experimental Biology*, **42**, pp. 153-175.

Rowell C.H.F. and Wells, M.J. (1961). Retinal orientation and the discrimination of polarized light by octopuses. *Journal of Experimental Biology*, **38**, pp. 827-831.

Russell, P. St.J., Birks, T.A., Lloyd-Lucas, F.D. (1995). Photonic Bloch waves and photonic band gaps, pp. 585-633. **In:** *Confined Electrons and Photons* (eds. E. Burstein and C. Weisbuch). New York: Plenum Press.

San Giovanni, G. (1819). Descrizione d'un particolare sistema di órgani cromophoro espansivo dermoideo e dei fenómeni ch'esso produce, scoperto nei molluschi cefalopodi. Giorn. *Enciclopedico di Napoli* **13** (9).

Sanderson, J.B. (1994). Biological microtechniques: *Royal Microscopical Society, Microscopic Handbook,* **28**. Oxford: BIOS Scientific Publishers.

Schäfer, W. (1937). Bau, entwicklung und farbenentstehung bei den flitterzellen von *Sepia officinalis. Z. f. Zellforschung u. mikr. Anatomie Bd.* **27** .222-245.

Shashar, N. and Cronin, T.W. (1996). Polarization contrast vision in octopus. *Journal of Experimental Biology*, **199**, pp. 999-1004.

Shashar, N., Rutledge P.S., and Cronin, T.W. (1996). Polarization vision in cuttlefish – A concealed communication channel? *Journal of Experimental Biology*, **199**, pp. 2077-2084.

Shashar, N., Hanlon, R.T. and Petz, A. deM. (1998). Polarization vision helps detect transparent prey. *Nature*, **393**, pp. 222-223.

Shashar, N., Hagen, R. Boal J.G. and Hanlon, R.T. (2000). Cuttlefish use polarization sensitivity in predation on silvery fish. *Vision Research*, **40**, pp. 71-75.

Shashar, N., Borst, D.T., Ament, S.A., Saidel, W.M., Smolowitz, R.M. and Hanlon, R.T. (2001). Polarization Reflecting Iridophores in the Arms of the Squid *Loligo pealeii. Biological Bulletin*, **201**, pp. 267-268.

Sinclair, N. (2002). Development of responsive surfaces for adaptive camouflage. *Department of Chemical Engineering, University of Bath* (Final year student project, CHEL0062). Supervisor: J. Hubble.

Sterio, D.C. (1984). The unbiased estimation of number and sizes of arbitrary particles using the dissector. *Journal of Microscopy*, **134**, pp. 127-136.

Swanson, G.J. and Weldkamp, W.B. (1990). Massachusetts Institute of Technology, Cambridge, Massachusetts. *High-Efficiency, multilevel, diffractive optical elements*. U.S. Patent no., 4,895,790.

Tang, M., Zhang, R., Bowyer, A., Eisenthal, R. and Hubble, J. (2003). A reversible hydrogel membrane for controlling the delivery of macromolecules. *Biotechnology and Bioengineering,* **82** (1), pp. 47-53.

Tilley, R. (2000). *Colour and the optical properties of materials*. Chichester: John Wiley and Sons.

Tompsett, D.H. (1939). *The anatomy of Sepia officinalis* L. Ph.D. Thesis. Reading University.

Young, R.E. (1977). Ventral bioluminescent countershading in midwater cephalopods. *Symposia of the Zoological Society of London*, **38**. **In:** *The Biology of Cephalopods* (eds. M. Nixon and J.B. Messenger), pp. 161-190. London: Academic Press.

Young, R.E. and Mencher, F.M. (1980). Bioluminescence in mesopelagic squid: Diel color change during counterillumination. *Science*, **208**, pp. 1286-1288.